A THESIS
entitled

A STUDY OF THE MODES OF GAS-SOLIDS FLOW IN PIPELINES

Submitted in partial fulfilment of the
requirements for the award of the

DEGREE OF DOCTOR OF PHILOSOPHY

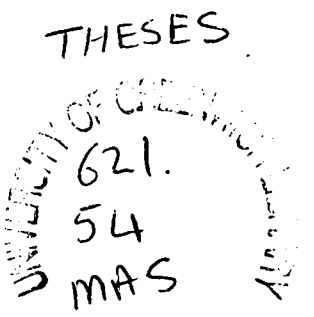

of the

COUNCIL FOR NATIONAL ACADEMIC AWARDS

by

DAVID JOHN MASON, BSc (Eng).

Centre For Numerical Modelling And Process Analysis
School Of Mathematics, Statistics And Computing
And School Of Engineering
Faculty Of Technology
Thames Polytechnic
LONDON

November 1991

So what you think? I ast.

I think us here to wonder, myself. To wonder. To ast. And that in wondering bout the big things and asting bout the big things, you learn about the little ones, almost by accident.

From The Color Purple by Alice Walker.

ABSTRACT

A variety of gas-solids flows can be observed in the pipeline of a pneumatic conveying system. These flows may be classified as one of three modes:

i. suspension flow;
ii. non-suspension moving-bed type flow;
iii. non-suspension plug type flow.

The modes of flow that a bulk material can achieve are dependent upon its particle and bulk properties as well as the pipeline conditions. This work describes the development of mathematical models for these modes of flow as well as experimental investigations to determine the validity of the models proposed.

The modelling technique was based upon the solution of the conservation equations for inter-dispersed continua. Mathematical models for phenomena, such as the aerodynamic drag force between the conveying gas and particles, were added to the general mathematical model so that the flow of the gas-solids mixture could be simulated. This resulted in successful development of models for the prediction of suspension flow and non-suspension moving-bed type flow.

In addition to providing data for validation of the mathematical models, the experimental programme produced a number of other observations. For example, it was found that the solids velocity in non-suspension moving-bed type flow could be determined non-intrusively by pressure measurements due to the variation in height of the moving-bed with time at a fixed location. More importantly, observation of plug type flow has led to the proposal of a mechanism to describe the development of the flow along a pipeline.

AUTHOR'S NOTE

All the work in this thesis is the sole and original work of the author, except where stated otherwise by acknowledgement or reference.

ACKNOWLEDGEMENTS

Numerous people have provided me with invaluable support throughout this work. Firstly, I would like to thank all those involved in the supervision of this project at various stages: Professor M Cross, Professor AR Reed, Professor NC Markatos and Dr MK Patel. I would also like to thank all my fellow reseach students in both the School of Mathematics and School of Engineering, especially Nicole and Cos whose managed to survive three years in the same office.

This work would not have been possible without the support of the staff of Computer Centre, and the technicians at the Laboratory. In particular I would like to acknowledge the support of Robert Painter and Andrew Mason.

Finally I would thank my Mum and Dad for their constant support during the production of this thesis.

This work was funded from the Science and Engineering Research Council's Specially Promoted Programme in Particulate Technology.

CONTENTS

3 THE MATHEMATICAL MODEL

4 EXPERIMENTAL EQUIPMENT

8 CONCLUSION

NOMENCLATURE

A	Flow area normal to the direction of flow.
A_{Proj}	Projected area of an object used in the calculation of aerodynamic drag (equation 5.3.2.1), defined in equation 5.3.2.5.
a	Coefficient in conservation equation.
b	Coefficient in conservation equation.
C_D	Coefficient of drag for an object.
C_d	Coefficient of dischage from an orifice.
C_P	Specific heat at constant pressure.
C_ϕ	Coefficient used in the linearisation of a source term, defined in equation 3.2.4.2.
c_1	Variable defined by equation 2.4.3.3.2.
c_2	Variable defined by equation 2.4.3.3.3.
D	Pipe diameter.
d_s	Particle diameter.
F_D	Drag force on an object.
F_i	Shear force due to the viscosity of the ith phase.
Fr	Froude number, defined by equation 2.4.3.3.3.
f_g	Gas pipe friction factor.
f_s	Solids pipe friction factor.
G	Multiplier used in the linearisation of a source term, defined in equation 3.2.4.2.
g	Acceleration due to gravity.
k	Turbulent kinetic energy.
$\dot{m}_g$	Gas mass flow rate.
$\dot{m}_i$	Mass flow rate of the ith phase.
$\dot{m}_m$	Mass flow rate of gas-solids mixture, defined in equation 5.3.1.1.
$\dot{m}_s$	Solids mass flow rate.
P	Pressure.
R	Gas constant from the ideal gas equation (equation 3.2.4.1).
R_g	Volume fraction of gas.
R_i	Volume fraction of ith phase, defined by equation 3.2.1.
R_s	Volume fraction of solids.
Re	Reynolds number.
Re_D	Pipe Reynolds number, defined in equation 5.4.1.2.
Re_s	Particle Reynolds number, defined in equation 5.3.2.3.
S_{Ri}	Source term for the conservation of mass equation for the ith phase.

S_P	Term used in the linearisation of a source term (equation 3.2.4.2), defined in equation 3.2.4.3.
$S_{Pressure}$	Pressure source term in the conservation of momentum equation.
S_{ui}	Source term for the conservation of momentum equation for the ith phase.
S_ϕ	Source term in the general conservation equation.
SLR	Solids loading ratio, defined by equation 2.2.1.
T_g	Temperature of gas.
T_m	Temperature of gas-solids mixture, defined in equation 5.3.1.3.
T_s	Temperature of solids.
U_g	Superficial gas velocity, $U_g = R_g u_g$.
u_g	Velocity of gas.
u_i	Velocity of the ith phase.
u_s	Velocity of solid particles.
u_{slip}	Slip velocity, $u_{slip} = u_g - u_s$.
u_{st}	Terminal velocity of a single particle.
V_{cv}	Volume of a control volume.
V_i	Volume occupied the ith phase in a control volume.
V_ϕ	Value used in the linearisation of a source term, defined in equation 3.2.4.2.
Z	Compressibility factor (Z=1 for an ideal gas).
α	Solids pressure drop function, defined by equation 2.4.2.1.
β	Variable defined by equation 2.4.2.4b.
Γ_ϕ	Diffusion coefficient.
γ	Ratio of specific heats, $\gamma = C_P/C_V$.
ΔP	Pressure drop.
ΔP_g	Pressure drop due to gas only.
ΔP_s	Pressure drop due to solids only.
Δx	Distance between two points in x direction.
ϵ	Turbulence dissipation rate.
λ_s	Solids friction factor, defined by 2.4.3.3.2.
μ_L	Dynamic viscosity of fluid.
μ_E	Effective dynamic viscosity used in turbulence models.
ν_L	Kinematic viscosity of fluid.
ξ	Variable defined by equation 2.4.2.4c.
ρ_{bulk}	Density of bulk material, $\rho_{bulk} = R_s \rho_s$.
ρ_g	Density of gas.
ρ_i	Density of the ith phase.
$\rho_{mixture}$	Density of gas-solids mixture, defined by equation 2.4.3.3.1.

ρ_s	Density of solid particle.
τ_s	Intergranular shear stress.
ϕ	Conserved variable in the general conservation equation.

1 INTRODUCTION

1.1 PNEUMATIC CONVEYING

Pneumatic conveying is the transportation of solid particles by a gas (generally air) through a pipeline. The origins of pneumatic conveying can be traced to the latter end of the nineteenth century. One of the earliest successful applications being the Duckham pneumatic grain elevator for ship unloading Anon.0 (1887). Pneumatic conveying systems are highly flexible, yet simple systems that may be used to transport a wide range of powdered and granular materials. A pneumatic conveying system may be considered as comprising of four elements, as illustrated in figure 1.1.1:

i. a source of compressed gas;
ii. a device to feed solid particles into the pipeline;
iii. the conveying pipeline;
iv. a device to separate the solids from the gas.

A multiplicity of industries employ pneumatic conveying. The following list indicates a small sample of these and some bulk particulate materials that are transported:

i.	food industry	floor, sugar, tea, fish;
ii.	agriculture	grain, rice, animal feed pellets;
iii.	oil industry	barytes, cement, bentonite;
iv.	power generation	pulverised coal, ash;
v.	chemical industry	polyethylene pellets, PVC powder.

The first trials to determine relationships between the properties of the gas and solid particles, and those of the flowing suspension were reported in the early nineteen-twenties, for example, the work of Cramp and Priestly (1925). These early systems transported solid particles in suspension, in the gas stream. By the late forties workers such as Albright et al (1949) had started to investigate alternative conveying systems employing modes of flow in which the solid particles were not suspended in the gas stream. Resistance to the adoption of these new systems was due to the frequency with which pipelines became blocked. This was especially true with poorly designed systems.

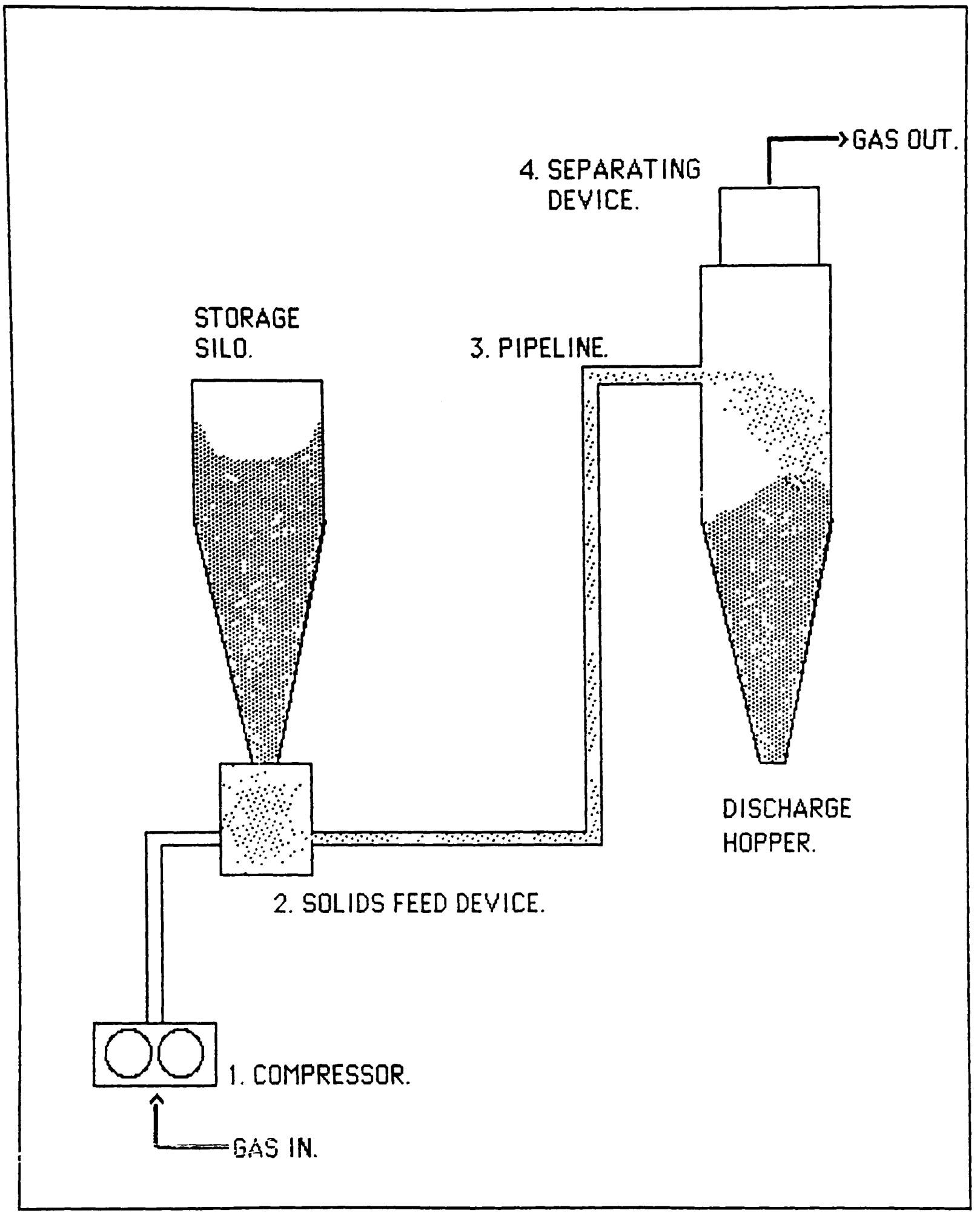

Figure 1.1.1 The Basic Elements of a Pneumatic Conveying System.

Some advantages of systems characterised by non-suspension modes of flow are:

i. lower energy consumption;
ii. reduced particle degradation;
iii. less pipeline erosion.

The second two effects result primarily from the lower velocities encountered in such systems. The first effect is dependent largely upon the type of bulk particulate material conveyed and the actual mode of flow achieved. The drawback to such systems is the increased complexity of the design procedure.

1.2 CURRENT SYSTEM DESIGN PRACTICE

When considering the design of a pneumatic conveying system, the designer starts with the following information:

i. the type of bulk particulate material to be conveyed;
ii. the required delivery rate for the bulk particulate material;
iii. the distance the bulk particulate material is to be transported.

Figure 1.2.1 shows the interdependence of the various parameters of the conveying system upon each other. This illustrates the importance of determining the pressure drop necessary to convey the bulk particulate material for a given set of operational parameters. From a knowledge of the gas requirements of the system the four system elements (illustrated in figure 1.1.1) may be selected. Current design practice employs one of the following methods to obtain this information:

i. the application of an empirical correlation, for example Rose and Barnacle (1957);
ii. the use of data acquired from similar existing systems;
iii. the use of data from tests on pilot size plant, for example Mills (1979).

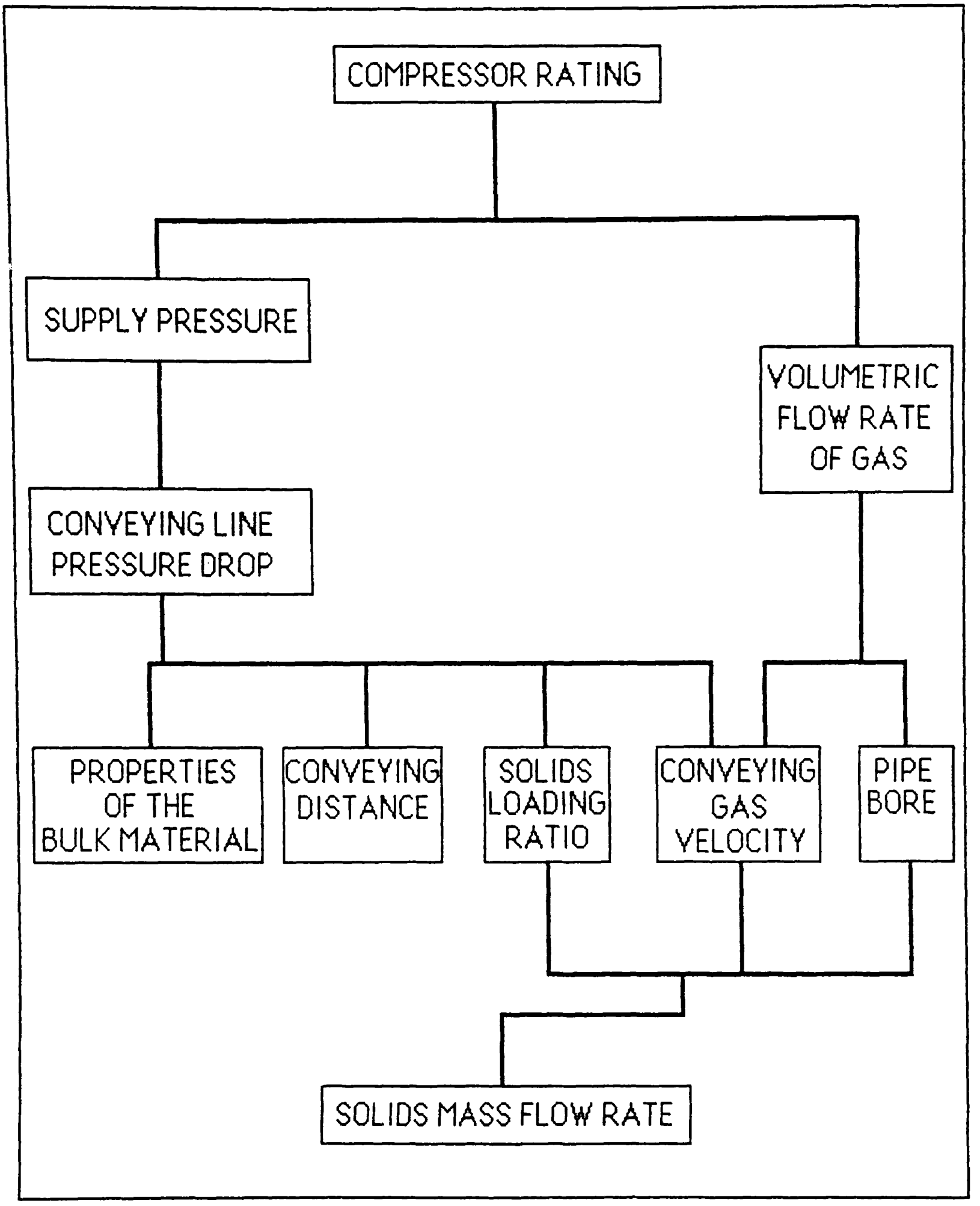

Figure 1.2.1 The Relationship Between System Performance Parameters and Components.

The difficulty with all these methods, to varying degrees, is the need to scale the data in order for it to be applicable to the actual system. The parameters involved in such a scaling process are:

i. the pipe diameter;
ii. the length and orientation of the pipeline;
iii. the number of bends in the pipeline.

From the results of this scaling procedure a suitable set of operating conditions may be used to define a system which can successfully transport the bulk material as specified.

1.3 OBJECTIVES OF THIS STUDY

While the procedure outlined in the previous section has proved reliable, considerable care is required when the actual system differs significantly from the pilot plant. The current demand for:

i. longer pipelines;
ii. higher throughputs;
iii. lower energy costs;
iv. better product quality (ie less particle degradation);

has exacerbated an already complex situation to a point which encourages the development of new design procedures. Consequently, those workers involved in the design of such systems have begun to explore alternative methods. The minimum requirement of any new design procedure is that it must provide a confidence check on the system parameters produced by a conventional design method. Therefore the aims of this research programme may be summarised as follows:

i. to analyse the physical phenomena that influence the flow of gas-solids mixtures in pipelines, with particular reference to situations in which the solid particles are not suspended in the gas;
ii. to develop mathematical models for these phenomena, and to use the models to predict the performance of a pneumatic conveying system;
iii. to acquire sufficient experimental data to validate these models.

1.4 STRUCTURE AND SCOPE OF THE THESIS

In accordance with the first objective of the research programme previously published work was reviewed to identify:

i. the possible modes of gas-solids flow in pipelines;
ii. a means of characterising bulk particulate materials according to their physical properties;
iii. the methods employed to develop models of gas-solids flow in pipelines.

A description of the general mathematical model employed in this programme is then given. An outline of the procedure used to solve the system of equations resulting from the general model is presented. Thus the tool for the computational simulations has been introduced. Subsequently the tool for the experimental element of the programme is described. Once the basic tools have been described, their application to the problem of gas-solids flow in pipelines is presented. Finally, comment is made on the success, or otherwise, of these experiments (computational and physical) and suggestions are made for further work.

2 REVIEW

2.1 INTRODUCTION

The starting point for the development of a mathematical model to describe a physical process is a conceptual view of the process. This conceptual view facilitates the identification of the important physical phenomena involved in the process. In the field of pneumatic conveying, this has led to numerous procedures for the classification of bulk particulate materials. These procedures use properties of both the bulk and the individual particles of the material to predict the potential modes of flow of the bulk material. This review assesses the various techniques, and demonstrates the reasoning behind the adoption of one of these methods.

The second part of this review considers the various methods available to analyse the process in light of the conceptual view of the process. The aim of this programme was to gain an insight into the mechanisms involved when a bulk material is transported through a pipeline by a gas. This insight also suggests certain types of mathematical approach for analysing the process.

2.2 MODES OF GAS SOLIDS FLOW IN PIPELINES

Pneumatic conveying systems have been classified traditionally according to the concentration of the bulk material in the pipeline. So-called *dilute phase* systems exhibit low solids concentrations, whilst *dense phase* systems have high solids concentrations. In general, *dilute phase* systems operate with gas velocities of sufficient magnitude to keep the majority of the bulk material suspended in the conveying gas. The *dense phase* description covers all other systems which operate generally at lower velocities. There is considerable ambiguity in the definition of *dense phase* according to the: classification method employed; the bulk material considered; and the type of system that is commercially marketed!

In order to avoid confusion by the use of the word phase to describe the components of the mixture flowing in the pipeline *dilute phase* systems will be referred to as suspension flow systems. This definition is different from that of Crowe (1982), who describes *dilute* gas-solids flow as a flow in which the particle motion is controlled by local aerodynamic forces and *dense* gas-solids flow as a flow in which particle motion is governed by particle-particle collisions. Both of these types of flow occur in suspension

flow systems, with the former characteristics dominating.

Zenz and Othmer (1960), show qualitative phase diagrams for the transport of bulk materials in both horizontal and vertical pipelines. These are reproduced in figures 2.2.1 and 2.2.2.

The saltation velocity, u_s, in the horizontal pipeline is the boundary between suspension and non-suspension flow. The choking velocity, u_c, in the vertical pipeline is the boundary between flow and no-flow. For a vertical pipeline the boundary between suspension and non-suspension flow is the velocity at which counter-flow of solids begins.

All other flowing gas-solid systems will be referred to as non-suspension flow systems. These operate in the region below u_s in horizontal pipelines. It should be noted that since the mass flow rate of the conveying gas is constant and the gas density falls as the pipeline exit is approached, a system may exhibit first non-suspension flow and then suspension flow as the gas expands. Numerous workers have used the dimensionless quantity, *phase density*, also known as the solids loading ratio, to define the boundary between suspension and non-suspension flow.

$$\textit{Solids Loading Ratio, } SLR = \frac{\dot{m}_s}{\dot{m}_g} \qquad 2.2.1$$

The following illustrate the variations that have occurred by using this approach:

i. Ramachandran et al (1970), SLR > 25 to 100 for non-suspension flow;
ii. Schuchart (1970), SLR > 100 for non-suspension flow;
iii. Klinzing and Mathur (1981), SLR > 10 for non-suspension flow.

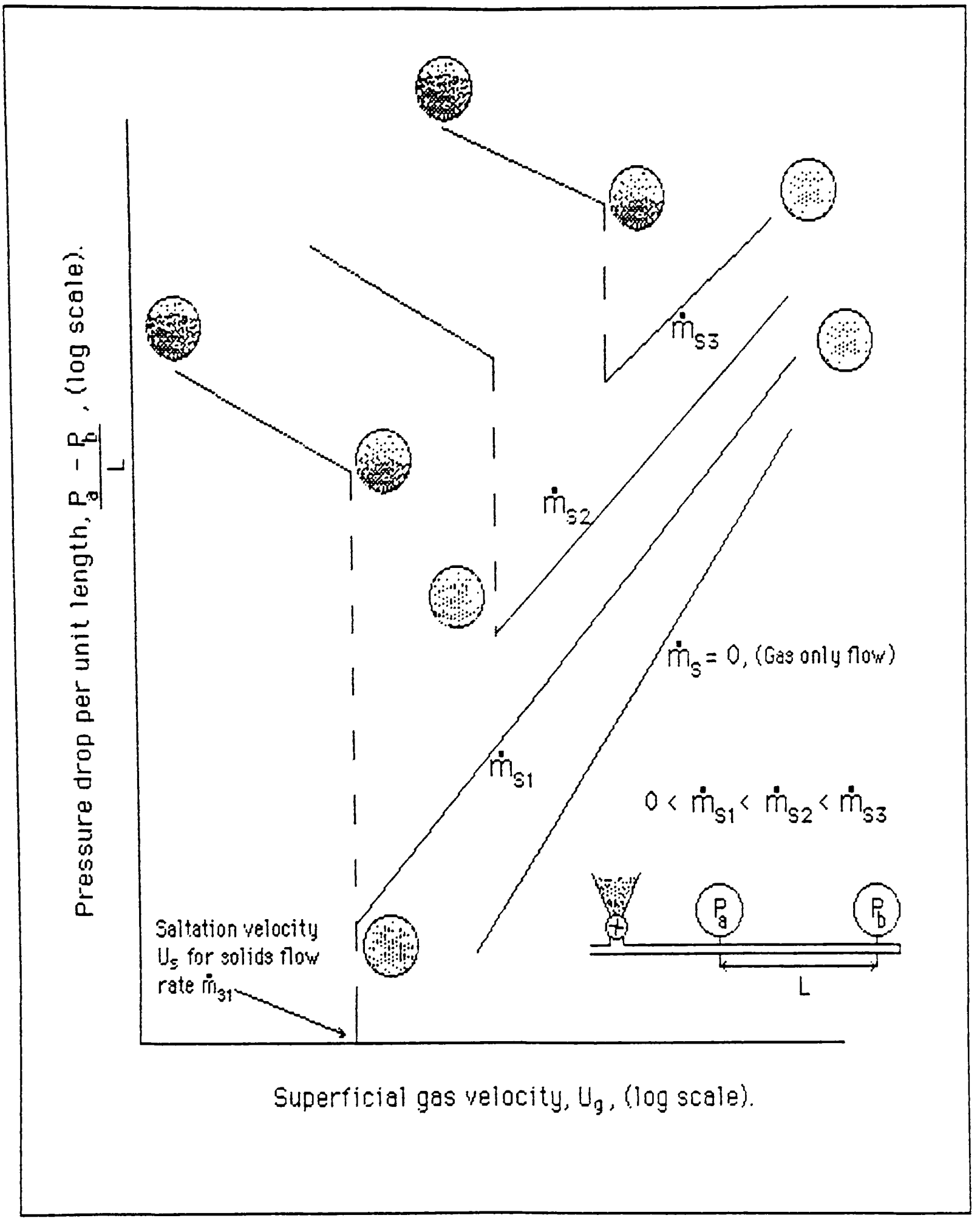

Figure 2.2.1 "Phase diagram" for horizontal gas-solids flow Zenz and Othmer (1960).

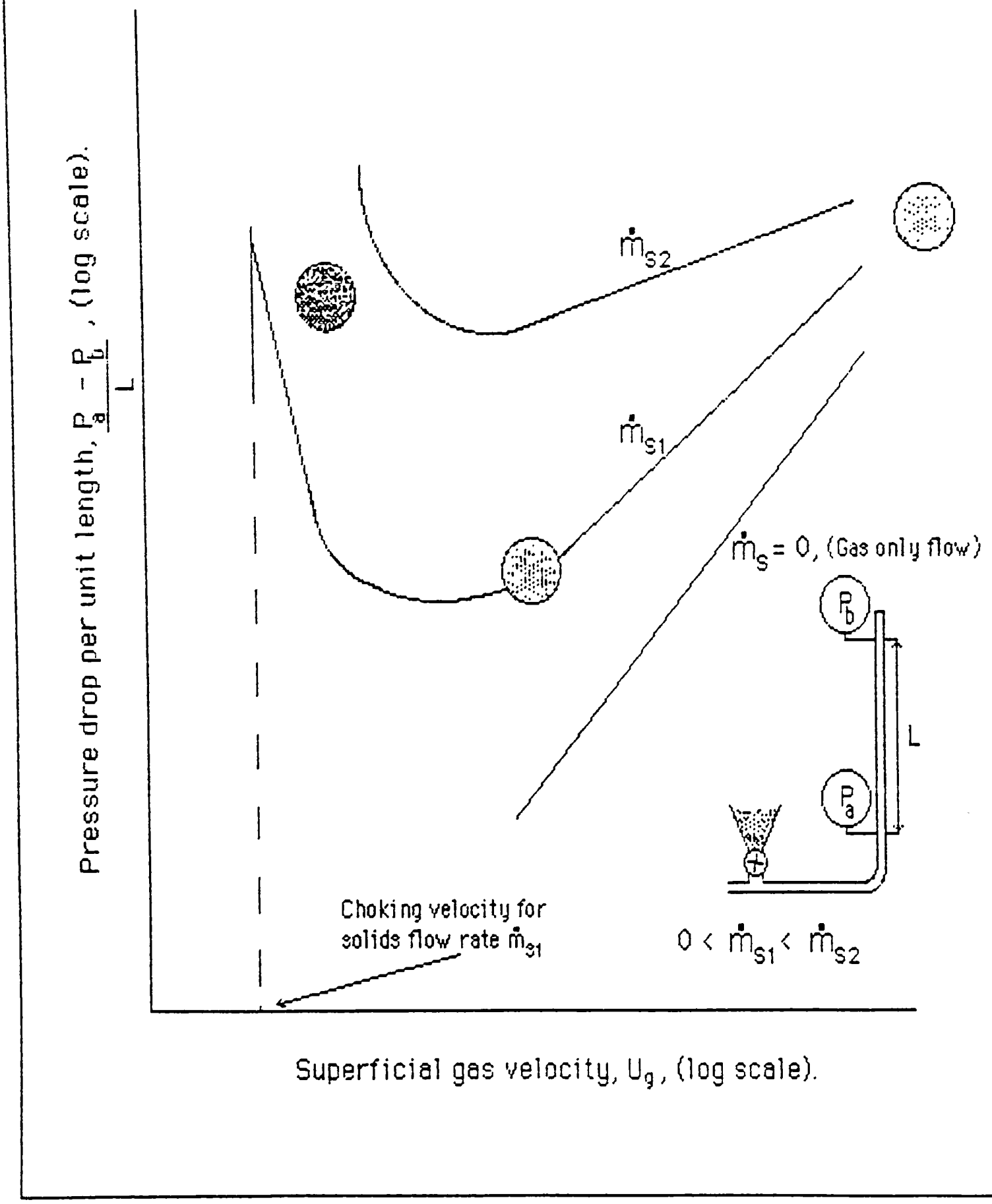

Figure 2.2.2 "Phase diagram" for vertically up gas-solids flow Zenz and Othmer (1960).

The use of SLR is clearly limited since it takes no account of the volumetric concentration, or the properties of the bulk material. Dixon (1979) identified this fact by describing the maximum SLR as a function of:

i. bulk material properties;
ii. pipeline geometry;
iii. system operating condition.

Zenz and Rowe (1976) emphasized this point, stating that there is no simple numerical division between suspension and non-suspension modes of flow.

Most workers subsequently subdivide the non-suspension flow mode according to the flow regimes that may be observed within the pipeline. Wen and Simons (1959) identify three modes of non-suspension flow. These are described in order of decreasing conveying gas velocity:

i. segregation into a dense formation;
ii. intermittent slugs of solids and gas;
iii. a stationary layer with ripples travelling along its surface.

This type of classification is both material and pipeline dependent, and is subjective in nature. Furthermore, Wirth and Molerus (1982) reverses the order of modes (ii) and (iii), and further subdivide mode (i). The most common subdivision of non-suspension flow is into moving-bed type flow and plug-type flow. Konrad et al (1980), Hitt (1985), and Legel and Schwedes (1984) all describe plug-type flow. Figure 2.2.3 illustrates the main features of this mode of flow. Moving-bed type flow encompasses the Wen and Simons groups (i) to (iii), and is illustrated in figure 2.2.4. In summary, the following modes of flow have been identified:

i. Suspension flow;
ii. Non-Suspension (moving-bed flow and plug flow).

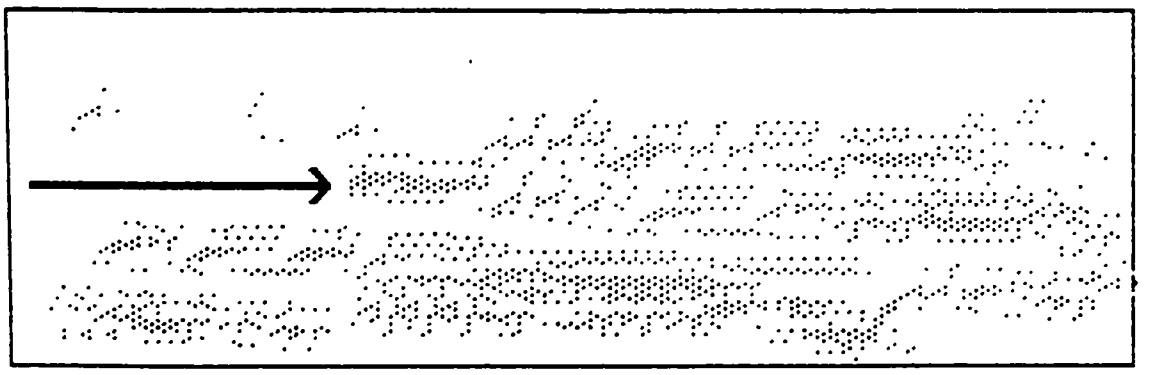

Particles suspended in the conveying gas.

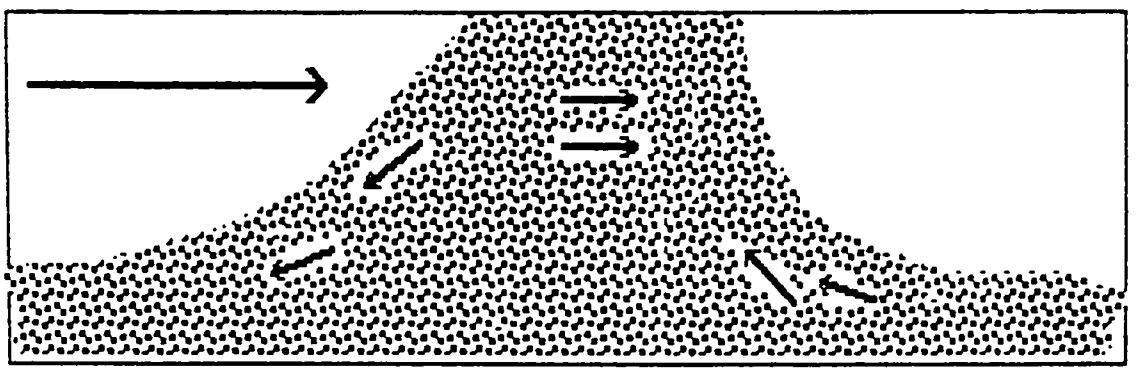

Plug flow, the material flows like a wave with material picked up from the stationary layer in front and falling off the back of the plug.

Increasing conveying gas velocity.

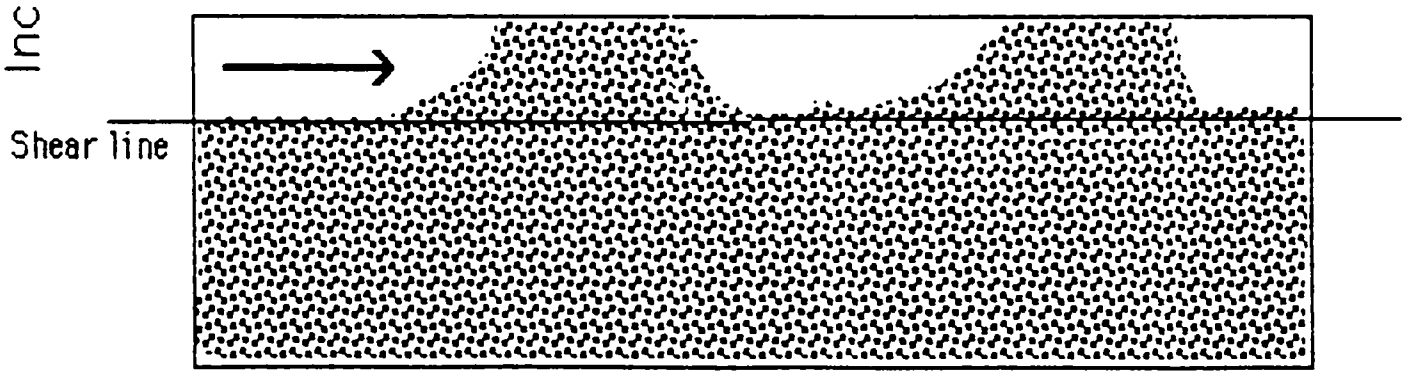

Small plugs of material flowing over a stationary layer.

Figure 2.2.3 Flow patterns in the development of non-suspension plug type flow.

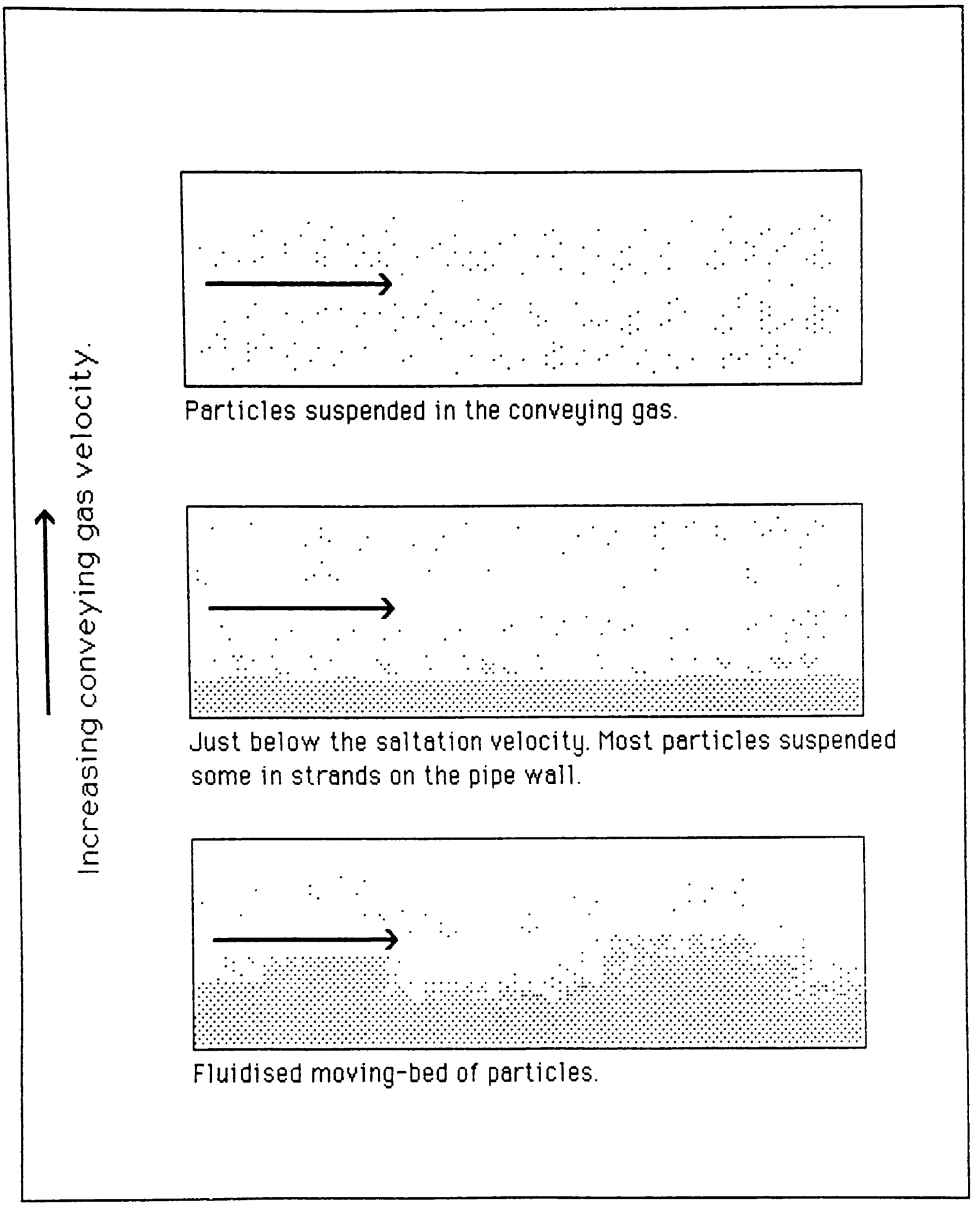

Figure 2.2.4 Flow patterns in the development of non-suspension moving-bed flow.

2.3 CLASSIFICATION OF BULK MATERIALS ACCORDING TO MODES OF FLOW

The type of pneumatic conveying system that is required to transport a bulk material is dependent upon the modes of flow that can be achieved with the particular bulk material. The ability to predict these modes of flow from the properties of the bulk material would be of considerable advantage to the system designer. Geldart (1973) developed a classification based upon the particle density and mean size of the particles forming the bulk material. This was developed to predict the fluidisation behaviour of bulk materials and was subsequently adapted to predict modes of flow of bulk materials in pipelines. Figure 2.3.1 shows the Geldart chart. Lohrman and Marcus (1983) identify Group A materials as good candidates for non-suspension flow. They also state that a classification based upon mean particle size and particle density is insufficient for the prediction of the potential conveying performance of a bulk material. Hitt (1985) identified Group D materials as good candidates for non-suspension plug flow.

Reproduced in figure 2.3.2 is the slugging diagram of Dixon (1979). The diagram was produced by using an analogy between fluidisation and vertical pipe flow. The diagram employs the same axes as the Geldart diagram, but the boundaries were determined from a comparison of the gas bubble velocity and the terminal velocity of a single particle. The application of this diagram for the prediction of flows in horizontal pipelines is justified on the basis of work of Zukoski (1966). This work shows that, for liquids, the gas bubble velocities in horizontal pipes were between 0 and 30% greater than that for vertical pipes. The Dixon chart has similar weaknesses as the Geldart diagram since the bulk material is only described by particle properties. Mainwaring and Reed (1987) correlated the results of conveying trials with bulk materials transported in non-suspension plug flows, with fluidisation tests of these materials. The bulk properties of permeability and de-aeration were measured in fluidisation tests and the mode of flows in the pipeline noted by visual observation. Permeability is the resistance of the bulk material to the flow of gas through it just before the bulk material becomes fluidised. De-aeration is a measure of the diffusion of gas from the fluidised bulk material. Jones and Mills (1989) reached a similar conclusion from conveying trials with bulk materials transported in non-suspension moving-bed flow. Figures 2.3.3 and 2.3.4 reproduce respectively the Mainwaring and Jones' classifications.

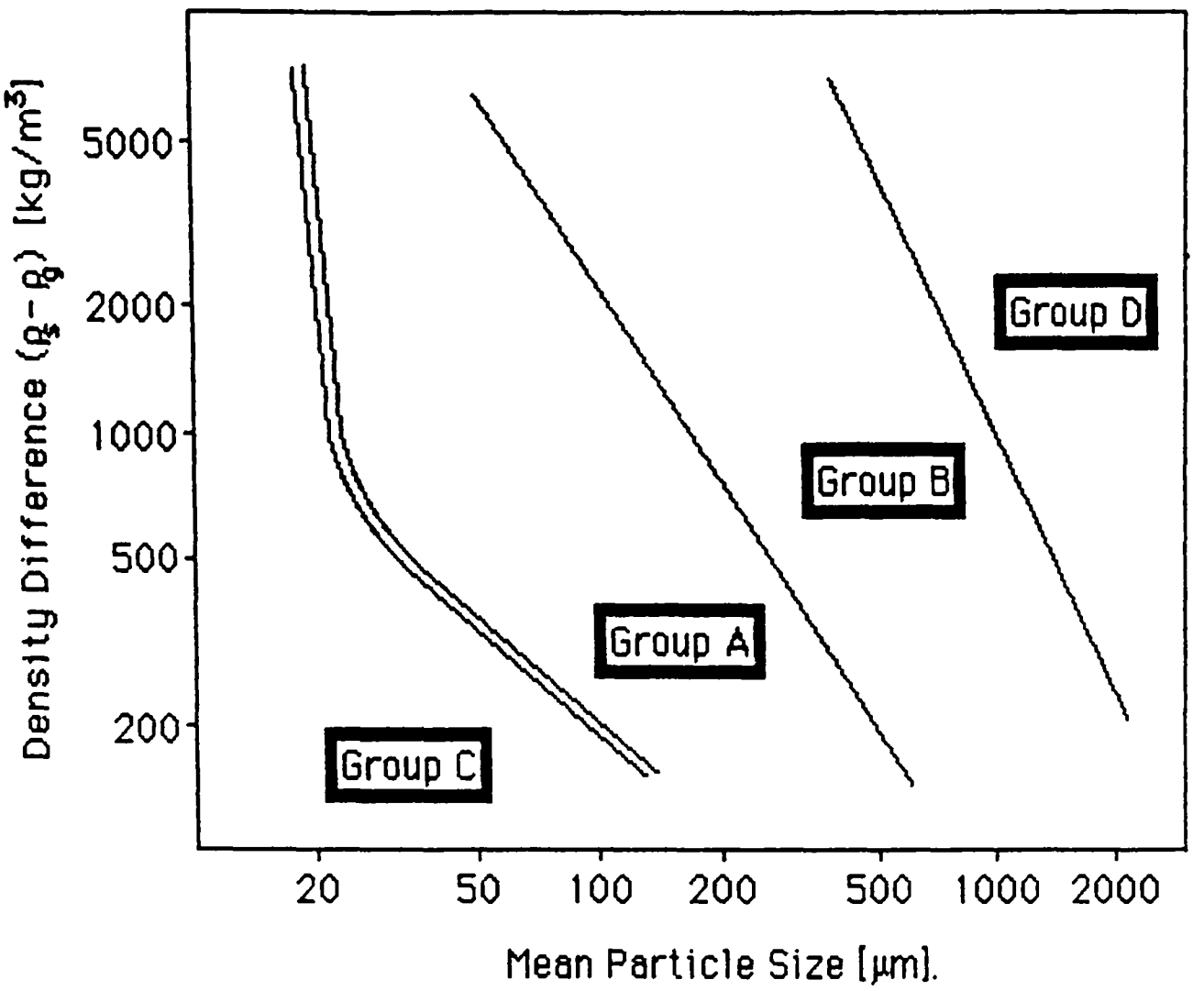

Group A: Small mean size and/or low particle density.
Bed expands considerably before bubbling commences.
Bed collapses slowly when the gas supply is cut off.

Group B: Bubbles form at or slightly above the minimum fluidisation velocity.
Bed expansion is small.
Bed collapses rapidly when the gas supply is cut off.

Group C: Cohesive powders.
Normal fluidisation is difficult.

Group D: Large mean size and/or very high particle density.
Bubble rise is slower than the interstitial gas velocity.

Figure 2.3.1 Geldart's powder classification diagram for fluidisation by air (ambient conditions).

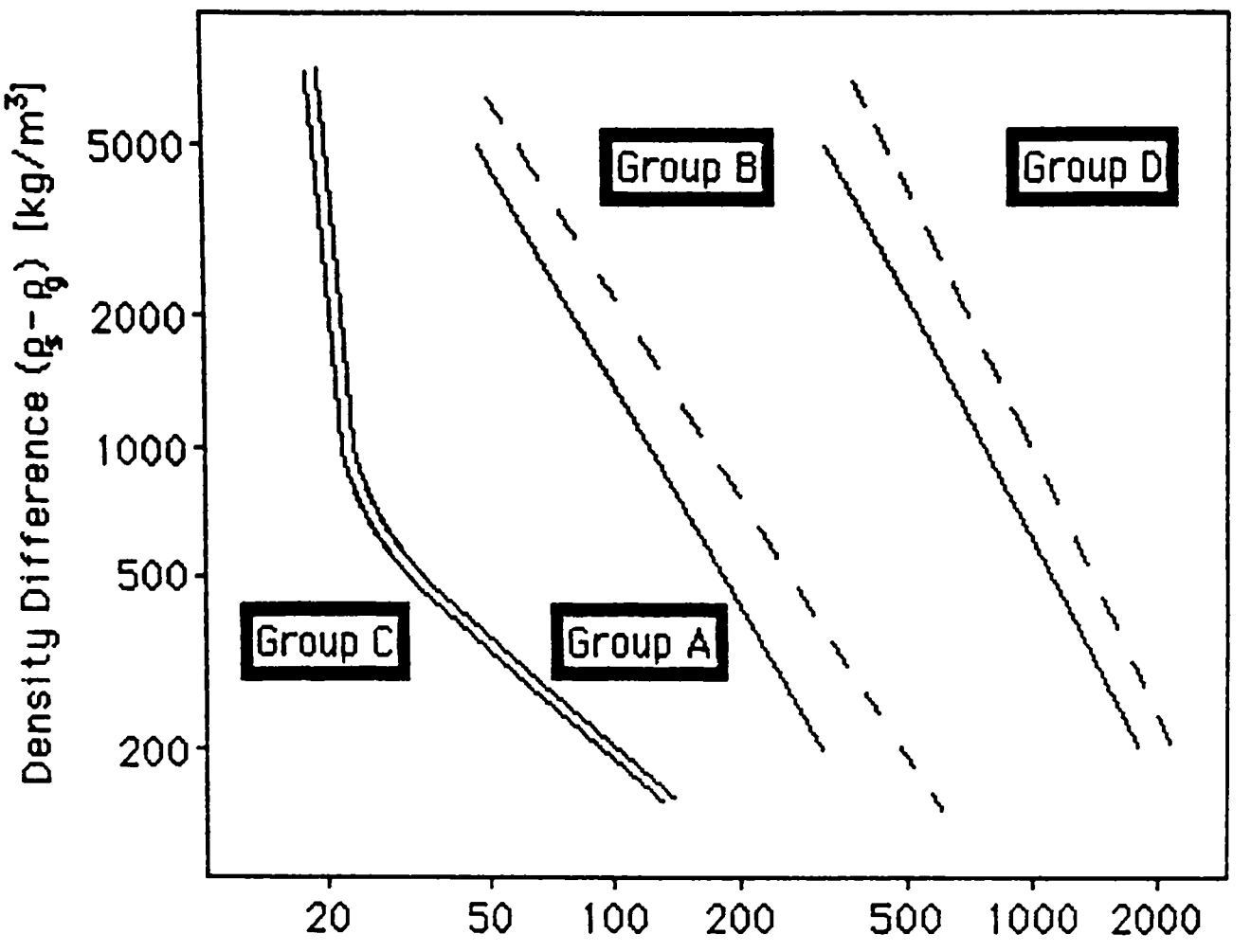

Group A: No slugging.
Group B: Weak asymmetric slugs (dunes).
Group C: The same as Geldart.
Group D: Strong Axisymmetric slugs.

Key:
——— Dixon's boundaries.
– — – Geldart's boundaries.

Figure 2.3.2 Dixon's slugging diagram for a 53mm bore pipeline.

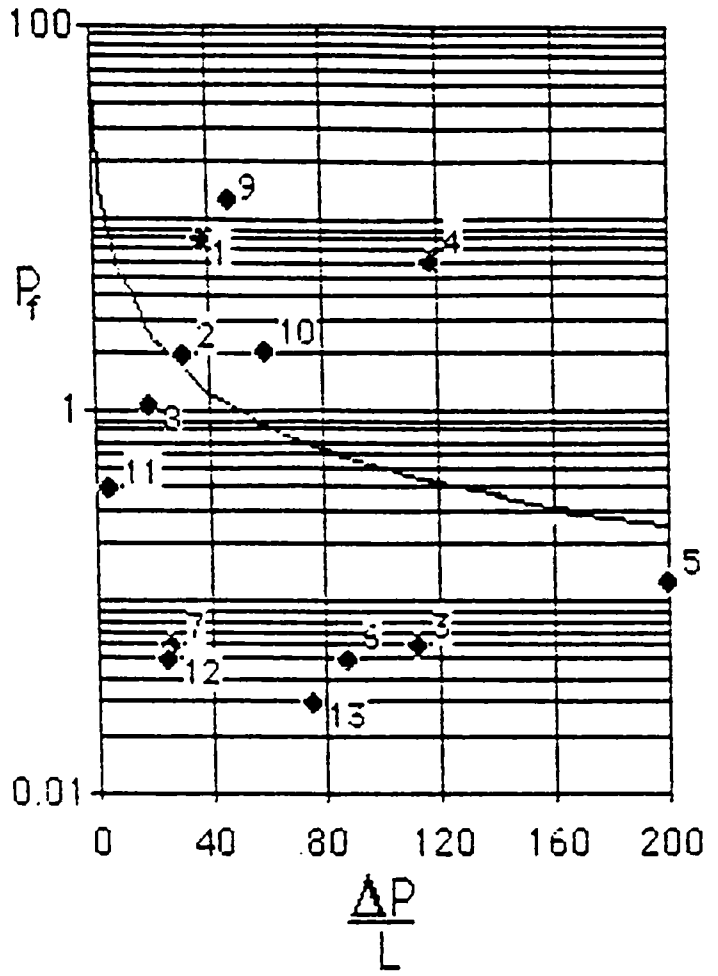

Boundary is a line of constant minimum fluidisation velocity equal to 50 mm/s.

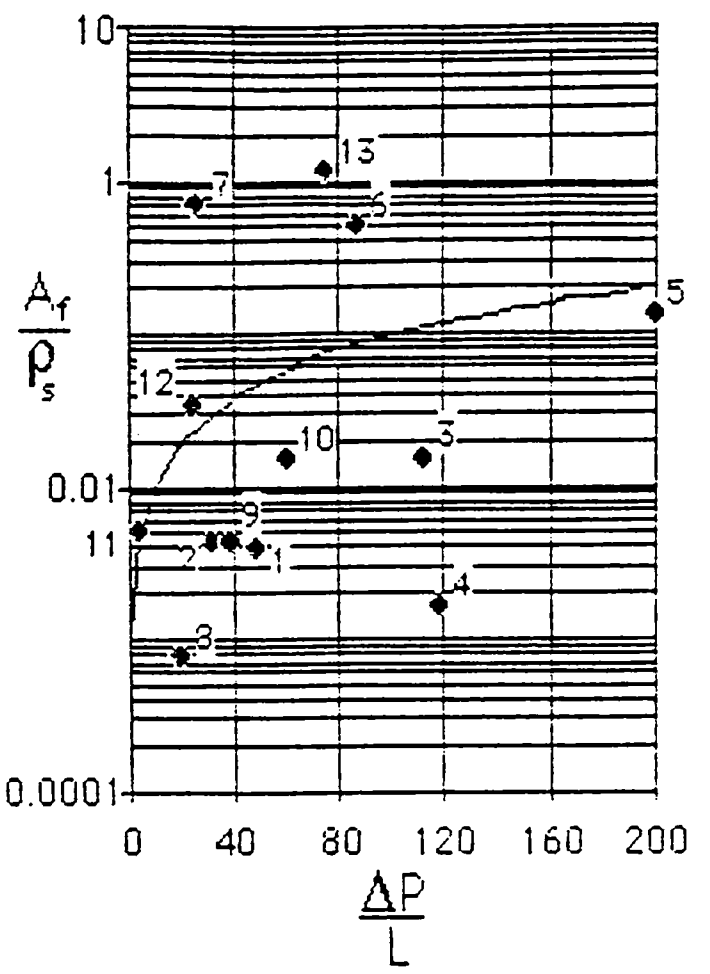

Boundary is a line of constant time / particle density equal to 0.001 s m^3/kg.

$\frac{\Delta P}{L}$ = Pressure drop per unit length [mbar/m].

P_f = Permeability factor [m^2/bar s].

$\frac{A_f}{\rho_s}$ = De-aeration factor / particle density [mbar s m^2/kg].

Materials:

1. Mustard seed.
2. Polyethylene Powder.
3. Slate dust.
4. 1000 µm sand.
5. Zircon sand.
6. Cement.
7. Pulverised coal.
8. PFA (grits).
9. Polyethylene pellets.
10. Granulated sugar.
11. Pearlite.
12. Flour.
13. PFA.

Figure 2.3.3 Mainwaring's classification for bulk materials.

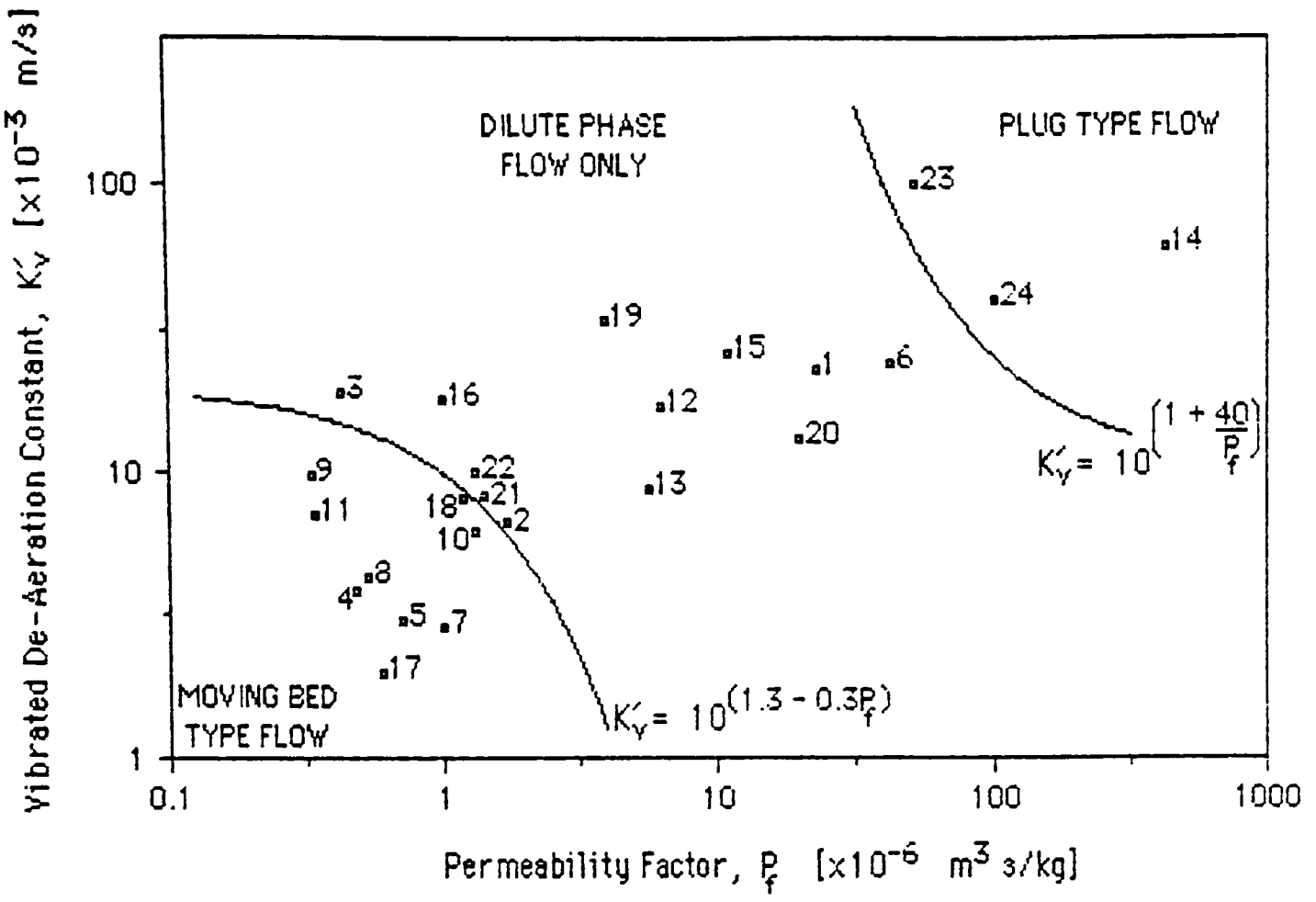

Boundaries separate bulk materials capable of being conveyed with a superficial gas velocity at inlet below 8 m/s (the dilute phase flow only materials must be conveyed at velocities greater than 8 m/s).

The equations for the boundaries were calculated as part of this thesis.

Key :

1	Agricultural Catalyst (ICI).	13	Pearlite.
2	Agricultural Catalyst (degraded).	14	Polyethylene Pellets (BP Rigidex).
3	Alumina.	15	Potassium Chloride.
4	Barytes.	16	Potassium Sulphate.
5	Cement (Ordinary Portland).	17	Pulverised Fuel Ash (PFA).
6	Coal (as supplied).	18	PVC Powder.
7	Coal (degraded).	19	Silica Sand.
8	Coal (pulverised fuel).	20	Granulated Sugar (as supplied).
9	Copper Ore.	21	Granulated Sugar (degraded).
10	Flour (RHM Democrat).	22	Zircon Sand.
11	Iron Powder.	23	Coarse Sand.
12	Magnesium Sulphate.	24	Mustard Seed.

Figure 2.3.4 Jones' bulk material classification.

Both workers use the same technique to measure permeability, which is illustrated in figure 2.3.5. The definitions used for de-aeration differ due to the nature of the bulk materials tested. Materials that exhibit non-suspension plug flow can have very rapid rates of fluidised bed height decay. Thus Mainwaring measured the decay of gas pressure in the fluidised bed from the time when the fluidising gas supply was switched off. Materials exhibiting non-suspension moving-bed flow can have bed height decay times measured in hours, thus Jones was able to measure this parameter successfully. Since the properties of permeability and de-aeration are those of the bulk material and are a function of: the particle properties; particle-particle interactions; and particle-gas interactions, these classifications have been taken as the indicators of the physical parameters which influence the flow of bulk materials in pipelines.

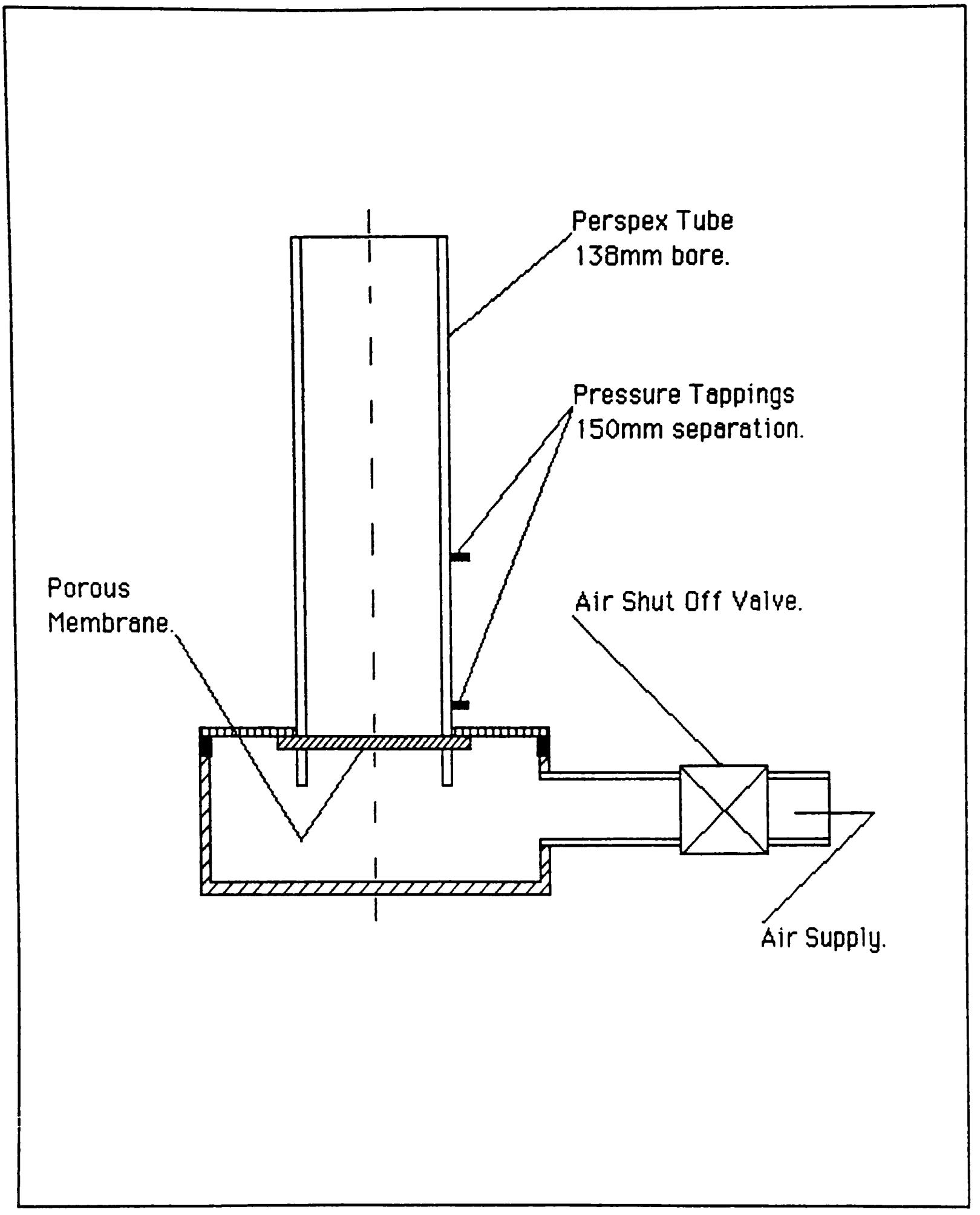

Figure 2.3.5 Diagram of fluidisation test equipment for determining the permeability factor for bulk materials.

2.4 MATHEMATICAL MODELS

2.4.1 INTRODUCTION

This section reviews the variety of methods that have been used to analyse gas-solids flows in pipelines. These methods range from the statistical analysis of experimental data to the solution of the differential equations governing the flow of solid particles in a gas. A review of experimental approaches will highlight the techniques available and the parameters that have been identified as characterising the flow. Similarly, for the analytical approach, the modelling techniques used and the mathematical description of the physical phenomena can be assessed.

2.4.2 EXPERIMENTAL INVESTIGATIONS

Gas-solids flows are found in many industrial applications such as: cyclone separators; pneumatic transport systems; spray drying and cooling; as well as sandblasting. The majority of experimental investigations have been attempts to produce correlations that can be used in the design of such systems. For pneumatic conveying systems the most frequently employed analysis is to sub-divide the total pressure drop required to transport the gas-solids mixture at the specified rate into a number of components.

These pressure drop components would account for some of the following effects:

i. the friction force due to the gas;
ii. the friction force due to the solids (often separated into vertical and horizontal components);
iii. the influence of the bends in the pipeline.

This may be generalised into an equation of the form:

$$\Delta P_{total} = \Delta P_{gas} (1 + \alpha) \qquad 2.4.2.1$$

The total pressure drop can be measured experimentally. The gas only value can be determined by one of the well established single phase flow equations, such as Darcy's equation, or experimentally. The task undertaken by the experimenters was to find the function that could be used to express α. In terms of the current work this will help to identify the key physical phenomena associated with gas-solids flows in pipelines.

For fully developed flow, the following is a representative example of correlations produced for α.

Rose and Barnacle (1957):

$$\alpha = \frac{\pi}{8} \frac{f_s}{f_g} \sqrt{\frac{\rho_s}{\rho_g} \frac{\dot{m}_s}{\dot{m}_g}} \qquad 2.4.2.2a$$

The solids friction factor, f_s, and the gas friction factor, f_g, are specified as functions of the pipe Reynolds number, with an acceptable value of f_s being:

$$f_s = 0.026 Re^{-0.85} + 0.0034 Re^{-0.6} \qquad 2.4.2.2b$$
$$for\ 1x10^4 < Re < 5x10^4$$

Richardson and McLeman (1960):

$$\alpha = \frac{k\ \dot{m}_s}{u_s^2\ u_{st}} \qquad 2.4.2.3$$

$$k = 3375 - 22148 D \qquad \left[\frac{m^3}{kg\,s^2}\right]$$

where $\dot{m}_s$ is the solids mass flow rate, u_s is solids velocity, u_{st} is the single particle terminal velocity, and k is a factor that depends upon the pipe diameter, D.

Michaelides (1987):

$$\alpha = \beta \frac{\dot{m}_s}{\dot{m}_g} \frac{\sqrt{Dg}}{u_g} \frac{1}{f_g} \qquad 2.4.2.4a$$

$$\beta = 2\left(\frac{1-\xi}{1+\xi}\right) \qquad 2.4.2.4b$$

$$\xi = \frac{\text{Axial velocity just after a collision with the wall}}{\text{Axial velocity just before the next collision}} \qquad 2.4.2.4c$$

Michaelides shows ξ to be material dependent but assumes a value from the range calculated which produces the best correlation for a range of data.

$$0.9 < \xi < 0.98 \qquad 2.4.2.4d$$

$$0.1 < \beta < 0.02 \qquad 2.4.2.4e$$

Unfortunately, Michaelides calculates 2β and uses this value instead of β in equation 2.4.2.4a! Fortunately Michaelides and Roy (1987) quote the same equation and use a value of $\beta = 0.076$ which lies within the allowable range for β.

All the correlations noted refer only to systems exhibiting the suspension mode of gas-solids flow. For non-suspension flows the behaviour is extremely material dependent, and hence the lack of general correlations for these modes of flow. What the various correlations do indicate are that α depends upon:

i. solids loading ratio;
ii. the Reynolds number of the gas (often in terms of the gas friction factor);
iii. the inverse of the Froude number;
iv. a material dependent parameter.

It is the definition of this final parameter which yields the most confusing range of answers. In general it is dependent upon the mode of flow and the bulk material type which the author assumed. In the case of equation 2.4.2.4a the particles are assumed to bounce along the pipe, exchanging momentum with the pipe wall and the conveying gas.

Thus far only fully-developed flow in a horizontal pipe has been considered. Common practice in single phase flow analysis is to replace all other components in a pipeline with a length of horizontal pipe that would have the equivalent flow resistance. Finally the pressure drop calculation is then determined for the total horizontal equivalent length.

Rose and Duckworth (1969) recognised that a significant proportion of the pressure drop in a pneumatic conveying system occurred in regions where the flow was developing (after the solids feed point and after bends). The basic assumptions of their analysis were:

i. the conveying fluid was incompressible;
ii. the flow was steady ie no time dependence;
iii. the static pressure was the average pressure over a particular cross-section.

From this the developing flow pressure drop depended upon:

i. the solids loading ratio;
ii. the particle to pipe diameter ratio;
iii. the density ratio;
iv. the Froude number;
v. the inclination of the pipe.

From these investigations a number of phenomena are highlighted. This may be divided into two areas:

i. flow conditions;
ii. material properties.

The flow conditions identified are:

i. the Reynolds number = $\frac{\text{Inertia Force}}{\text{Viscous Force}}$

ii. the Froude number = $\frac{\text{Inertia Force}}{\text{Gravity Force}}$

iii. the solids loading ratio which is a measure of the solids concentration, by mass.

The final quantity may be more useful in analysis if it was the ratio of volumes, but it is used since it remains constant throughout the pipeline. The material properties identified are the particle size and density. As discussed previously these may only be suitable for suspension modes of flow (which is the mode employed in the majority of experimental investigations reported here).

2.4.3 MATHEMATICAL MODELS FOR MULTI-PHASE GAS-SOLIDS FLOW

2.4.3.1 INTRODUCTION

This section will review the analytical approaches used to describe gas-solids flow. In general these approaches can be assessed on the basis of four criteria:

i. coupling between the phases;
ii. the number of dimensions used;
iii. the general mathematical descriptions of the phases;
iv. the key physical phenomena that need to be modelled.

After discussing the implications of each of these criteria they will be used to assess two groups of mathematical models:

i. low solids concentration flows;
ii. high solids concentration flows.

This division is made for two reasons. Firstly, although the physical phenomena that occur are generally the same, their respective influences are very different. For example, particle-particle collisions are often

neglected in low solids concentration flows, whereas particles could be in almost continuous contact in high concentration flows. The second reason is due to the type of investigations made into these flows. Most of the models developed to assess gas-solids flow in pipelines have examined low solids concentration flows. Most high solids concentration investigations have examined the behaviour of fluidised beds. As noted in previous sections the fluidisation properties of a bulk material can be used to assess its likely conveying performance in a pneumatic conveying system.

2.4.3.2 CRITERIA FOR ANALYSING GAS-SOLIDS FLOW MODELS

The coupling between the phases describes how the phases interact with each other. Models that assume one-way coupling assume that the gas flow field controls the solids flow field, but that the presence of solids has no effect on the gas. Two-way coupling assumes that all the phases interact with each other. Two-way coupling is obviously what happens in the physical system, but Crowe (1982) states that the influence of the solid particles on the gas may be neglected if:

$$\frac{(1 - R_g)\ \rho_s}{R_g\ \rho_g} < 0.1 \qquad 2.4.3.2.1$$

ie the mass concentration of the solids is very low.

The flow of a gas-solids mixture in a pipeline is a three-dimensional transient flow. The types of models used to describe gas-solids flow range from this to one dimensional steady flow. Reducing the number of dimensions simplifies the analysis of the problem and the effort required to generate solutions. This simplification of the problem can only be justified by restricting the model to a certain mode of gas-solids flow. The phases (gas and solids) may be described in one of two ways, either:

i. continuous;
ii. discrete.

A material may be defined as a continuum if:

$$\rho = \lim_{V \to 0} \frac{m}{V} \qquad 2.4.3.2.2$$

ie the volume must contain sufficient mass so that the density is a stationary average. Reif (1965) states that a volume containing 10^4 gas molecules will ensure a variation of density less than 1%. At standard conditions ($P = 1x10^5$ Pa_{abs} and $T = 293K$) for air then this would be a cube with sides 0.07 μm long. For a bulk material with a mean particle size of 100 μm this would be a cube with sides 2mm long ($R_g = 0.35$), or 5mm long ($R_g = 0.95$). In order to consider a phase as a continuum then the minimum dimension of the flow domain must be less than the critical size for the cube. All models consider the gas to be continuum, the difference is seen in the model for the solid particles. In low solids concentration flows the bulk material is often considered as a series of discrete particles. In this case the trajectory of each particle is calculated separately. In the case of one-dimensional analysis this only has to be done once, but for multi-dimensional flows many trajectory calculations are required before stationary averages for solids concentration are achieved, Tsuji et al (1985).

The final criteria for judging a model are the physical phenomena that are modelled. This depends upon the analysis of the mode of flow and the simplifying assumptions made. Some of these assumptions are more restrictive than others.

2.4.3.3 LOW SOLIDS CONCENTRATION FLOWS

Most mathematical models for gas-solids flow in pipelines fall into this category. The models are developed from an analysis of the suspension mode of flow.

The most simple approach is the single fluid analysis, exemplified by Michaelides (1984), where Navier-Stokes partial differential equations were solved for the one-dimensional steady flow. The influence of the solid particles is accounted for via the mixture density:

$$\rho_{mixture} = R_g \rho_g + (1 - R_g) \rho_s \qquad 2.4.3.3.1$$

ie the flow is treated as that of a dense gas. In order to reduce the problem to a one-dimensional case empirical correlations for the distribution of solids concentration were employed. This type of approach is very limited, since it takes little account of the physical phenomena that occur in the flow.

Tsuji, Oshima and Morikawa (1985) use a one-way coupling model to analyse gas-solids flow in a horizontal pipeline. They state that although this is not the actual case, the differences are only small for low concentration flows. Their model treats the bulk material in a discrete manner. Particles are released from slightly different locations and their trajectories calculated in three dimensions. The key physical phenomena modelled are the aerodynamic forces on the particle and the particle-wall collisions. The impact angle between the particle and the wall is modified by an abnormal bouncing model. This is required in order to produce realistic results. The adjustment of the parameters for the abnormal bouncing model is made to achieve good results. The model is compared with experimental data by considering the solids friction factor as a function of the Froude number, as proposed by Welschof (1962):

$$\lambda_s = \frac{\Delta P_S}{\Delta x} \frac{D}{(1-R_g)\rho_s \frac{1}{2} u_s^2} = c_1 D \qquad 2.4.3.3.2$$

$$Fr = \frac{u_s}{\sqrt{gD}} = c_2 D^{-\frac{1}{2}} \qquad 2.4.3.3.3$$

$$\lambda_s = c_1 c_2^2 Fr^{-2} \qquad 2.4.3.3.4$$

The functions c_1 and c_2 are dependent upon the mode of flow. Figure 2.4.3.1 plots the relationship (with $c_1 = c_2 = 1$) together with the range of experimental values shown by Tsuji.

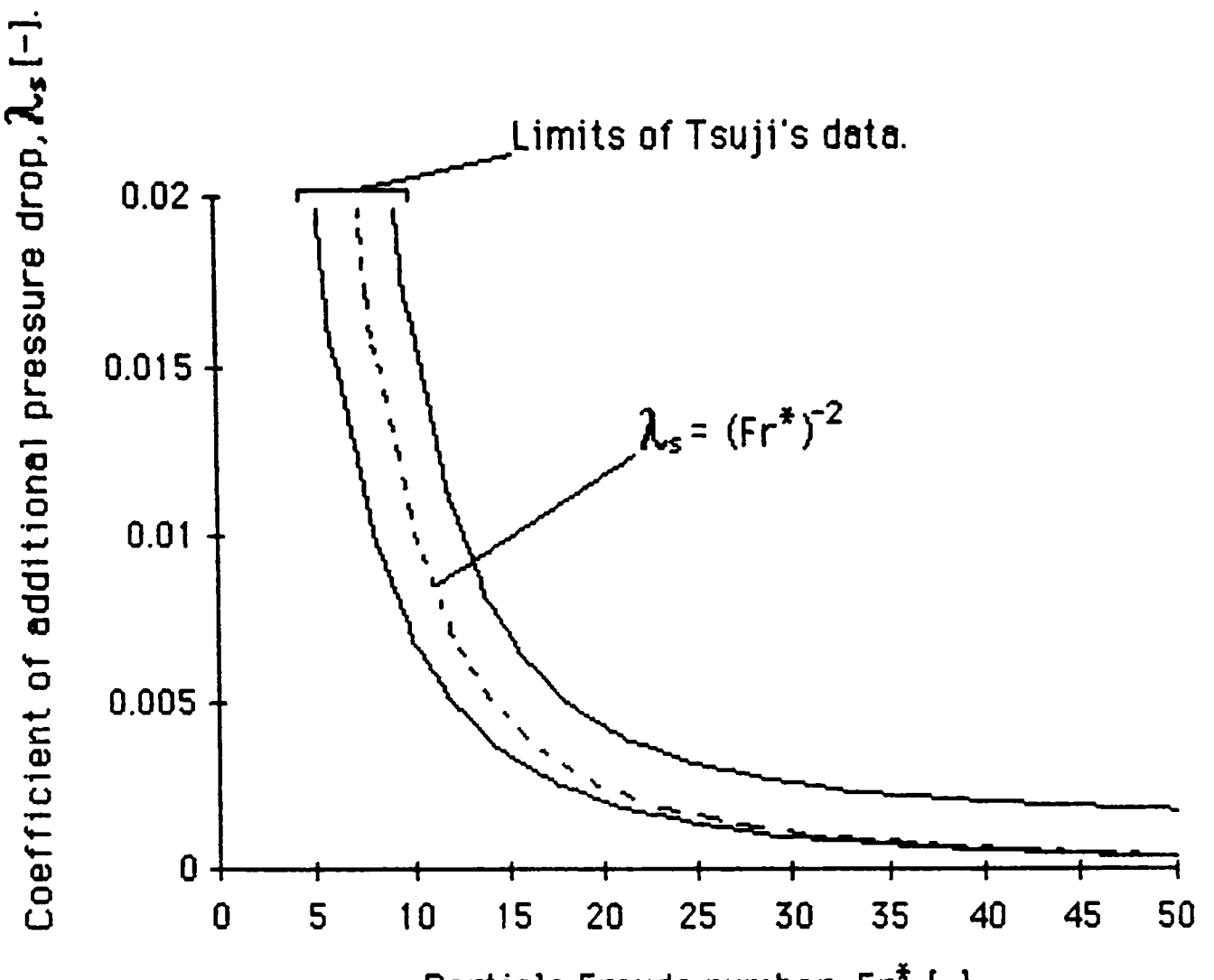

$$Fr^* = \frac{U_s}{\sqrt{gD}}$$

$$\lambda_s = \frac{\Delta P_s}{L} \Big/ \frac{1}{D} R_s \rho_s \frac{1}{2} U_s^2$$

Figure 2.4.3.1 The relationship between particle pressure drop and Froude number.

Since the curve $\lambda_s = Fr^{-2}$ fits the data, the only information provided is that the particles have only a small influence on the flow, which justifies the one-way coupling assumption and nothing else.

The majority of mathematical models employ two-way coupling. All the models considered subsequently use this assumption. The major difference between these models is whether they describe the solids phase as a continuum, or as discrete particles. Each of these groups may be sub-divided according to the number of dimensions considered.

The multi-phase gas-solids flow can be reduced to a single phase calculation by considering the solid particles to be a source of mass, momentum and energy for the gas. This was first proposed by Migdal and Agosta (1967). The gas and solids are considered to be continuum and the gas conservation equations for the flow of mass, momentum and energy are derived. The solid particles are assumed to occupy zero volume. This paper only notes that various analytical and empirical models are available to evaluate the solids source terms.

Crowe, Sharma and Stock (1977) took this approach to derive their Particle Source in Cell (PSI-Cell) model for gas-droplet flows. The difference being that the particles are considered discretely. An interactive procedure is developed where the gas flow field is calculated and then particle trajectories evaluated based upon this flow field. The particle source terms are calculated on the basis of these trajectories and the gas flow field is corrected to account for the new particle source terms.

A separate trajectory is calculated for each inlet condition (location of injection and velocity) and size of particle. The magnitude of a source term is modified by the number of particles that would follow this trajectory. Only the aerodynamic and gravitational forces on the particle are considered. Particle-wall interactions are not included, though the model does not preclude this. A model for the turbulence is included, which is a direct application of a single phase flow model. The lack of particle-wall interaction and the influence of particles on turbulence mean that this model cannot be applied directly to a pneumatic conveying system without modification.

Modifications of the PSI-Cell model have been used by several authors to describe gas-solids flow in pipelines at concentrations similar to those in suspension flow pneumatic conveying systems. Sharma and Crowe

(1978) developed a one-dimensional form of the PSI-Cell model. Particle-particle collisions were neglected since only low solids concentrations were considered. In addition, no model for particle to wall collisions was implemented. This approach was used to model a venturi metering device with solids loading ratios of up to two. Woodcock and Mwabe (1984) and Mason, Yenetchi and Woodcock (1990) describe the adaptation of this technique to suspension flow pneumatic conveying systems. Models for particle-wall interactions and the effect of pipeline geometry (bends) are implemented. Though these refinements to the basic mathematical description are based largely upon empirical work the results have predicted the performance of pneumatic conveying systems with reasonable accuracy. In this case the one-dimensional approach serves to reduce the complexity of the problem and the computer time required to generate a solution.

The work of Tsuji, Oshima and Morikawa (1985) was developed by Tsuji et al (1987). The model employed originally was simplified to a two-dimensional channel. The PSI-Cell model was used to take account of two-way coupling effects. The abnormal bouncing model used to describe the particle-wall interactions was modified (mainly to compensate for the reduction in the dimensions). Though this produced good agreement with experimental data, some of this could be attributed to *tuning* the parameters of the bouncing model. In two papers Tsuji, Shen and Morikawa (1989a and 1989b) replaced the abnormal bouncing model with an irregular particle model. Thus the change in particle-wall interactions was related to a physical property of the particle. The results of the simulation show a similar performance to their abnormal bouncing model. This is probably one of the most sophisticated models for particle-wall interactions. It is based upon physical quantities that can be measured relatively easily, but does rely upon estimating the orientation of the particle just before each collision.

An alternative to this approach is to consider the flow as a mixture of inter-dispersed continua. Soo (1965) defined a multi-phase system in terms of dynamic phases. For example, in the case of a particulate suspension with a distribution in particle size but of similar particle material, as the suspension is accelerated, particles of a given size range will be similarly accelerated, thus constituting a dynamic phase. Some averaging procedures are needed in formulating the conservation equations. Averaging of the conservation equations was first suggested by Birkhoff (1964). Spalding (1980) derives the volume-averaged

conservation equations for multi-phase, multi-dimensional flow. The successful application of this technique depends upon the mathematical models used to describe the physical phenomena that occur in gas-solids flow.

Di Giacinto, Sobetta and Piva (1982) analyse low solids concentration flows using similar concepts. In the momentum conservation equation the pressure and viscous terms are neglected since these are attributed to particle-particle interactions which are considered to be negligible. The aerodynamic force on the particles and the relationship between the volumetric concentration of the phases are the only two-way coupling effects considered.

It must be noted that Spalding (1980) uses the concept of a *shared pressure*, ie one pressure for all the phases. Many formulations use separate pressures for each phase. Spalding states: "There are some cases in which this [different pressures] is indeed desirable but the shared-pressure presumption is correct for most practical circumstances.". The treatment of the pressure term is discussed in more detail when high concentration flows are considered. Using Spalding's procedure Mason, Markatos and Reed (1987) developed a model to describe the developing flow region in the pipeline of a pneumatic conveying system using suspension flow. In this analysis the main gas-solids interaction was considered to be the aerodynamic force on the particles. The particle-wall interaction was considered to be of the same magnitude as the gas-wall interaction force. The influence of turbulence was noted. Since there is no general formulation for turbulence in multi-phase flows (particles are known to influence the level of turbulence, Boothroyd (1966) and Hishida, Takeroto and Maeda (1987)), a simple model relating to the apparent viscosity due to turbulence effects to a multiple of the fluid viscosity was employed. The lack of experimental investigations to quantity the relationship between particles and the gas turbulence results in the use of such arbitrary models. The constant tends to mask the deficiencies in other areas of the flow model. The benefit of such an approach is that some account is taken of the turbulence phenomena, but effort is not expended in solving equations that are only applicable to single-phase flow.

2.4.3.4 HIGH SOLIDS CONCENTRATION FLOWS

The majority of mathematical models for high solids concentration flows have been related to fluidised beds. Of these investigations most have examined liquid-solids beds. Among others, Foscolo and Gibilaro (1987), note the difference between liquid-solids and gas-solids fluidised beds as a stable homogeneous bed and an unstable bubbling bed respectively. Geldart (1973) observed stable fluidised beds when fine particles were fluidised by air (group A materials in Geldart's classification). Thus the results from liquid-solids beds can be applied to the flow of certain bulk materials. The problem of extending models for low solids concentrations to those for high solids concentrations is a matter of modelling the particle-particle interactions. Two modes of flow can be identified:

i. moving-bed flow;
ii. plug flow.

The flow patterns for each of these are very different. Bulk materials that have a moving-bed mode of flow can be classified as Geldart group A materials. Thus the investigation of relationships for fluidised beds is relevant to this type of material.

The pressure term in the solids phase momentum equation is often termed the particle pressure. Markatos (1986) considered an intergranular stress where the particle pressure comprises two components, the gas pressure and the intergranular stress. The intergranular stress is:

$$\tau_s = k\,(R_s - R_{s,critial})^n \qquad R_s > R_{s,critical}$$
$$\tau_s = 0 \qquad R_s < R_{s,critical} \qquad \text{2.4.3.4.1}$$

where k is a constant and n = 1, ie the particle pressure is due to particle-particle interactions. Foscolo and Gibilaro (1987) review a number of such approaches and conclude that this does not fully explain the particle pressure term since it does not predict a stable gas-solids fluidised bed for Geldart group A materials. They conclude that a fluid dynamic influence is also important. This is expressed through the fluid-solids interaction force, which is expressed as the force on a single particle modified by a function of the solids concentration.

The method of relating the single particle force to the force on a particle within a fluidised bed was developed by Richardson and Zaki (1954). They derived a relationship for the fluid velocity in terms of a function of the fluid concentration and the single particle terminal velocity in the fluid. The former was derived from experiment while the latter can be derived from theoretical considerations. This technique provides a link between the single particle analysis and the actual phenomena via an empirical correlation. Rowe (1961), Foscolo and Gibilaro (1984), and Gidaspow (1986) have all employed this technique with different functions of solids concentration depending upon the data used for correlation. It must be noted that the term voidage is most often used in these investigations. Voidage is the ratio of the gas volume to the total volume ie the gas concentration, or gas volume fraction.

A different approach is employed by Zuber (1963). The equation of motion for a single particle is formulated. The viscosity used in this equation is the apparent viscosity. This is the viscosity of the fluid *seen* by the particle as a result of the distortion of the fluid by neighbouring particles. Thus the influence of solids concentration is accounted for by a relationship for the apparent viscosity in terms of the fluid viscosity and a function of solids concentration. This approach is common in the analysis of rheological suspensions (liquid-solids). The result is similar to that from fluidised bed investigations ie a quantity is modified by a function of the solids concentration before being used in the relevant equation.

2.5 SUMMARY

This chapter has reviewed the modes of gas-solids flow that have been considered in pneumatic conveying systems. The bulk properties that can be used to classify a bulk material in terms of its possible modes of flow have been identified. These bulk properties indicate the key physical phenomena for each of these modes of flow.

The approaches used to analyse gas-solids flow in pipelines have been assessed. Analysis of the empirical correlations derived provides a useful indication of the variables that should be investigated and their relative importance. A review of mathematical models has shown the variety of methods that have been used to analyse gas-solids flow. Most investigators have concentrated on the suspension mode of flow. An extension of these approaches is indicated by work analysing fluidised beds.

THE MATHEMATICAL MODEL

3.1 INTRODUCTION

This chapter presents the general mathematical model that forms the basis of those models subsequently developed to describe the flow under consideration. This flow is the confined flow of a gas-solids mixture. This type of flow is multi-phase, multi-dimensional, and transient in nature. In this context a phase is any component of the flow mixture with a motion relative to the other components of the mixture. Two phases have been considered, the gas and the solid particles. More phases may be considered if say the solid particles vary in size, where each phase could represent a group of particles of a particular mean size.

The multi-dimensional nature of the flow is found in the variations of concentration of the solid particles both axially and radially within the pipeline. As noted in the previous chapter these variations are dependent upon the mode of flow achieved within the pipeline (suspension, moving bed, or plug flow). All the modes of flows identified are transient in nature. Though the overall pressure drop necessary to maintain the flow is substantially steady, the concentration of solid particles at a point in the pipeline can vary significantly with time.

3.2 THE CONSERVATION EQUATIONS

A multi-phase flow is one which requires for its characterisation more than one set of velocities, temperatures, masses per unit volume etc, at each location in the calculation domain. This implies that more than one phase can exist at the same location at the same time, Spalding (1980). This is a convenient concept, and it rests on the ideas of time and space averaging. Thus for any small volume of space, at any particular time:

$$V_{cv} = \sum_{i=1}^{i=n} V_i$$

$$R_i = \frac{V_i}{V_{cv}} \qquad 3.2.1$$

$$\sum_{i=1}^{i=n} R_i = 1$$

Equation 3.2.1 states that the sum of the individual volumes of each phase in the total volume is equal to the total volume considered. The mass flow rate of a phase through a surface within the domain at any time is:

$$\dot{m}_i = R_i A \rho_i u_i \qquad 3.2.2$$

This approach considers each phase as a continuum in the domain and the phases share the space and may interpenetrate as they move within the domain. The conservation equations will be developed for one-dimensional steady flow by considering the flow through a control volume shown in figure 3.2.1. This simplified case is considered so that the concept may be presented with clarity.

3.2.1 THE CONSERVATION OF MASS

Considering the control volume with centre at P.

$$\rho_{i,w} R_{i,w} A_w u_{i,w} = \rho_{i,e} R_{i,e} A_e u_{i,e} - S_{R_i} \qquad 3.2.1.1$$

ie the mass flow rate into the control volume is the same as the mass flow rate out of the control volume for the ith phase plus any changes that occur inside the control volume. This source of mass may result from an evaporating liquid, or a combustion process. For the type of control volume employed all scalar quantities, such as pressure, volume fraction, and temperature are calculated at the centres of the control volumes. Vector quantities (velocity components) are calculated at the faces of the control volumes.

This staggered grid approach for the velocity components was first used by Harlow and Welch (1965). The advantage of this method is that the pressure difference between two adjacent control volumes becomes the driving force for the velocity component at their joint face.

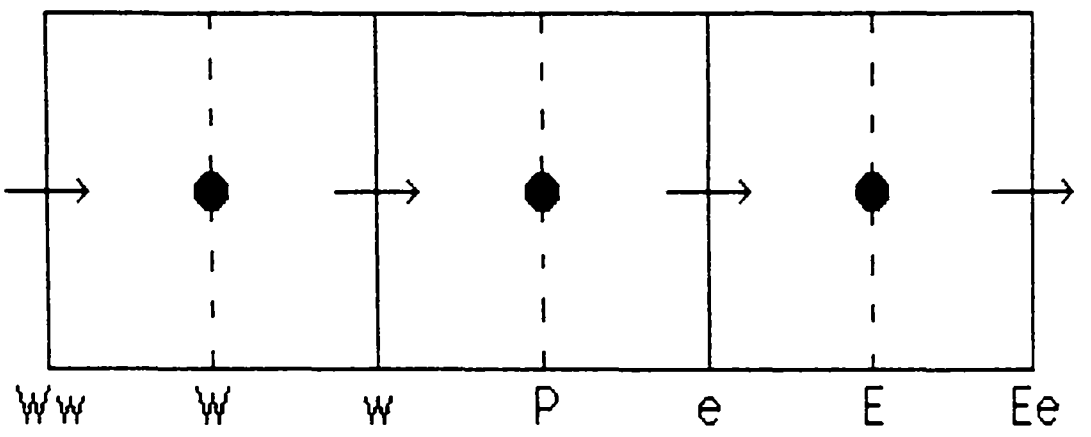

Figure 3.2.1 One-dimensional domain for the derivation of the conservation equations.

Some method for averaging is required to obtain the values of the scalar quantities at the face of the control volume. Patankar (1980), discusses a number of options available, in this case the upwind scheme will be illustrated, where:

$$\begin{aligned} \phi_{i,e} &= \phi_{i,P} \qquad u_{i,e} > 0 \\ \phi_{i,e} &= \phi_{i,E} \qquad u_{i,e} < 0 \\ ie \quad \phi_{i,e} u_{i,e} &= \phi_{i,P} [\![u_{i,e}, 0]\!] - \phi_{i,E} [\![-u_{i,e}, 0]\!] \end{aligned} \qquad 3.2.1.2$$

where $[\![A,B]\!]$ means the greater of A and B. This averaging scheme can introduce errors into the solution of the problem, often known as *false diffusion*. This results from the assumption that the flow is locally one-dimensional when in fact it is multi-dimensional. Patel et al (1987) evaluate a number of averaging schemes and conclude that although the upwind scheme has deficiencies, for high shear flows its accuracy is only marginally worse than higher order schemes. In addition it is more stable, easier to implement, and frequently, changes in the physical model (such as for turbulence) far outweigh the *false diffusion* error.

Using equation 3.2.1.2 in 3.2.1.1 the conservation of mass principle can be expressed by:

$$\begin{aligned} a_P \rho_{i,P} R_{i,P} &= a_W \rho_{i,W} R_{i,W} + a_E \rho_{i,E} R_{i,E} + S_{R_i} \\ a_W &= A_w [\![u_{i,w}, 0]\!] \\ a_E &= A_e [\![-u_{i,e}, 0]\!] \\ a_P &= A_w [\![-u_{i,w}, 0]\!] + A_e [\![u_{i,e}, 0]\!] \end{aligned} \qquad 3.2.1.3$$

3.2.2 THE CONSERVATION OF MOMENTUM

Considering the staggered control volume for u with its centre at e, and applying Newton's second law of motion:

> *The rate of increase of momentum of a body is proportional to the net force acting on the body, and takes place along the direction in which that force is applied.*

$$\dot{m}_{i,E}u_{i,E} - \dot{m}_{i,P}u_{i,P} = F_{i,E} - F_{i,P} + P_P A_P R_{i,P} - P_E A_E R_{i,E} + S_{u_i} \qquad 3.2.2.1$$

where the left hand side is the change of momentum and the right-hand-side is the net shear force due to the viscosity of the ith phase. S_{ui} is the sum of all the other forces on the ith phase which includes:

i. body forces, such as gravity;
ii. inter-phase friction forces;
iii. wall friction.

Applying the upwind difference scheme:

$$\begin{aligned}[\![\dot{m}_{i,E},0]\!]u_{i,e} - [\![-\dot{m}_{i,E},0]\!]u_{i,eE} - [\![\dot{m}_{i,P},0]\!]u_{i,w} - [\![-\dot{m}_{i,P},0]\!]u_{i,e} \\ = \mu_{i,E}R_{i,E}A_E\frac{u_{i,eE}-u_{i,e}}{\Delta x_{e,eE}} - \mu_{i,P}R_{i,P}A_P\frac{u_{i,e}-u_{i,w}}{\Delta x_{w,e}} \\ + P_P R_{i,P}A_P - P_E R_{i,E}A_E + S_{u_i}\end{aligned} \qquad 3.2.2.2$$

$$
\begin{aligned}
a_e u_{i,e} &= a_w u_{i,w} + a_{eE} u_{i,eE} + S_{Pressure} + S_{u_i} \\
a_w &= \frac{\mu_{i,P} R_{i,P} A_P}{\Delta x_{w,e}} + [\![\dot{m}_{i,P}, 0]\!] \\
a_{eE} &= \frac{\mu_{i,E} R_{i,E} A_E}{\Delta x_{e,eE}} + [\![-\dot{m}_{i,E}, 0]\!] \\
a_e &= \left\{ \frac{\mu_{i,P} R_{i,P} A_P}{\Delta x_{w,e}} + [\![-\dot{m}_{i,P}, 0]\!] \right\} + \\
&\qquad \left\{ \frac{\mu_{i,E} R_{i,E} A_E}{\Delta x_{e,eE}} + [\![\dot{m}_{i,E}, 0]\!] \right\}
\end{aligned}
\qquad 3.2.2.3
$$

The mass flow rates can be evaluated by:

$$
\begin{aligned}
\dot{m}_{i,P} &= \rho_{i,P} R_{i,P} A_P u_{i,P} \\
&= \rho_{i,P} R_{i,P} \frac{1}{2} (A_w u_{i,w} + A_e u_{i,e}) \\
\dot{m}_{i,E} &= \rho_{i,E} R_{i,E} A_E u_{i,E} \\
&= \rho_{i,E} R_{i,E} \frac{1}{2} (A_e u_{i,e} + A_{eE} u_{i,eE})
\end{aligned}
\qquad 3.2.2.4
$$

and the pressure source term by:

$$
\begin{aligned}
S_{Pressure} &= P_P R_{i,P} A_e - P_E R_{i,E} A_e + \\
&\qquad \left(\frac{P_P + P_E}{2} \right) (R_{i,E} - R_{i,P}) A_e
\end{aligned}
\qquad 3.2.2.5
$$

all other contributions to the momentum source term are problem dependent and will be discussed in the relevant chapters.

3.2.3 THE GENERAL CONSERVATION EQUATION

The previous discussion has shown how the conservation equations may be developed by consideration of the steady flow through a one-dimensional control volume. For a general quantity ϕ the conservation equation for the ith phase may be written in differential form as:

$$\frac{\partial(\rho_i R_i \phi_i)}{\partial t} + \nabla.(\rho_i R_i \vec{v}_i \phi_i) = \nabla.(\Gamma_\phi R_i \nabla(\phi_i)) + S_\phi \qquad 3.2.3.1$$

where the terms on the left-hand-side represent the transient variation, convection, and diffusion of the quantity ϕ. The source term $S_{\phi i}$ represents all the other phenomena that cannot be represented in this format.

Integration of equation 3.2.3.1 over a finite volume results in the general form of the conservation equation for the control volume, ie

$$\left\{ b_P + \sum b_{nb} + C_\phi \right\} \phi_{i,P} = \left\{ \sum a_{nb} \phi_{nb} \right\} + C_\phi V_\phi \qquad 3.2.3.2$$

where subscript nb represents a neighbour of p, in space and time. The (a) coefficient represents inflow terms and the (b) coefficient outflow terms. The source term has been linearised to acknowledge its dependence upon the value of ϕ in the control volume, ϕ_p.

Considering the conservation of momentum equation derived earlier, equation 3.2.2.4:

$$u_{i,e} = \frac{a_w u_{i,w} + a_{eE} u_{i,eE} + S_{u_i}}{b_w + b_{eE}} \qquad 3.2.3.3$$

note the subscript changes since the u-control volume is staggered.

$$a_w = \frac{(\mu_i R_i A)_P}{\Delta x_{w,e}} + [\![\dot{m}_{i,P}, 0]\!] \qquad 3.2.3.4$$

$$b_w = \frac{(\mu_i R_i A)_P}{\Delta x_{w,e}} + [\![-\dot{m}_{i,P}, 0]\!]$$

Thus the a's consist of an inflow convection and a diffusion contribution. The b's consist of an outflow convection and a diffusion contribution.

3.2.4 PROBLEM SPECIFIC RELATIONSHIPS

The general conservation equations that have been presented have to be solved in conjunction with observance of constraints on the values of the variables used. These relationships are the expression of physical laws, which:

i. describe the behaviour of a variable in terms of other auxiliary equations, such as the ideal gas equation:

$$\rho_g = \frac{P_g}{R\, T_g} \qquad 3.2.4.1$$

ii. describe the interactions between the phases and other problem specific source terms, which are discussed further in subsequent chapters;

In addition to these relationships a set of initial conditions and boundary conditions are also required.

The boundary conditions and problem specific source terms are specified by a value and the extent of the domain to which the particular phenomena applies. These source terms are taken as a linear function of ϕ_p, the value of the dependent variable at the centre of the control volume under consideration.

Source terms are specified by a linear expression of the form:

$$S_\phi = G(C_\phi + [\![S_P, 0]\!])(V_P - \phi_P) \qquad 3.2.4.2$$

$$\begin{aligned} S_P &= GC_P(V_P - P_P) \qquad V_P > P_P \\ S_P &= GRC_P(V_P - P_P) \qquad V_P < P_P \end{aligned} \qquad 3.2.4.3$$

Equations 3.2.4.3 represent the mass sources for inflow and outflow respectively. G is a multiplier (often geometric) C_ϕ and V_ϕ are the coefficient and value that are used to describe the required phenomena, or boundary condition. For example, in order to specify a gravitational force, a source term is required for the momentum conservation equations:

$$\begin{aligned} G &= \frac{1}{2}(R_{i,P}\rho_{i,P} + R_{i,E}\rho_{i,E})\, A_e\, \Delta x_{P,E} \\ C_\phi &= 1x10^{-10} \\ V_\phi &= 1x10^{10}\ 9.81\, ms^{-2} \\ S_\phi &= R_{i,e}\rho_{i,e}\Delta x_{P,E} 9.81\, ms^{-2} \end{aligned}$$

this is an example of a fixed flux source term. The practice of assigning a large (10^{10}), or small value (10^{-10}) to the coefficient and value is illustrated by Rosten and Spalding (1986). The purpose of this practice is make the source term the dominant value in the equation.

3.3 THE SOLUTION PROCEDURE

3.3.1 SOLVING THE CONSERVATION EQUATIONS

The next step in the process is to develop an algorithm to solve the conservation equations. For single phase flows Patankar and Spalding (1972) developed SIMPLE (Semi-Implicit Method for Pressure Linked Equations). The pressure linked equations are the conservation equations. Semi-Implicit refers to the solution method which is iterative.The following steps are taken in SIMPLE to solve the conservation equations:

i. guess the pressure field;

ii. solve the momentum equations to find the velocity field;
iii. calculate the errors in the mass conservation equation;
iv. use these errors to correct the pressure field;
v. and velocity field;
vi. solve the conservation equations for the other variables such as enthalpy and turbulence quantities;

vii. repeat until a converged solution is obtained.

SIMPLE worked well for a wide variety of problems, but in some cases such as the use of very small control volumes heavy under-relaxation was necessary. Relaxation in this case relates to the practice of altering the rate at which a variable is allowed to change during iterations to promote a converged solution. Thus, in stages (iv) and (v) of SIMPLE the pressure and velocity would only be changed by a small fraction of the correction value (heavy under relaxation). Allowing only a small rate of change then requires a much higher number of iterations to achieve the solution.

Patankar (1980) recognised that some improvement was necessary and devised SIMPLER (SIMPLE Revised). The problem with SIMPLE was traced to the guessed pressure field. SIMPLER was devised to avoid this by only calculating the pressure field from the velocity field.

Using the same numbering as for SIMPLE the algorithm for SIMPLER is:

i. guess the velocity field;

iia. solve the modified momentum equations (without the pressure term) to find the pseudovelocity field;
iib. use the pseudovelocity field in the calculation of the pressure field;
iic. solve the full momentum equations using the pressure field from iib to find the velocity field;
iii. calculate the errors in the mass conservation equation;
iv. **DO NOT** correct the pressure field;
v. correct the velocity field;
vi. solve the conservation equations for the other variables such as enthalpy and turbulence quantities;

vi. repeat until a converged solution is obtained.

This method works well and will produce a converged solution in fewer iterations. The drawback is that each iteration requires greater computational effort. The other half of the team that produced SIMPLE, also developed a solution to its problems. In SIMPLEST (SIMPLE ShorTened), Spalding traced the poor convergence when using small control volumes to the convection term of the momentum conservation equation. The conservation equation was modified so that its coefficients contained only the diffusion terms. The convection terms were added to the source term. This approach allows the SIMPLE algorithm to be used to solve the modified equations.

In order to solve for a multi-phase flow, methods such as SIMPLE need to be extended. The obvious approach would be to solve for each variable in each phase in turn, but in practice this results in very slow convergence.

3.3.2 THE INTER-PHASE SLIP ALGORITHM

IPSA is the method developed by Spalding to generalise SIMPLE from a single phase to a multi-phase algorithm. In order to improve the rate of convergence, advantage is taken of the fact that a change in the local value of the property of the ith phase will affect all the other phases in that locality. For example, consider a two phase flow where:

$$\phi_1 = \frac{\alpha_1 + \beta_1\phi_2}{\gamma_1}$$
$$\phi_2 = \frac{\alpha_2 + \beta_2\phi_1}{\gamma_2} \qquad 3.3.2.1$$

where α, β, and γ are coefficients that contain contributions of ϕ from neighbouring control volumes. For large values of β the convergence is slow, because the new value of ϕ_1 is approximately the current value of ϕ_2 and similarly $\phi_2 \approx \phi_1$. The partial elimination algorithm (PEA) attempts to solve this by removing the contribution of other ϕ's from the equation for ϕ_i:

$$\phi_1 = \frac{\alpha_1 + \dfrac{\beta_1\alpha_2}{\beta_2+\gamma_2}}{\gamma_1 + \beta_1\left(1 - \dfrac{\beta_2}{\beta_2+\gamma_2}\right)}$$
$$\phi_2 = \frac{\alpha_2 + \dfrac{\beta_2\alpha_1}{\beta_1+\gamma_1}}{\gamma_2 + \beta_2\left(1 - \dfrac{\beta_1}{\beta_1+\gamma_1}\right)} \qquad 3.3.2.2$$

This approach allows the value of ϕ to vary at a faster rate and hence improve the rate of convergence to a solution.

The main features of the Inter-Phase Slip Algorithm are:

i. The conservation equations are solved in the following order: enthalpy, volume fraction, velocity, pressure.

ii. The enthalpy equations are solved by use of the partial elimination algorithm, since the enthalpy of the phases are likely to be closely linked.

iii. The mass conservation equation is solved next, because the inter-phase mass transfer that forms the source term of each equation is closely connected with the enthalpy. For example, the source of gas from a burning particle is closely related to the enthalpy of the particle. The conservation equations for all but one of the phases are solved, and the volume fractions are determined. The remaining volume fraction can be calculated:

$$R_n = 1 - \sum_{i=1}^{i=n-1} R_i \qquad 3.3.2.3$$

Alternatively, all the conservation equations can be solved, and then corrected so that:

$$R_i = \frac{R_i}{\sum_{j=1}^{j=n} R_j} \qquad 3.3.3.3$$

The first method is more suited to flows where one of the phases has a significantly higher volume fraction. The phases with low volume fractions are solved for and that for the higher value calculated from equation 3.3.2.3. This avoids numerical problems were small errors in the high value can be of the same order as that for the low values of volume fraction.

iv. Using a guessed pressure field the momentum conservation equations are solved. Overall mass conservation is now not satisfied.

v. The volume fractions calculated from iii and the velocities from iv are used in the overall mass conservation equation to determine the mass error in each of the control volumes.

vi. Differentiating the overall mass conservation equation with respect to pressure leads to a pressure correction equation. From this the velocity corrections can be deduced. Applying these corrections will restore satisfaction of the overall mass conservation equation.

v. This process is iterative, and the cycle is repeated until the size of the errors in the conservation equation have been minimised ie a converged solution has been achieved.

3.4 SUMMARY

The previous sections have described the general mathematical model employed in this work. The control volume formulation of the conservation equations and the Inter-Phase Slip Algorithm (IPSA) to solve them have been implemented in the PHOENICS package, Rosten and Spalding (1986). This was the general model employed in this work. The mathematical models added to this general framework to describe phenomena specific to the flow of gas-solids mixtures in pipelines are described in subsequent chapters.

The PHOENICS package used in this work was run on a NORSK DATA ND-500 computer, which operates at 0.19 MFLOPS, Dongarra (1985), ie 230 times slower than a CRAY X-MP-1, and 16 times faster than an IBM PC AT with math coprocessor. The size of control volumes and time steps employed in this work were constrained by the requirement to produce solutions within a reasonable timeframe.

4 EXPERIMENTAL EQUIPMENT

4.1 INTRODUCTION

The pneumatic conveying system employed in the experimental phase of this project was an existing design. The system was designed by Hitt (1985). This reference provides a detailed description of the design philosophy and construction of this particular system. Mainwaring (1988), altered the system by changing the configuration of the pipeline and the data acquisition system. In the present work the system has been essentially unaltered. The only difference being the requirement for more detailed measurements of the flow. As noted previously most system design methods only require the overall pressure drop at a particular mass flow condition (ie the pressure at the inlet end of the pipeline minus that at the outlet end). In order to validate the models developed a more detailed pressure distribution is necessary. Thus a great deal of the available experimental data is of limited value, and hence the necessity for this test programme.

4.2 SYSTEM OVERVIEW

A positive pressure pneumatic conveying system is one in which the pressure at the inlet to the pipeline is greater than that at the outlet. This type of system may be considered to comprise of four elements:

i. a supply of compressed gas;
ii. a solids feed device;
iii. the pipeline;
iv. a disengaging device.

The system may operate on a continuous basis, or on a batch basis. The design philosophy adopted for this system may be summarised as follows:

i. the ability to operate over the widest possible range of flow conditions;
ii. of proportions such that only a small scale-up is required for comparison with industrial scale systems.

A schematic diagram of the system is shown in figure 4.2.1.

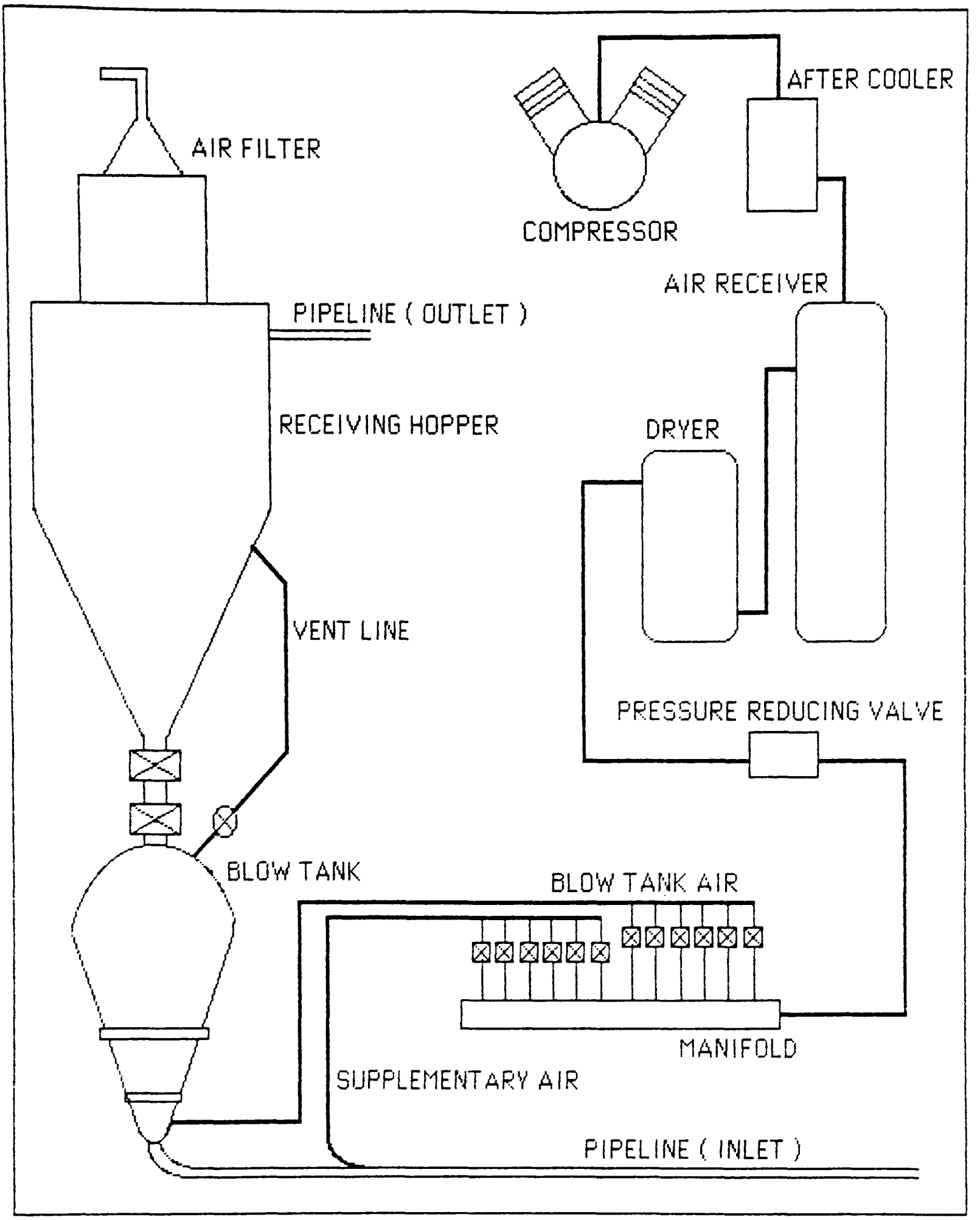

Figure 4.2.1. Schematic Diagram of Experimental Test System.

4.2.1 THE SUPPLY OF COMPRESSED GAS

The air mover was an oil free reciprocating compressor type Broomwade V200 DAF2, which can produce $0.097m^3s^{-1}$ free air delivery at 6.8 bar gauge.

The performance at free conditions equates to a superficial gas velocity at the outlet end of the pipeline of $42ms^{-1}$ (for a pipe bore of 54mm). This allowed the full range of flow conditions to be investigated. The compressed gas passes through an aftercooler and into an air receiver having a capacity of $0.87m^3$. Before being supplied to the system the air passes through a deliquescent air dryer Anon-1. Thus a large reservoir of pulsation-free dry gas at 6.8 bar gauge and essentially ambient temperature was available for the conveying of bulk particulate materials.

4.2.2 THE SOLIDS FEED DEVICE

The choice of solids feed device was restricted to a pressure vessel, or *blow tank*, due to the high pressure drops necessary to convey materials in certain non-suspension modes of flow. A possible alternative solids feed device is the high pressure rotary valve Anon-2, as shown in figure 4.2.2. Tests were conducted with such a valve as part of another study and reported by Reed et al (1988).

Figure 4.2.3 shows the alteration made to the test rig to accommodate this valve. The valve was able to operate with a high pressure drop across its rotor, thus allowing non-suspension modes of flow to be achieved within the pipeline. When operating under these conditions a large percentage of the air supplied to the pipeline leaked through the valve into the supply hopper above the valve.

The advantage of using such a valve is to permit continuous operation, as opposed to the batchwise operation of a single pressure vessel shown in figure 4.2.4. In this case the amount of material available in the supply hopper above the valve is the same as that used to charge the pressure vessel, thus no advantage exists with this test facility. The air leakage through the valve poses the problem of monitoring accurately, the actual amount of air passing into the pipeline.

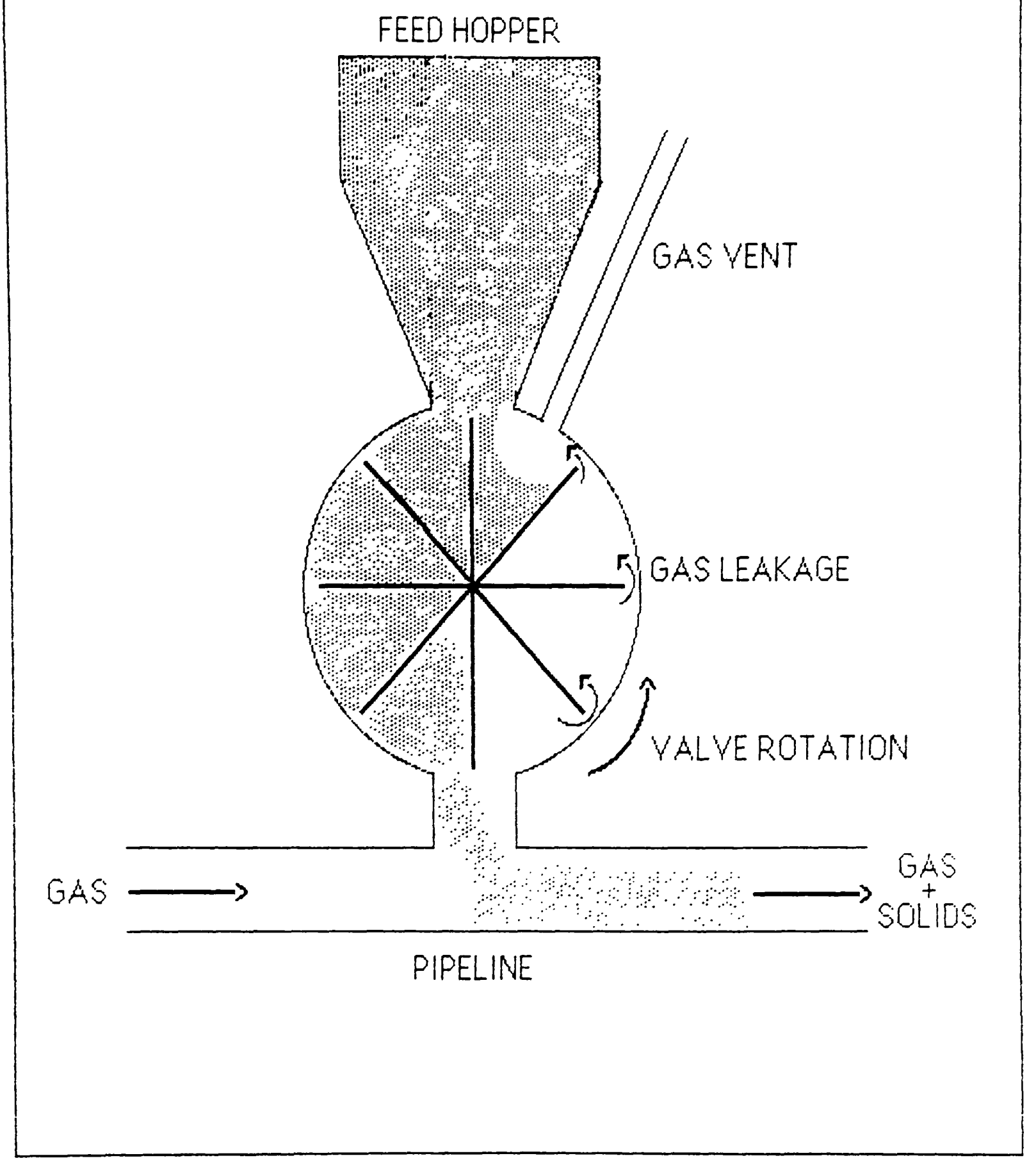

Figure 4.2.2. Schematic Diagram of a Rotary Valve.

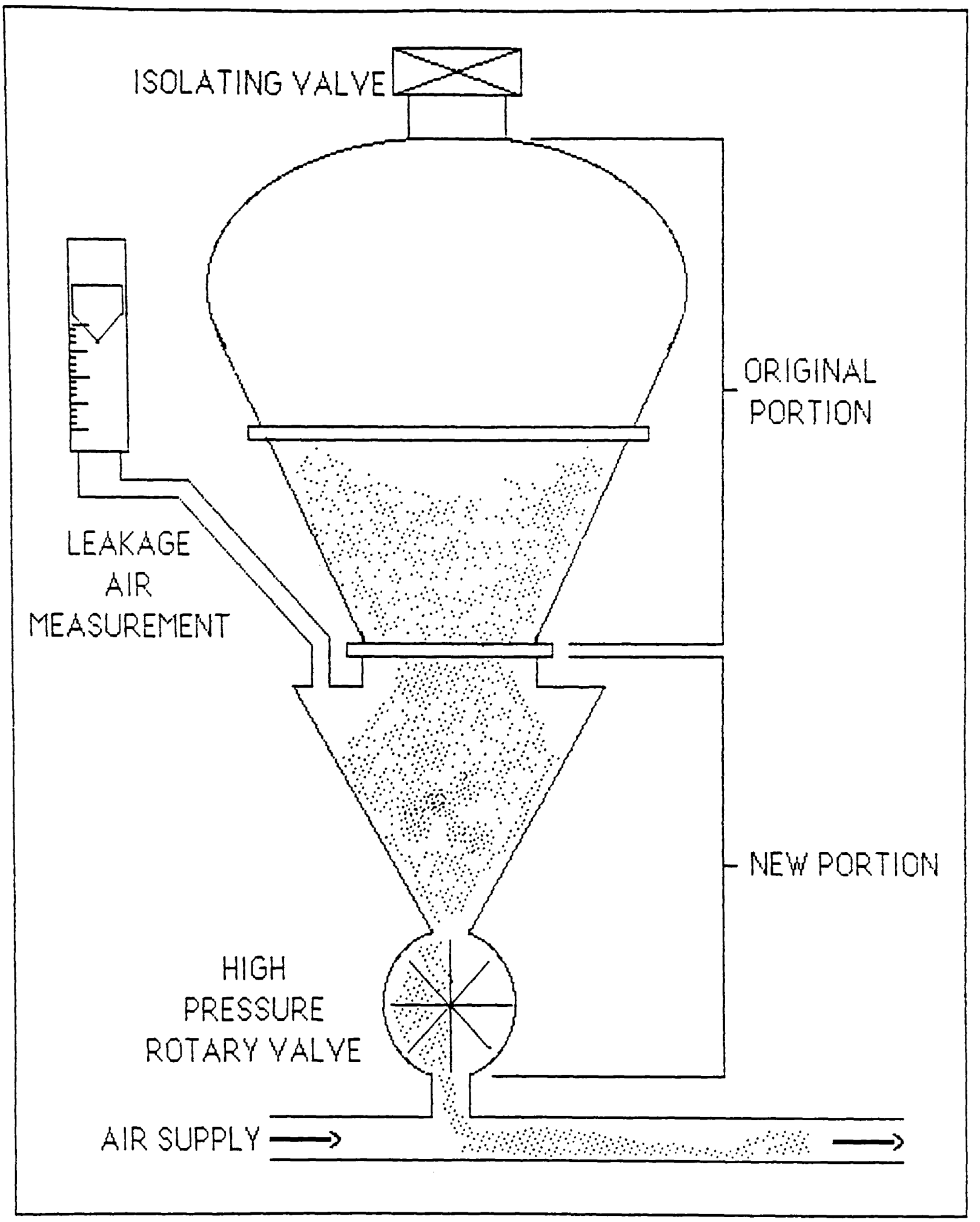

Figure 4.2.3. Modification to Convert the Solids Feeder From a Blow tank to a High Pressure Rotary Valve.

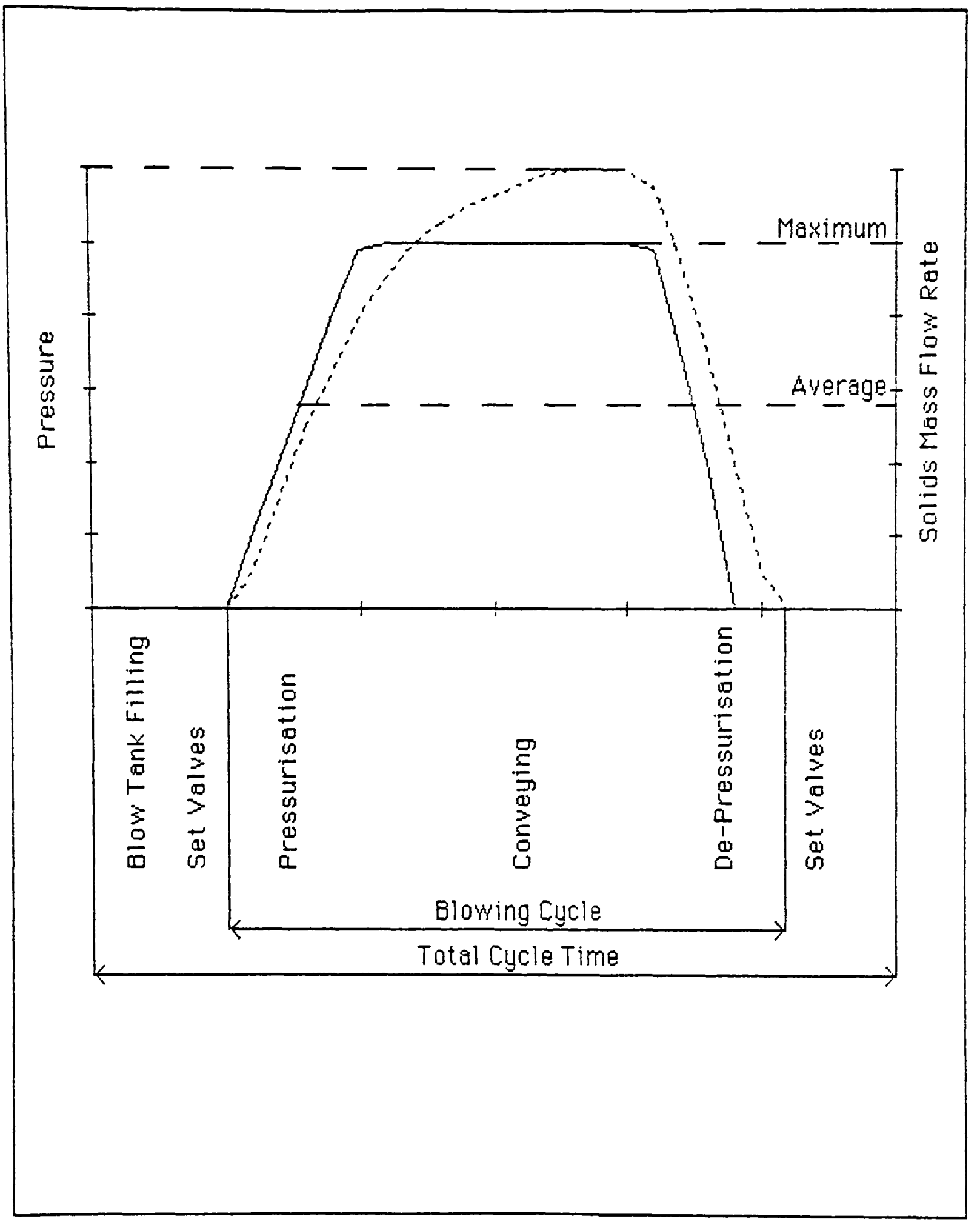

Figure 4.2.4. Batchwise Operation of a Single Blow Tank.

It is interesting to note that among the advantages listed for p conveying systems employing non-suspension modes of flow ar energy costs. This is due to the lower volume flow rates of air to achieve the specified solids mass flow rate. The air leakage through the valve greatly reduces this advantage.

The performance of the pressure vessel as a pipeline feed device is shown in figure 4.2.5.

The starting point for this figure is a pressure vessel fully charged with the bulk material and an empty pipeline point t_0. As high pressure air is introduced into the pressure vessel the bulk material is aerated and flows out of the vessel. The material flows along the pipeline and begins to be collected in the receiving hopper at point t_1. At point t_2 the resistance to flow in the pipeline and the pressure in the vessel balance and a steady pressure condition is reached. Numerous workers, including Waghorn (1977), and Lohrman and Marcus (1982) have analysed the performance of pressure vessels as pipeline feed devices. In this work the important factor is the ability to achieve the desired modes of flow within the pipeline. Once the steady pressure condition has been achieved experimental measurements may be taken. It must be noted that at a nominally steady pressure condition the flow is still transient in nature.

4.2.3 THE PIPELINE

For this work one pipeline arrangement of 54mm nominal bore has been used, as shown in figure 4.2.6. The pipe loop is essentially horizontal with one short vertical lift 8.0m from the inlet of the pipeline and a remaining vertical section at the end of the pipeline to return the solids to the receiving hopper above the pressure vessel. Special features to note about the pipeline are the two glass observation sections near the start and end of the pipeline and the three possible arrangements for the pressure transducers:

i. distributed along the whole pipeline;
ii. in the measuring section located in the straight pipe;
iii. in the measuring section located after the bend.

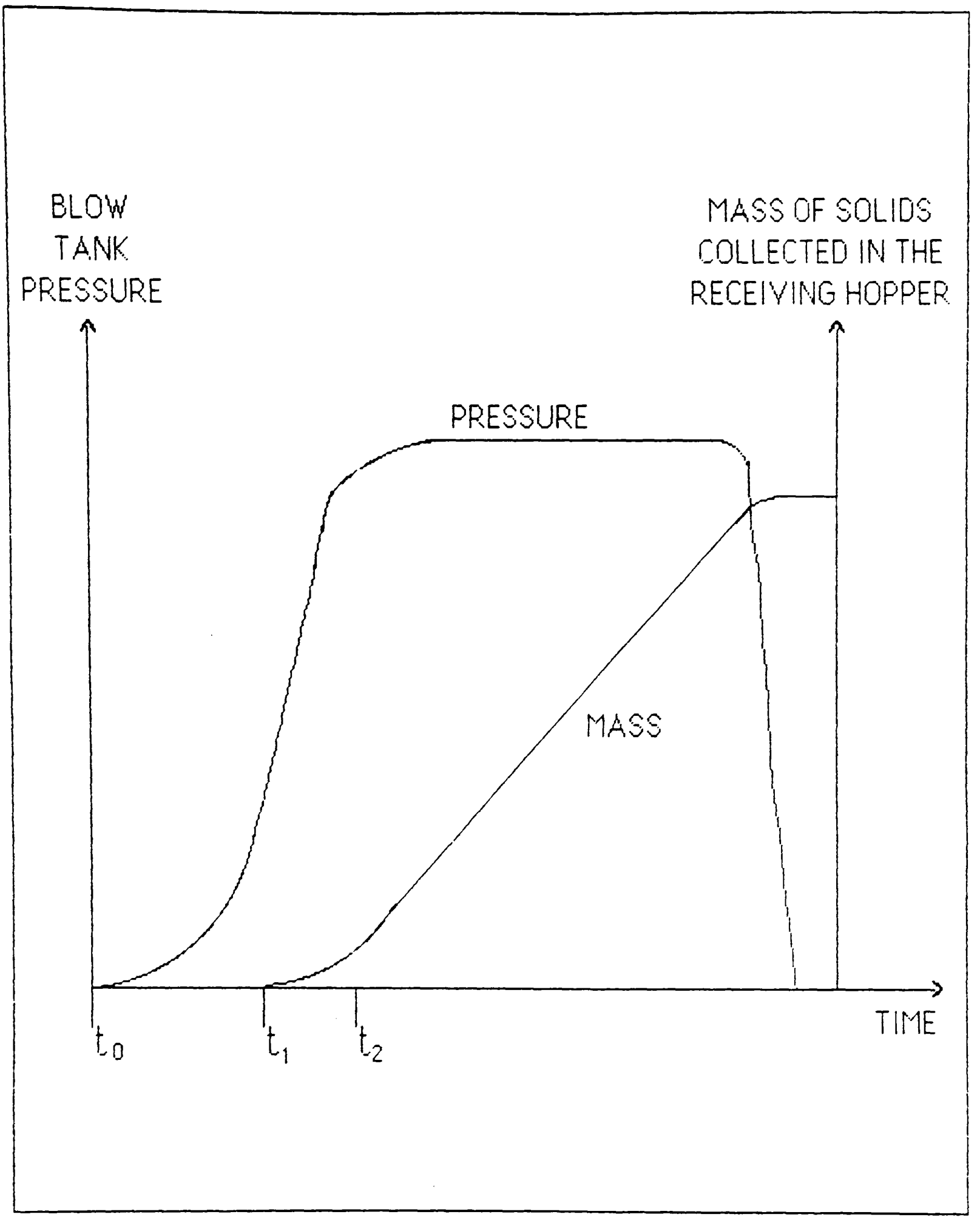

Figure 4.2.5. Pressure Transient for a Blow Tank Without a Discharge Valve.

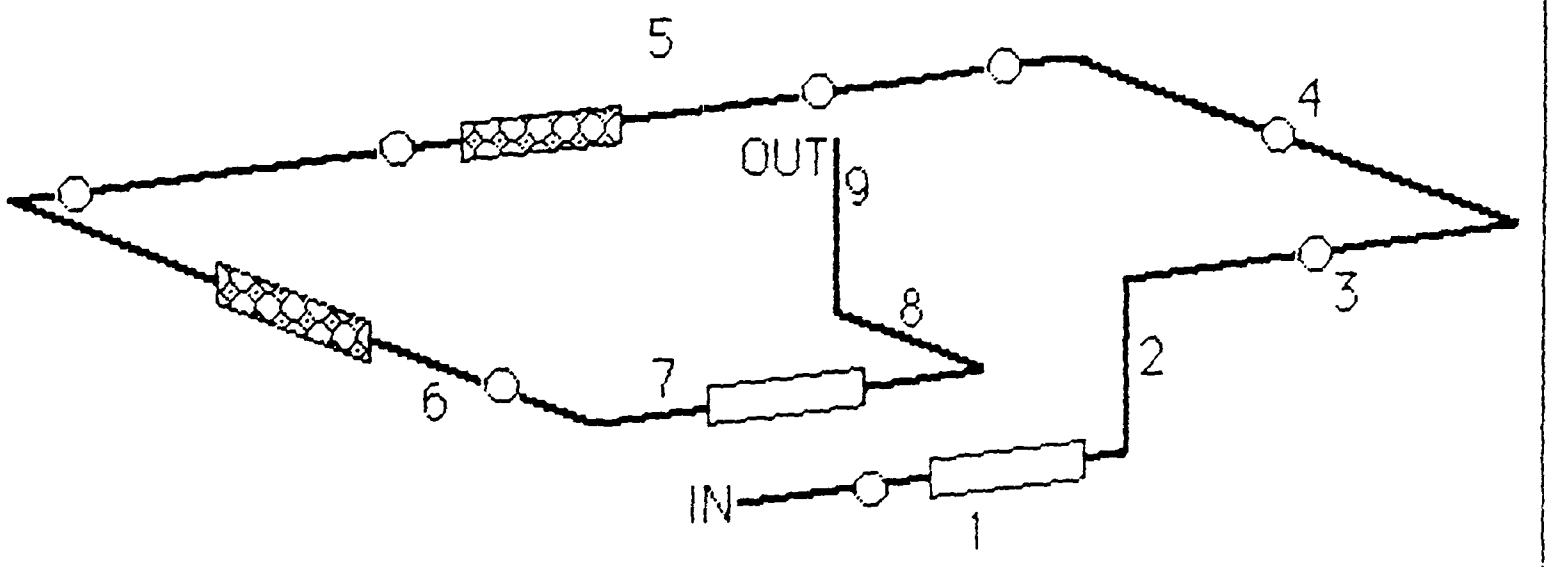

Section	Orientation	Length
1	horizontal	7.25m
2	vertical	1.11m
3	horizontal	3.65m
4	horizontal	6.15m
5	horizontal	17.00m
6	horizontal	7.42m
7	horizontal	6.05m
8	horizontal	0.60m
9	vertical	2.25m

System Summary	
Total Length	54.77m
Pipe Bore	53.00mm
Bend Radius	127.00mm

Key

- Steel Pipeline.
- Glass Pipeline
- Pressure Tapping.
- Measuring Section.

Figure 4.2.6. Pipeline Arrangement.

4.2.4 THE RECEIVING HOPPER

The bulk material is collected in a hopper resting upon three load cells. This allows the mass of solids conveyed to be measured. A bag filter above the hopper provides the means of separating the air from the solid particles. A mechanical vibrator attached to the filter facilitates periodic cleaning of the filter media. The air is exhausted to atmosphere.

4.3 SYSTEM CONTROL

The control of a pressure vessel system is achieved by proportioning the total air supply between the pressure vessel and the inlet of the pipeline. The former is generally referred to as *blow rank air* and the latter as *supplementary air*. Blow tank air pressurises the pressure vessel and may also aerate the bulk material (this depends upon the bulk properties of the material), and then discharges the bulk material into the pipeline. Supplementary air is used to *dilute* the flow. The effect of proportioning the air between these two points is shown in figure 4.3.1.

The air supplied to these two locations passes through a bank of critical-flow nozzles. The mass flow rate of air may be set by selecting one or more of the nozzles to supply air to the pressure vessel, or to the supplementary air line. If the air pressure in the manifold beneath the nozzle bank is kept constant and the downstream pressure is reduced, the air mass flow rate will increase until the velocity at the throat of the nozzle is sonic. Any further reduction will not alter the air mass flow rate. Thus, provided the downstream pressure is sufficiently low the air mass flow rate is known. Brain and Reid (1974) give the following equation for the air mass flow rate when the flow is sonic at the throat:

$$\dot{m}_{air} = C_d A \frac{P_0}{\sqrt{T}} \left(\frac{\gamma}{ZR}\right)^{\frac{1}{2}} \left(\frac{2}{\gamma + 1}\right)^{\frac{\gamma+1}{2(\gamma-1)}} \qquad 4.3.1$$

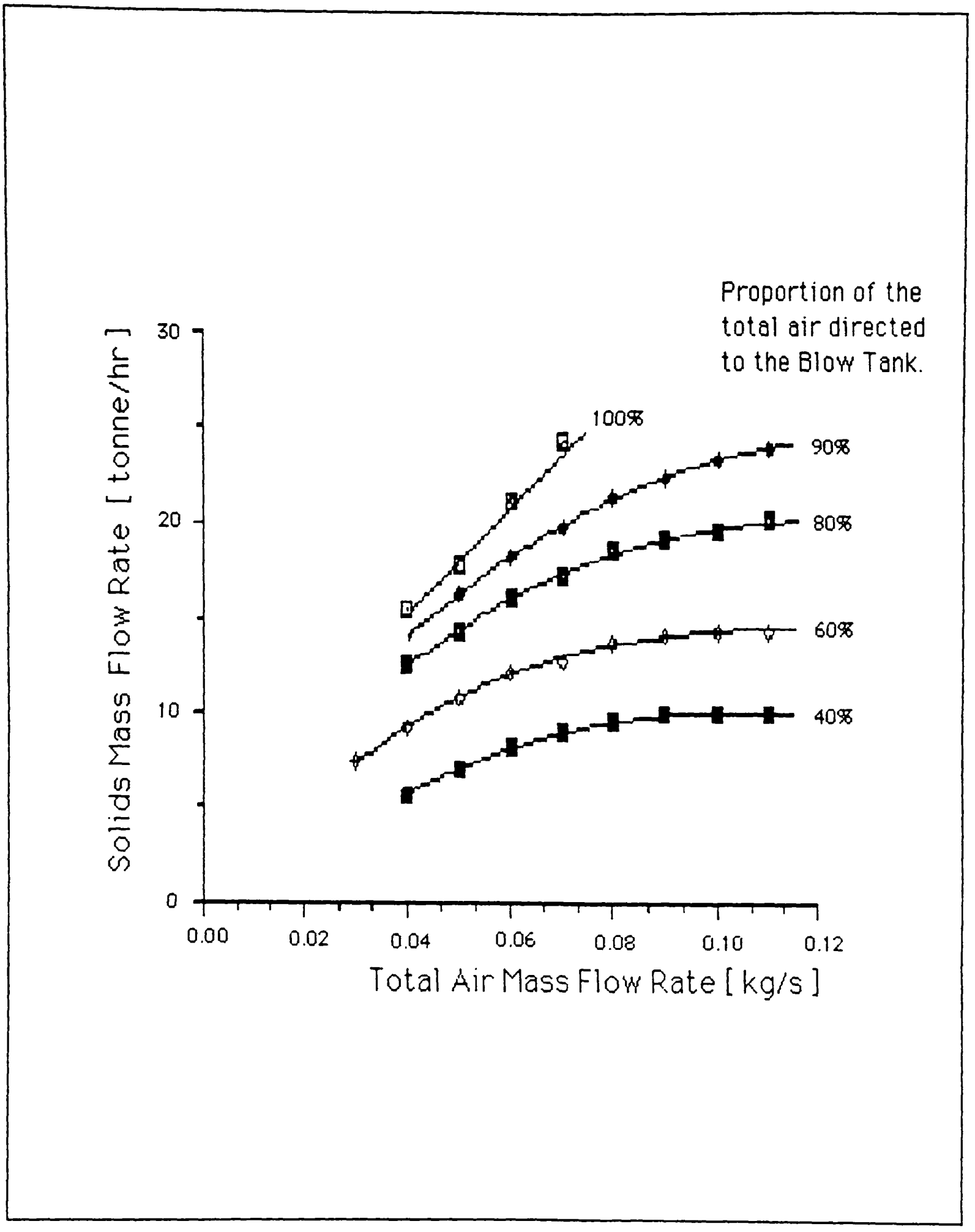

Figure 4.3.1. Typical Blow Tank Discharge Characteristics.

Hitt (1985) modified this equation to

$$\dot{m}_{air} = Q \frac{P_0}{\sqrt{T}} \qquad 4.3.2$$

where Q is the mass flow number obtained by calibration of the nozzles according to BS1042 (1964), and listed in table 4.3.1.

The critical pressure ratio, the ratio of the downstream pressure to the manifold pressure, was found to be 0.7 for these nozzles. To ensure that the downstream pressure was independent of both the flow rate and the upstream pressure, a pressure of 5.0 bar gauge was set as the maximum manifold pressure. Thus the maximum pressure in the pressure vessel is:

$$\begin{aligned} P_{vessel} &= 0.7\ (5.0\ bar_{gauge} + P_{ambient}) \\ &= 3.196\ bar_{gauge} \qquad 4.3.3 \\ when\ P_{ambient} &= 1.013\ bar_{abs} = 760\ mm_{Hg} \end{aligned}$$

Thus the total mass flow rate of air into the pipeline is reliably known provided that the pressure in the vessel does not exceed 3.2 bar gauge.

	BANK 'A'			BANK 'B'	
NOZZLE COMBINATION	MASS FLOW NUMBER Q	MASS FLOW NUMBER FOR COMBINATION PLUS NOZZLE NUMBER 6	NOZZLE COMBINATION	MASS FLOW NUMBER Q	MASS FLOW NUMBER FOR COMBINATION PLUS NOZZLE NUMBER 6
		81.50			81.67
1	4.06	86.48	1	5.02	86.69
2	5.85	87.35	2	5.92	87.59
3	7.75	89.25	3	7.63	89.30
4	9.65	91.17	4	9.62	91.29
1+2	10.82	92.32	1+2	10.94	92.61
1+3	12.73	94.32	1+3	12.65	94.32
2+3	13.60	95.10	2+3	13.55	95.22
1+4	14.64	96.14	1+4	14.64	96.31
2+4	15.51	97.01	2+4	15.54	97.21
3+4	17.42	98.92	3+4	17.25	98.92
1+2+3	18.57	100.07	1+2+3	18.57	100.24
1+2+4	20.49	101.99	1+2+4	20.56	102.23
1+3+4	22.38	103.88	1+3+4	22.27	103.94
2+3+4	23.26	104.76	2+3+4	23.17	104.84
1+2+3+4	28.24	109.74	1+2+3+4	28.19	109.86
5	34.25	115.75	5	35.42	117.09
1+5	39.23	120.73	1+5	40.44	122.11
2+5	40.10	121.60	2+5	41.34	123.01
3+5	42.00	123.50	3+5	43.05	124.72
4+5	43.92	125.40	4+5	45.04	126.71
1+2+5	45.07	126.75	1+2+5	46.36	128.03
1+3+5	46.98	128.48	1+3+5	48.07	129.74
2+3+5	47.85	129.35	2+3+5	48.97	130.64
1+4+5	48.89	130.40	1+4+5	50.06	131.73
2+4+5	49.76	131.262	2+4+5	50.96	132.63
3+4+5	51.67	133.17	3+4+5	52.63	134.34
1+2+3+5	53.00	134.50	1+2+3+5	53.99	135.66
1+2+4+5	54.74	136.24	1+2+4+5	55.98	137.65
1+3+4+5	56.67	138.13	1+3+4+5	57.69	139.45
2+3+4+5	57.51	139.01	2+3+4+5	58.59	140.26
1+2+3+4+5	62.49	143.99	1+2+3+4+5	63.61	145.28

TABLE 4.3.1 CRITICAL FLOW NOZZLE COMBINATIONS

4.4 DATA MEASUREMENT AND COLLECTION

Figure 4.4.1 shows a typical set of operating points achieved by a pneumatic conveying system. Lines of constant pressure drop (blow tank pressure minus receiving hopper pressure) are shown for combinations of solids and air mass flow rates. The data recorded to produce this conveying characteristic are:

i. the steady pressure value in the blow tank;
ii. the mass of solids collecting in the receiving hopper with time, at this condition;
iii. the mass flow rate of air supplied to the pipeline.

Though a single operating point may be taken and the pressure predicted by a mathematical model compared with the actual value, this is not sufficient to validate fully the model. The aim of this experimental programme is to obtain additional detailed data.

It was decided that no intrusive methods would be employed to measure flow parameters. Such intrusive methods are generally based upon single phase flow techniques, such as orifice plates and venturi-meters employed by McVeigh and Craig (1972), and have proved to be less than satisfactory.

One novel approach developed by Hitt (1985) and shown in figure 4.4.2 was considered, but this was designed for measuring flow in one particular mode of non-suspension flow, and thus was not implemented. Woodhead et al (1989) have reviewed non-intrusive methods for solids mass flow measurement in the pipeline, but these systems are of limited application, and can be highly dependent upon the condition of the material within the pipeline.

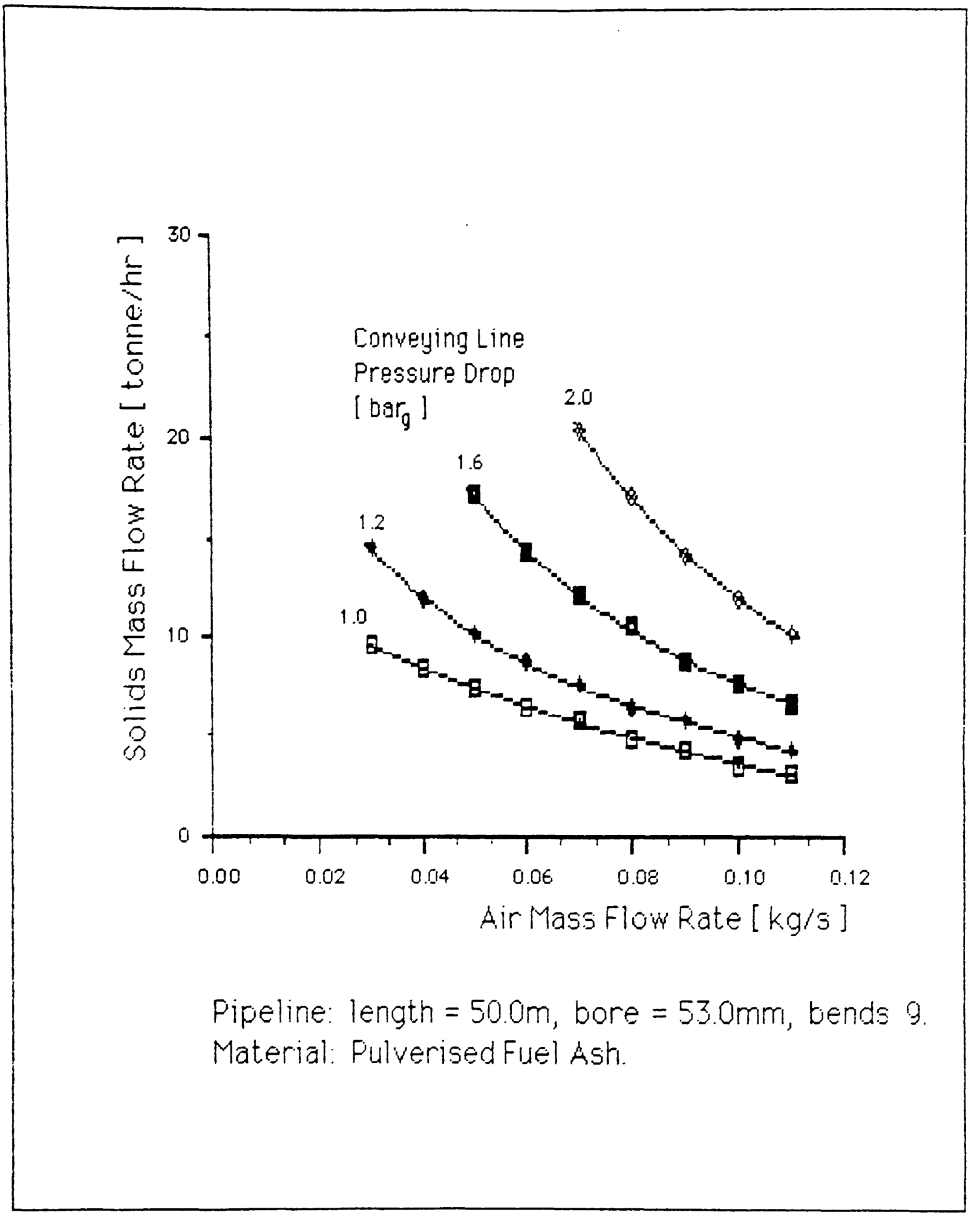

Figure 4.4.1. A Typical Conveying Characteristic.

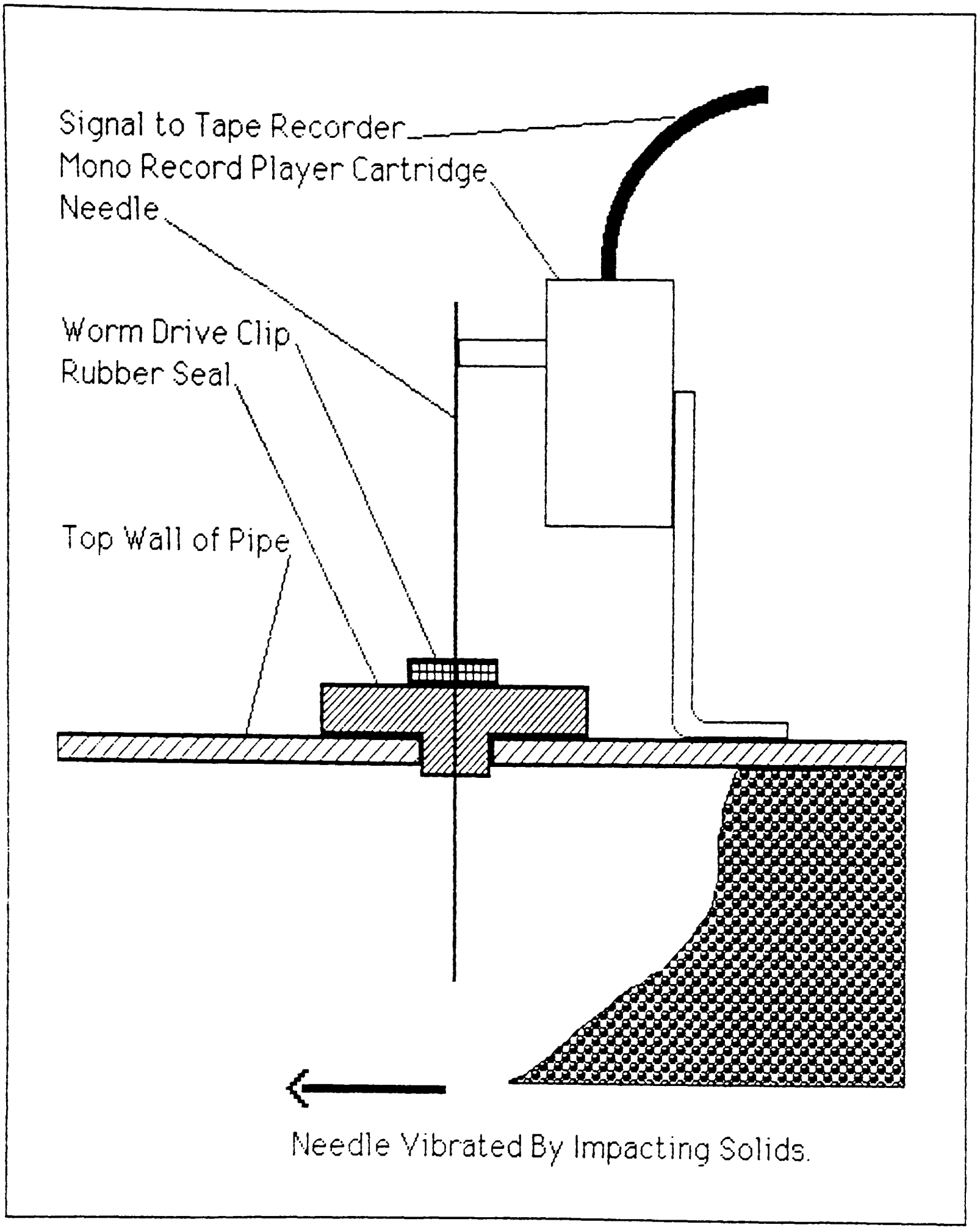

Figure 4.4.2. Hitt's Plug Measuring Device.

For example, the capacitive technique places electrodes around a point in the pipeline. The capacitance changes according to the value of the dielectric, in this case the gas-solids mixture within the pipeline at the point of measurement. This can be significantly affected by the presence of even small amounts of water vapour. The use of laser doppler velocimeters, Birchenough and Mason (1980) is also limited to very low values of solids loading ratio, which restricts the technique to suspension flows where the volume concentration of solid particles is low.

From this analysis of the state of the art it was decided to measure only pressure and to record the flow patterns by visual means. Figure 4.2.6 shows the distribution of pressure transducers along the pipeline and the location of glass sections within the pipeline. The output of the transducers was recorded by a data logger, which also recorded the blow tank pressure and load cell readings at various times during the conveying cycle, to produce a pressure distribution with time and axial distance.

Three options were available for the location of the pressure transducers:

i. distributed along the entire length of the pipeline;
ii. in a 5.0m section in the middle of a straight section of the pipeline;
iii. in a 5.0m section after a bend in the pipeline.

The second and third options provide detailed pressure distributions and a means of investigating the effect of a bend upon the overall pressure drop. This has been reported by Bradley (1989) as significant in systems employing suspension flow, but negligible in some non-suspension flow systems, Hitt (1985).

Figure 4.4.3 shows the construction details of the sight glasses employed at two locations in the pipeline. The flow patterns observed were recorded on video tape during certain tests when a different flow pattern was expected. The presence of the perspex guard reduced the quality of the pictures, but was regarded as an essential safety feature, especially after one exploded while the author was video-recording the flow patterns.

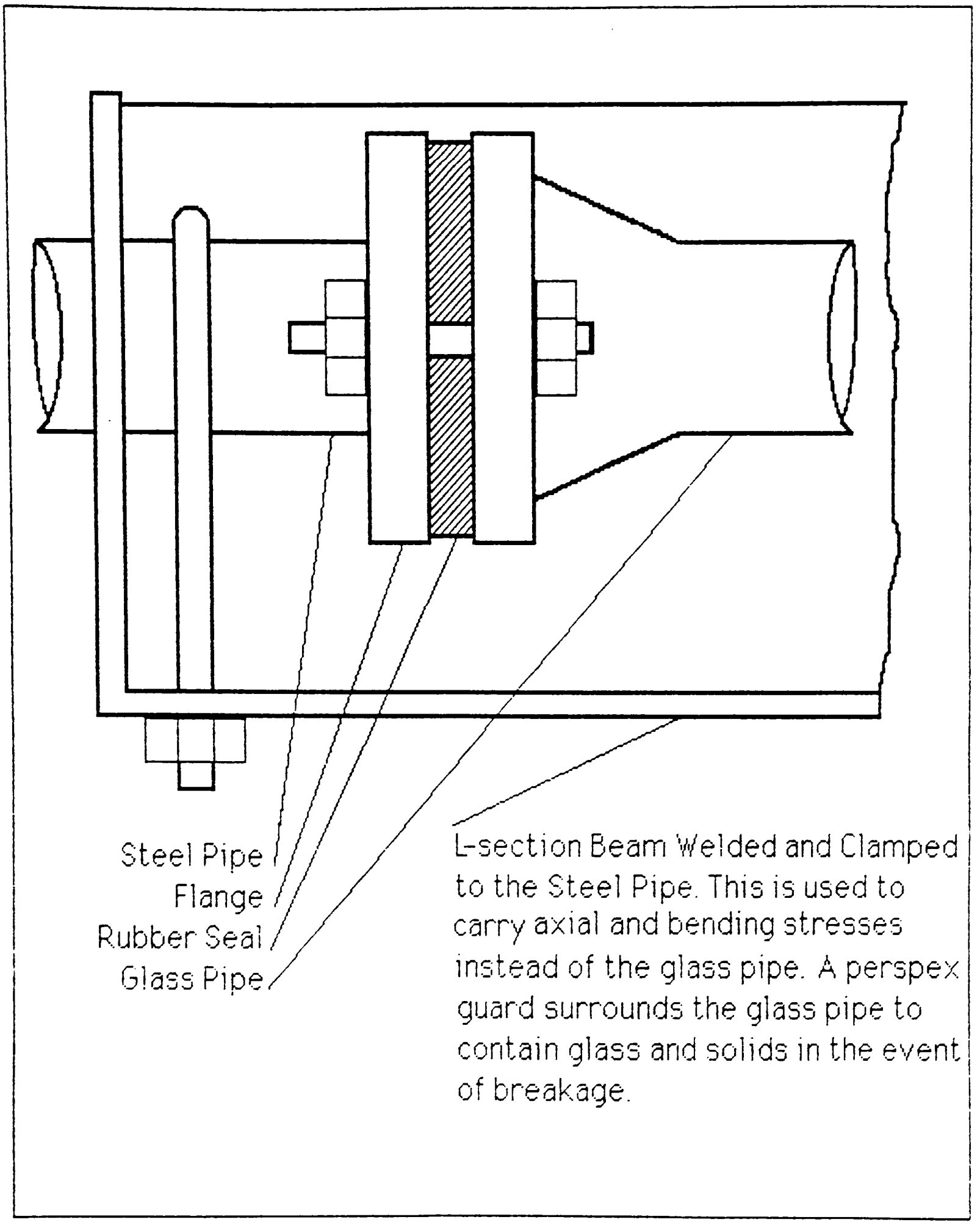

Figure 4.4.3. Construction Details of the Glass Pipeline Section.

4.5 SUMMARY

The previous sections have described the experimental facilities available for the author's use. With a knowledge of the bulk properties which characterise materials according to mode of flow, a test programme was commenced with representative materials in order to gather sufficient information for validation of the mathematical models developed to describe these flows.

5 MODELLING OF SUSPENSION FLOW

5.1 INTRODUCTION

This chapter describes the application of the general mathematical model to the case of suspension flow of a bulk material in a pipeline. The sub-models included to make the general model problem specific are presented. The predictions of the model are compared with experimental data. In the light of this comparison the sub-models are developed and key parameters discussed.

Dilute phase pneumatic conveying systems are employed in a wide variety of industries. A typical system employing this mode of flow could be characterised as follows:

i. a low value of solids loading ratio, usually less than 10, but possibly as high as 20;
ii. high gas and solids velocities, typically in excess of 15 ms^{-1}.

The two key aspects of the design of such systems are:

i. the need to determine the minimum conveying velocity for the bulk material;
ii. the need to determine the effect of the bends in the pipeline.

The former is important since this defines the point at which particles will begin to fall out of suspension. This minimum velocity occurs at the pipeline inlet, and once this and the pressure drop are known the volume flow rate of the gas is determined. The latter aspect is often accounted for by the use of equivalent lengths. This approach has been used extensively for single-phase flows in pipelines. All bends, and fittings are replaced by a length of horizontal pipe that would produce the same pressure drop.

Thus the calculation of total pipeline pressure drop is reduced to a calculation for a single horizontal pipe. Publications such as the Chemical Engineer's Handbook, have produced tables of equivalent lengths for bends in pneumatic conveying systems. It was noted by Bradley (1989), that the equivalent length of a bend will increase if it is located nearer to the exit of the pipeline. This is due to the increase in velocity as the pressure falls and the conveying gas expands.

5.2 RELATIONSHIP BETWEEN FLOW CONDITIONS AND SLIP VELOCITY

This section provides an estimation of the variation of the solids volume fraction with the slip velocity between the conveying gas and the solid particles. Consider the one-dimensional flow of a gas-solids mixture.

$$R_g + R_s = 1 \qquad 5.2.1$$

$$u_i = \frac{\dot{m}_i}{R_i A \rho_i} \qquad i = g,s \qquad 5.2.2$$

Defining two quantities, the solids loading ratio, and the density ratio:

$$\phi = \frac{\dot{m}_s}{\dot{m}_g} \qquad 5.2.3$$

$$\lambda = \frac{\rho_s}{\rho_g} \qquad 5.2.4$$

As a result of gas-particle interactions the particles will be accelerated by the gas, steadily reducing the slip velocity:

$$u_s = u_g - u_{slip} \qquad 5.2.5$$

Substituting for velocity in equation 5.2.5 using 5.2.2 produces the following expression for slip velocity:

$$u_{slip} = \frac{\dot{m}_g}{R_g A \rho_g} - \frac{\dot{m}_s}{R_s A \rho_s} \qquad 5.2.6$$

This may be rewritten in terms of the solids values and the solids loading and density ratios:

$$u_{slip} = \frac{\dot{m}_s}{R_s A \rho_s}\left(\frac{\lambda}{\phi}\frac{R_s}{1-R_s} - 1\right) \qquad 5.2.7$$

If a slip factor is defined such that:

$$u_g = \alpha u_s \qquad 5.2.8$$

where $\alpha = 1$ gives the no slip condition, then

$$u_{slip} = (\alpha - 1)\, u_s \qquad 5.2.9$$

$$(\alpha - 1) = \left(\frac{\lambda}{\phi}\frac{R_s}{1-R_s} - 1\right) \qquad 5.2.10$$

$$\alpha = \frac{\lambda}{\phi}\frac{R_s}{1-R_s}$$

$$R_s = \frac{\phi\alpha}{\phi\alpha - \lambda} \qquad 5.2.11$$

Figure 5.2.1 shows the variation of slip factor, α, with solids volume fraction, R_s.

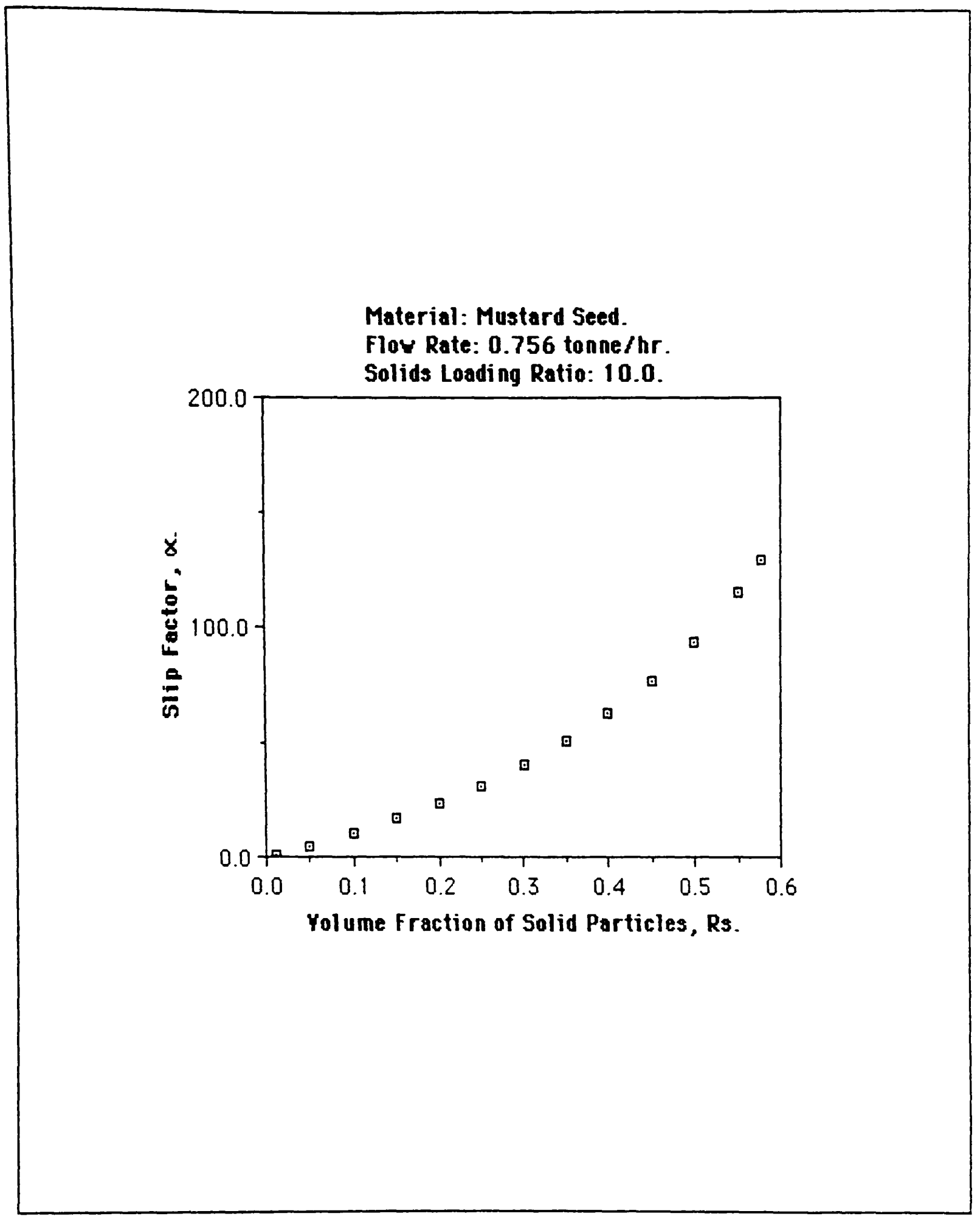

Figure 5.2.1 The variation of slip factor with solids volume fraction.

Consider a typical *dilute phase* pneumatic conveying system transporting mustard seed where:

$$\phi = \frac{0.21\ kg/s}{0.021\ kg/s} = 10.0$$

$$\lambda = \frac{1130.0\ kg/m^3}{1.2\ kg/m^3} = 941.7$$

$$\frac{\rho_{bulk}}{\rho_s} = \frac{654.0\ kg/m^3}{1130.0\ kg/m^3} = 0.579 = R_{s,max}$$

When the slip velocity is zero, ie $\alpha = 1$, then the solids volume fraction, R_s, is 0.011.

When the the solids volume fraction, R_s, is 0.02 then $\alpha = 1.92$, ie the solids velocity is approximately half the gas velocity.

Therefore, for a constant solids mass flow rate the slip velocity may be up to half of the conveying gas velocity without the solids volume fraction exceeding 2%. Thus, for most *dilute-phase* systems the volume fraction will be expected to be very low.

5.3 GAS SOLIDS INTERACTIONS

5.3.1 HEAT AND MASS TRANSFER

The conservation equations contain a source term which represents the source of the conserved quantity due to the other phases present. A source of mass transfer may be due to factors such as:

i. burning of the particles, generating gases;
ii. evaporation of water vapour from the surface of the particles.

The first may be neglected since the particles do not burn in a pneumatic transport system. The second may be neglected if there is no heat transfer. Heat transfer in a pneumatic conveying system may normally result from either:

i. a hot conveying gas, as could be supplied by a Roots type blower;
ii. hot particles, such as those produced during one stage of a chemical process and requiring transport to the next stage.

Since the majority of pneumatic conveying systems operate with particles at ambient temperature the latter case may be neglected. Figure 5.3.1.1 shows the operation of a Roots type blower. The compression of the gas occurs across a shock wave at the exit of the machine. Considering a control volume around the solids feed point of a pneumatic conveying pipeline, as shown in figure 5.3.1.2, the gas-solids mixture can than be analysed as follows:

$$\dot{m}_m = \dot{m}_s + \dot{m}_g = \dot{m}_g(1+\phi) \qquad 5.3.1.1$$

$$(\dot{m} C_P T)_m = (\dot{m} C_P T)_s + (\dot{m} C_P T)_g \qquad 5.3.1.2$$

$$T_m = \frac{(\dot{m} C_P)_s}{(\dot{m} C_P)_m} T_s + \frac{(\dot{m} C_P)_g}{(\dot{m} C_P)_m} T_g \qquad 5.3.1.3$$

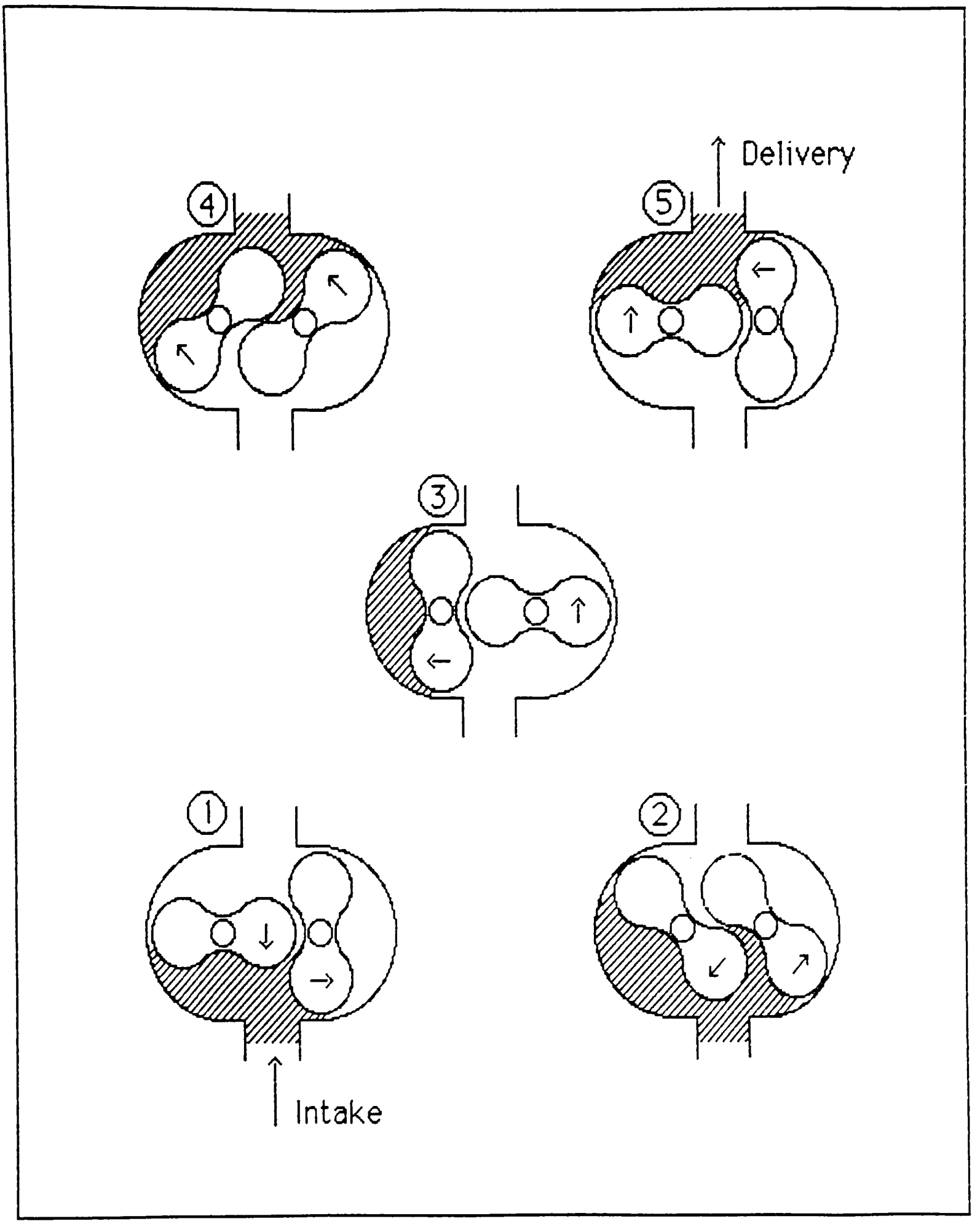

Figure 5.3.1.1 The operating principle of a Roots-type blower.

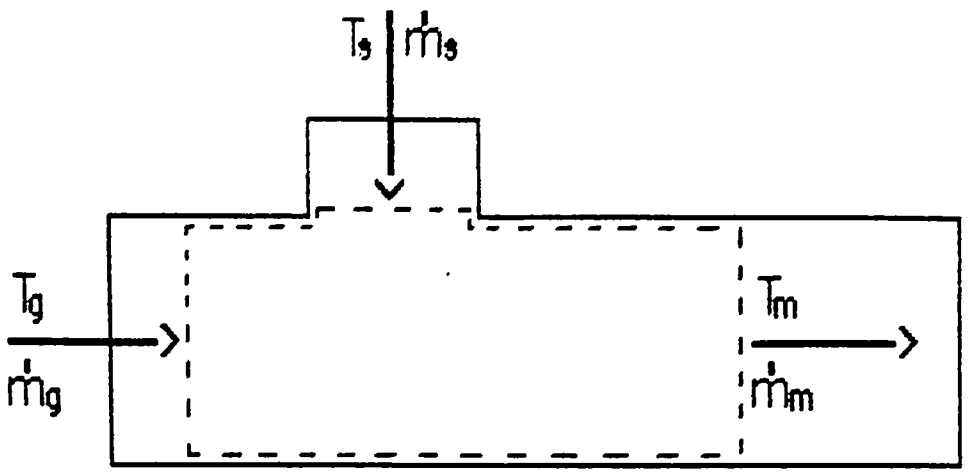

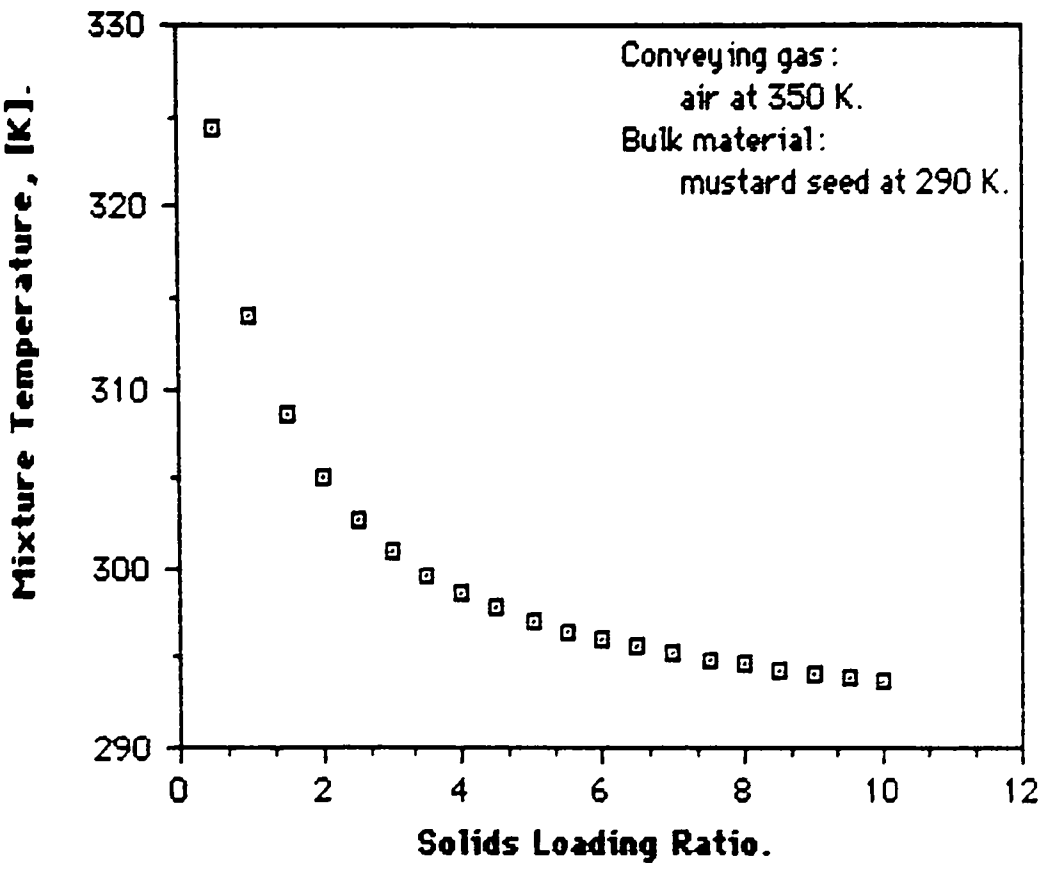

Figure 5.3.1.2 The influence of a hot conveying gas on the gas-solids mixture temperature at the feed point of a pneumatic conveying system.

$$C_{P,m} = \frac{(\dot{m} C_P)_g + (\dot{m} C_P)_s}{\dot{m}_g + \dot{m}_s} \qquad 5.3.1.4$$

$$T_m = \frac{\phi C_{P,s} T_s + C_{P,g} T_g}{\phi C_{P,s} + C_{P,g}} \qquad 5.3.1.5$$

Considering the case of the transport of mustard seed where:

$T_g = 77\ C = 350\ K$
$T_s = 17\ C = 290\ K$

$C_{Pg} = 1.0\ kJ/kg\ K$
$C_{Ps} = 1.5\ kJ/kg\ K$

Figure 5.3.1.2 shows the variation of the mixture temperature, T_m, with solids loading ratio, ϕ. This shows that the heat transfer effect is only influential at very low solids loading ratios. Thus the influence of a hot conveying gas has been neglected in this work, which is an important point since many industrial *dilute-phase* pneumatic conveying systems are supplied with air from a Roots type blower.

In summary:

i. no mass transfer has been considered;
ii. the flow is assumed to be isothermal.

The former greatly simplifies the mass conservation equations. The latter means that the conservation of enthalpy need not be considered.

5.3.2 MOMENTUM TRANSFER

The final conservation equation is that for momentum. Momentum is transferred between the conveying gas and particles as a result of the aerodynamic drag of the particles. Consider a single particle in an infinite gas stream:

$$F_D = C_D A_P \frac{1}{2} \rho_g u_{slip}^2 \qquad 5.3.2.1$$

where the drag coefficient is calculated from the Schiller and Naumann (1933) equation:

$$C_D = \frac{24}{Re_s}\left(1 + 0.15 Re_s^{0.687}\right) \qquad Re_s \leq 800 \qquad 5.3.2.2$$

$$Re_s = \frac{d_s u_{slip}}{\nu_L} \qquad 5.3.2.3$$

For particle Reynolds numbers greater than 800, Newton's law is used, giving:

$$C_D = 0.44 \qquad 5.3.2.4$$

In order to avoid a step change in the drag coefficient function, equations 5.3.2.2 and 5.3.2.4 are equated so that the Schiller and Naumann equation (5.3.2.2) was applied up to a particle Reynolds number of 989.

In order to calculate the total momentum transfer due to all the particles in a control volume, the projected area, A_P, is evaluated as the sum of all the individual particle projected areas.

$$A_{Proj} = n \frac{\pi}{4} d_s^2$$

$$= \frac{R_s V_{cv}}{\frac{\pi}{6} d_s^3} \frac{\pi}{4} d_s^2 \qquad 5.3.2.5$$

$$= \frac{3}{2} R_s \frac{V_{cv}}{d_s}$$

Since a two-phase model has been employed, the solids phase is characterised by a mean particle diameter. For bulk materials with a wide size distribution this assumption can be a significant cause of error. Without employing any further phases to describe parts of the size range, the following approach has been employed:

$$F_{D,total} = \sum_{i=1}^{n} f_i \, F_{D,i} \qquad 5.3.2.6$$

The size range is divided into parts with f_i being the fraction having a particle diameter of $d_{s,i}$. Thus the drag force is calculated for each diameter range and the weighted sum is taken to be the drag force exerted by the gas phase. In this case n=3 was used.

The exchange coefficient, Γ_ϕ, for the momentum conservation equation is equal to the effective viscosity, μ_E. This is the mechanism by which the effect of turbulence is modelled.

$$\mu_E = \mu_L \qquad \textit{for laminar flow} \qquad 5.3.2.7$$

In turbulent flows, energy is transferred from the kinetic energy of the mean flow to internal thermal energy of the fluid, via eddies. Large eddies, with dimensions comparable to the linear dimensions of the flow domain, determine the energy transfer from the kinetic energy of the mean flow to the eddy system. The viscosity of the fluid determines the smallest eddies at which energy is transferred to internal thermal energy

of the fluid. Thus, large eddies are mainly responsible for the transport of momentum and heat.

Transport models for turbulent effects do not model the physical modes of turbulence, such as eddies, velocity patterns, and high vorticity regions. Even so, Markatos (1986) shows that good results have been achieved using such models for single phase flows. The Reynolds stress due to turbulence is modelled using an analogy with molecular viscous stress. The *molecules* are eddies, which collide and exchange momentum, obeying the kinetic theory of gases. Two models are employed to evaluate the effective viscosity:

$$\mu_E = 0.09 \frac{k^2}{\epsilon} \qquad 5.3.2.8$$

$$\mu_E = \beta \mu_L \qquad 5.3.2.9$$

Equation 5.3.2.8 is the *two-equation model* of Launder and Spalding (1972). This solves extra conservation equations for turbulent kinetic energy, k and the turbulence dissipation rate, ϵ. The presence of particles in the gas can significantly affect the levels of turbulence. Figure 5.3.1.3 shows how the ratio of gas-solids friction factor to gas only friction factor varies with solids loading ratio. With zero solids the ratio is, obviously, unity. As the mass flow of solids increases the ratio falls below unity, then increases. This effect was noted by Boothroyd (1966) in his study of duct flow of fine particle suspension flows.

In equation 5.3.2.9, β, is a constant value. Although β was taken as a constant it is a function of the flow conditions and particle properties. Theory to calculate β is nonexistent and considered beyond the scope of present work. β was evaluated in the light of comparison of flow predictions with experimental data. By employing equation 5.3.2.9 an estimate of the influences of particles on turbulence was obtained.

It was found that β predicted by equation 5.3.2.8 was approximately 1500, whereas a value of 300 gave good agreement with experimental data. Thus equation 5.3.2.9 was used as the turbulence model.

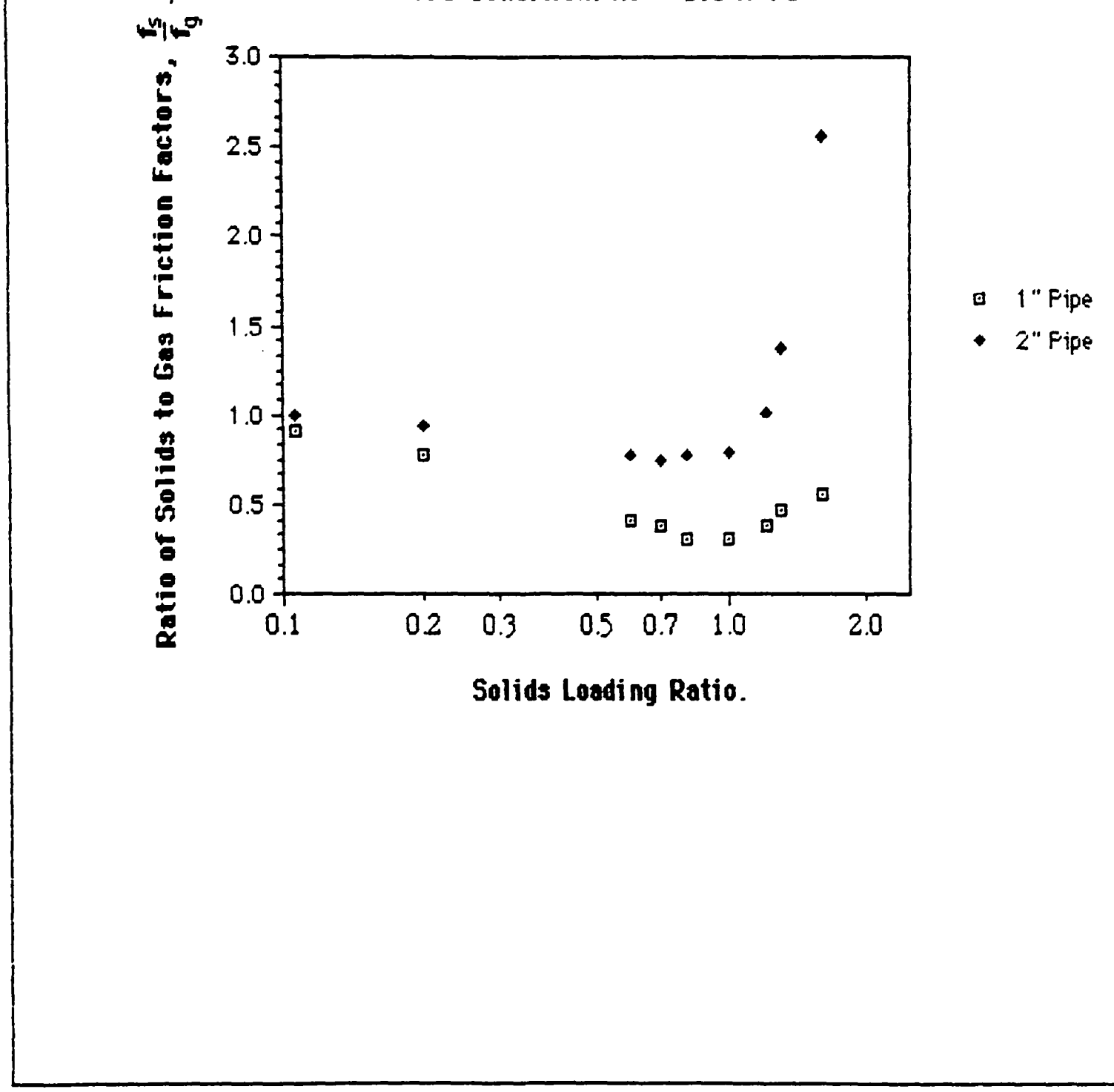

Figure 5.3.1.3 The variation of pipe friction factor with solids loading ratio.

5.4 OTHER RELATIONSHIPS

5.4.1 WALL EFFECTS

At the pipe wall the no slip condition was used for the gas phase. The Blasius formula for the friction factor, f, which is based upon the flow of a single fluid in a smooth pipe, was used for this phase where:

$$f_{g,wall} = 0.079\ Re_D^{-0.25} \qquad 5.4.1.1$$

$$Re_D = \frac{D\ u_g}{\nu_L} \qquad 5.4.1.2$$

The interaction of the particles with the pipe wall is more difficult to model. The manner in which particles collide with the walls of a pipe has been investigated by many authors, including Adam (1957), Owen (1969) and Brauer (1980). Tsuji et al (1985) developed a random bouncing model for numerical simulation of confined horizontal gas-solids flows. Unfortunately this relies upon a random function for which no details have been published. Initially it was assumed that the particles lost no momentum to the pipe wall, ie there were no particle-wall collisions. If this phenomenon is significant then the pressure drop measured experimentally would be expected to be higher.

5.4.2 DESCRIPTION OF THE PHASES

The conveying gas was considered to be a perfect gas. All gases at low pressure and high temperature have an equation of state approximating the perfect gas equation:

$$\rho_g = \frac{P}{R\ T}$$
$$R = C_P - C_V \qquad 5.4.2.1$$
$$C_P = \frac{dh}{dT}$$

The bulk material was described by the particle density and mean particle size. In addition, equations such as 5.3.2.5 treat the particle as being spherical in shape. This problem is often countered by the use of an effective diameter, ie the diameter of a sphere that would have the same effect as the actual particle. Ergun (1952) defines an effective diameter as follows:

$$d_{s,eff} = \frac{6}{S_v} \qquad 5.4.2.2$$

$$S_v = \frac{S_T}{ALR_s}$$

where
- A is the cross-sectional area of a tube;
- L is the height to which the tube is filled;
- R_s is the volume fraction of solids in the tube;
- S_T is the total geometric surface area of the solids in the tube.

5.5 COMPARISON WITH EXPERIMENTAL DATA

5.5.1 INTRODUCTION

The validity of a mathematical model can only be determined by a comparison with the behaviour of the physical system that it is being used to describe. This comparison can be used to highlight the areas of the model that require refinement. From the point of view of system operation three key variables can be identified:

i. the solids mass flow rate;
ii. the gas mass flow rate;
iii. the pressure drop along the pipeline.

The mass flow rate of solids is the prime design requirement of a commercial pneumatic conveying system. The other two variables govern the specification of the air-mover, one of the major capital costs of a system. It is important for the model to be able to predict these values, but in order to validate the model more detailed measurements are

required, where the variation of the dependent variables (ie pressure, velocity, volume fraction) is measured along the pipeline.

5.5.2 EXPERIMENTAL DATA

The data used to validate the mathematical model for suspension flow was taken from the work of Jones (1983). The experimental rig used is shown in figure 5.5.2.1, and the test data used for validation is reproduced in table 5.5.2.1. The data used for comparison was carefully chosen so that the influence of the assumptions made in the model was minimised. The bulk material used in these tests was mustard seed. Figure 5.5.2.2 shows a microscope slide of the bulk material together with its properties. It is reasonable to assume that mustard seeds are monosized and nearly spherical. The validation can be used to assess other features of the model.

For dynamic similarity of the flow where the boundaries are geometrically similar and the flow is only affected by viscous, pressure and inertia forces, the Reynolds number must be constant. The data used for comparison was selected so that the pipe Reynolds number values:

$$Re_D = \frac{\rho_g D \overline{u_g}}{\mu_L} = \frac{4\dot{m}_g}{\pi \mu_L D} \qquad 5.5.2.1$$

were as close as possible and the solids loading ratio:

$$SLR = \frac{\dot{m}_s}{\dot{m}_g} \qquad 5.5.2.2$$

covered the range of values tested.

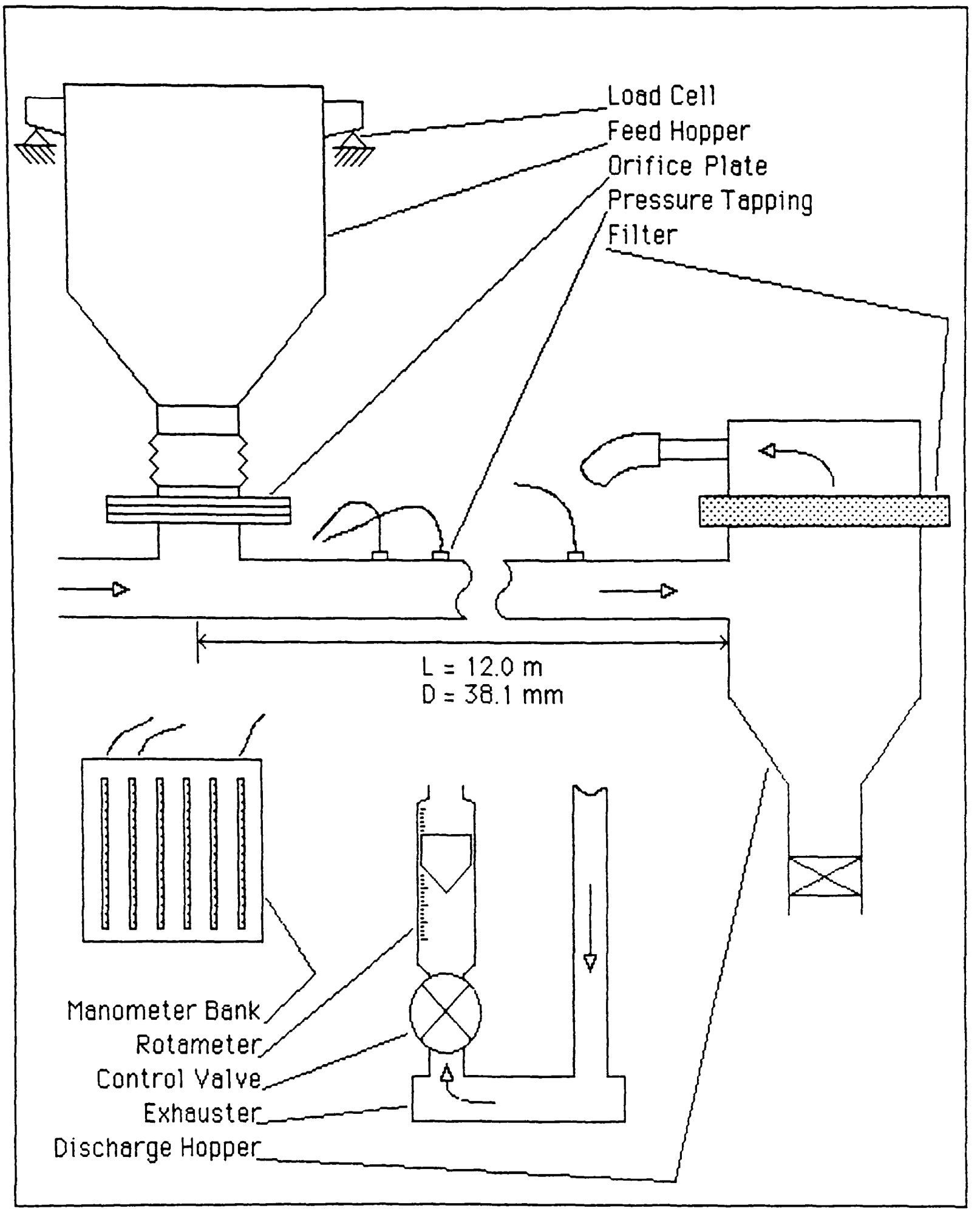

Figure 5.5.2.1 Experimental test rig used to determine *acceleration* region pressure gradients.

Mass flow of gas	[kg/s]	0.0340	0.0340	0.0320	0.0368
Mass flow of solids	[kg/s]	0.161	0.197	0.352	0.463
Solids Loading Ratio		4.74	5.71	10.16	12.58
Distance along pipe	[m]		Pressure drop	[Pa]	
	0.0	0.0	0.0	0.0	0.0
	0.5	89.0	102.0	195.0	250.0
	1.0	127.0	143.0	275.0	370.0
	1.5	160.0	180.0	330.0	455.0
	2.0	192.0	220.0	370.0	535.0
	2.5	213.0	245.0	420.0	580.0
	3.25	239.0	275.0	470.0	640.0
	4.0	267.0	305.0	510.0	700.0
	5.0	283.0	328.0	545.0	760.0
	6.0	314.0	360.0	585.0	815.0
	7.0	343.0	393.0	625.0	860.0
	8.0	364.0	413.0	665.0	895.0
	9.0	387.0	440.0	700.0	925.0
	10.0	399.0	450.0	740.0	955.0

TABLE 5.5.2.1 Data for suspension flow of mustard seed.

In this set of experiments the following values were measured:

i. mass flow rate from the supply hopper;
ii. mass flow rate of gas out of the exhauster;
iii. pressure variation along the conveying line.

In addition a perspex section in the pipeline was used for flow visualisation. The limitation of this data is that there were no measurements of velocities and only subjective information on the distribution of the solid particles in the pipe. Morikawa et al (1986) measured both of these variables using an optical probe situated in the pipeline. This data provides a useful comparison for the model. It must be noted that the probe will have had an effect on the flow patterns measured. Birchenough and Mason (1976) used laser doppler anemometry techniques to measure particle velocities and gas turbulence intensities. Although this is a less intrusive technique, measurements were limited to solids loading ratios of about one. This is an order of magnitude less than Jones' data and the values of solids loading ratio commonly found in industrial systems.

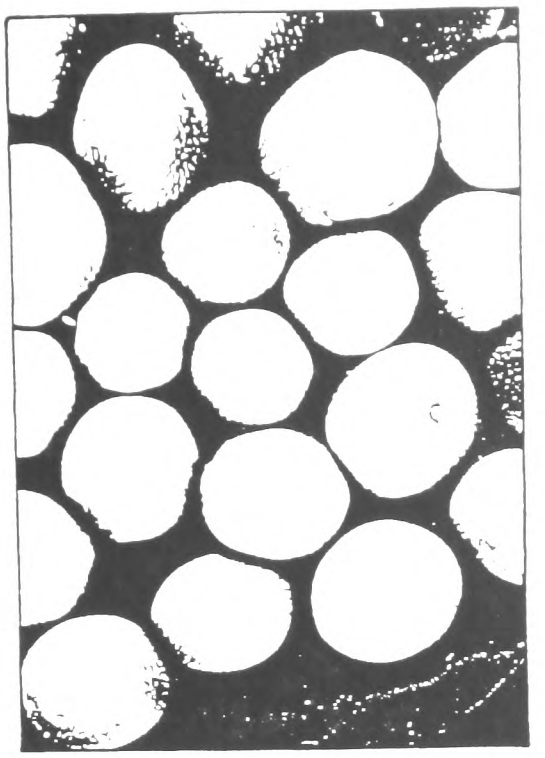

Mean particle size:	1.54 mm
Mass median particle size:	1.54 mm
Particle size range (2.5% / 97.5%):	NIL
Particle density:	1130 kg/m^3
Poured bulk density:	654 kg/m^3
Tapped bulk density:	670 kg/m^3

Comments: This bulk material is composed of nearly monosized particles which are spherical in shape. This material will degrade after being conveyed several times.

Figure 5.5.2.2 The properties of mustard seed.

5.5.3 DISCRETISATION OF THE FLOW DOMAIN, AND CALCULATION PROCEDURE

The flow was modelled as two-dimensional. This assumption reduces the number of variables that need to be solved for and hence the computer time taken to produce a solution. In order to maintain the same flow area the thickness of the two-dimensional channel was specified. This assumption will result in inaccuracies due to the difference in the surface area used for calculating the pipe wall friction. The error introduced by this difference is not significant, because only the gas wall friction is calculated and the gas only pressure drop for the pipe (ie that due to the wall friction) is only a small proportion of the total pressure drop for the gas-solids flow.

The following boundary conditions were employed:

i. at the inlet the mass flow rate per unit area was specified for each phase, and was assumed to be uniform over the entire cross-section;
ii. at the outlet the pressure was specified.

The grids of control volumes used are shown in figure 5.5.3.1. Initially a uniform grid of 20 control volumes in the axial direction and 4 in the direction normal to the channel axis was employed. This size was chosen so that:

i each control volume was large enough to contain sufficient particles so that the model of the solids as a continuum was applicable;
ii the aspect ratio of each control volume (the ratio of length to width) was not too large (this is difficult to achieve in a pipe where the length is many diameters);
iii the time taken to compute the solution of the model was reasonable.

The original grid was subsequently modified as part of the study to determine the dependence of the solution on the grid.

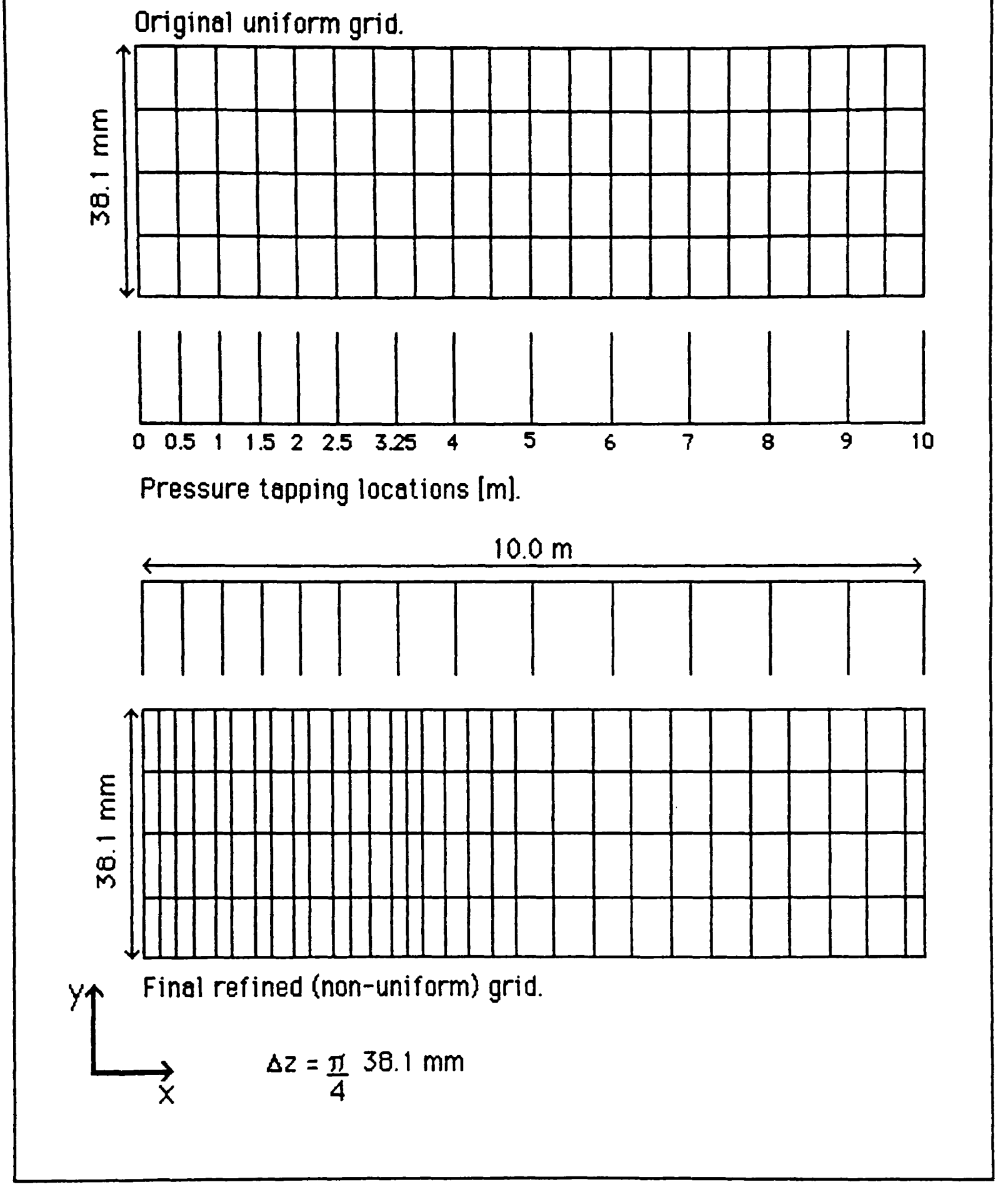

Figure 5.5.3.1 Control volume grids used to model the test pipeline.

The grid used for the final calculations was finer in the *acceleration* region where the change in pressure gradient was largest. This grid was also adjusted so that control volume centres (where the pressure is calculated) were at the same locations as the pressure tappings in the experimental work.

By monitoring the manometer readings and the flow in the perspex section, Jones' noted that it took approximately 10 seconds to achieve a steady pressure distribution. This was simulated by undertaking a transient simulation of the flow into the pipe from empty pipe state, for 10 seconds. This provided the initial field of values for a steady simulation. Since the purpose of the transient simulation was to achieve an initial estimate of the flow field, less strict convergence criteria was used to reduce the solution time. Subsequently, it was discovered that by increasing the inertial relaxation:

$$(a_P + I)\phi_P = \sum_{i=1}^{n} a_{nb}\phi_{nb} + b + I\phi_P^* \qquad 5.5.3.1$$

where I is the inertial relaxation factor, ϕ_P^* the old iteration value and ϕ_P the new value. Using more iterations the transient analysis could be omitted. The reciprocal of I is termed the *false time step*.

5.5.4 PREDICTION OF THE PRESSURE DROP

Rose and Duckworth (1969) divided the flow of a gas-solids suspension into two regions:

i the *acceleration* region where the flow is developing and the slip velocity of the solid particles relative to the gas is large;

ii the *established flow* region where the slip velocity is small.

Figure 5.5.4.1 shows this division graphically. They, along with Bradley (1989), and Mills and Mason (1985), noted that the *acceleration* region often represented the major component of the total pressure drop. Such flow regions occur at the solids feed point and after all bends in the pipeline.

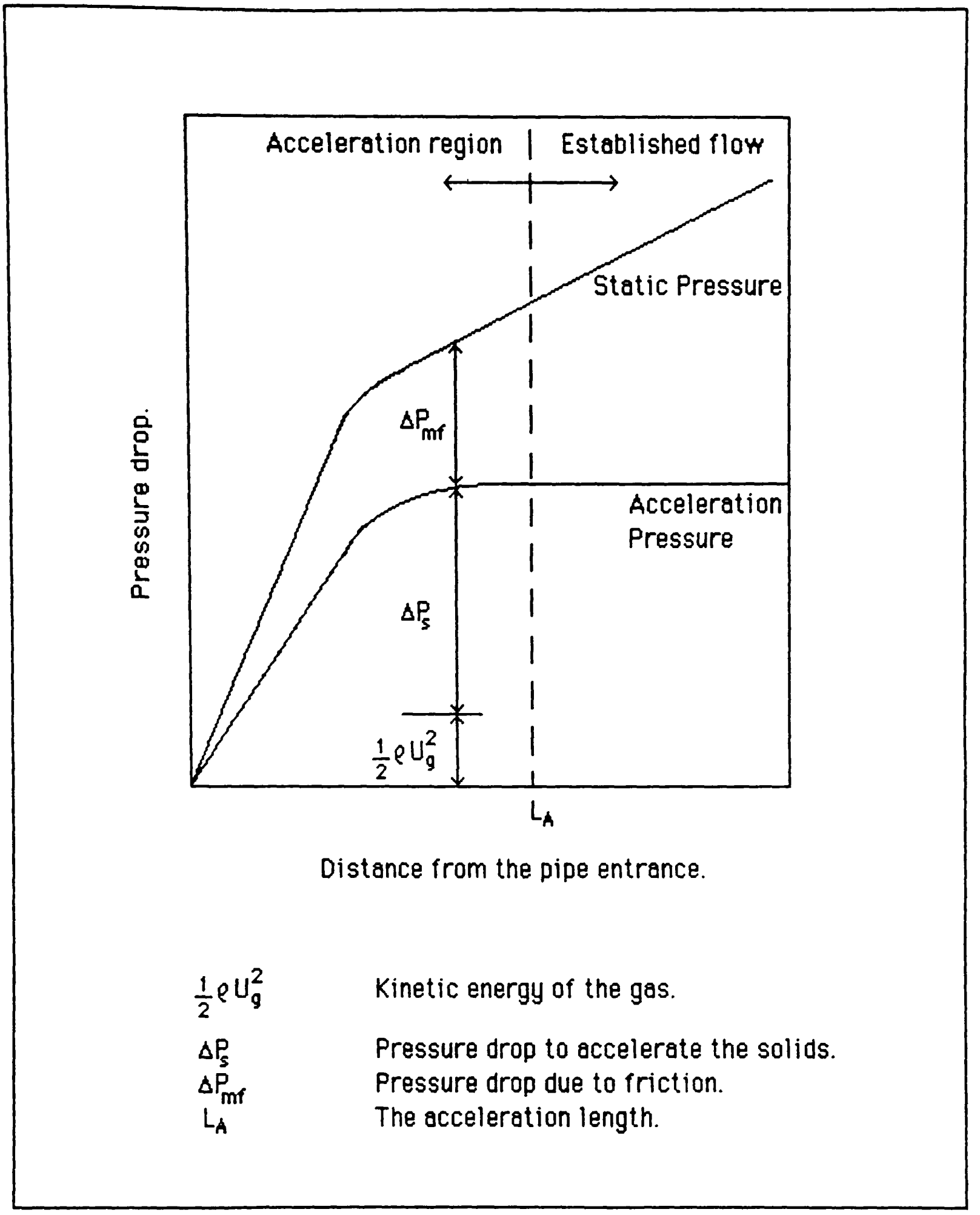

$\frac{1}{2}\rho U_g^2$	Kinetic energy of the gas.
ΔP_s	Pressure drop to accelerate the solids.
ΔP_{mf}	Pressure drop due to friction.
L_A	The acceleration length.

Figure 5.5.4.1 The composition of the drop in static pressure for the transport of solids in a gas.

The performance of the mathematical model was assessed on the basis of three criteria:

i the prediction of the total pressure drop;
ii the prediction of the *acceleration* length;
iii the prediction of the pressure gradient in the *established flow* region.

Figures 5.5.4.2 and 5.5.4.3 show the variation of pressure along the pipeline from experimental data and the predictions of the mathematical model.

Considering the lower values of solids loading ratio (4.74 and 5.71) the prediction of the model judged on each criteria is very good. The total pressure drop prediction and the pressure gradient in the *established flow* region are very close.

In the *acceleration* region the pressure gradient is not as steep initially, but the *acceleration* length (the distance for the flow to become fully developed) is similar. At the pressure tapping 2.0 m from the inlet the errors in pressure prediction for the solids loading ratios 4.74 and 5.71 are 15.8% and 17.6% respectively. This is comparable to the accuracy of the experimental measurements where:

i the mass flow rate of solids could be measured to within 10%;
ii the pressure to within 5 mmH_2O (0.5 mbar).

Although the error in the pressure measurement is negligible, the error in mass flow measurement could be significant since there is only 20% difference in the solids mass flow rate from a solids loading ratio of 4.74 to 5.71.

For comparisons at solids loading ratios of 10.16 and 12.58 a different picture is presented. The total pressure drop is predicted reasonably well, as is the initial part of the *acceleration* region. The major difference is seen in the pressure gradient in the *established flow* region.

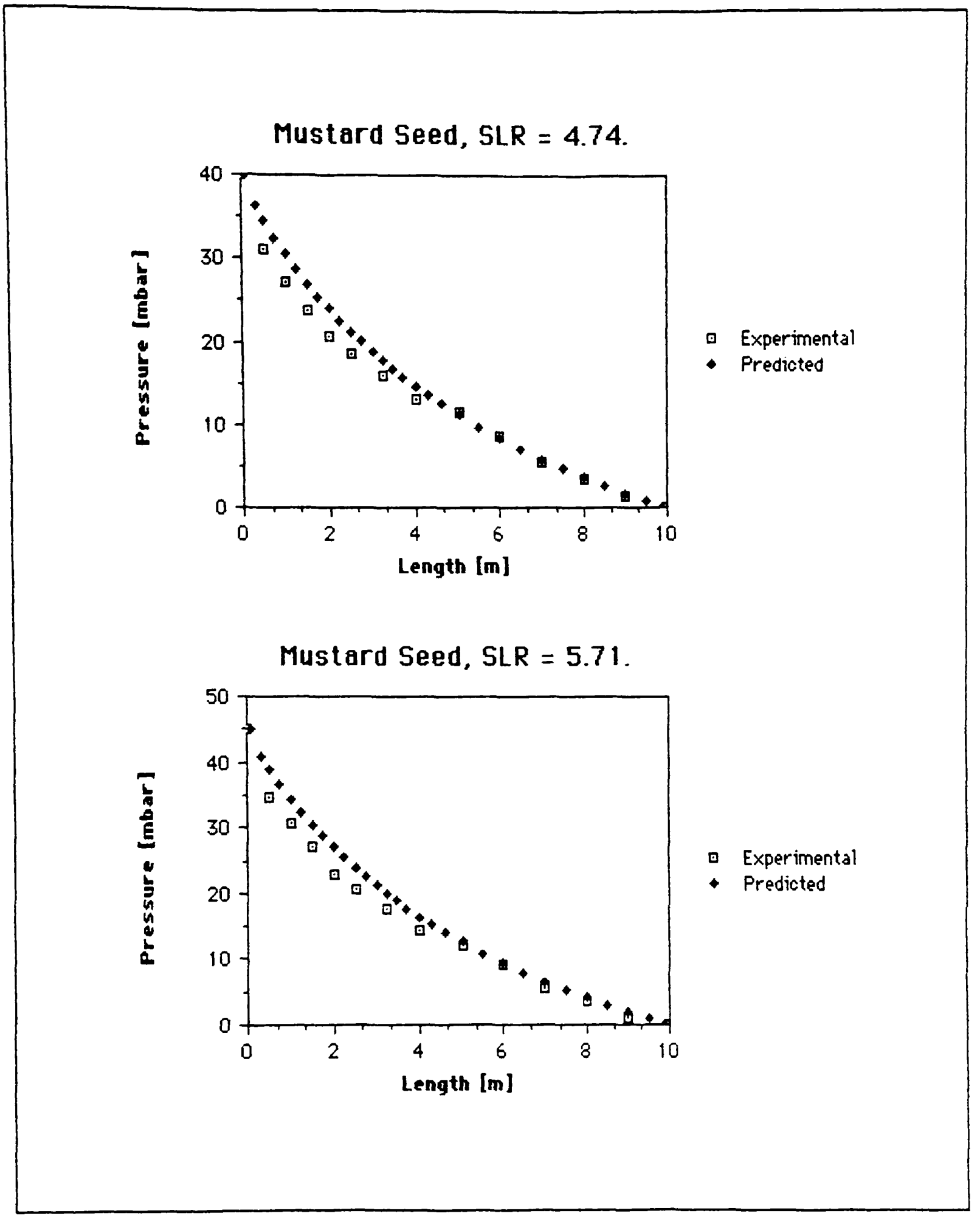

Figure 5.5.4.2 A comparison of the pressure drop prediction of the model with experimental data (SLR =4.74 and 5.71).

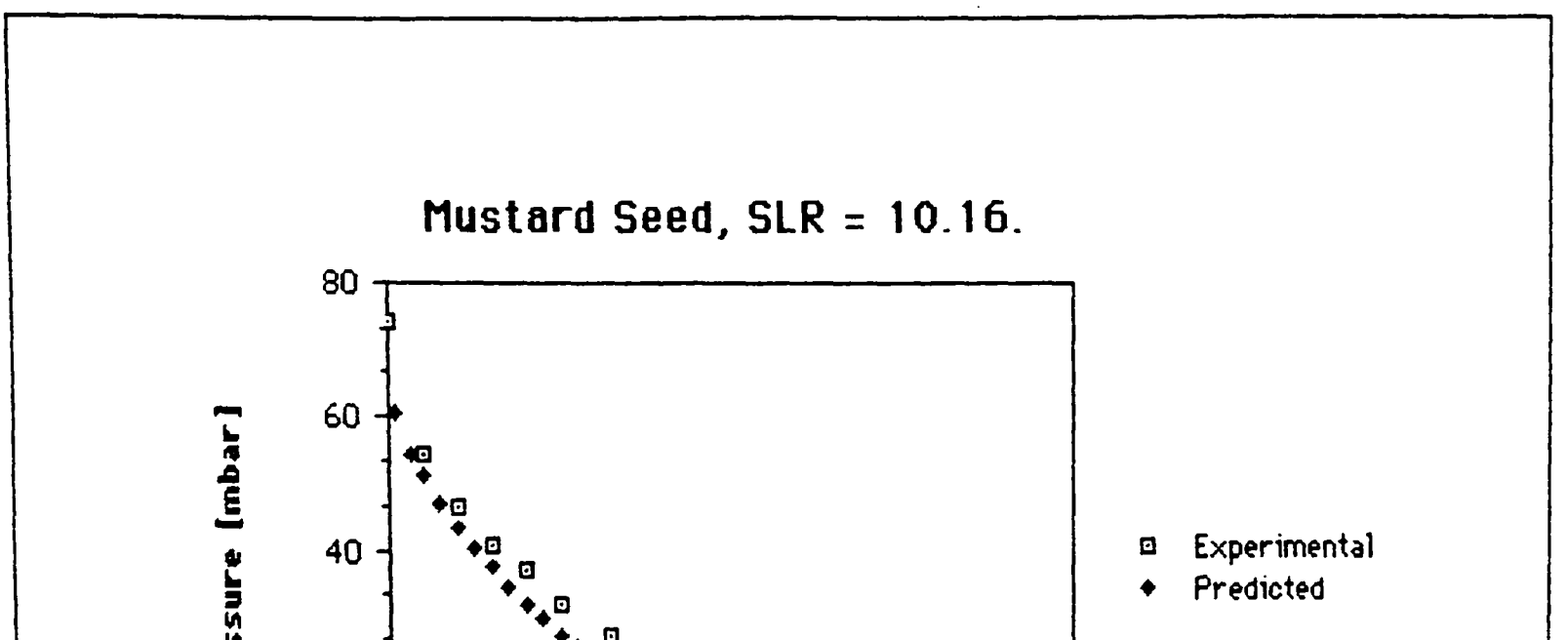

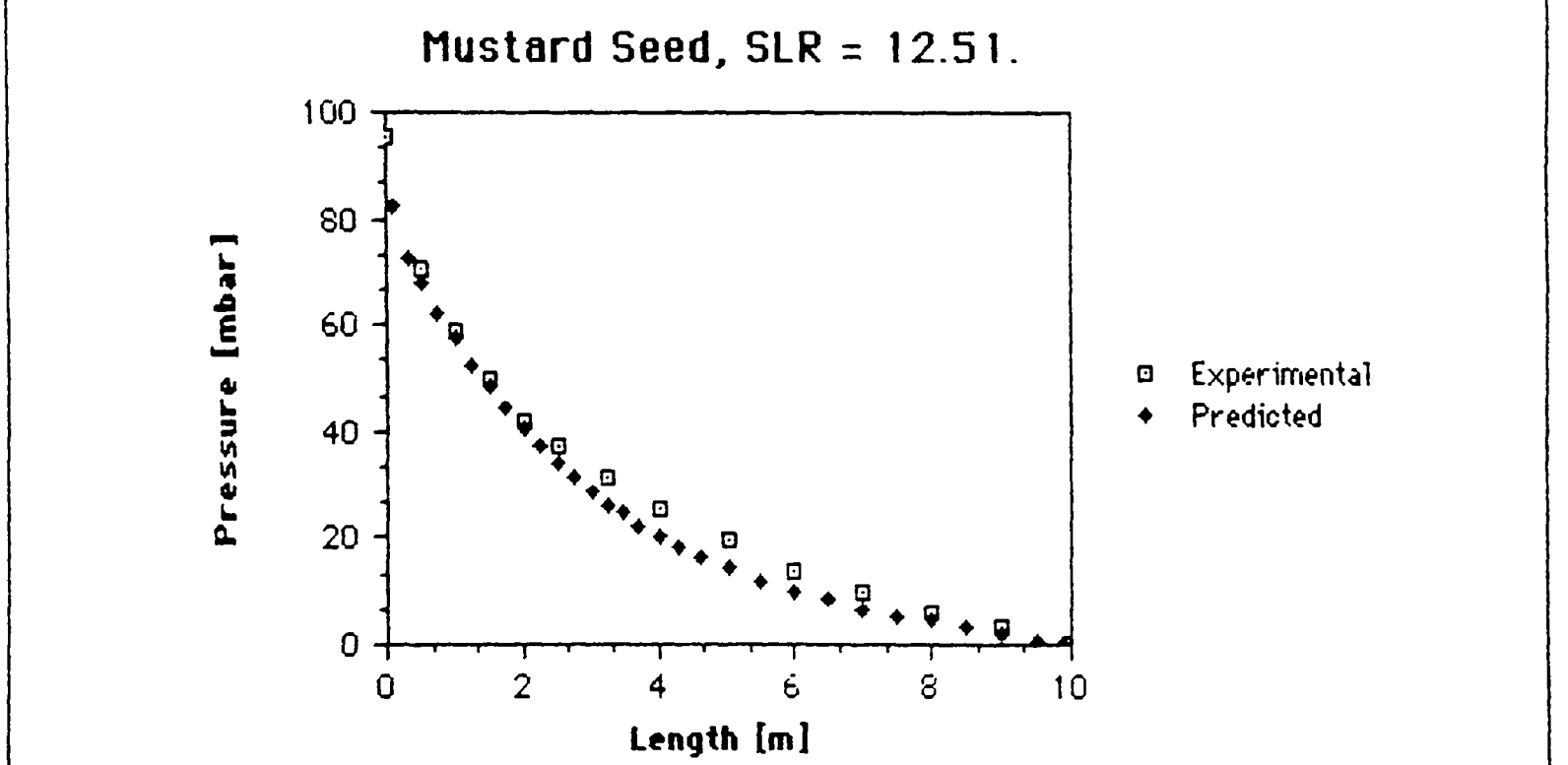

Figure 5.5.4.3 A comparison of the pressure drop prediction of the model with experimental data (SLR=10.16 and 12.51).

Figure 5.5.4.4 shows all the experimental data plotted together and all the predicted values on a separate graph. In the case of the experimental data the pressure gradient in the *established flow* region increases with the solids loading ratio and there is a notable difference between a solids loading ratio of 5 and a ratio of 10. The model predicts a similar pressure gradient for all values of the solids loading ratio. The difference between the experimental data and model predictions is due to the simplified model for the particle-wall interactions, ie the assumption of negligible particle-wall effects is only reasonable for a bulk material when the solids loading ratio is less than 5. The major component of the pressure drop occurs in the *acceleration* region where the assumption of the drag force as the dominant effect is accurate for the whole range of solids loading ratios tested.

5.5.5 THE PREDICTION OF SOLIDS CONCENTRATIONS

Visual observation of suspension flow in a pipeline is difficult since at velocities between 15 ms^{-1} and 30 ms^{-1} the flow is a blur, figures 5.5.5.1 to 5.5.5.3 show the predicted variations of solids volume fraction. Morikawa et al (1986) used an optical fibre probe to count particles flowing in a pipeline. Figure 5.5.5.4 reproduces their measurements of solids concentration. The following points should be noted about these measurements:

i the material conveyed was polystyrene in the form of spherical pellets (d_s = 0406 mm, ρ_s is not stated but is approximately 1050 kgm^{-3});
ii measurements were made in the *established flow* region (5.21 m downstream of the solids feed device);
iii the measuring device is intrusive and could have influenced the results.

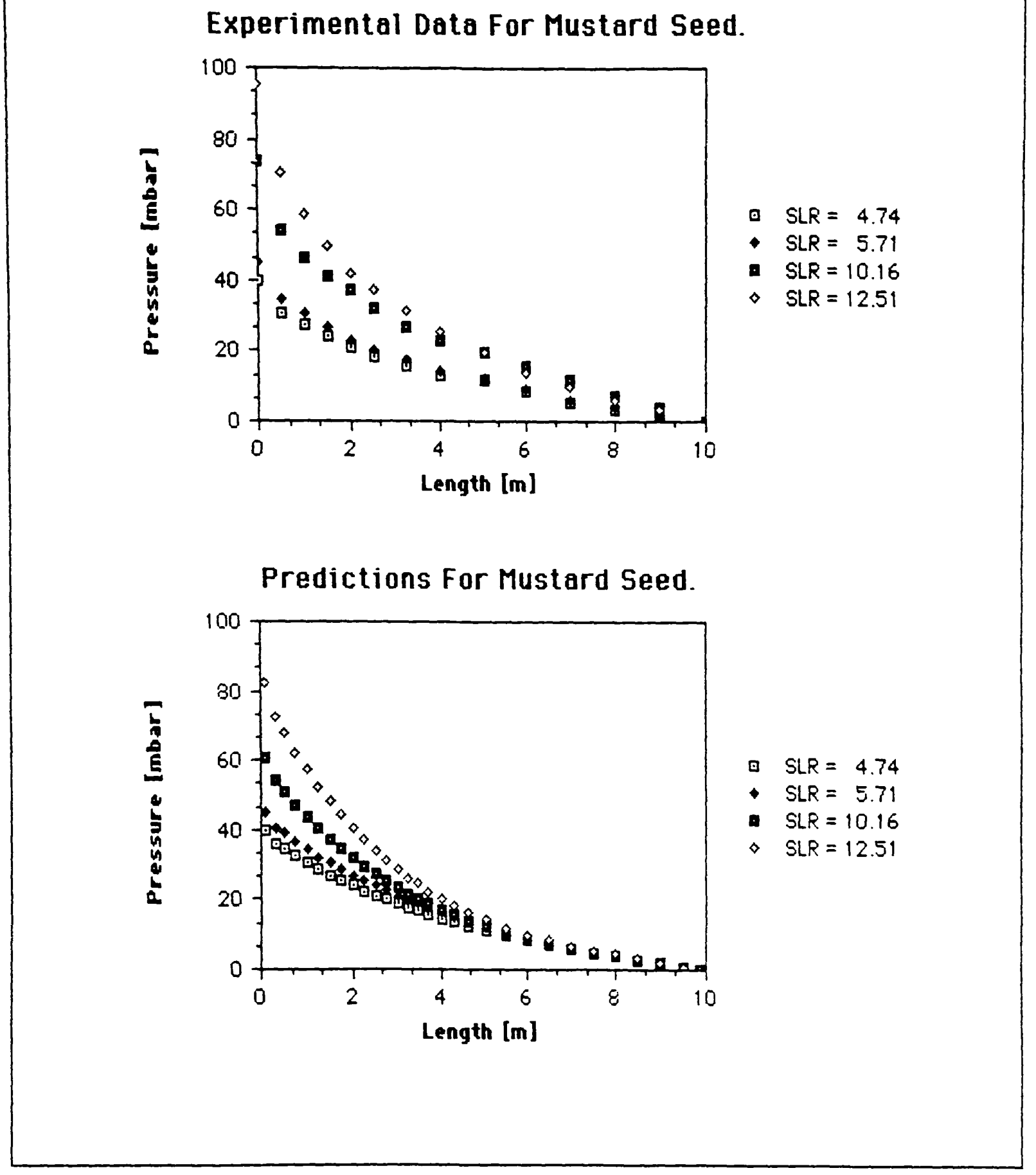

Figure 5.5.4.4 Comparison of the experimental data and predictions of the model separately.

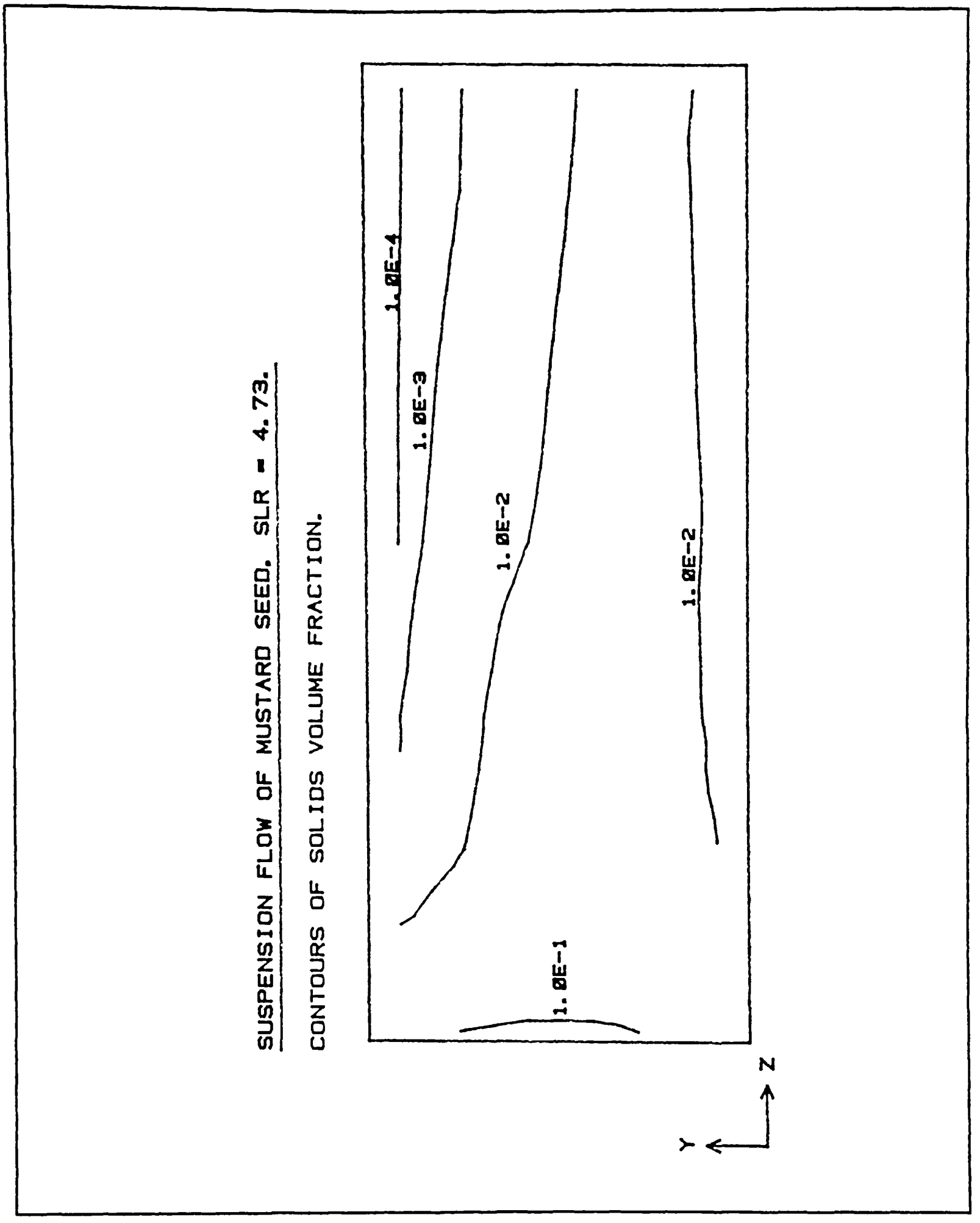

Figure 5.5.5.1 Contours of solids volume fraction for suspension flow of mustard seed (SLR = 4.73).

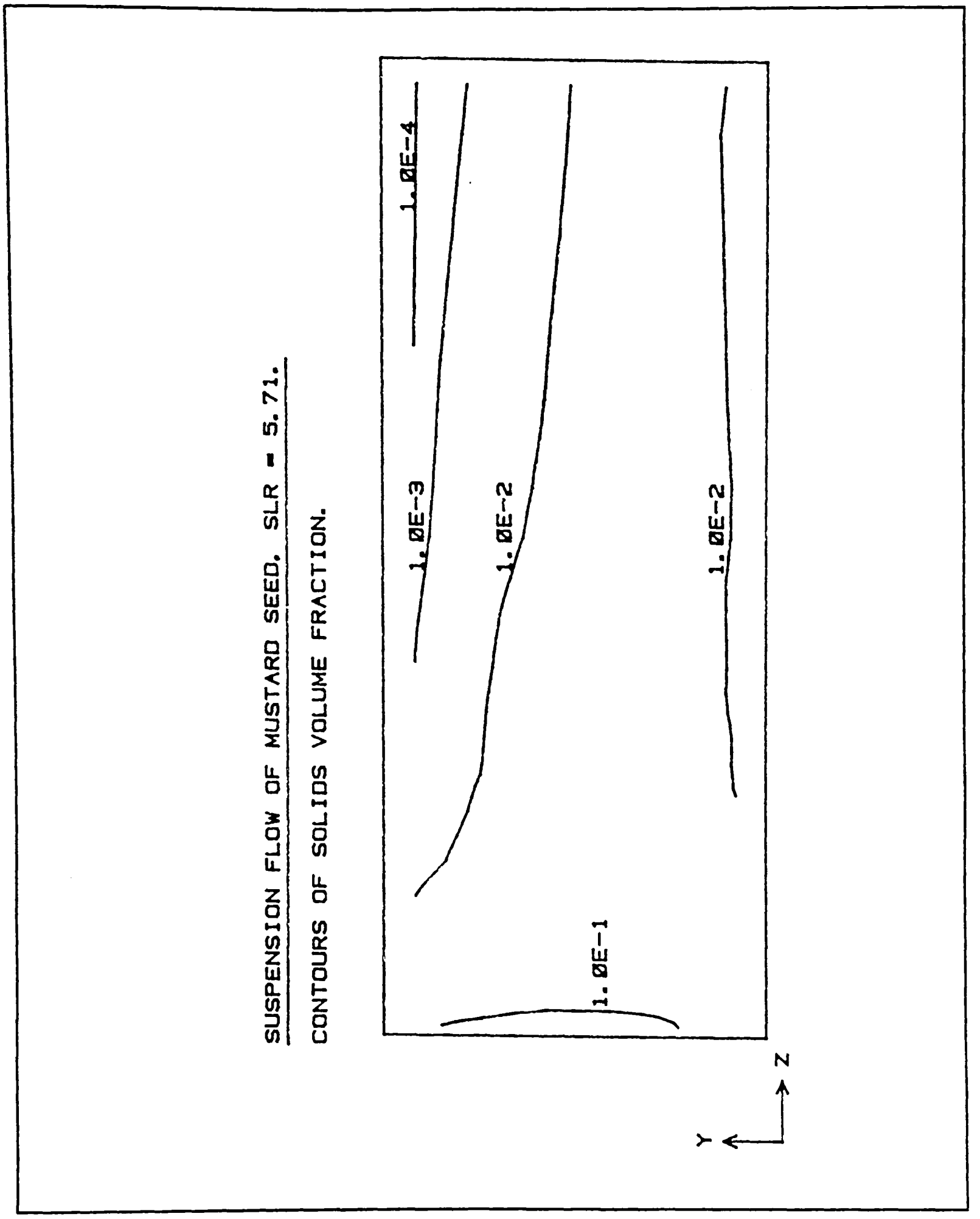

Figure 5.5.5.2 Contours of solids volume fraction for suspension flow of mustard seed (SLR = 5.71).

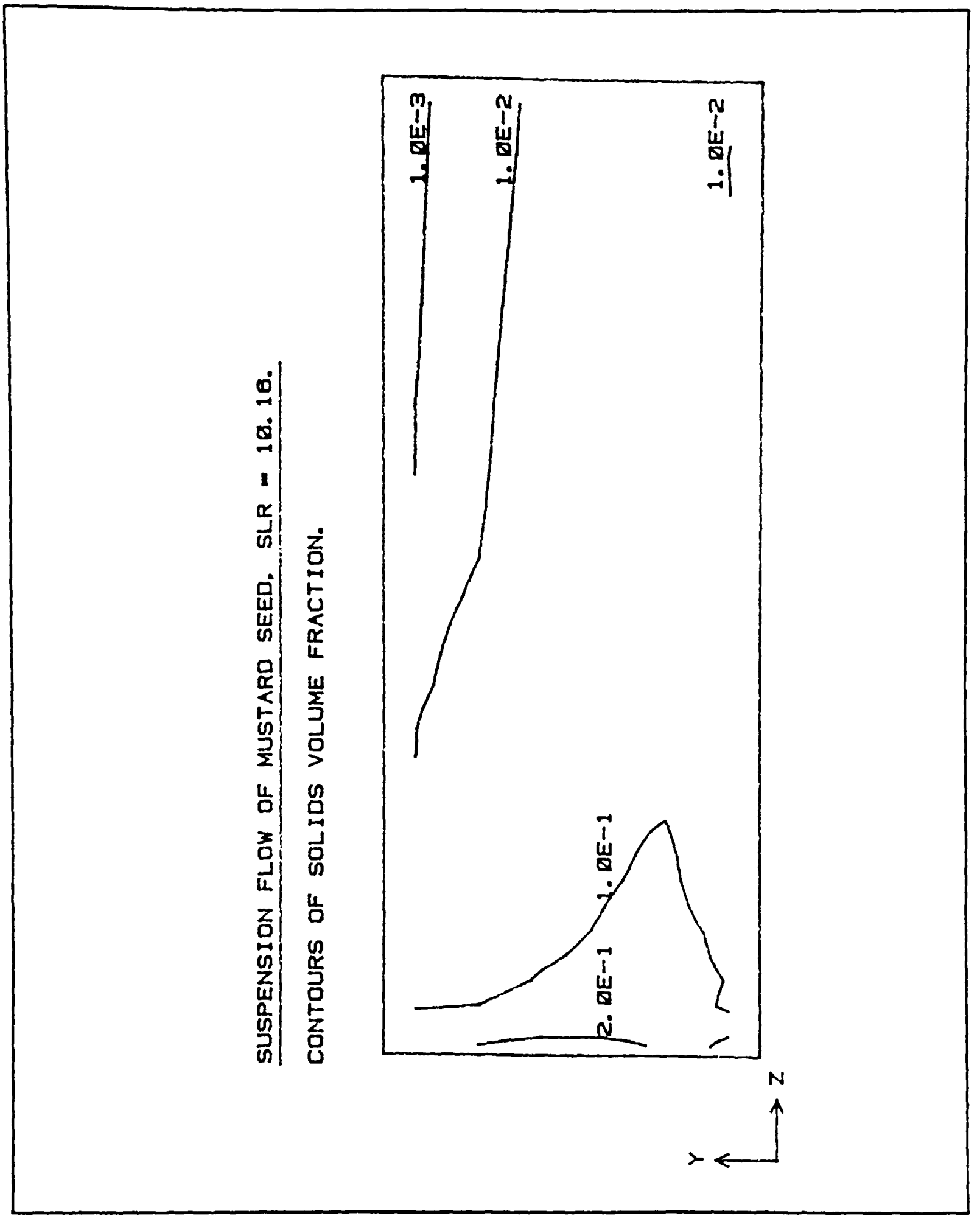

Figure 5.5.5.3 Contours of solids volume fraction for suspension flow of mustard seed (SLR = 10.16).

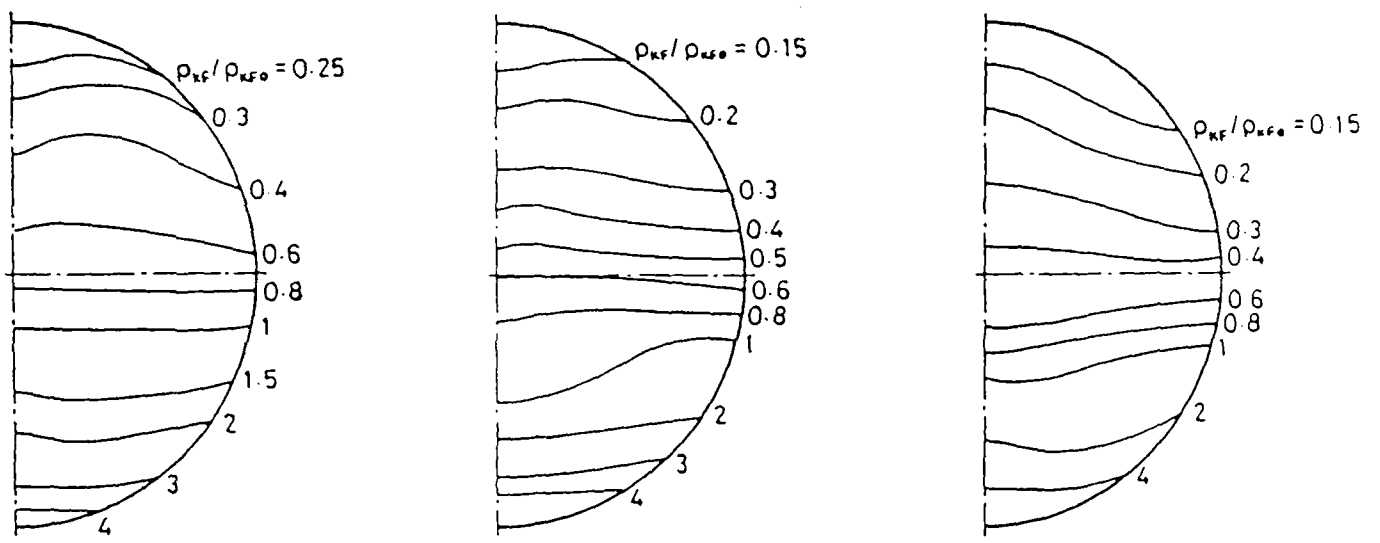

Figure 5.5.5.4 Solids concentration in the established flow zone Morikawa et al (1986).

The dispersed density, ρ_{KF}, is defined by:

$$\rho_{KF} = \frac{m_s n}{\frac{\pi}{6} d_s^3 A} = \rho_s R_s \qquad 5.5.5.1$$

The mean dispersed density, ρ_{KFO}, is defined by:

$$\rho_{KFO} = \frac{1}{A} \int_A \rho_{KF}\, dA = \sum_{i=1}^{n} \rho_{s,i} R_{s,i} \qquad 5.5.5.2$$

ie the mean dispersed density at a cross-section is the sum of $\rho_s R_s$ for each control volume in the cross-section. Figure 5.5.5.5 shows Morikawa's data in terms of solids volume fraction, R_s, along the vertical centre-line of the pipe, and the model's predictions for a solids loading ratio of 5.71 in the *established flow* region 8.1 m from the inlet. Table 5.5.5.1, shows the difference between Morikawa's data and the values used in the model:

QUANTITY	MORIKAWA	PRESENT STUDY
Bulk material	Polystyrene pellets	Mustard seed
Particle shape	Spherical	Spherical
Particle size	0.406 mm	1.54 mm
Particle density	1050 kg m^{-3}	1130 kg m^{-3}
Solids loading ratio	6.66	5.71
Superficial gas velocity (at ambient conditions)	9.99 ms^{-1}	25.0 ms^{-1}

TABLE 5.5.5.1 Comparison of Morikawa's test data with data used in the present study.

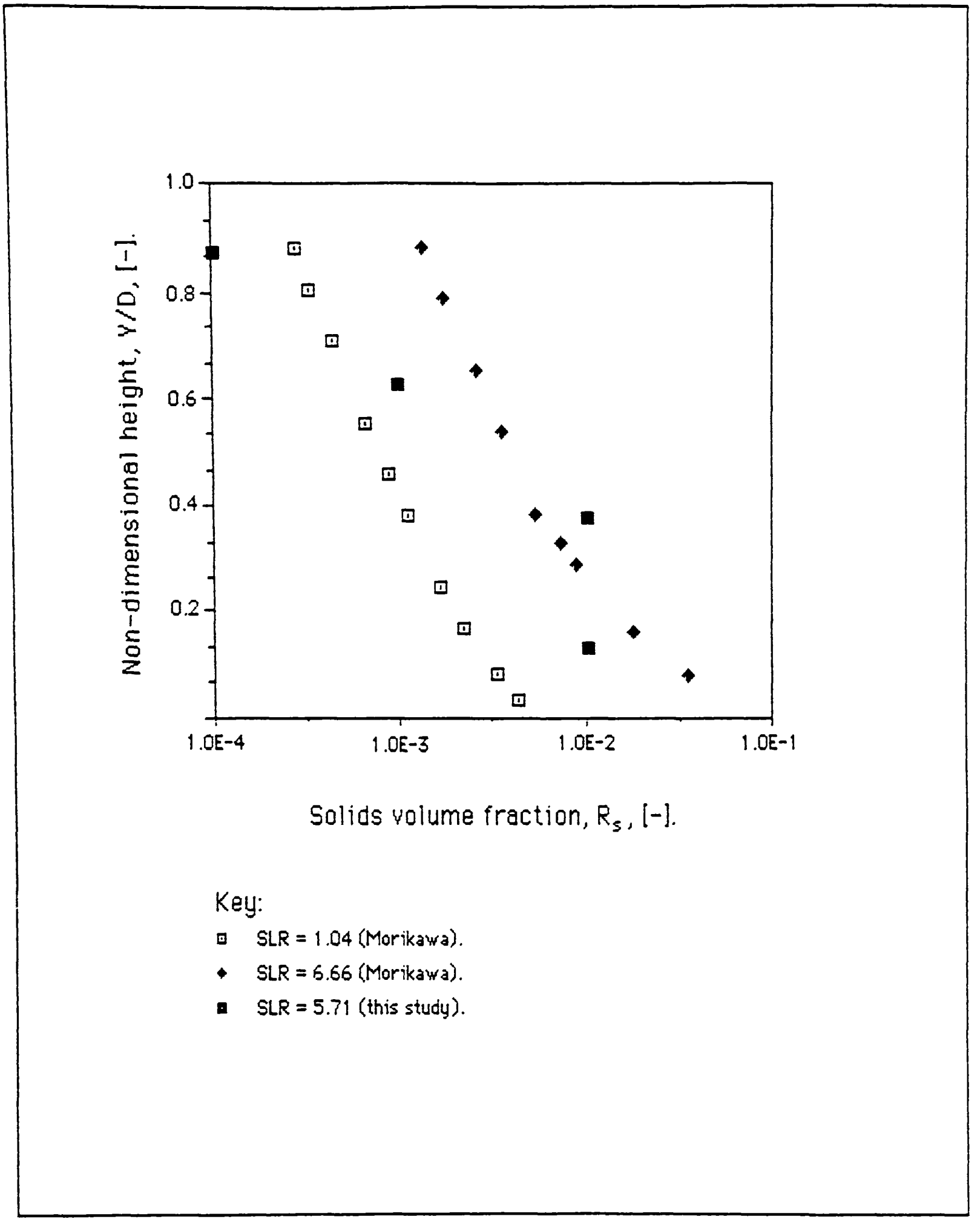

Figure 5.5.5.5 The distribution of solids in a horizontal pipe in the established flow region.

The main difference between the two cases is the superficial gas velocity. The higher gas velocity leads to a more uniform distribution in the lower half of the horizontal pipe. The solids volume fraction is distributed similarly and the order of magnitude is the same.

5.6 SUMMARY OF MODEL PERFORMANCE

Comparison of the performance of the mathematical model with experimental data over a range of solids loading ratios has shown that:

i. the pressure distribution in the pipeline and the total pressure drop are well predicted;
ii. the distribution of solids in the pipeline is similar to that expected;
iii. in the *acceleration* region of the pipe the dominant force on the particles is the aerodynamic drag force;
iv. as the solids concentration increases the assumption that particle-wall effects are of the same order as gas-wall effects is less accurate, and indicates a need to refine the model.

All results must be judged on the assumption made of the interaction of the particles with turbulence in the gas phase. The lack of experimental correlations for this phenomenon give little scope for anything except the assumption of a constant effect.

6 NON-SUSPENSION MOVING-BED FLOW

6.1 INTRODUCTION

When the conveying gas velocity is reduced to a value below the saltation velocity the mode of flow begins its transition from suspension flow to non-suspension flow. Figure 6.1.1 shows the development of the moving-bed mode of non-suspension flow. Jones and Mills (1989) correlated the mode of flow of a bulk material in a pneumatic conveying system with its fluidisation properties. Bulk materials such as cement, flow and pulverised fuel ash often exhibit a non-suspension moving-bed mode of flow. These products are characterised by a low de-aeration rate constant and a low permeability factor. Table 6.1.1 shows a list of bulk materials with their fluidisation properties and observed modes of non-suspension flow.

The starting point for the development of a mathematical model for moving-bed non-suspension flow is the suspension flow model that had been developed previously. Examination of the deficiencies of this model, together with an analysis of the extra physical phenomena that are encountered, will lead to the evolution of a mathematical model for this mode of non-suspension flow.

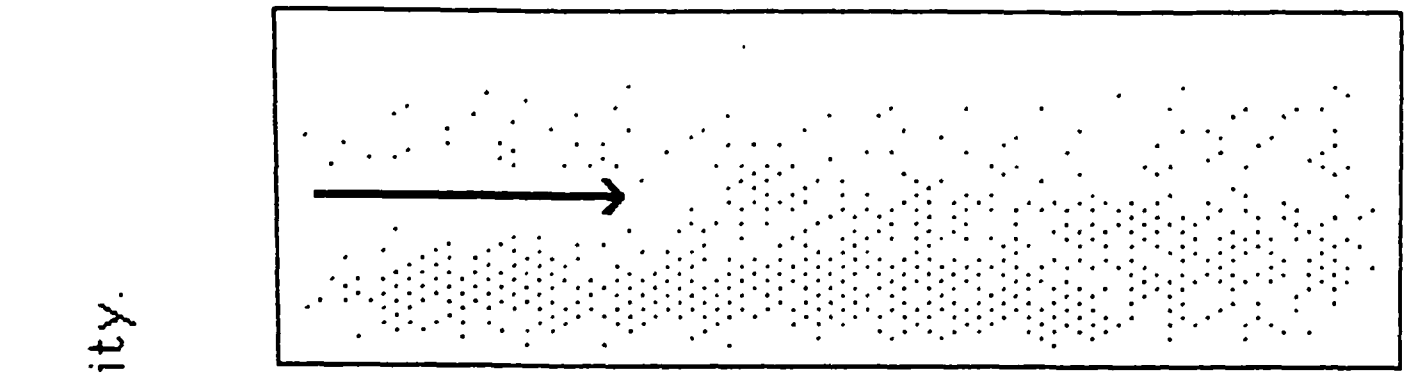

Particles suspended in the conveying gas. Main concentration is in the lower half of the pipe.

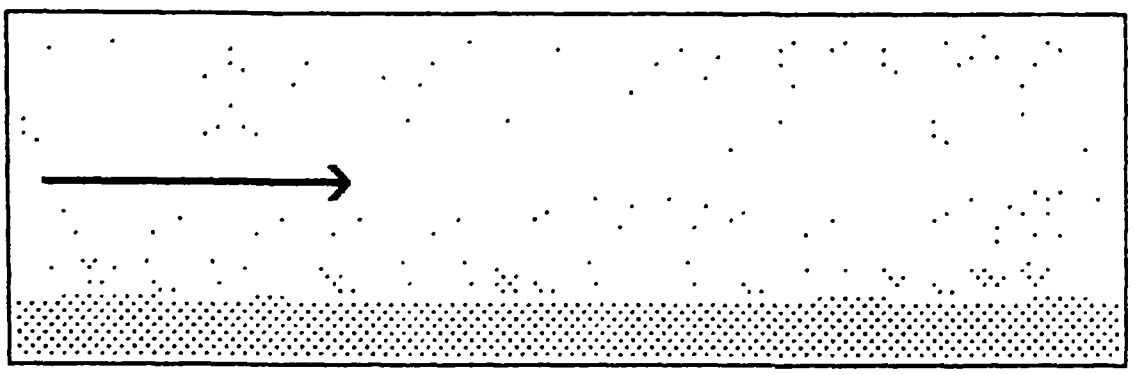

Just below the saltation velocity. Most particles suspended some in strands on the pipe wall. Particles in the strands roll along the pipe wall.

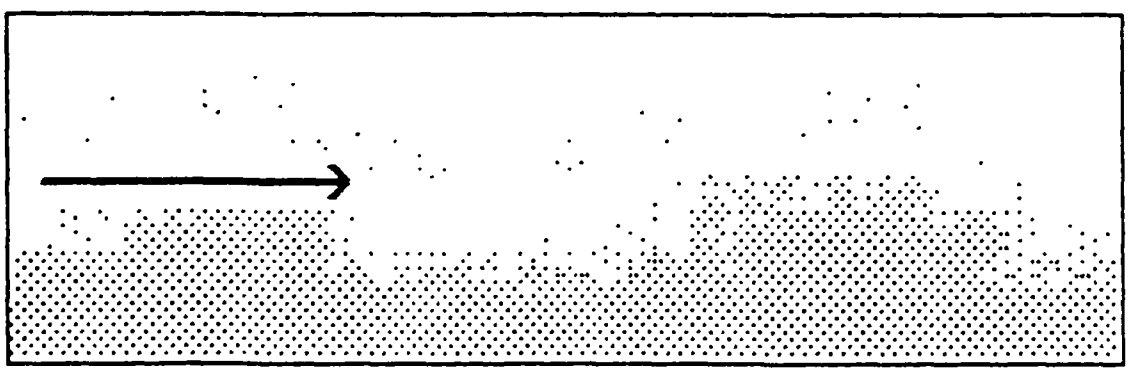

Moving-bed flow. The bulk material in the moving-bed is fluidised. The depth of the bed fluctuates with the amplitude increasing as the velocity is reduced ie the flow becomes pulsatile.

Increasing conveying gas velocity.

Figure 6.1.1 Flow patterns in the development of non-suspension moving-bed flow in a horizontal pipeline.

No.	Product Name	Geldart Classifi-cation	Dixon Classifi-cation	Density Particle (Bulk) kg/m^3	Particle Size Mean (2.5% / 97.5%) μm	Observed Mode of Conveying
1	Mustard Seed	D	D	1180 (680)	11650 (1100/2350)	Plug
2	Polyethylene Powder	B	D	990 (480)	825 (209/2100)	Plug
3	Slate Dust	B	D	2860 (1280)	500 (10/1850)	Dilute
4	Coarse Sand	D	D	2620 (1540)	1020 (820/1400)	Plug
5	Zircon Sand	B	B	4610 (2600)	115 (75/185)	Dilute
6	Cement	A	A	3160 (1030)	22 (2/64)	Moving bed
7	Pulverised Coal	A	A	1500 (610)	44 (1/90)	Moving bed
8	Pulverised Fuel Ash (Grits)	D	D	2380 (400)	700 (20/2250)	Dilute
9	Polyethylene Pellets	D	D	914 (558)	3850 (-)	Plug
10	Granulated Sugar	B	D	1590 (820)	720 (-)	Plug
11	Pearlite	A	B	800 (100)	200 (50/900)	-
12	Flour	A	A	1470 (514)	78 (40/120)	-
13	Pulverised Fuel Ash	A/C	A/C	2450 (980)	20 (-)	Moving bed

Table 6.1.1. A summary of bulk material characteristics.

6.2 DEVELOPMENT OF THE MATHEMATICAL MODEL

6.2.1 DEFICIENCIES OF THE SUSPENSION FLOW MODEL

One of the major assumptions made in the suspension flow model was that no particle-particle interactions occurred and that the gas flow field around each particle was unaffected by neighbouring particles. This was reflected in the model by the absence of a particle-particle force and by the use of a drag coefficient based upon the flow of an individual particle.

As the volume fraction of solids increased the accuracy of the prediction of the pressure in the established flow region worsened due to the simplified model for particle-wall interactions. Collision of particles with the pipe wall is an additional loss of momentum. The exclusion of this phenomenon was highlighted by the lower pressure gradient predicted by the model when compared to experimental data.

The suspension flow model contains no mathematical model that would limit the solids volume fraction. When the particles which comprise a bulk material pack together there are always gaps between the particles. These gaps, or voids, are most frequently measured by the bulk density of the material. The bulk material is poured into a container of known volume and then weighed. The mass in the container divided by the volume of the container is the poured bulk density. This can be related to the volume fraction of the bulk material by the particle density.

$$R_s = \frac{\rho_B}{\rho_s} \qquad 6.2.1.1$$

The assumption that the solids phase is a continuum requires a mathematical model for particle packing. In the absence of such a model the solids volume fraction could reach unrealistic values.

6.2.2 PARTICLE-PARTICLE EFFECTS

Workers in the field of fluidised beds have approached the analysis of the fluidised bed by correlating the behaviour of a particle within the bed with that of a single unhindered particle. Richardson and Zaki (1954), Rowe (1961), Wen and Yu (1966) and Foscalo and Gibilaro (1984) have all used this approach. The outcome of the approach is a relationship between the single particle value and that in the fluidised bed, in terms of the voidage or gas volume fraction.
This approach combines a number of particle-particle effects into a single correlation. Phenomena such as particle collisions and alteration of the flow field are all included in such correlations. The application of fluidised bed relationships is valid since the key to successful moved-bed non-suspension pneumatic conveying is the ability of the bulk material to remain fluidised.

The majority of bulk materials that flow in a moving-bed type flow are Geldart (1973) group A materials. These exhibit a homogeneous expansion in a gas fluidised bed similar to liquid fluidised beds. Thus a wide range of correlations, such as Richardson and Zaki (1954), that were developed for liquid fluidised beds could be used. The correlation used was developed by Foscolo and Gibilaro (1984). The drag coefficient of a single particle was modified by a function of the gas volume fraction:

$$C_{D\ multi\text{-}particle} = C_{D\ single\ particle}\, R_g^{\,n} \qquad n = -3.8 \qquad 6.2.2.1$$

This relationship was most accurate in the laminar ($Re_s < 0.2$) and fully turbulent ($Re_s > 500$) regions. This formulation allows a simple extension of the suspension flow model by modifying the interphase friction force.

6.2.3 PARTICLE-WALL EFFECTS

In horizontal pipes the majority of the particles flow in a fluidised strand of material along the bottom of the pipe. Observation of the flow in the glass sections of the test pipeline show that the particle-wall interaction is a frictional one, due to particles sliding along the wall rather than particles colliding with and bouncing off the wall. Konrad (1980) assumed Coulomb-type friction, that is, the wall friction is proportional to the weight of material above the wall. Hitt (1985) evaluated several methods to determine a reliable value for the coefficient of sliding friction between a bulk material and pipe material. The difficulty is in relating the results of a static shear test to the flow of a fluidised material. Figure 6.2.3.1 shows an annular ring shear cell that was regarded as most reliable by Hitt (1985). For a fluid the shear stress at the pipe wall is described by:

$$\tau_w = f \frac{1}{2} \rho \overline{U}^2 \qquad 6.2.3.1$$

where

$$f = \frac{\Delta P^*}{4} \frac{D}{L} \frac{1}{\frac{1}{2}\rho \overline{U}^2} \qquad 6.2.3.2$$

ΔP^* is the difference in piezometric pressure, which is the same as the static pressure difference when there is no change in elevation. For Coulomb friction:

$$\tau_w = \mu_w \rho g h \qquad 6.2.3.3$$

where μ_w is the coefficient of sliding friction and ρgh is the weight of material above the wall. Figure 6.2.3.2 shows the arrangement of control volumes for a typical two-dimensional channel. The static pressure of the solids above the bottom wall of the channel was evaluated by:

$$\rho g h = \sum_{iy=1}^{ny} R_s \rho_s \cdot g \cdot \frac{\sum_{iy=1}^{ny} R_s y}{ny \sum_{iy=1}^{ny} R_s} \qquad 6.2.3.4$$

This relationship allows contributions to the wall friction by particles flowing in suspension above the moving-bed. This was deemed reasonable since the error would be small due to the very low volume fraction, Rs, in the region. This also eliminated the need to specify a critical volume fraction, or find the level of the surface of the moving-bed. This latter point is important since the general mathematical model assumes a uniform distribution of each quantity throughout the central volume (which is not the case when the surface passes through the control volume).

The formulation of the wall friction for the solids replaces the friction factor for a fluid with one based upon the Coulomb sliding friction between the particles and the pipe wall. The assumption of a velocity profile is still required. This was assumed to be similar to that for a fluid with zero velocity at the pipe wall. This represents the *worst case* since the particles will have some velocity, but it is reasonable in view of the lack of experimental data for this phenomenon.

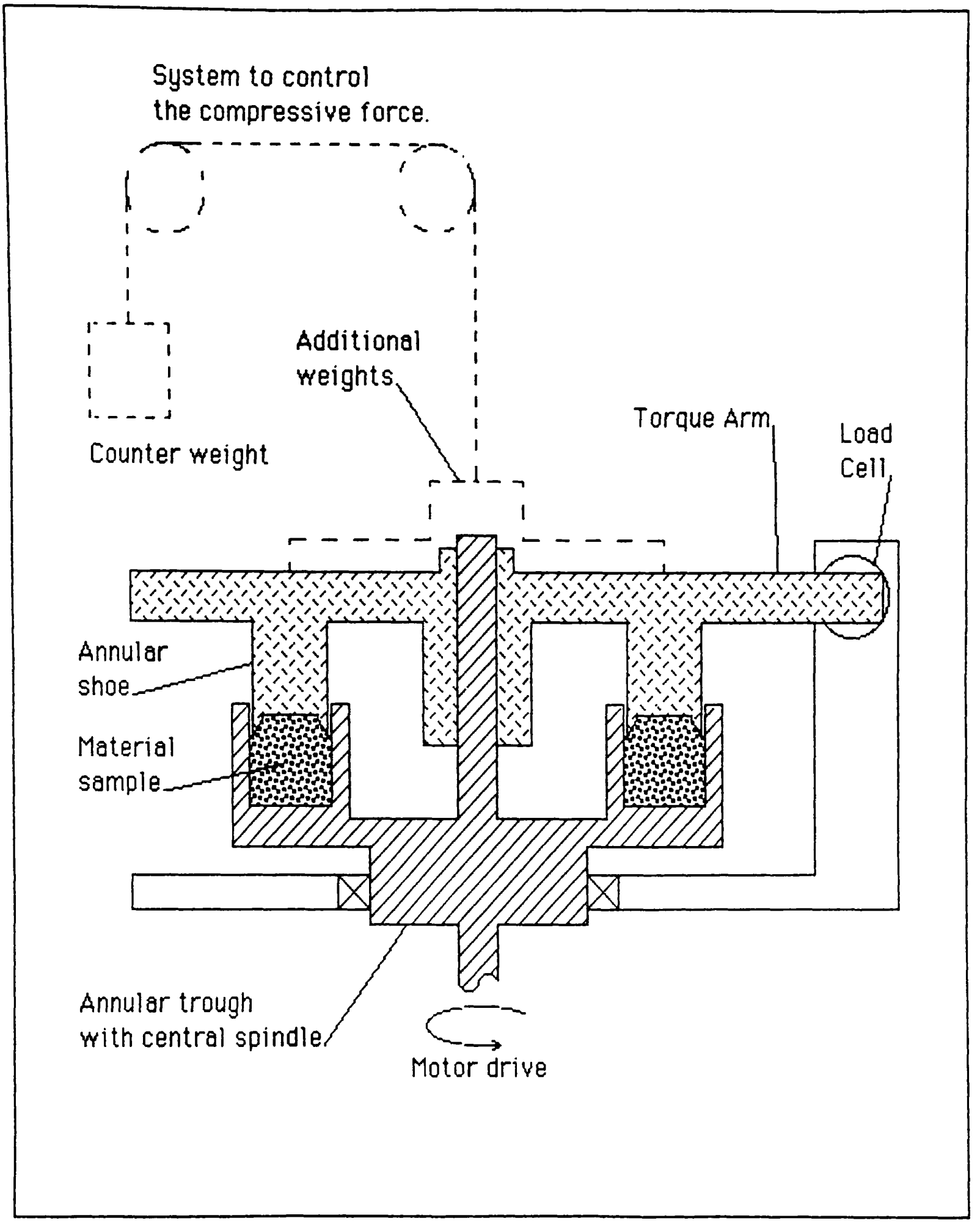

Figure 6.2.3.1 The annular ring shear cell.

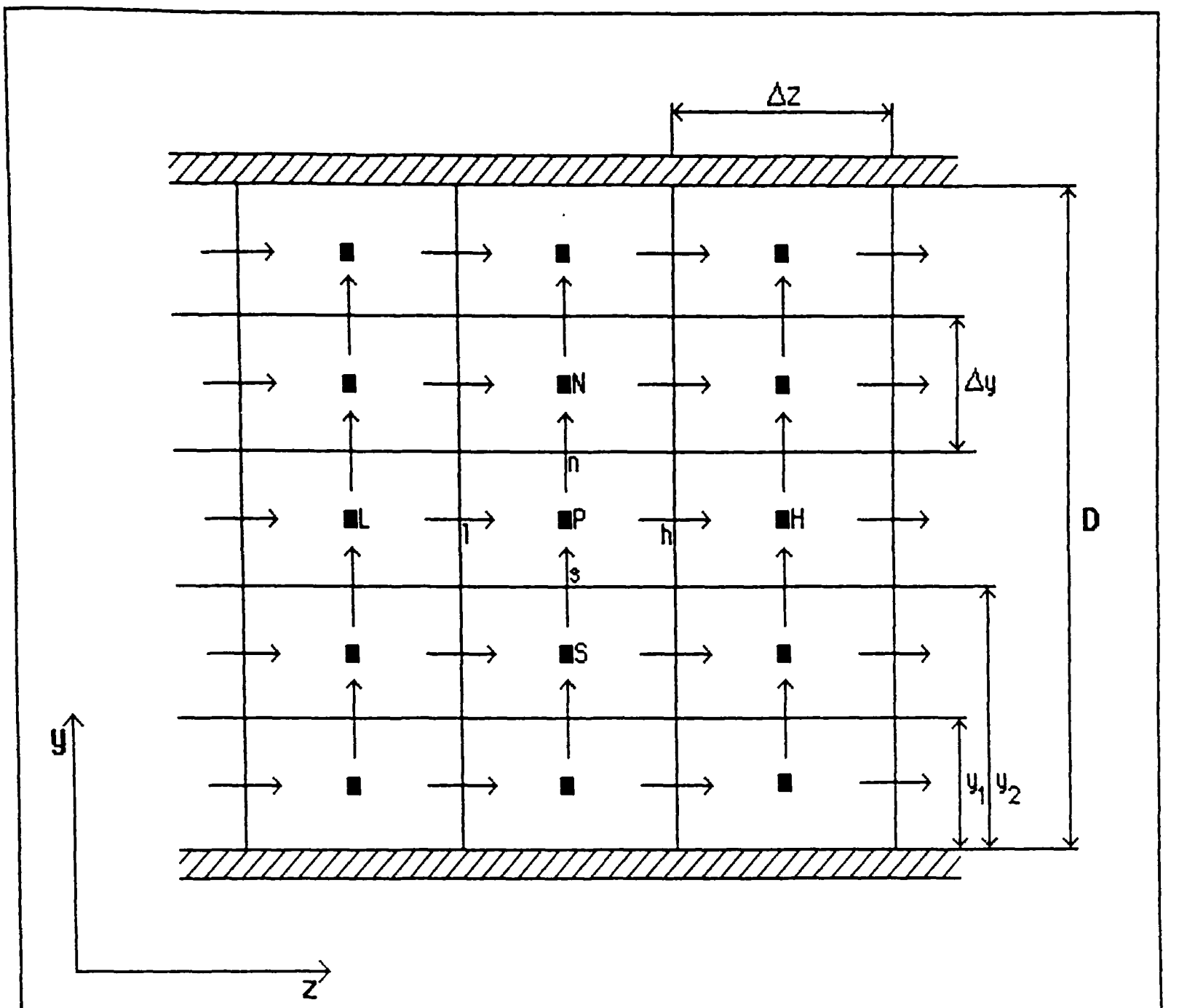

Width of channel, $\Delta x = \frac{\pi}{4} D$

Control volume size, $V_{cell} = \Delta x \Delta z \Delta y$

Coefficient of friction, μ_{wall}

$$\rho = \sum_{iy=1}^{ny} (R_s \rho_s)_{iy} \qquad H = \frac{\sum_{iy=1}^{ny} (R_s y)_{iy}}{ny \sum_{iy=1}^{ny} (R_s)_{iy}} \qquad \tau_{wall} = \mu_{wall} \rho g H$$

Figure 6.2.3.2 Wall friction model for the solids phase in a horizontal two-dimensional channel.

6.2.4 PARTICLE PACKING

A mathematical model is required to describe the forces due to the packing of particles so that the volume fraction of solids does not become physically unrealistic. Markatos (1986) introduced a source term for the momentum conservation equation to describe this *intergranular stress*:

$$\begin{aligned} \tau &= 0 && 0 \le R_s \le R_{s,critical} \\ \tau &= k(R_s - R_{s,critical})^n && R_{s,critical} < R_s \end{aligned} \qquad 6.2.4.1$$

k is a constant that represents the rate of change of stresses with respect to R_s. Markatos (1986) assumed a linear variation of stress with volume fraction, R_s, that is, n = 1.

6.2.5 DIFFUSION OF THE GAS OUT OF THE BULK MATERIAL

In the case of the momentum conservation equation the diffusion coefficient is specified by:

$$D = \rho_g R_g \left(\frac{\nu_T}{Pr_T} + \frac{\nu_L}{Pr_L} \right) \qquad 6.2.5.1$$

ν_T is the effective viscosity due to turbulence evaluated from a turbulence model such as the k-ϵ model. In this case no turbulence model is used since these only apply to single-phase flows. The effective viscosity is calculated from a function of the solids volume fraction:

$$D = \rho_g \, R_g \, \frac{\nu_L}{Pr_L} \, f(R_s) \qquad 6.2.5.2$$

Zuber (1963) reviews a number of such expressions where the effective viscosity of the two phase mixture is correlated with solids volume fraction. Most of these correlations are not suitable since they include physical phenomena that have been accounted for in the extension of the

inter-phase drag force to high concentration flows.

Sutton and Richmond (1973) apply Fick's law of diffusion to a fluidised bed and relates the de-aeration rate constant of the bed after the fluidising gas has been shut off to the diffusion coefficient.

$$\frac{dR_g}{dt} = k'.\frac{R_{g,t=\infty} - R_g}{Z} \qquad 6.2.5.3$$

Fick's law may be stated as:

$$\frac{\partial P}{\partial t} = \frac{\partial}{\partial z}\left(D\frac{\partial P}{\partial z}\right) \qquad 6.2.5.4$$

assuming a linear variation of pressure through the fluidised bed then

$$\frac{\partial P}{\partial t} = \frac{\partial D}{\partial z}.\frac{P - P_{t=\infty}}{z} \qquad 6.2.5.5$$

where $P_{t=\infty}$ is atmospheric pressure.

Since the pore pressure is linearly proportional to the mean voidage (gas volume fraction) in the bed:

$$-\frac{\partial R_g}{\partial t} = \frac{\partial D}{\partial z} \cdot \frac{R_{g,t=\infty} - R_g}{z} \qquad 6.2.5.6$$

and

$$\frac{\partial D}{\partial z} = -k' \qquad 6.2.5.7$$

This analysis shows good agreement with experimental data for homogeneous beds, that is, Geldart group A materials which flow in a moving-bed mode of non-suspension flow.

6.2.6 PARTICLE PRESSURE

Numerous approaches have been used to specify the *pressure* of the solids phase for use in the conservation equations. Spalding (1980), in his derivation of the general equations states that the shared pressure assumption (one pressure for all the phases that comprise the flow) is "correct for most practical circumstances". Markatos (1986) uses this assumption in a model for a gas barrel where a granular propellant is used. In this case a source term similar to the pressure gradient was added to the solids phase momentum equation to account for the shear stress due to particle packing. Foscolo and Gibilaro (1987) review a number of approaches to the *particle pressure* term. They conclude that physical phenomena such as particle-particle collisions and cohesive forces do not fully explain the behaviour of Geldart group A materials. The stable behaviour of gas fluidised beds of group A materials correlates well with particle size and density which "points strongly to a fluid dynamic controlling influence". The model developed in this work uses the shared pressure assumption.

6.2.7 DISCRETISATION OF THE FLOW DOMAIN

Unlike suspension flow, the convenient assumption of steady flow cannot be applied to non-suspension flow. The pipeline of the pneumatic conveying system was modelled as a two-dimensional channel with the same cross-sectional area as the pipe. The section of the pipeline modelled corresponded to the measuring section of the pipeline. This was located in the middle of the longest straight section, away from any bend effects. The pressure transducers were located at uniform intervals along the section. Similarly, the channel was divided into a number of control volumes of equal length in the axial direction. Figure 6.2.7.1 shows the grid of control volumes used. The size of the time-step was based upon the requirement to limit the distance travelled by particles to the length of a control volume in a single time-step.

In the model for suspension flow a transient analysis was used to produce a reasonable set of initial values for the steady state solution. In this case a fully converged solution is required for each time-step so that the variation of the flow with time can be assessed in addition to the time-averaged effects.

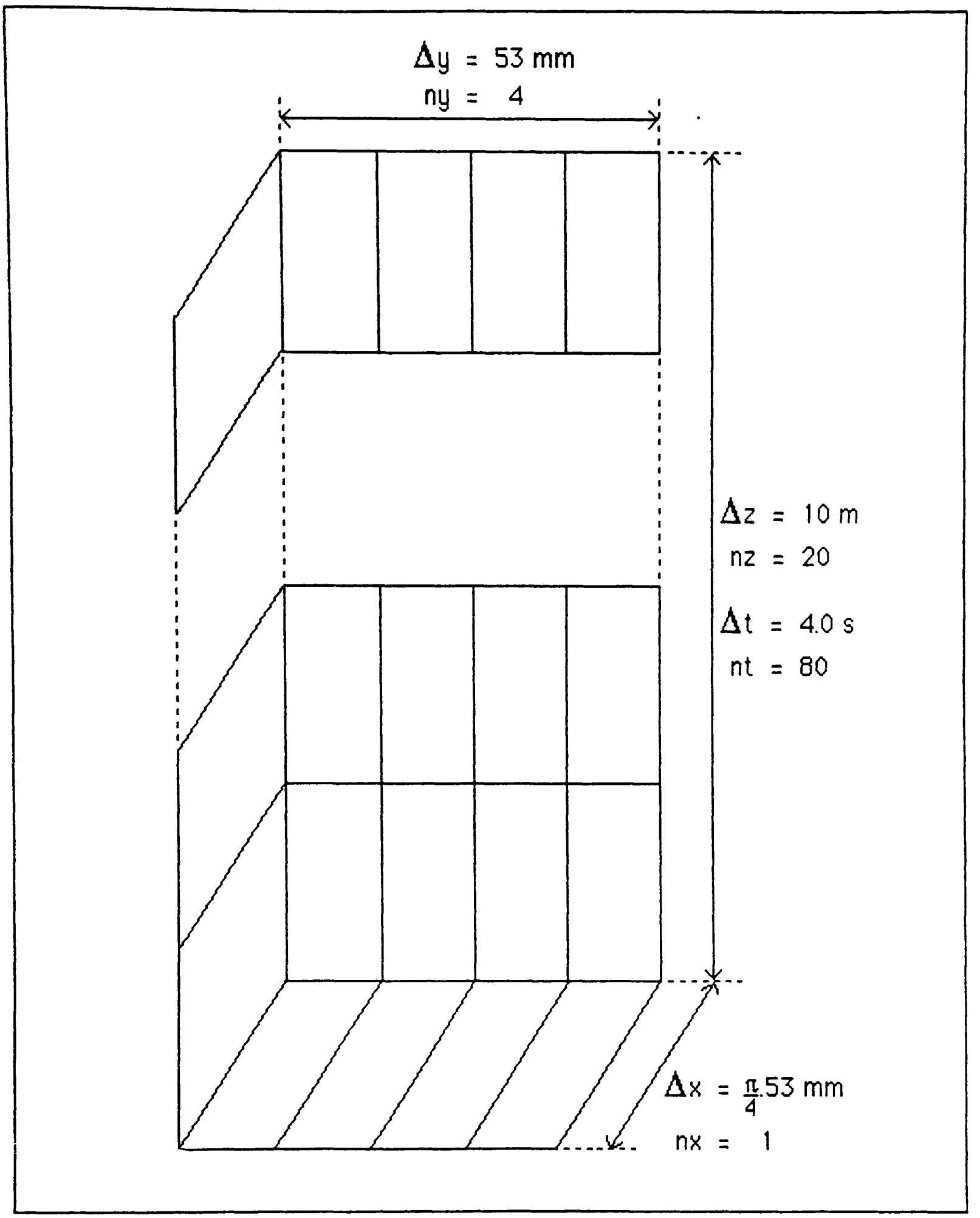

Figure 6.2.7.1 A typical control volume grid used for the moving-bed flow simulations, (transient two-dimensional).

6.3 EXPERIMENTAL INVESTIGATION

6.3.1 INTRODUCTION

The scope of the experimental investigation was determined by the data required to validate the mathematical model. Since the refinement of the model requires experimental data the experimental method and the mathematical model were developed in parallel. This section describes the evolution of the experimental technique and the interpretation of the data.

The development can be divided into two parts:

i. gathering global data;
ii. gathering detailed local information.

The former is necessary for control of the conveying system and for comparison with data from other sources. The latter provides the information required for the validation process. Figure 6.3.1.1 shows the system used to record both the global and local information. The data logger records information for subsequent analysis. The x, t chart recorder was used to monitor the current operating conditions of the pneumatic conveying system.

In order to conduct any experiments, a bulk material must be selected. Using Jones (1989) classification, figure 6.3.1.2, Ordinary Portland Cement was chosen as representative of bulk materials that are capable of moving-bed non-suspension flow. Figure 6.3.1.3 shows the properties of this bulk material.

6.3.2 GLOBAL DATA

Three variables describe the operating point of a pneumatic conveying system:

i. the conveying gas mass flow rate;
ii. the solids mass flow rate;
iii. the pipeline pressure drop.

By conducting a number of conveying trials a map of successful

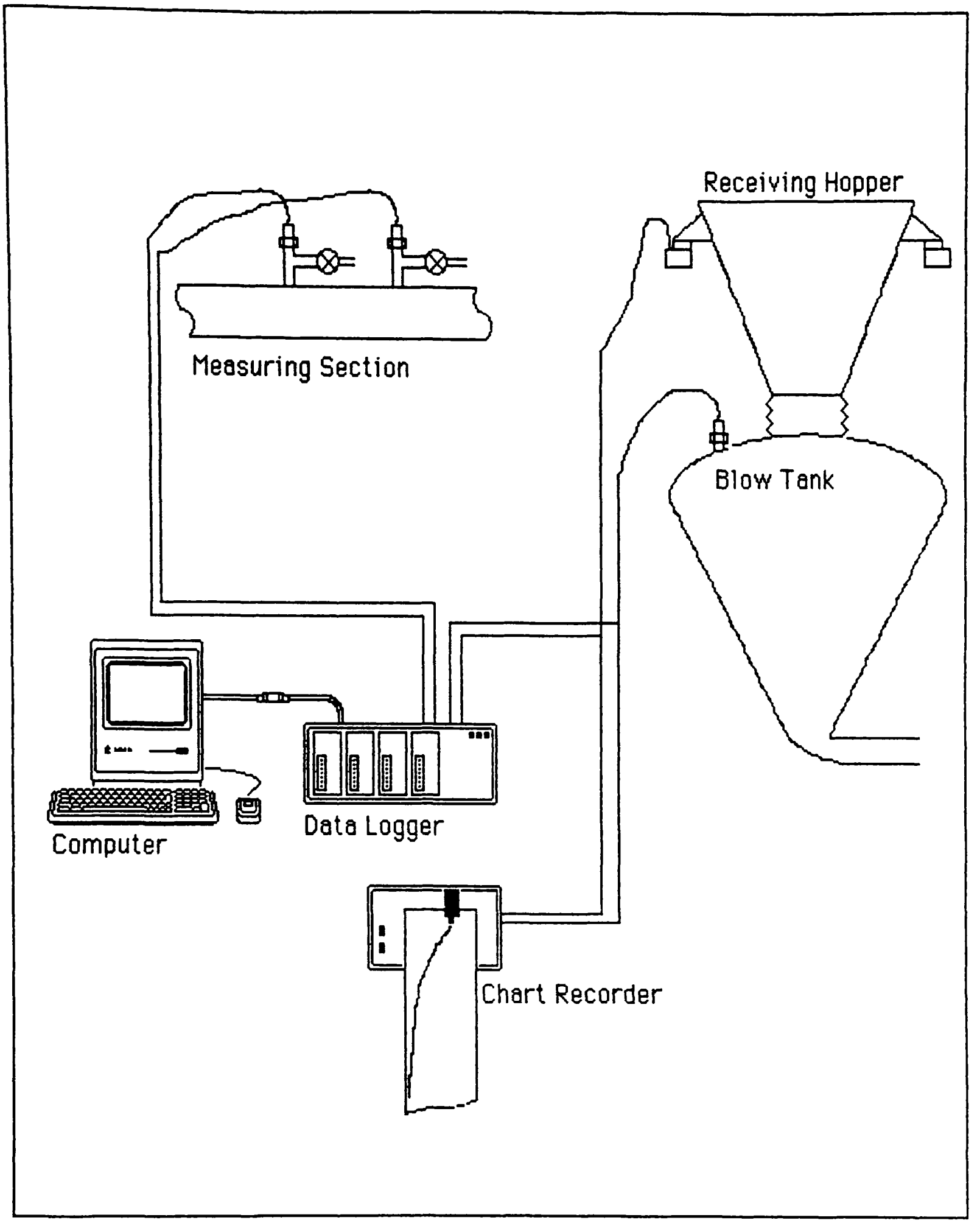

Figure 6.3.1.1 The data aquisition system.

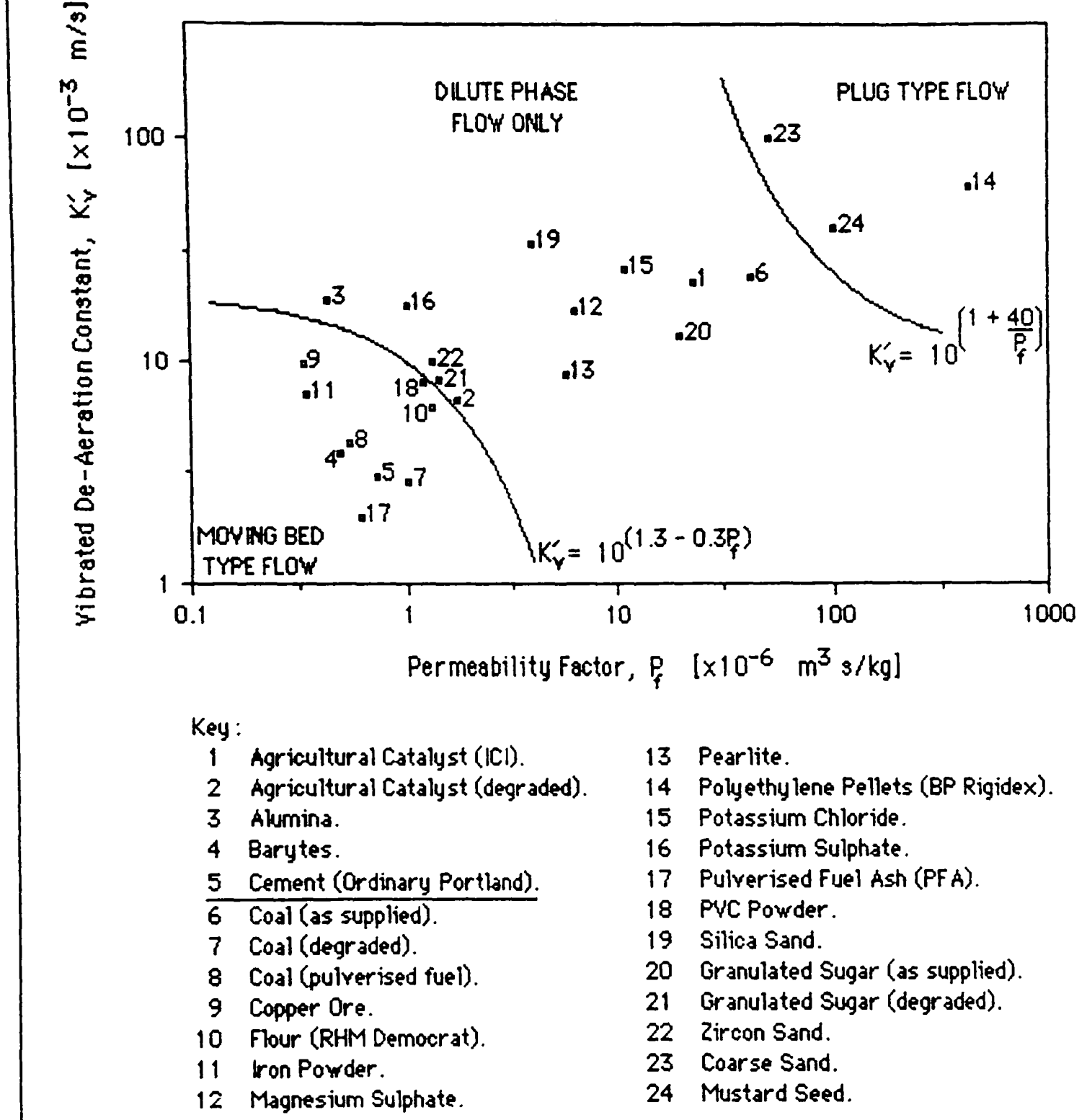

Key :

1	Agricultural Catalyst (ICI).	13	Pearlite.
2	Agricultural Catalyst (degraded).	14	Polyethylene Pellets (BP Rigidex).
3	Alumina.	15	Potassium Chloride.
4	Barytes.	16	Potassium Sulphate.
5	Cement (Ordinary Portland).	17	Pulverised Fuel Ash (PFA).
6	Coal (as supplied).	18	PVC Powder.
7	Coal (degraded).	19	Silica Sand.
8	Coal (pulverised fuel).	20	Granulated Sugar (as supplied).
9	Copper Ore.	21	Granulated Sugar (degraded).
10	Flour (RHM Democrat).	22	Zircon Sand.
11	Iron Powder.	23	Coarse Sand.
12	Magnesium Sulphate.	24	Mustard Seed.

Figure 6.3.1.2 Jones' characterisation of bulk materials according their potential modes of flow.

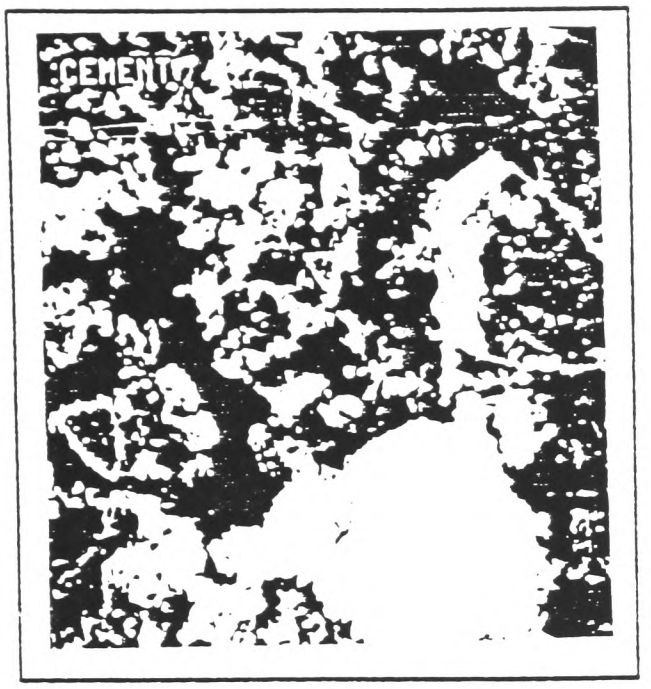

50 µm

Micrograph.

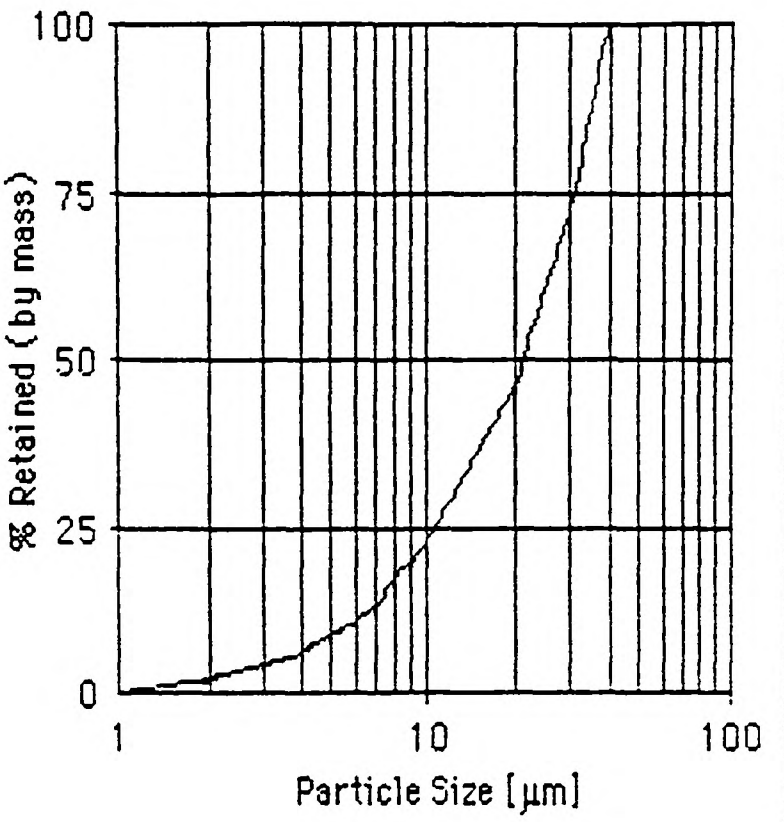

Particle Size Analysis.

Summary.

Mean particle size:	14	µm.
Mass median particle size:	21	µm
Particle size range (2.5%/97.5%):	4/37	µm
Particle density:	3060	kg/m^3
Poured bulk density:	1070	kg/m^3
Tapped bulk density:	1500	kg/m^3
Compaction:	40	%
Permeability factor:	0.71×10^{-6}	m^3 s/kg
Vibrated de-aeration constant:	3.0×10^{-3}	m/s

Data from Jones (1988).

Figure 6.3.1.3 The properties of ordinary portland cement.

operating points, the conveying characteristics, can be determined. For a single trial the following procedure was followed:

i. transfer the bulk material from the receiving hopper into the flow tank;
ii. select the nozzles to supply air to the blow tank and conveying line;
iii. start recording the pressure in the blow tank and the mass of the bulk material in the receiving hopper.

The pressure and temperature in the manifold used to supply the choke flow nozzles were measured. Equation 4.3.2 and table 4.3.1 enable the mass flow rate of air to be calculated. As noted in section 4.3 the balance of air supplied to the blow tank and directly to the pipeline governs the rate at which solids are fed into the pipeline.

Figure 6.3.2.1 shows the data collected during a conveying trial. Values were sampled every 5 s throughout the trial. The pressure in the blow tank nears a steady value as an equilibrium between the potential driving the flow (the pressure) and the flow resistance (a combination of the pipeline geometry and flow rates) is approached. The duration of the steady pressure was determined as follows:

i. find the maximum pressure;
ii. assume this is 5% greater than the mean steady pressure;
iii. find the first point where the pressure is 95% of the mean value;
iv. find the last point where the pressure is 95% of the mean value.

The steady period is shows on figure 6.3.2.1. The mean and standard deviation of the pressures during this time were then calculated. The mass flow rate during this period was found by fitting a straight line to the values of mass collected using the least squares method.

Figure 6.3.2.2 shows the operating points measured during this work. Superimposed are the pressure contours measured by Jones (1988). Jones' pipeline was:

i. the same diameter;
ii. had the same number of bends (though of longer radius);
iii. similar in length (only 4 m shorter);
iv. similar in layout (mostly horizontal).

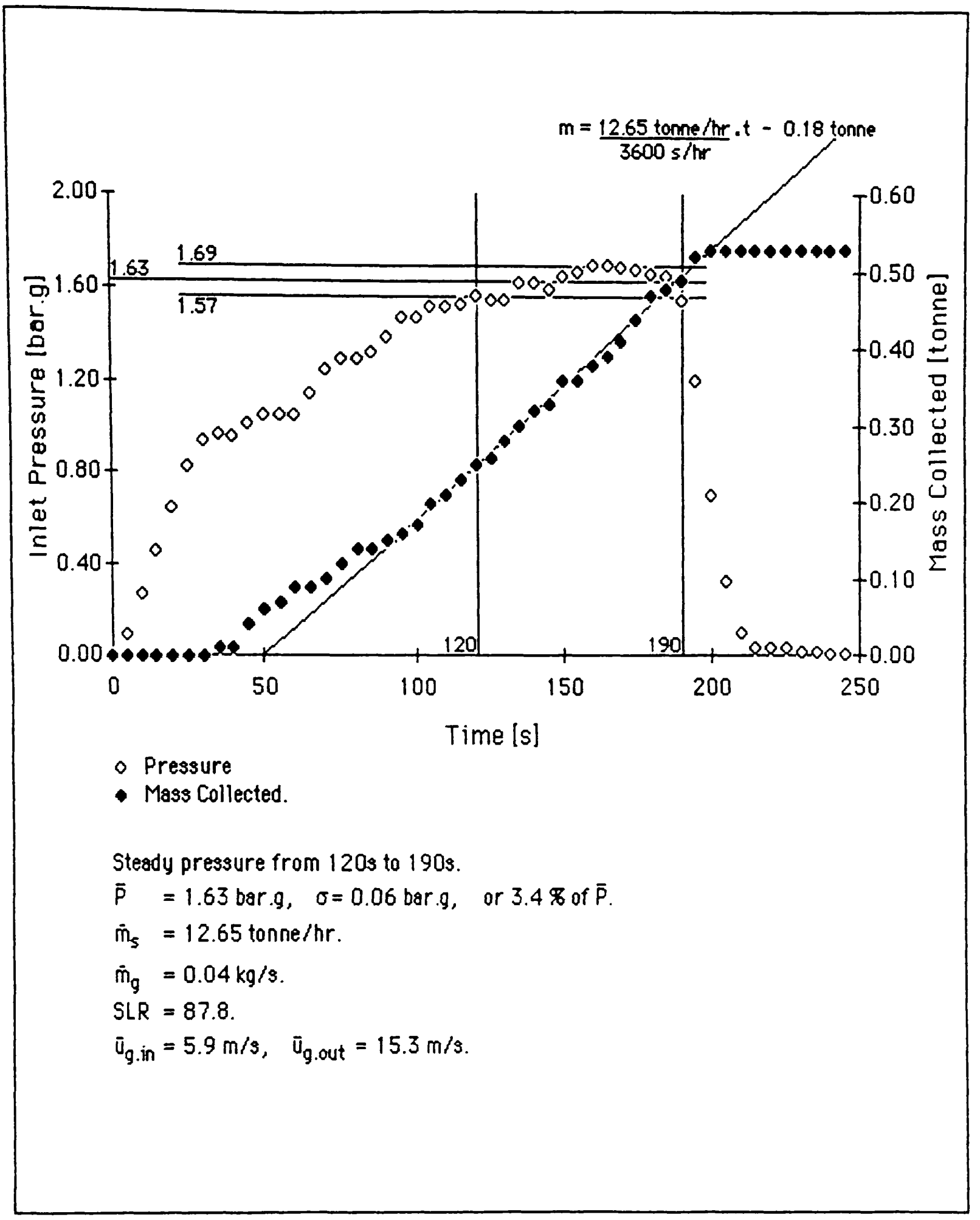

Figure 6.3.2.1 The variation of pressure and mass collected with time during a conveying trial.

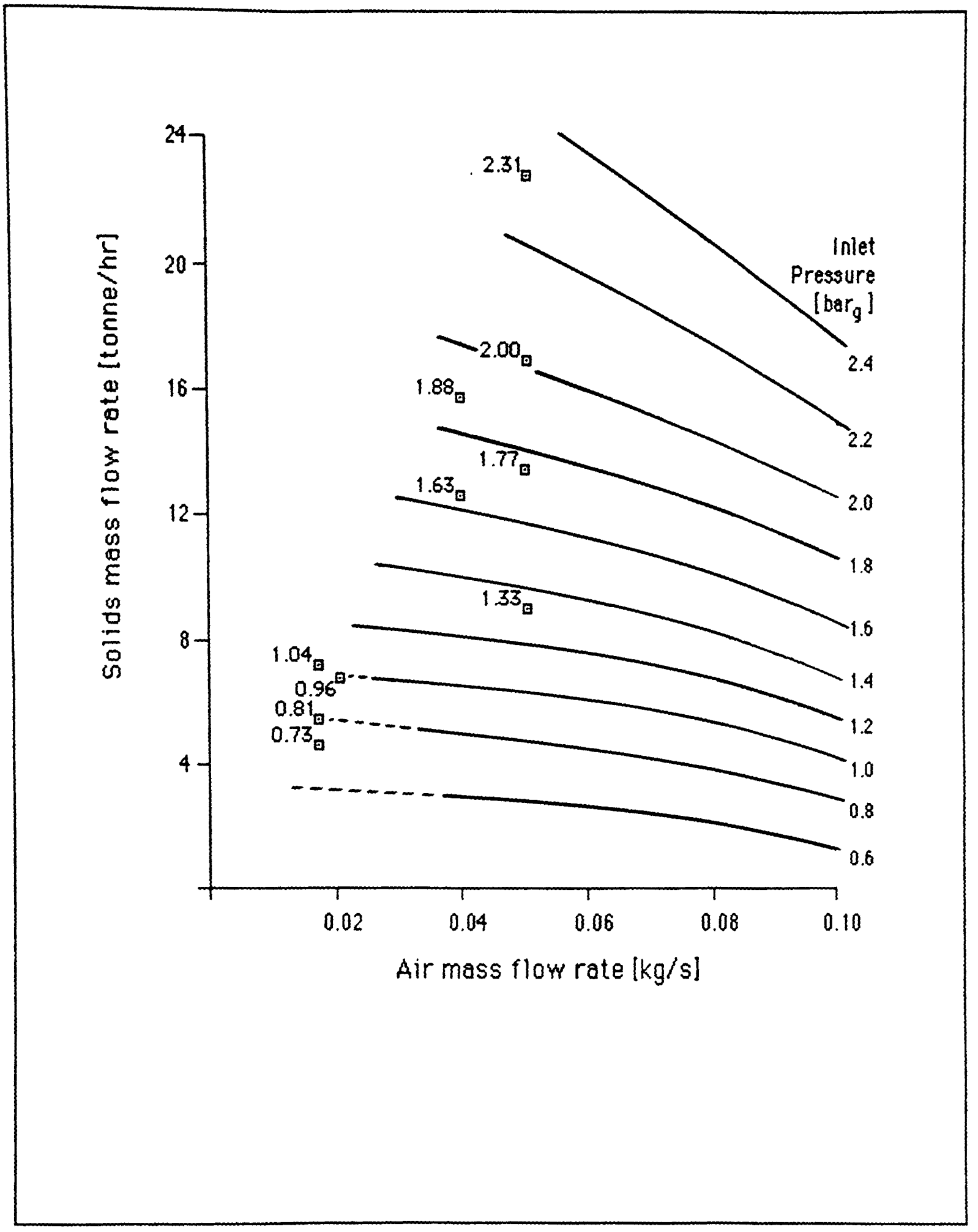

Figure 6.3.2.2 Conveying characteristics for ordinary portland cement.

Conventional scaling would treat the pipelines as similar, thus a direct comparison can be made. From figure 6.3.2.2 the data points from the current work are in good agreement with Jones' data.

An important region of the conveying characteristic is the left-hand limit of the pressure contours. This marks the minimum conveying condition, ie the lowest flow rate of gas that can convey the solids without the pipeline blocking. Since this study was to investigate low velocity pneumatic conveying the majority of trials were conducted near this boundary. The result of this was a better definition of the flow/no-flow boundary (and some considerable experience in unblocking the pipeline).

Figure 6.3.2.3 shows the data from another conveying trial. While the superficial gas velocity at the inlet is in the non-suspension flow region the expansion of the gas through the pipeline has resulted in a velocity at the outlet consistent with suspension flow. Thus a number of tests were conducted at the lowest possible gas mass flow rate to ensure non-suspension flow throughout the pipeline. From figure 6.3.2.2 these trials can be seen to have established a lower minimum conveying condition than Jones' data.

In addition to determining the operating point of the pneumatic conveying system the global data was used to determine when to start recording the detailed local information.

Test Number	Manifold P [bar_g]	Manifold T [C]	Nozzle BT	Nozzle SU	Blow Tank Air Ratio [%]	$\dot{m}_g$ [kg/s]	$\dot{m}_s$ [tonne/hr]	P [bar_g]
1	5.0	23.0	129.35	14.64	89.8	0.0503	17.02	2.0
2	5.0	22.0	97.01	17.25	84.9	0.04	12.65	1.63
3	5.0	25.0	129.35	14.64	89.8	0.0503	22.8	2.31
4	5.0	26.0	51.67	7.63	87.1	0.0206	6.76	0.96
5	5.0	26.0	45.07	5.02	90.0	0.0174	7.23	1.04
6	5.0	26.0	45.07	5.02	90.0	0.0174	5.48	0.81
7	5.0	24.0	45.07	5.02	90.0	0.0174	4.65	0.73
8	5.0	25.0	129.35	14.64	89.8	0.0503	9.0	1.33
9	5.0	25.0	115.75	28.19	80.4	0.0501	13.46	1.77
10	5.0	25.0	97.01	17.25	84.9	0.04	15.76	1.88

TABLE 6.3.2.1 Summary of Conveying Trial Results.

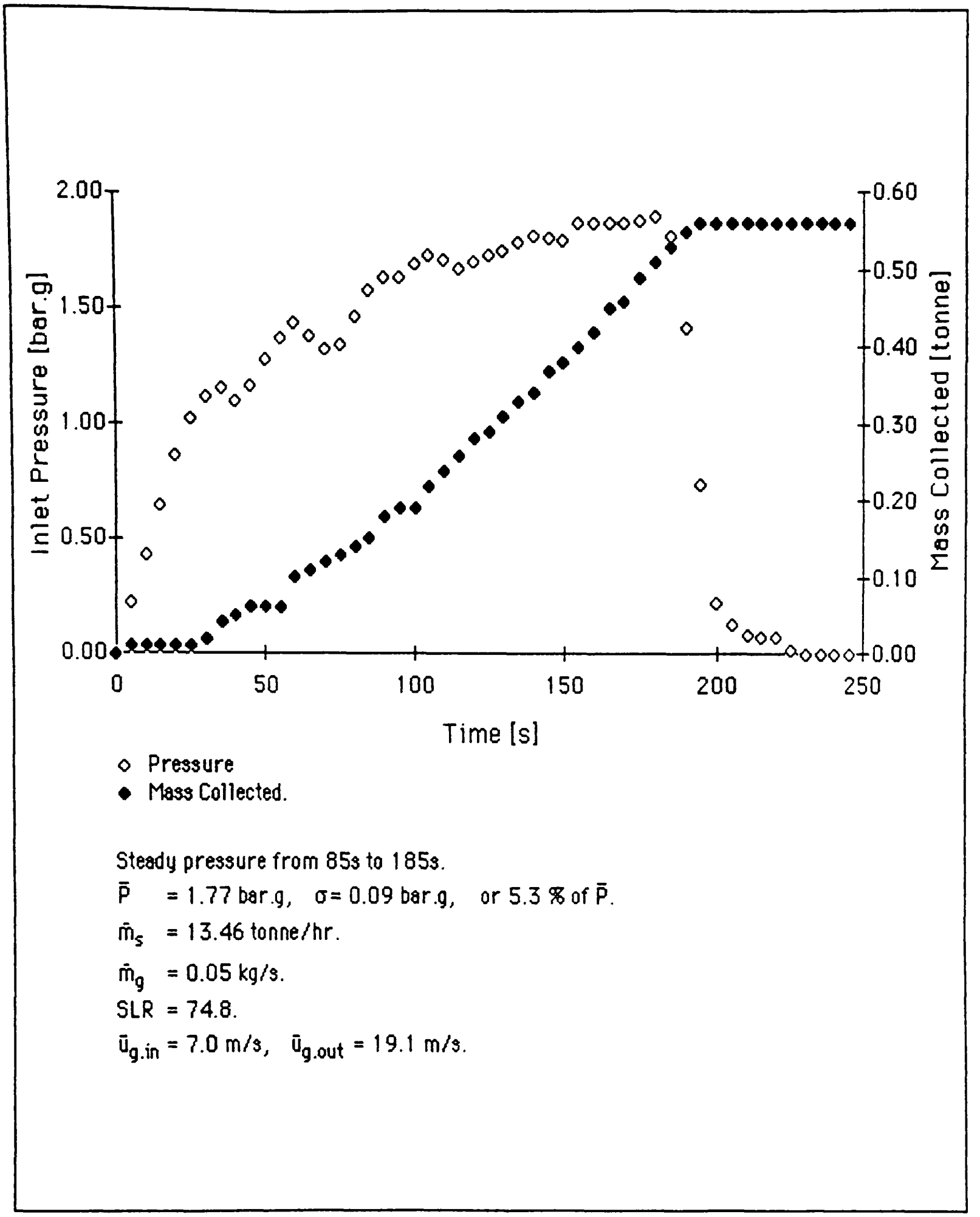

Figure 6.3.2.3 The results of conveying trial 5.

6.3.3 LOCAL DATA

Detailed information about how the flow varies with distance and time is required for validating the mathematical model. Figure 6.3.3.1 shows the arrangement of pressure transducers along the measuring section and the design of each pressure tapping. Each tapping was cleaned by blowing high pressure air through it before starting a conveying trial. Figure 6.3.3.2 shows the location of the measuring section in the pipeline. This location was chosen to minimise the influence of the bends on the flow measured.

The data logger scanned its channels in a sequential manner. Firstly the time was recorded followed by all the channels specified by the current test. The time taken to scan a channel attached to a pressure transducer was 0.001 s. Thus there was a minimum time lag of 0.01 s between scanning the first and last pressure transducers in the measuring section. This limited the frequency at which the pressures could be sampled.

The number of samples that can be recorded was limited by the memory of the data logger:

i. the maximum memory available was 14076 bytes;
ii. the size of header for each test was from 100 to 200 bytes;
iii. each value required 2 bytes;
iv. for a global test 2 channels and the time were recorded every 5 s, C = 2 and R = 500 s/5 s = 100.
v. for a local test all 12 channels and the time were recorded, C = 12 and R = 500.

Memory required = Σ (200 + (C+1)*R*2 bytes)
= 14000 bytes

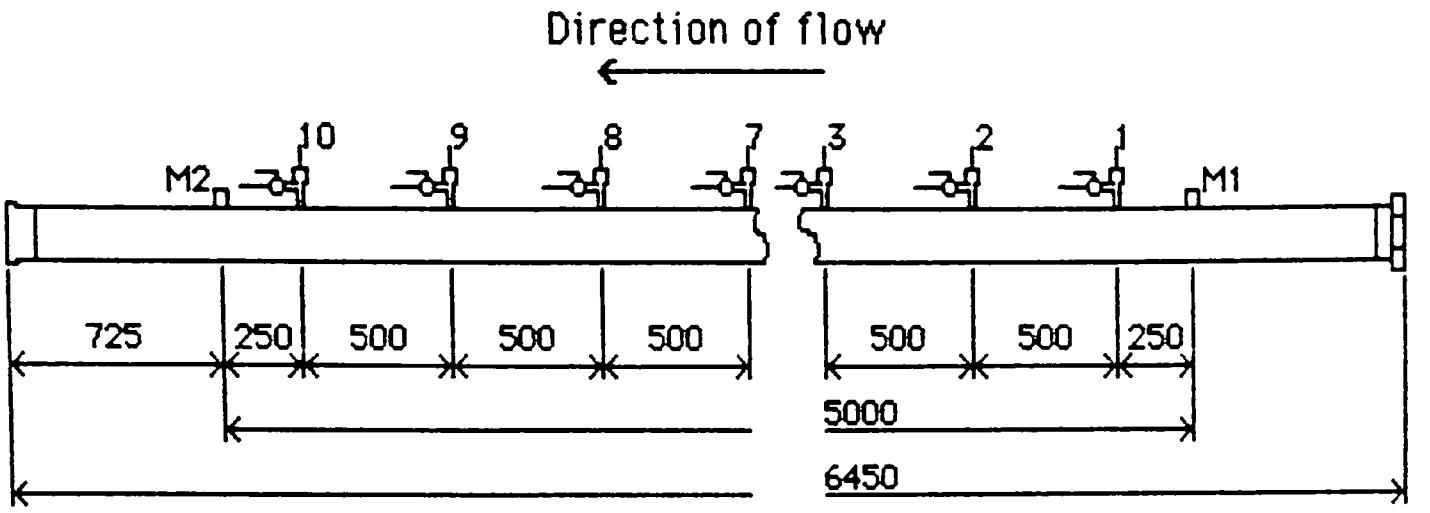

Location of pressure tappings in the measuring section.
M1 and M2: Manometer tappings
1 thro' 10: Tappings for transducers
All dimensions in mm

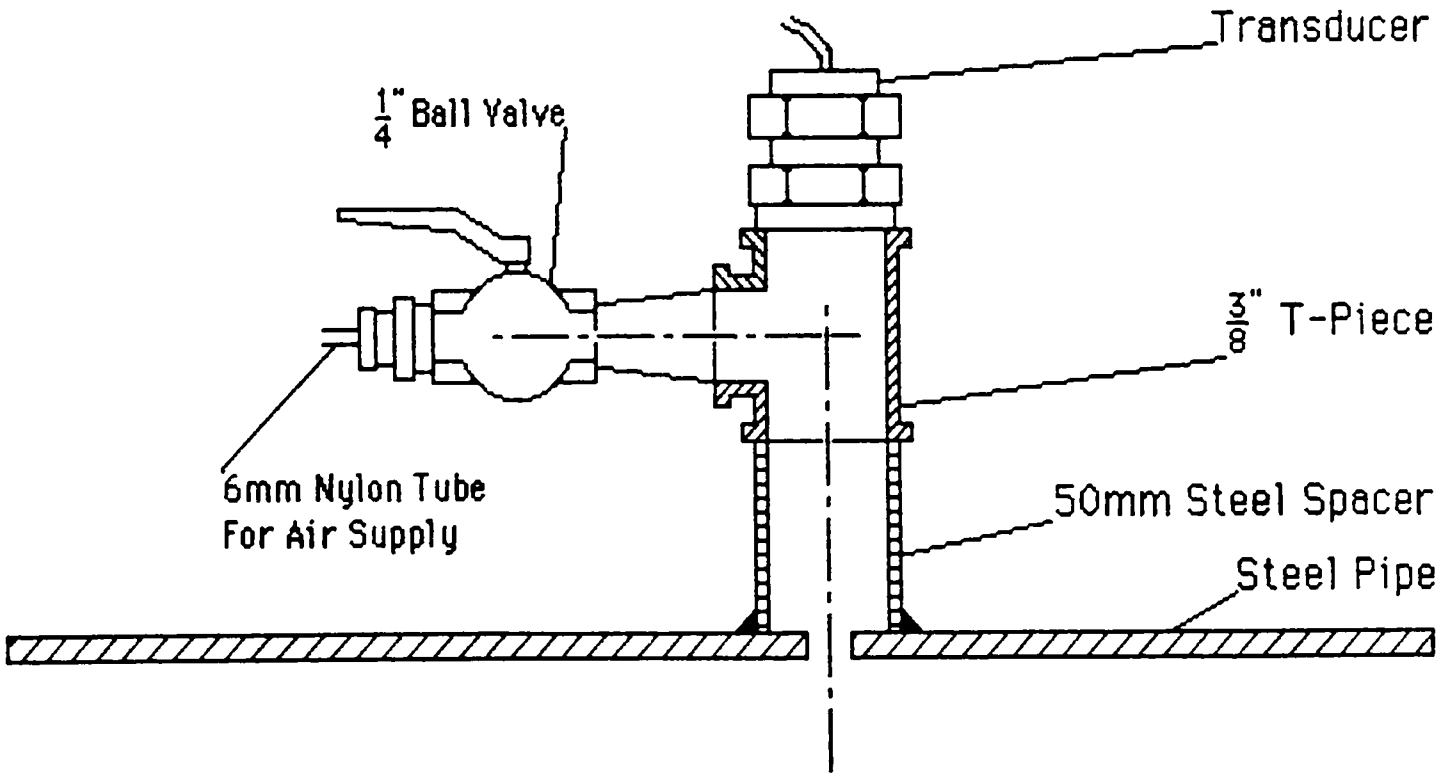

Detail of a pressure tapping.

Figure 6.3.3.1 Design and arrangement of pressure tappings in the measuring section.

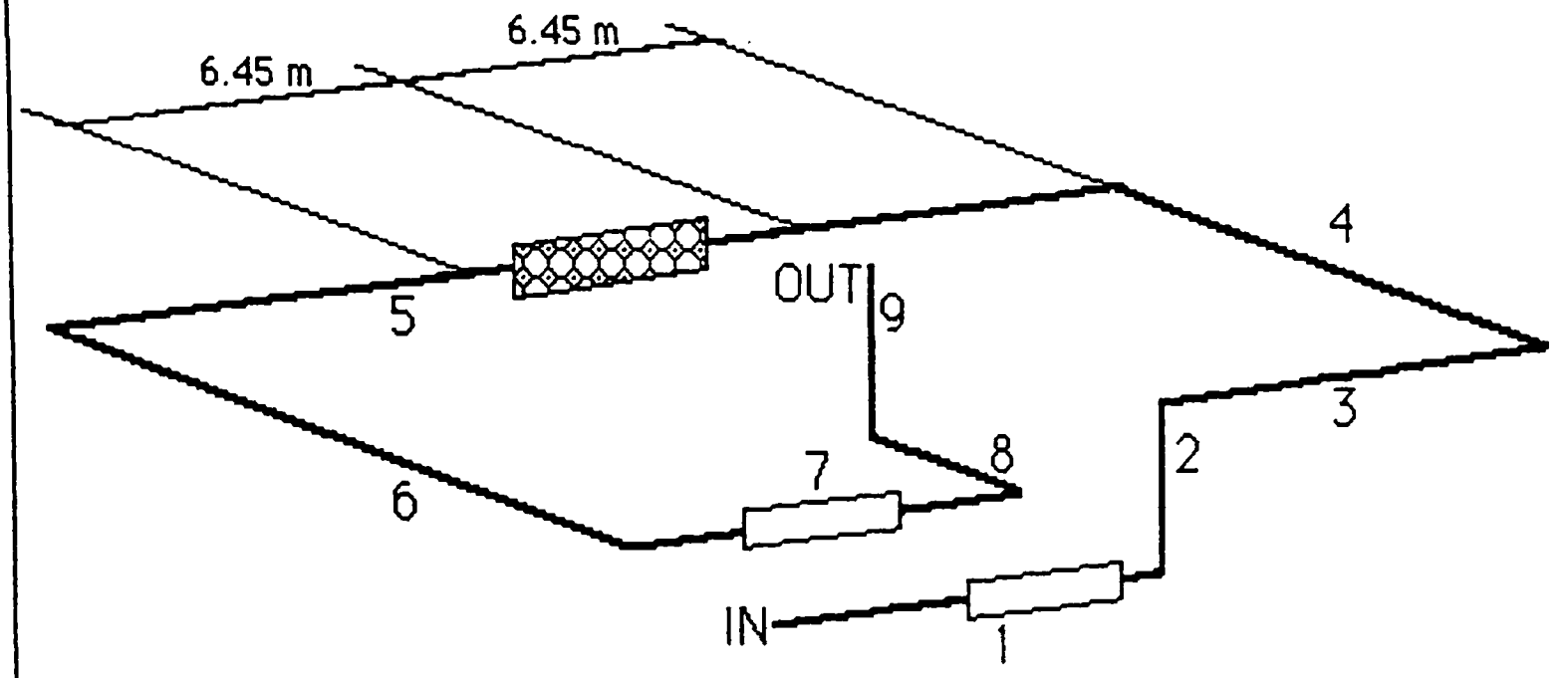

Section	Orientation	Length
1	horizontal	7.25m
2	vertical	1.11m
3	horizontal	3.65m
4	horizontal	6.15m
5	horizontal	17.00m
6	horizontal	7.42m
7	horizontal	6.05m
8	horizontal	0.60m
9	vertical	2.25m

System Summary	
Total Length	54.77m
Pipe Bore	53.00mm
Bend Radius	127.00mm

Key

Steel Pipeline.

Glass Pipeline

Measuring Section.

Figure 6.3.3.2 Location of the measuring section in the pipeline.

It was decided to sample at the maximum possible rate so that the time scale of variations in the flow could be determined. Since it would take 0.012 s to sample all the channels, the interval between samples was set to 0.02 s. With a limit of 500 readings per channel this allows the flow to be monitored for up to 10 s. Thus, two tests were performed by the data logger during a conveying trial:

i. a SLOW SCAN test recording the time, blow tank pressure and mass collected at 5 s intervals;
ii. a FAST SCAN test recording the time, all the pressure transducers in the measuring section, blow tank pressure and mass collected at 0.02 s intervals.

The slow scan test was run for the duration of the conveying trial. The fast scan test was only started after the pressure in the blow tank had reached the steady condition.

In order to minimise differences in the data recorded between conveying trials the following procedure was devised. At the start of a day of tests the conveying line was broken at the end of the eighth section and plugged. The empty blow tank and pipeline were then pressurised. Each joint in the pipeline was checked for leakage, which could be significant when operating at very low flow rates. This is particularly important for the joints on the glass sections, since these needed to be removed at intervals for cleaning (the union connections used throughout the pipeline are more prone to leaking if they are frequently disconnected). The pressurisation was carried out in increments of 0.5 bar so that the calibration of the transducers could be checked. At each increment 10 readings were sampled in 100 s. The results of a typical calibration series are shown in figure 6.3.3.3. At the maximum pressure tested:

$$\text{Pressure Ratio, } R_P = \frac{1.01325\ \text{bar}_a + 3.5\ \text{bar}_g}{1.01325\ \text{bar}_a + 5.0\ \text{bar}_g} = 0.75$$

No conveying trials could be conducted at, or above this pressure, because the pressure ratio exceeds the critical value necessary to ensure sonic velocity in the choke-flow nozzles and hence a known gas mass flow rate.

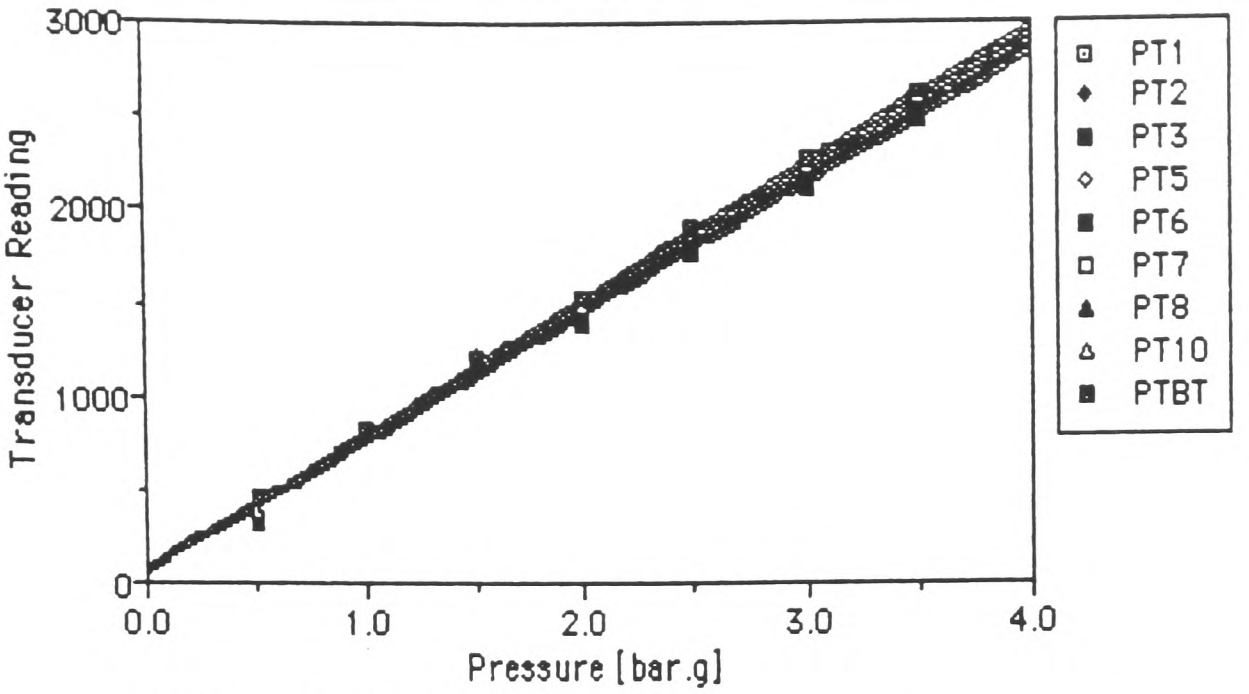

Individual calibration lines.

PT1	= 65.943 + 698.69x	ρ^2 = 0.994	PT6	= 66.386 + 689.45x	ρ^2 = 0.994
PT2	= 78.414 + 711.44x	ρ^2 = 0.997	PT7	= 69.700 + 705.07x	ρ^2 = 0.995
PT3	= 67.457 + 700.74x	ρ^2 = 0.994	PT8	= 67.786 + 703.03x	ρ^2 = 0.994
PT5	= 76.571 + 712.03x	ρ^2 = 0.997	PT10	= 80.900 + 718.84x	ρ^2 = 0.997
			PTBT	= 102.97 + 723.77x	ρ^2 = 1.000

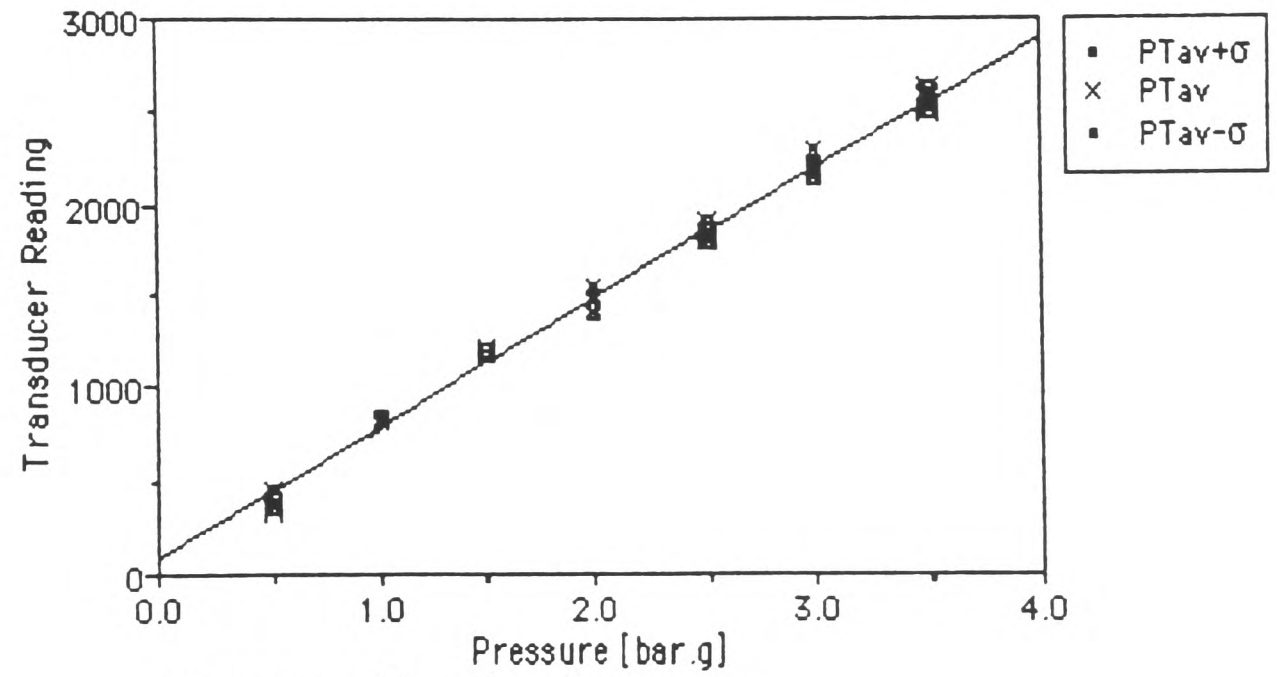

Average calibration lines.

PTav + σ	= 76.253 + 707.10x	ρ^2 = 0.994
PTav	= 75.125 + 707.00x	ρ^2 = 0.994
PTav - σ	= 73.998 + 706.91x	ρ^2 = 0.994

Figure 6.3.3.3 Typical calibration results for the measuring section and blow tank pressure transducers.

The load cells used to measure the mass of product in the receiving hopper were calibrated when the bulk material was loaded. Each bag of material was weighed and then loaded. Subsequently, the load cell reading was checked for variation after each conveying trial.

6.3.4 INTERPRETATION OF DATA FROM A FAST SCAN TEST

The raw values from a fast scan are shown in figure 6.3.4.1. This shows a noticeable fluctuation in the pressure measured at each point.

The first step in processing the data was to calculate the time-averaged mean pressure gradient in the measuring section. The result of this is show in figure 6.3.4.2. Superimposed on this figure are the values for plus and minus one standard deviation from the mean. This data would be used later for validation.

The variation of the mass flow rate of solids through the measuring section could not be measured directly. Figure 6.3.4.3 shows the approach taken. During a fast scan test the pressure in the blow tank is recorded 0.011 s after the first transducer in the measuring section. The effect of this change will only be seen by the measuring section some seconds later.

Calculating the superficial gas velocity at both the inlet of the pipeline and the start of the measuring section:

$$U_{g,\ \text{inlet to pipeline}} = 7.07\ \text{m/s}$$

$$U_{g,\ \text{measuring section}} = 11.42\ \text{m/s}$$

$$\text{Time delay} = \frac{7.25+1.11+3.65+6.15+6.45\ \text{m}}{0.5*(7.07+11.42)\ \text{m/s}} = 2.7\ \text{s}$$

The pressure history over the previous four readings was examined and the mean value calculated. Since the standard deviation was only a small percentage of the mean, the pressure in the blow tank that influenced the flow in the measuring section was taken as the mean pressure.

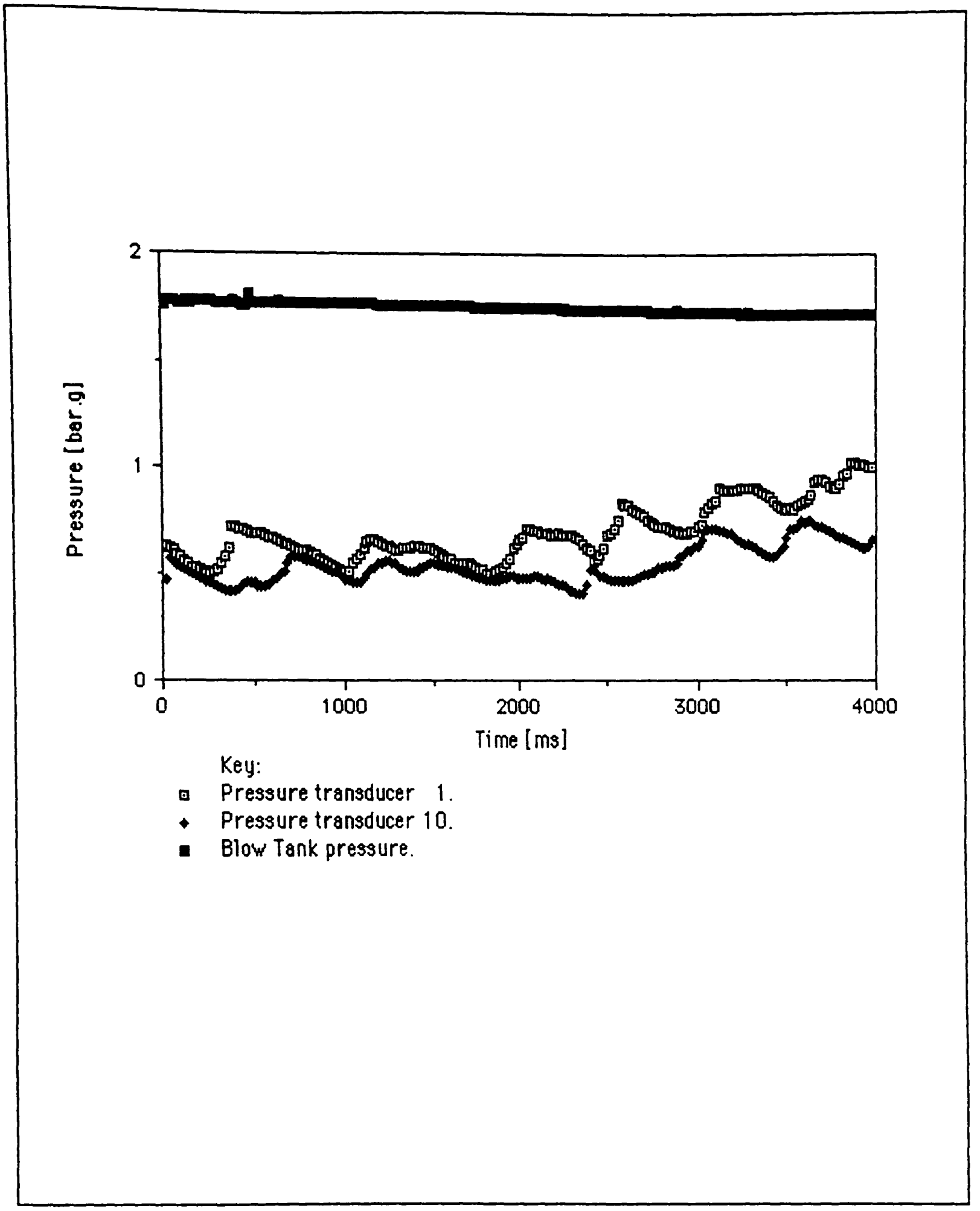

Figure 6.3.4.1 The pressure fluctuation with time during the fast scan test in conveying trial 5.

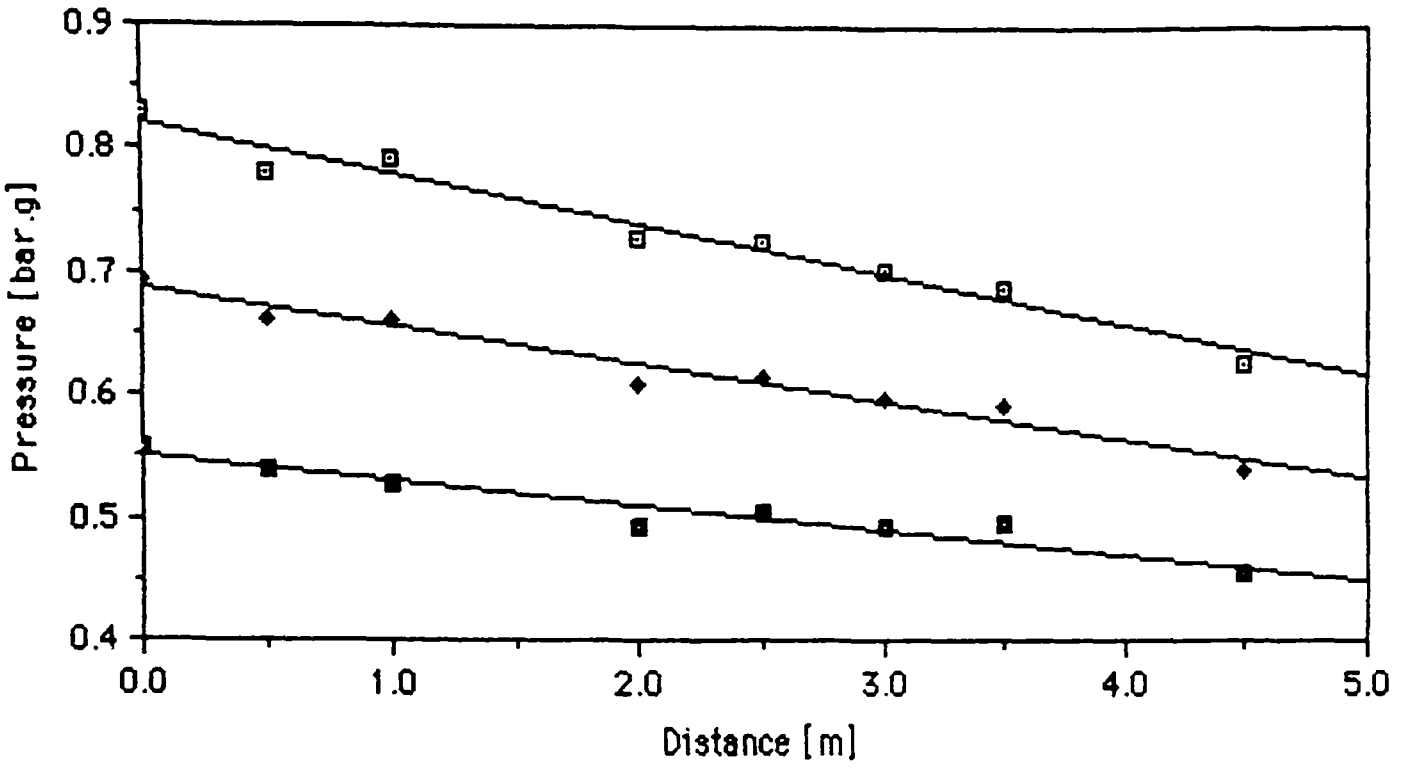

- ▫ $\bar{P} + \sigma$ = 0.82209 - 4.1145E-2.x, ρ^2 = 0.967.
- ◆ $\bar{P}$ = 0.68640 - 3.0612E-2.x, ρ^2 = 0.961.
- ■ $\bar{P} - \sigma$ = 0.55071 - 2.0079E-2.x, ρ^2 = 0.914.

At each transducer location, $\bar{P}$ represents the mean of 200 readings sampled every 0.02s for 4s.

The mean pressure gradient = 0.0306 bar/m = 3061 Pa/m.

The mean standard deviation = 0.0131 bar = 1308 Pa.

Figure 6.3.4.2 The time averaged mean pressures in the measuring section during the fast scan in conveying trial 5.

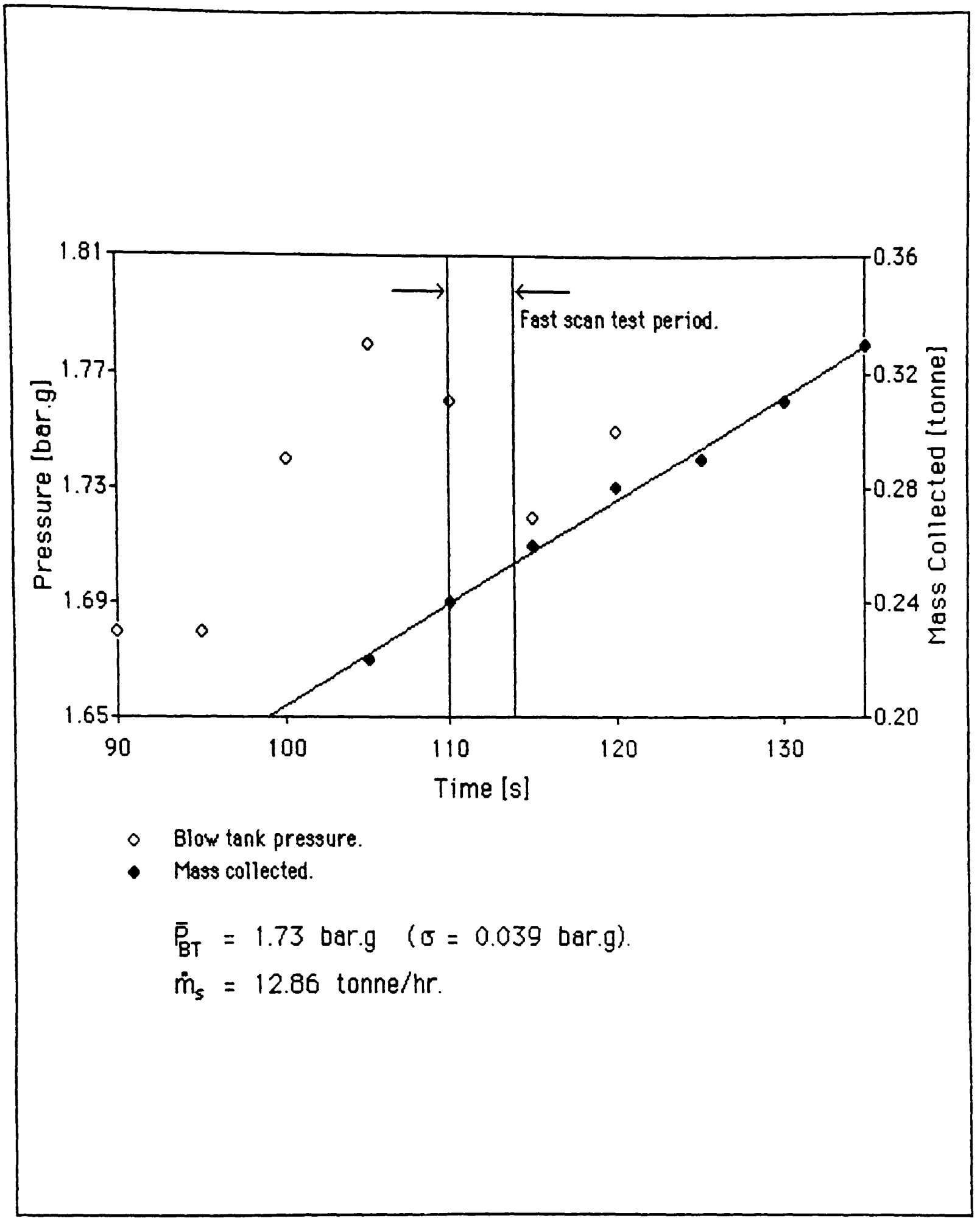

Figure 6.3.4.3 Solids mass flow rate during the fast scan test in conveying trial 5.

The aim of starting the fast scan test only after the pressure in the blow tank had been steady was met in this case, since the small deviation would not have been detected by the chart recorder that was used to monitor the system during the conveying trial.

A similar analysis can be applied to the mass collected readings. This is measured at the end of the pipeline and the four readings after the fast scan was completed were used in calculating the mean solids mass flow rate. A number of readings must be included, because the signal from the load cells varies due to solids hitting the hopper wall after leaving the pipe.

The variation of the signal from the pressure transducers in the measuring section can be attributed to:

i. environmental effects such as temperature and electrical noise;
ii. the flow in the pipeline.

From previous discussions the former effects would be expected to be constant for all the transducers. Figure 6.3.4.4 shows the variation of the pressure measured by the first and last transducers in the measuring section. This shows that the form of the trace from the first transducer is repeated at a later time by the last transducer. This indicates that the variation of the readings is due to flow phenomena.

Observation of the flow in the glass sections of the pipeline shows that the level of the moving-bed is not constant. Using this as the starting point an analogy with a piston in a cylinder was used to model the effect of bed level on the pressure.

The 1st law of thermodynamics states:

$$q - w = U_2 - U_1 \qquad 6.3.4.1$$

where U_1 is the initial internal energy and U_2 is the final internal energy.

For an adiabatic process, the heat flow into the system, q, is:

$$q = 0 \qquad 6.3.4.2$$

For a reversible process the work done by the system, w, is:

$$w = \int_1^2 P\,dV \qquad 6.3.4.3$$

From the definition of a perfect gas:

$$\begin{aligned} u &= C_V T \\ RdT &= PdV + vdP \\ R &= C_P - C_V \\ \gamma &= \frac{C_P}{C_V} \end{aligned} \qquad 6.3.4.4$$

Hence

$$C_V dT + P dv = 0 \qquad 6.3.4.5$$

$$\gamma \frac{dv}{v} + \frac{dP}{P} = 0 \qquad 6.3.4.6$$

$$P v^{\gamma} = constant \qquad 6.3.4.7$$

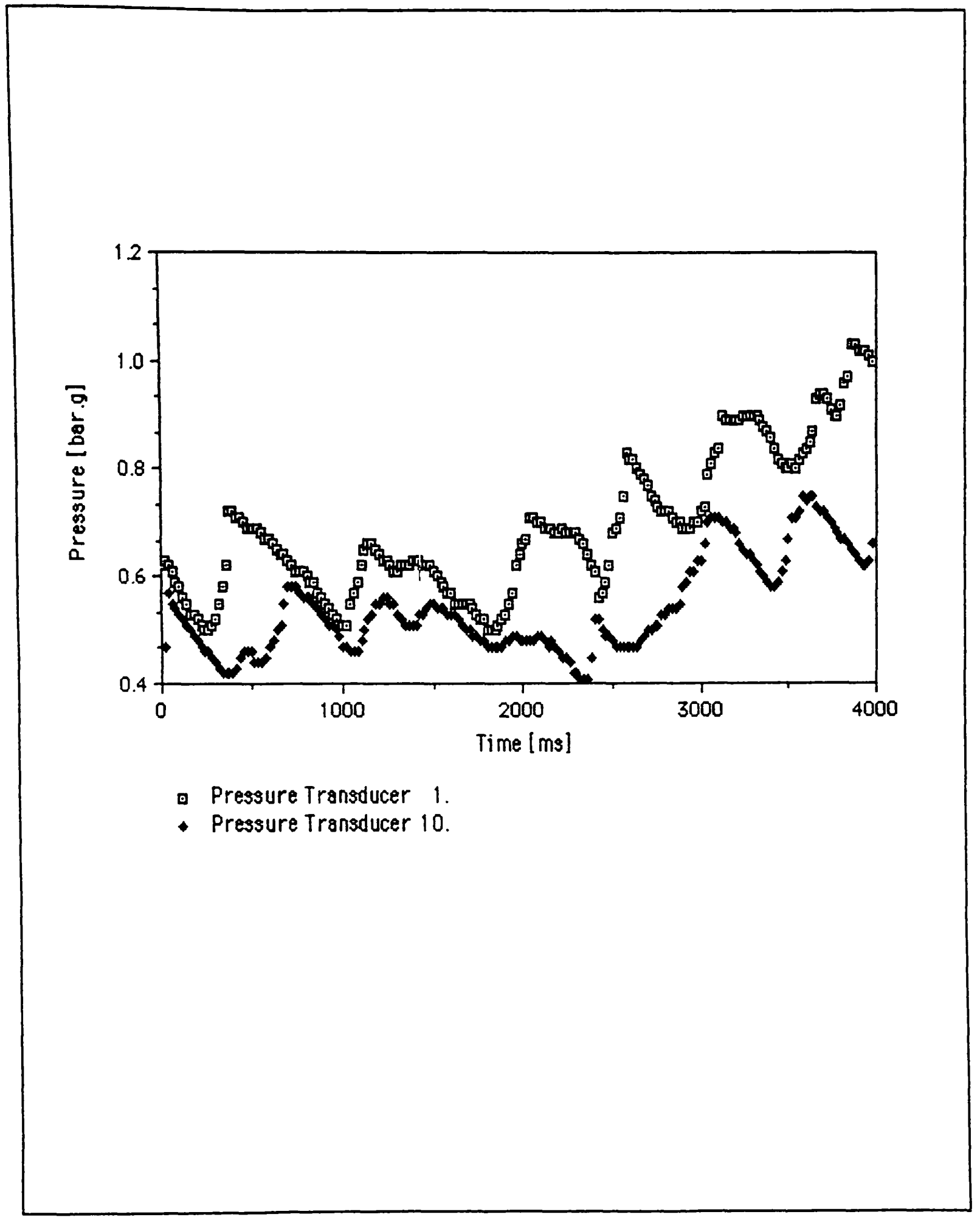

Figure 6.3.4.4 A comparison of the pressure variation with time at the first and last transducers in the measuring section during the fast scan in conveying trial 5.

Equation 6.3.4.7 applies to a perfect gas undergoing an isentropic (reversible adiabatic) process. Figure 6.3.4.5 shows the analogy between the flow in the pipe beneath the pressure transducer and the piston in cylinder model. An increase in the height of the moving-bed of solids is equated to the piston compressing the gas in the cylinder from point 1 to point 2.

From equation 6.3.4.7

$$(Pv^{\gamma})_1 = (Pv^{\gamma})_2 \qquad 6.3.4.8$$

Let

$$\begin{aligned} P_2 &= P_1 + \Delta P \\ v &= \frac{Ax}{m} \\ x_2 &= x_1 - \Delta x \end{aligned} \qquad 6.3.4.9$$

Hence

$$\Delta x = \left(1 - \left(\frac{P_1}{P_1 + \Delta P}\right)^{\frac{1}{\gamma}}\right) x_1 \qquad 6.3.4.10$$

Using equation 6.3.4.10 the expected change in height of the moving-bed of solids may be calculated. For the following conditions:

$$\begin{aligned} H &= 60 \text{ mm} \\ D &= 53 \text{ mm} \\ X_1 &= H + D - 0.5*D = 86.5 \text{ mm} \end{aligned}$$

The change in bed height due to an increase in pressure, using equation 6.3.4.10, is shown in figure 6.3.4.6.

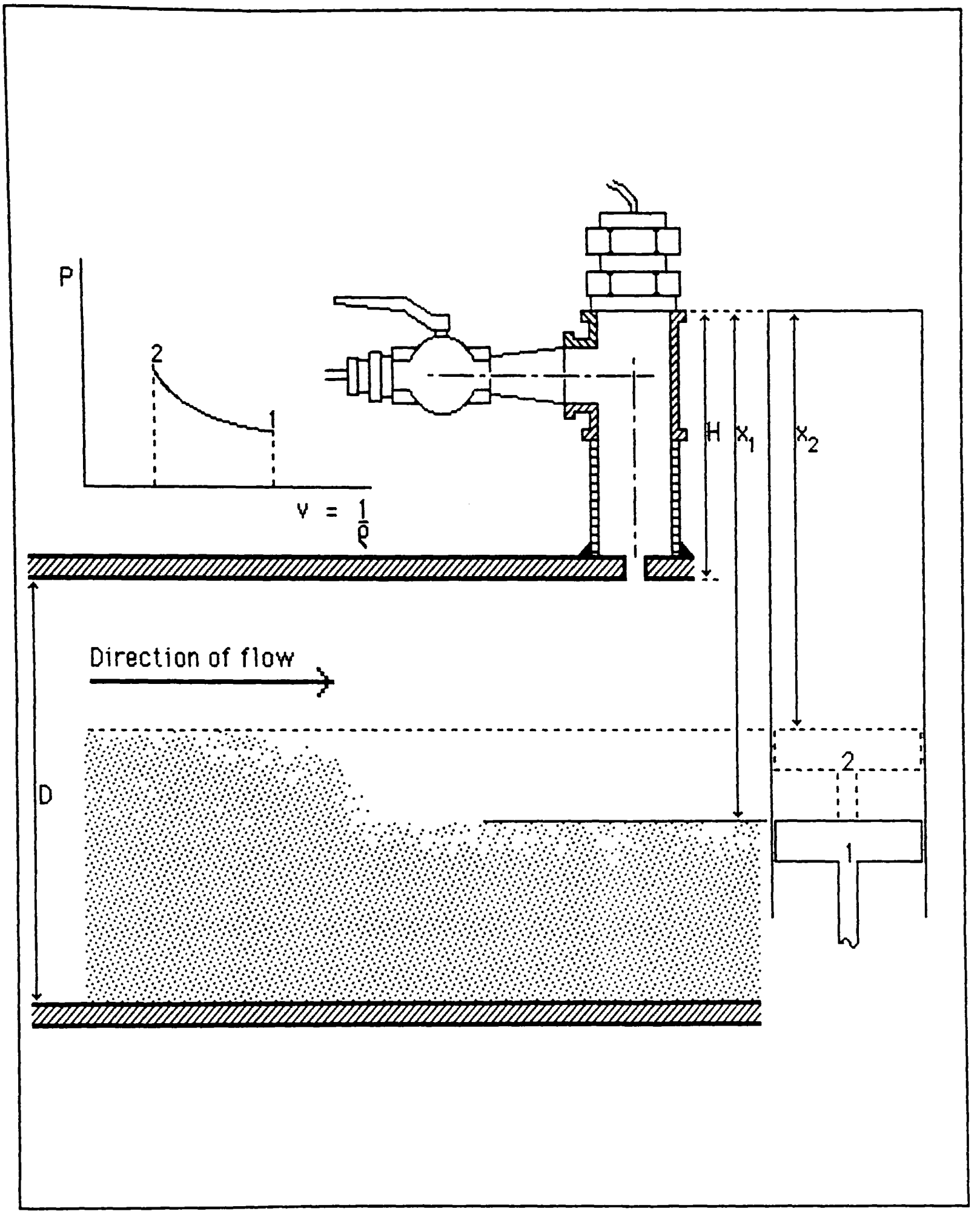

Figure · 6.3.4.5 The piston in cylinder model for the change in pressure due to the flow.

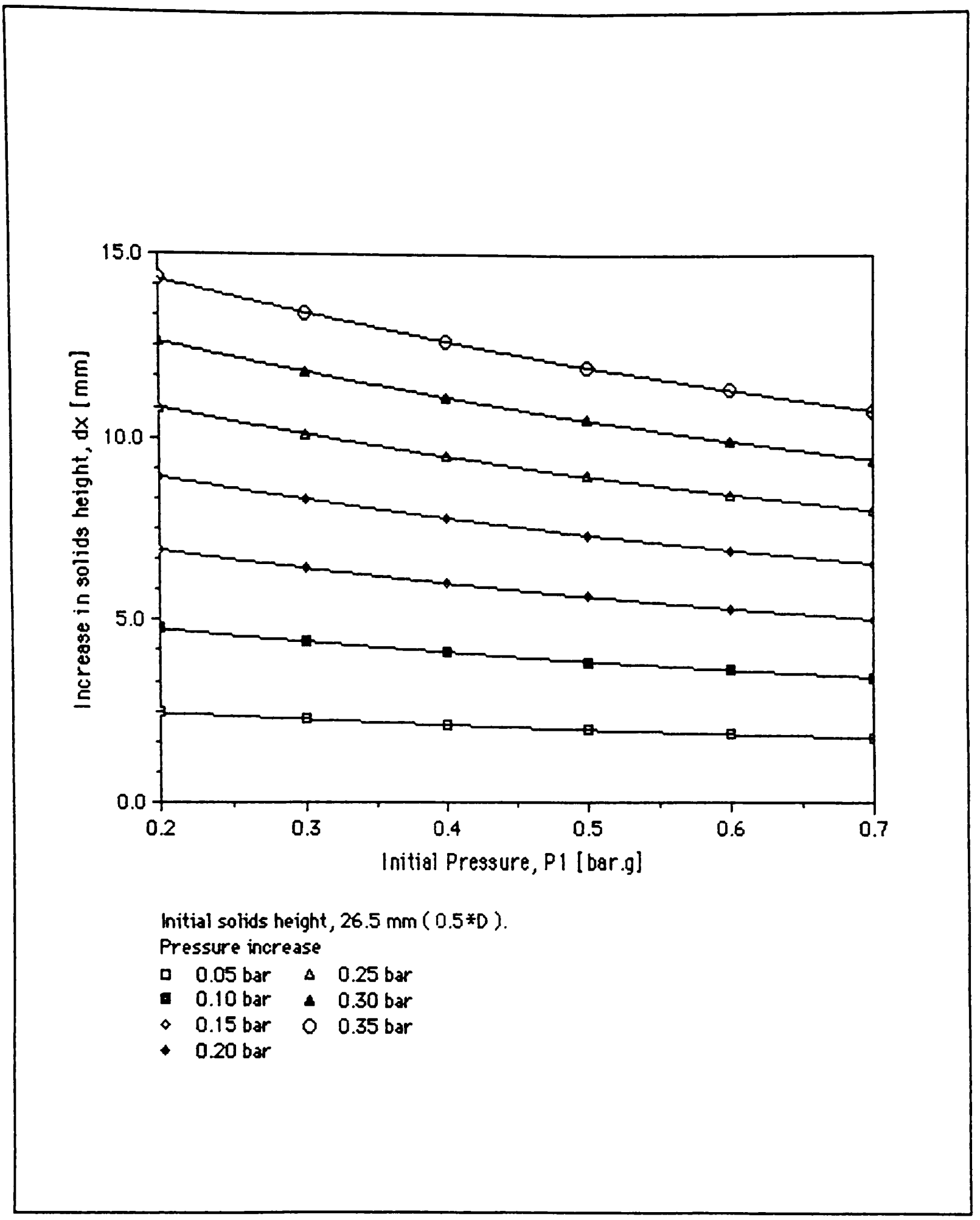

Figure 6.3.4.6 The variation of solids height using the piston in cylinder analogy.

Considering the first peak in pressure in figure 6.3.4.4, then assuming that the pipe is half full of solids:

$P_1 = 0.50\ bar_g$ $\quad x_1 = 86.5$ mm
$P_2 = 0.72\ bar_g$ then $\quad x_2 = 38.5$ mm
$\Delta P = 0.22\ bar_g$ ie $\quad \Delta x = 15.1\%$ of D

Assuming that the pipe is one third full of solids:

$P_1 = 0.50\ bar_g$ $\quad x_1 = 95.3$ mm
$P_2 = 0.72\ bar_g$ then $\quad x_2 = 86.5$ mm
$\Delta P = 0.22\ bar_g$ ie $\quad \Delta x = 16.6\%$ of D

Values of this order of magnitude are in agreement with visual observations of the flow. Even though this is an idealised model for the influence of the flow on the pressure transducer, it demonstrates that the variation of the transducer readings during a fast scan test is a function of the flow within the pipeline.

Further analysis of the fast scan pressure data is now possible. The velocity of the pressure peak can be calculated and the velocity of the solids estimated. Figure 6.3.4.7 shows the detail of the first peak in the pressure. Figure 6.3.4.8 shows two subsequent peaks. From this data the mean velocity of the pressure pulse is 11.13 m/s.

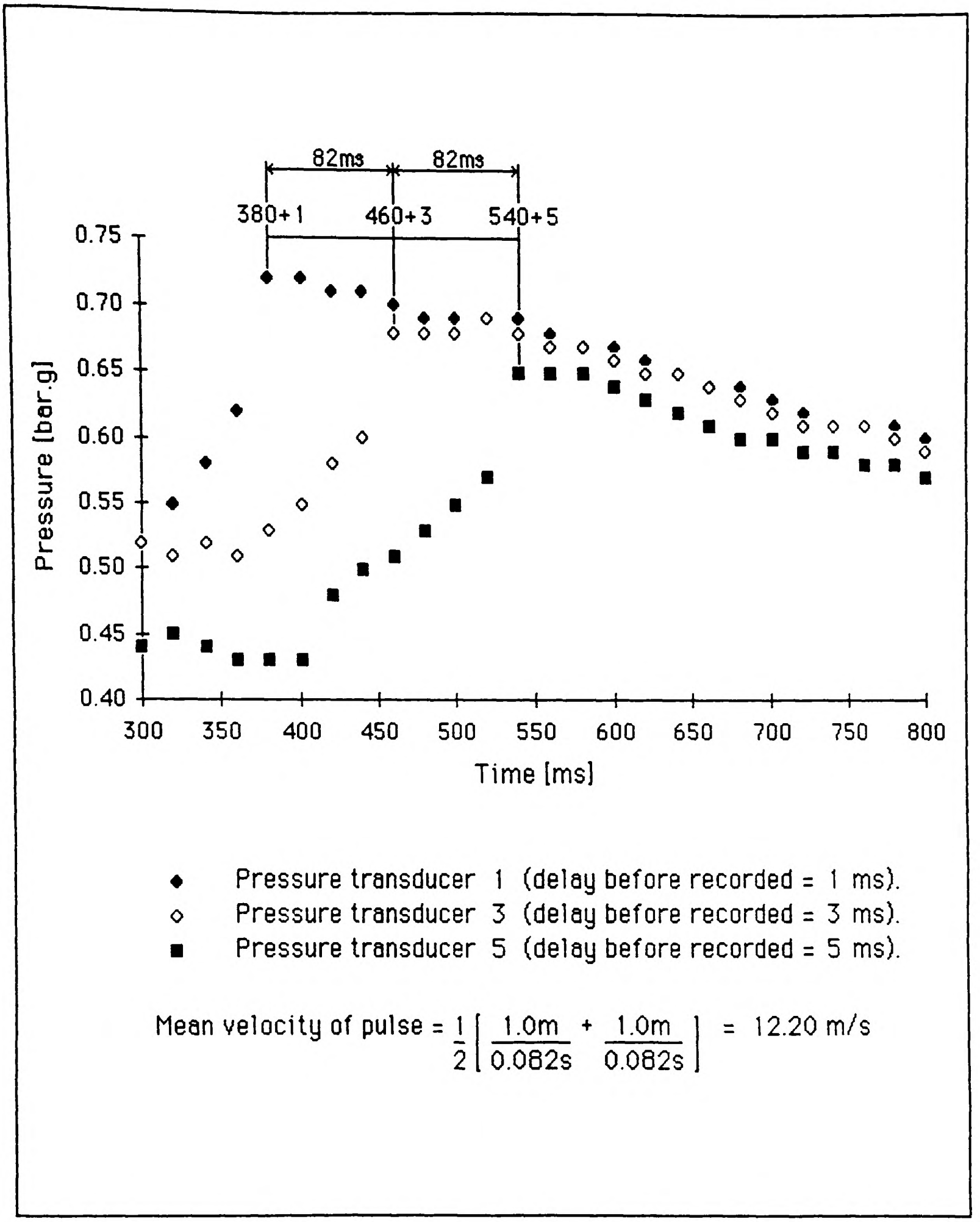

Figure 6.3.4.7 Velocity of pressure pulse during the fast scan in conveying trial 5.

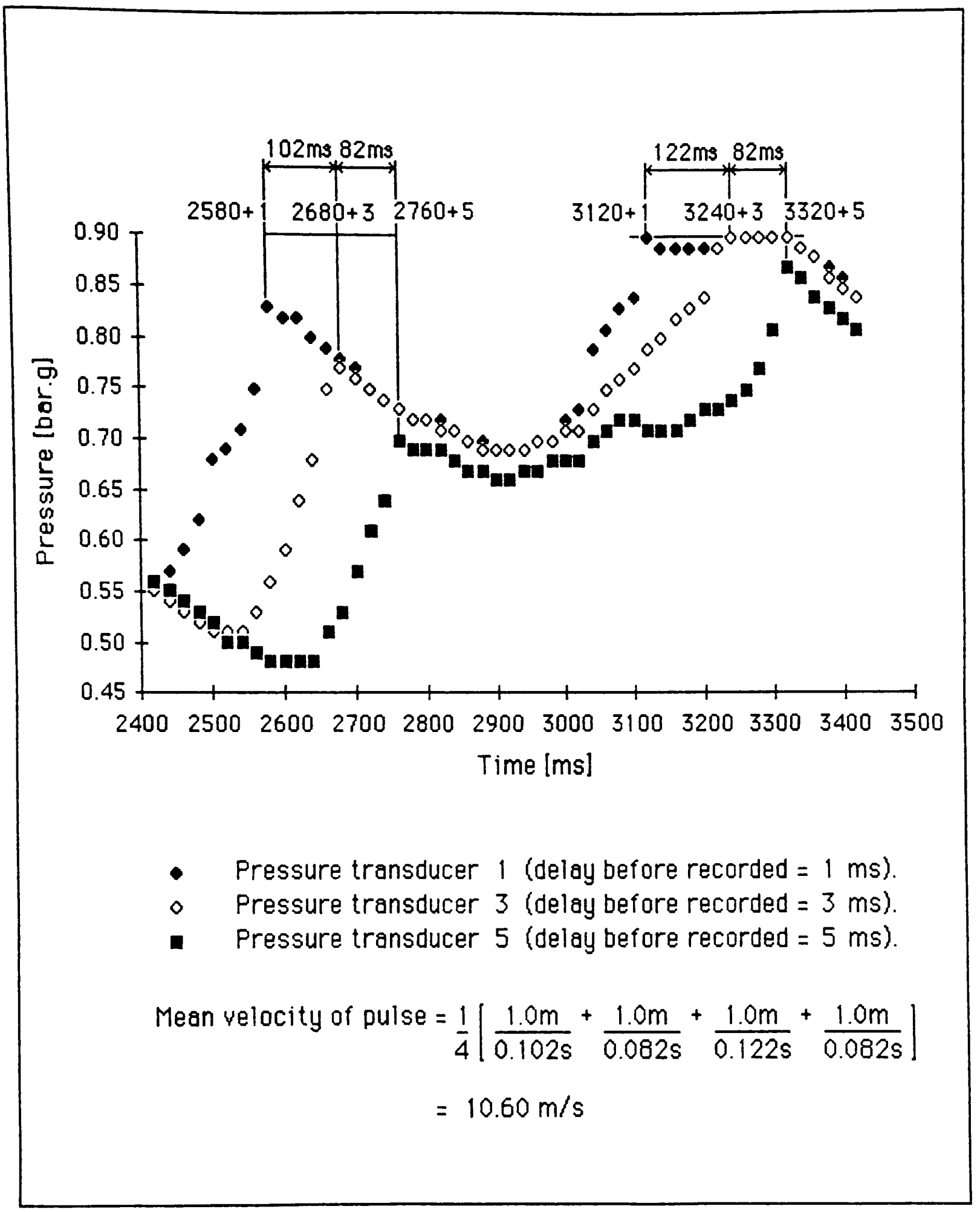

Figure 6.3.4.8 Velocity of pressure pulse during the fast scan in conveying trial 5.

Thus,

$$\dot{m}_s = \rho_s R_s A u_s$$

$$R_s = \frac{\dot{m}_s}{\rho_s A u_s} = \frac{12.86\ tonne/hr}{3060\ kg/m^3\ 0.002211\ m^2\ 11.13\ m/s} \qquad 6.3.4.11$$

$$R_s = 0.048$$

where R_s is the solids volume fraction for the entire pipe cross-section. Figure 6.3.4.9 shows how this value can be related to the depth of the moving-bed and the solids volume fraction in the bed. At its bulk density the solids volume fraction of cement is 0.35. Assuming that the bed is at this concentration then the depth of the bed is approximately 0.3 of the pipe diameter. Comparing this result with the piston-in-cylinder model for the variation of the pressure shows good agreement.

6.3.5 SUMMARY OF TEST RESULTS

A series of conveying trials have been conducted to investigate the moving-bed mode of non-suspension flow. Using Jones' classification for bulk materials according to their mode of flow, ordinary portland cement was chosen as the test material. Comparison of the system operating points used during the test programme compare well with other workers data. The minimum conveying boundary was investigated and found to be approximately 3 m/s for this material.

The main point of the test programme was to gather data suitable for the validation of the mathematical models of the flow. A test procedure was devised that could monitor the flow with sufficient detail by non-intrusive means. The variation of pressure with time was measured. The velocity of the flow could be determined by monitoring the variation of pressure with time at closely spaced pressure transducers. This method relies upon the flow patterns that occur in moving-bed non-suspension flow.

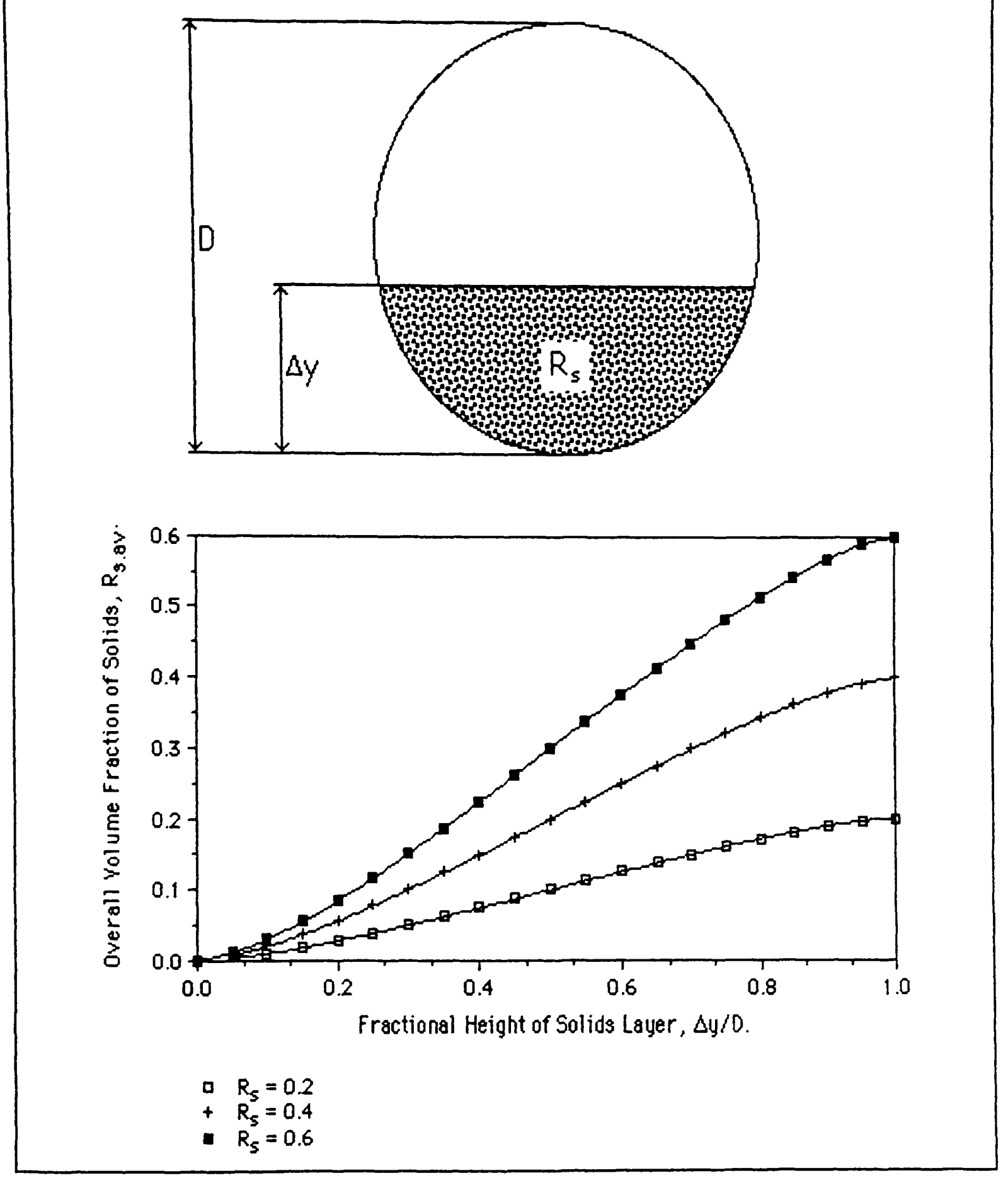

Figure 6.3.4.9 The variation of overall solids volume fraction with the height of the solids layer in a horizontal pipeline.

6.4 VALIDATION OF THE MATHEMATICAL MODEL

6.4.1 SIMULATION OF THE FLOW

The starting point for the mathematical model for moving-bed non-suspension flow was the successful model for suspension flow. The steps taken to adapt this model for another mode of flow have been described previously. This section concerns the comparison (qualitatively and quantitatively) between the model and the experimental data. The simulation of the flow was set up as follows:

i. Initial conditions:
   - The pipeline was empty (no solids).

ii. Boundary conditions:
   - Both phases flow in through the entire cross-section of the pipeline.
   - Mass flux (mass flow rate per unit area) and velocity are specified at the inlet.
   - The pressure at the outlet is fixed.

The length of pipeline modelled was 10 m. The flow was modelled for a time period that was sufficient to allow the solids to reach the outlet. The aim of this approach was to develop the flow in a similar manner to that in an actual system. The results from the middle of the pipeline were used for comparison with the experimental data. This was done to minimise the influence of any differences between the specified boundary and the actual conditions.

The variation of solids volume fraction with time for a typical test is shown in figures 6.4.1.1 and 6.4.1.2. In these figures only three contours of solids volume fraction are plotted:

i. $R_s = 10^{-4}$ which corresponds to low concentration suspension flow;

ii. $R_s = 0.1$;

iii. $R_s = 0.2$ which is the concentration at approximately 60% of the bulk density.

From a uniform flow of gas and solids across the inlet boundary, the solid particles fall under the influence of gravity. The solids form a layer, or moving-bed, in the lower half of the horizontal pipe. The $R_s = 0.2$ contour indicates a depth of 12.6 mm (2.4% of the diameter).

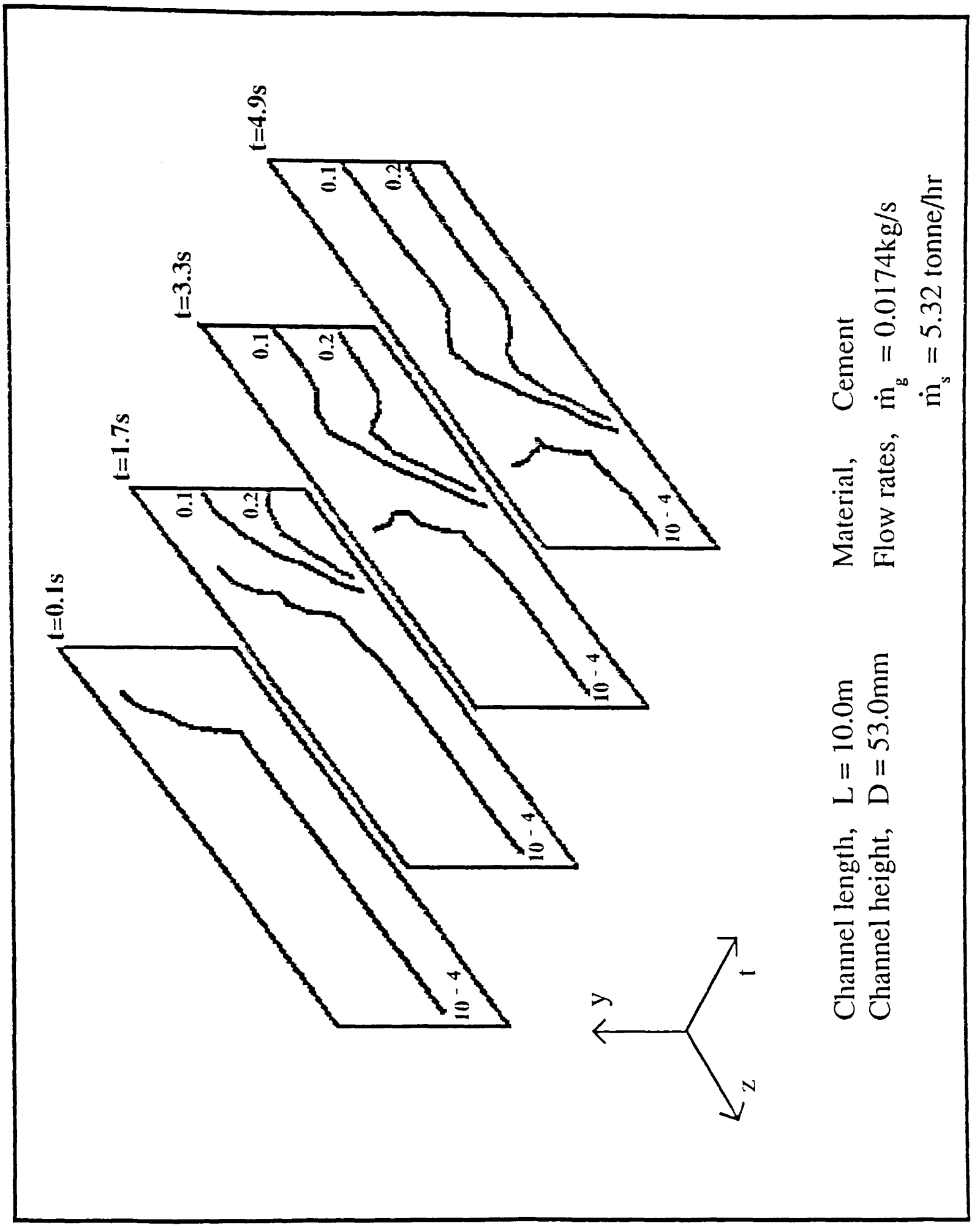

Figure 6.4.1.1 The variation of solids volume fraction in the 2D channel with time.

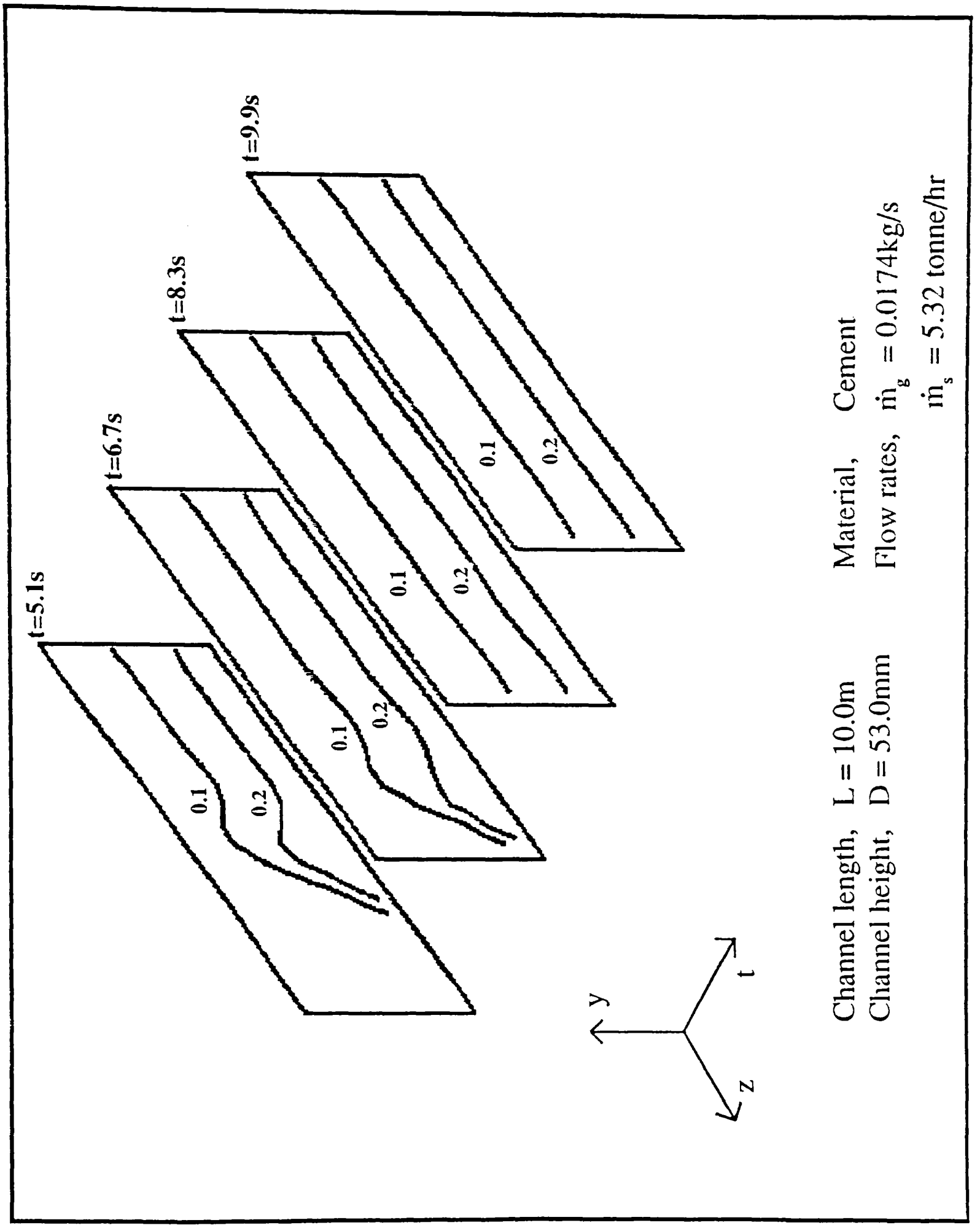

Figure 6.4.1.2 The variation of solids volume fraction in the 2D channel with time.

Figure 6.4.1.3 shows the change in the $R_s = 0.15$ contour with time. During the *pipe filling* phase the same phenomenon was observed for a number of simulations. Material builds up at the material *front*, increasing the local height of the moving-bed of solids. Observation of the flow in the experimental pipeline shows a similar phenomenon during the initial stages of the conveying trial (similar to a wave breaking and rolling up the beach). Calculating the mass flow rate of solids through the pipeline cross-section at the maximum height of the layer typically shows a 50% increase over the value at the inlet. The region at the material front is shown in detail in figure 6.4.1.4. The front is spread over two, or three control volumes in the axial direction, 1 m to 1.5 m (the length of the glass observation sections in the experimental pipeline was 2 m) and the increase in height is one control volume, or 13.25 mm. The *pipe filling* phase is only a means to an end in the computation (and actual system) and was not investigated further.

The calculated solids velocities are shown in figures 6.4.1.5 and 6.4.1.6. The velocities have been multiplied by the solids volume fraction. Thus only velocity vectors plotted in the region of the moving-bed have any length, in fact this value is the local superficial velocity:

$$\dot{m}_s = \rho_s R_s A u_s$$

$$\overline{U}_{pipe} = \frac{\dot{m}_s}{A_{pipe}\rho_s} \qquad 6.4.1.1$$

The variation of pressure with time is shown in figure 6.4.1.7. Several points should be noted from this figure:

i. the pressure in the top control volume is taken since this is closest to the upper pipe wall where the pressure tappings were located in the measuring section of the experimental pipeline;
ii. the initial pressure gradient is steep, but this can be neglected since it is a function of the inlet boundary condition;
iii. the overall pressure gradient is 1459 Pa/m.

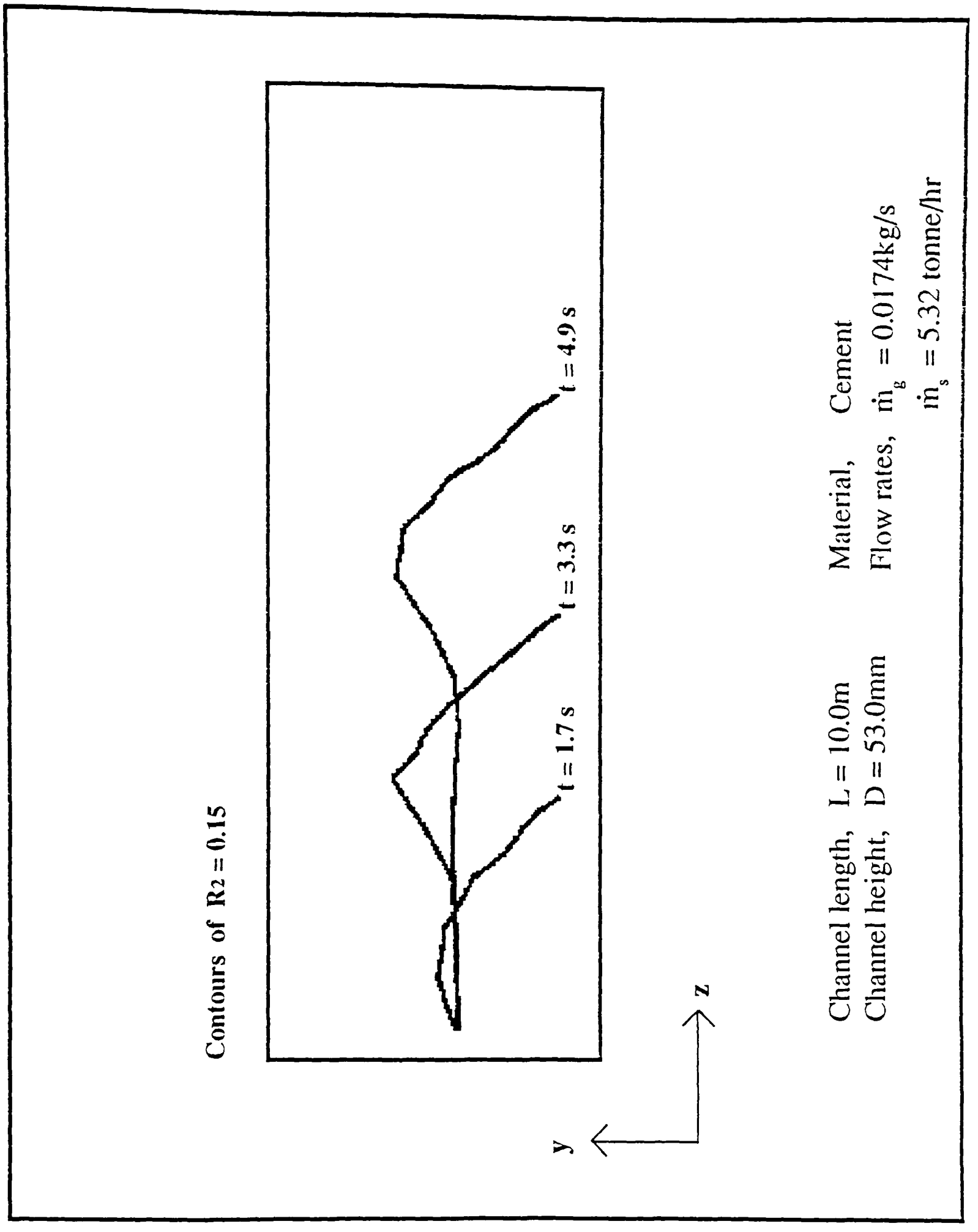

Figure 6.4.1.3 The advance of the solids front during the pipeline filling period.

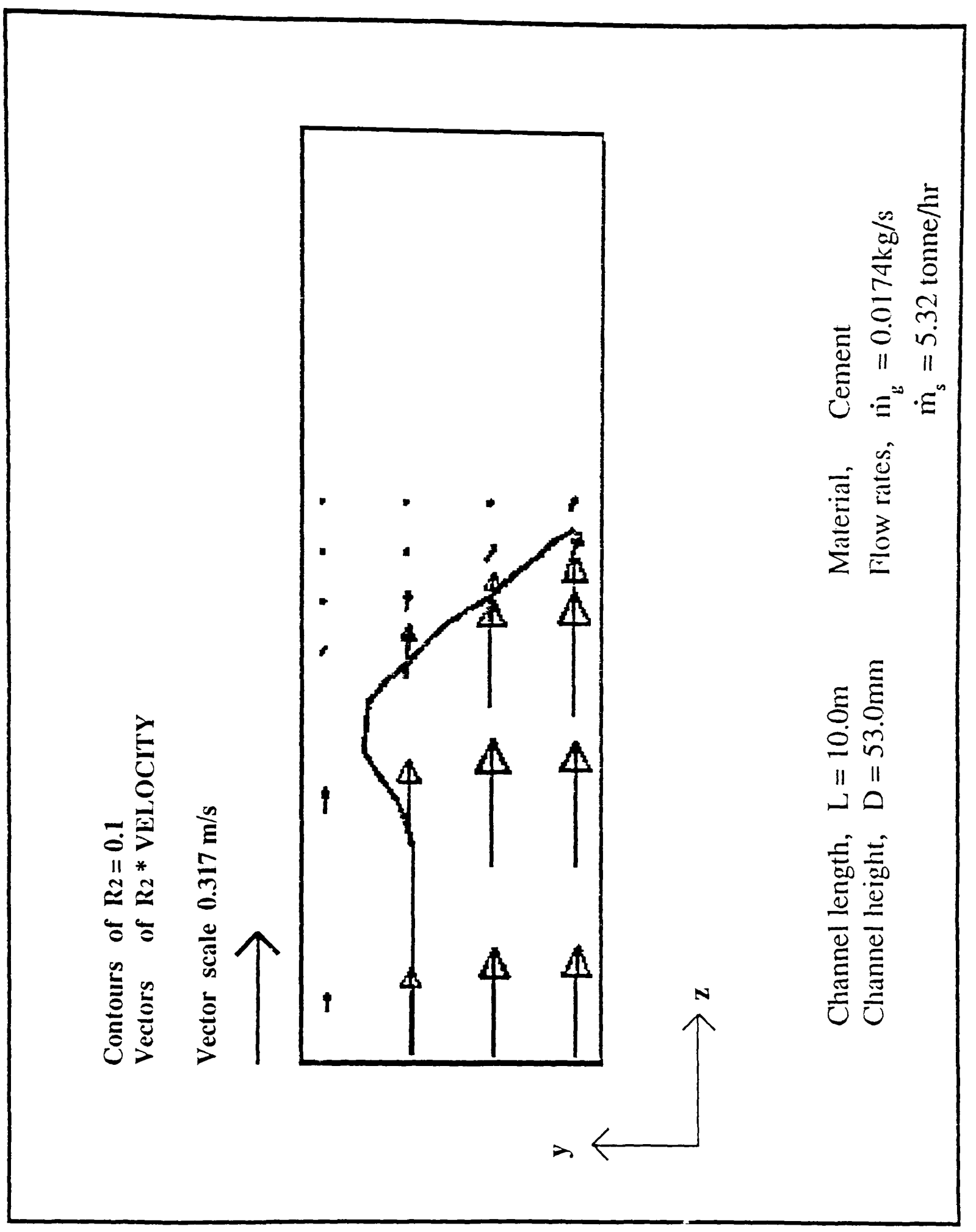

Figure 6.4.1.4 Velocity vectors in the moving-bed, showing the rolling motion of the material front during the pipeline filling period.

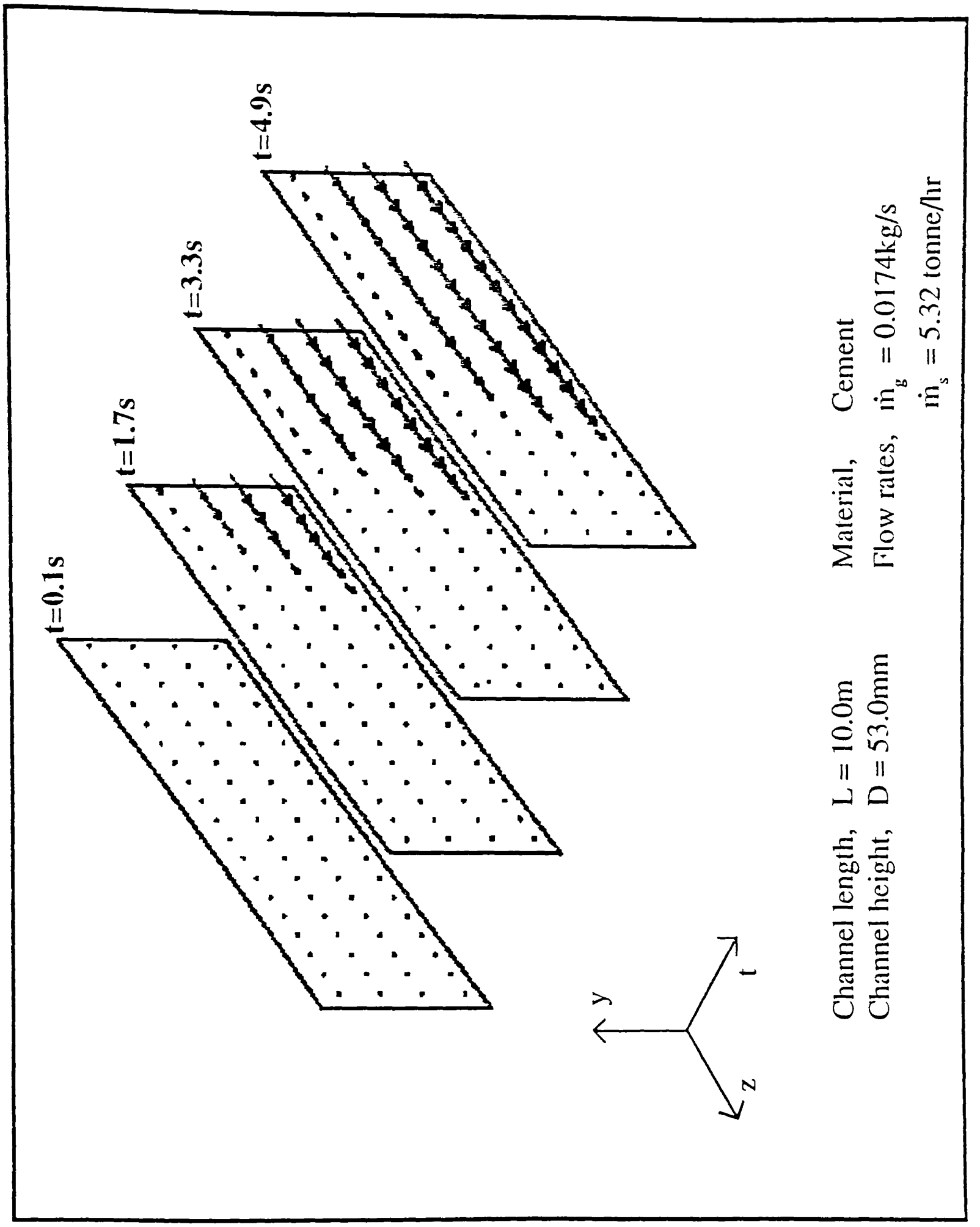

Figure 6.4.1.5 The variation velocity in the 2D channel with time (vectors of solids volume fraction times solids velocity).

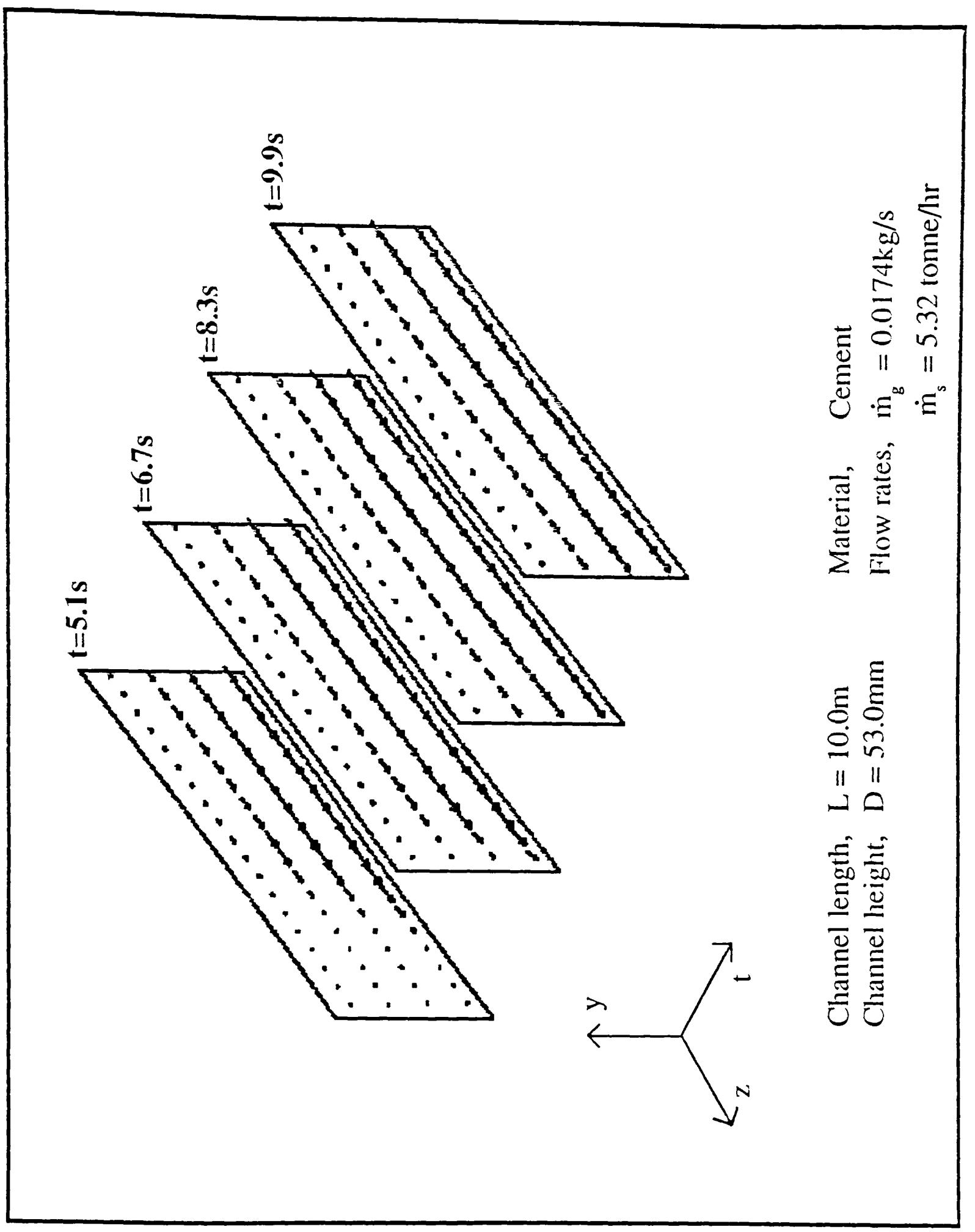

Figure 6.4.1.6 The variation of velocity in the 2D channel with time (vectors of solids volume fraction times solids velocity).

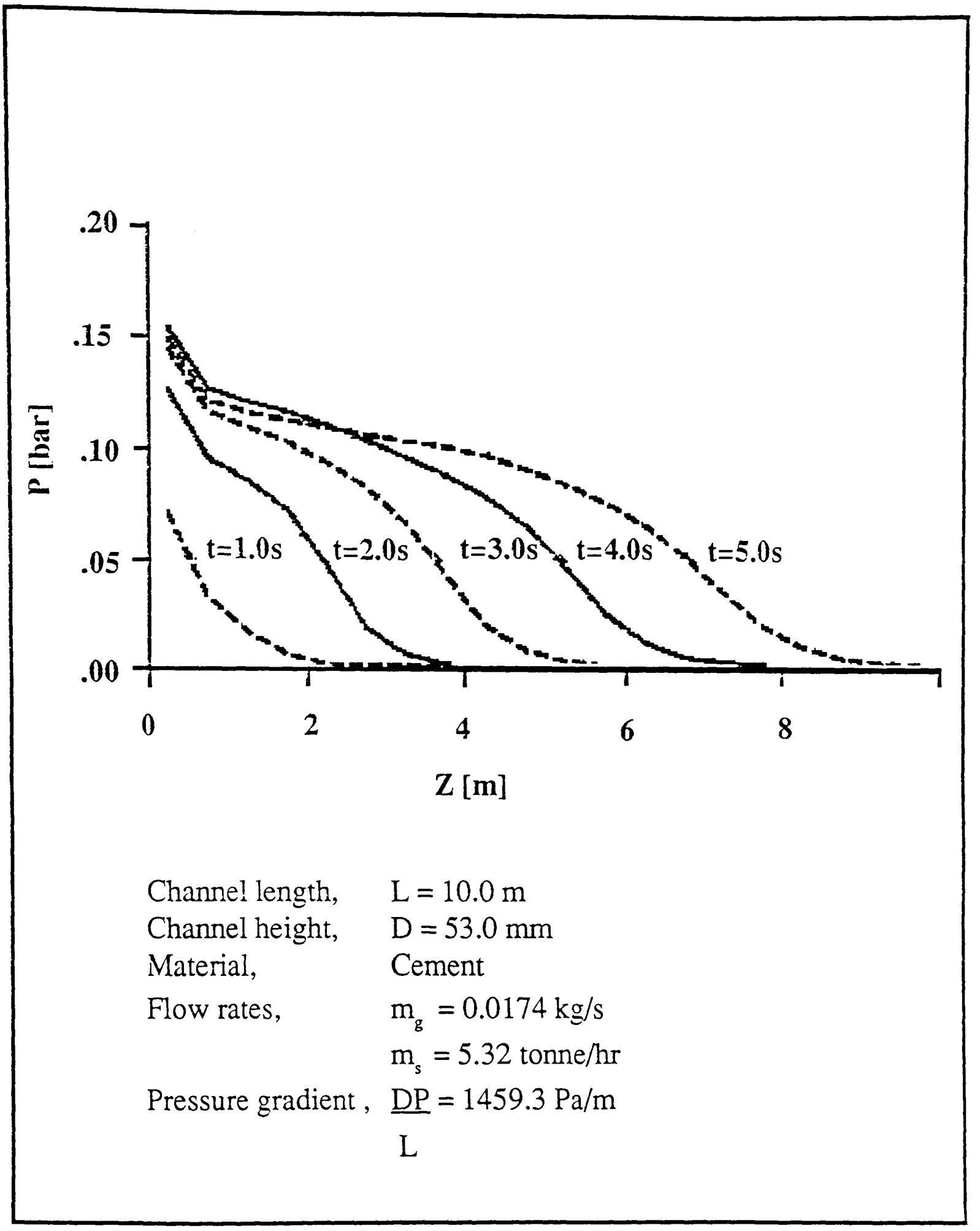

Channel length, L = 10.0 m
Channel height, D = 53.0 mm
Material, Cement
Flow rates, m_g = 0.0174 kg/s
m_s = 5.32 tonne/hr
Pressure gradient , $\frac{DP}{L}$ = 1459.3 Pa/m

Figure 6.4.1.7 The variation of pressure with axial distance and time.

Figure 6.4.1.8 shows the data from the conveying trial with the same operating point:

i. gas mass flow rate, $\dot{m}_g$ = 0.0174 kg/s;

ii. solids mass flow rate, $\dot{m}_s$ = 5.48 tonne/hr;

iii. inlet pressure, P = 0.81 bar_g.

The flow conditions during the fast scan test are shown in figure 6.4.1.9:

i. mean solids mass flow rate, $\dot{m}_s$ = 5.32 tonne/hr;

ii. mean inlet pressure, P = 0.714 bar_g

The time averaged values for the pressure at each location in the measuring section are shown in figure 6.4.1.10:

i. mean pressure gradient, $\frac{\Delta P}{L}$ = 1656 Pa/m

ii. standard deviation of the pressure = 5922 Pa

Using equation 6.3.4.10, and assuming a pipe that is one third full, then a standard deviation of this magnitude represents a variation of 3 mm in the depth of the solids moving-bed.

Comparison of the depth of the moving-bed predicted in figure 6.4.1.2 and observation of the flow in the glass sections show that this is of the correct order (ie between 30% and 50% of the pipe diameter). This assumes that the cement is concentrated at 50% to 60% of its bulk density. The measured pressure gradient is 11.8% greater than the value predicted by the mathematical model. This comparison shows the basic mathematical model is reasonable.

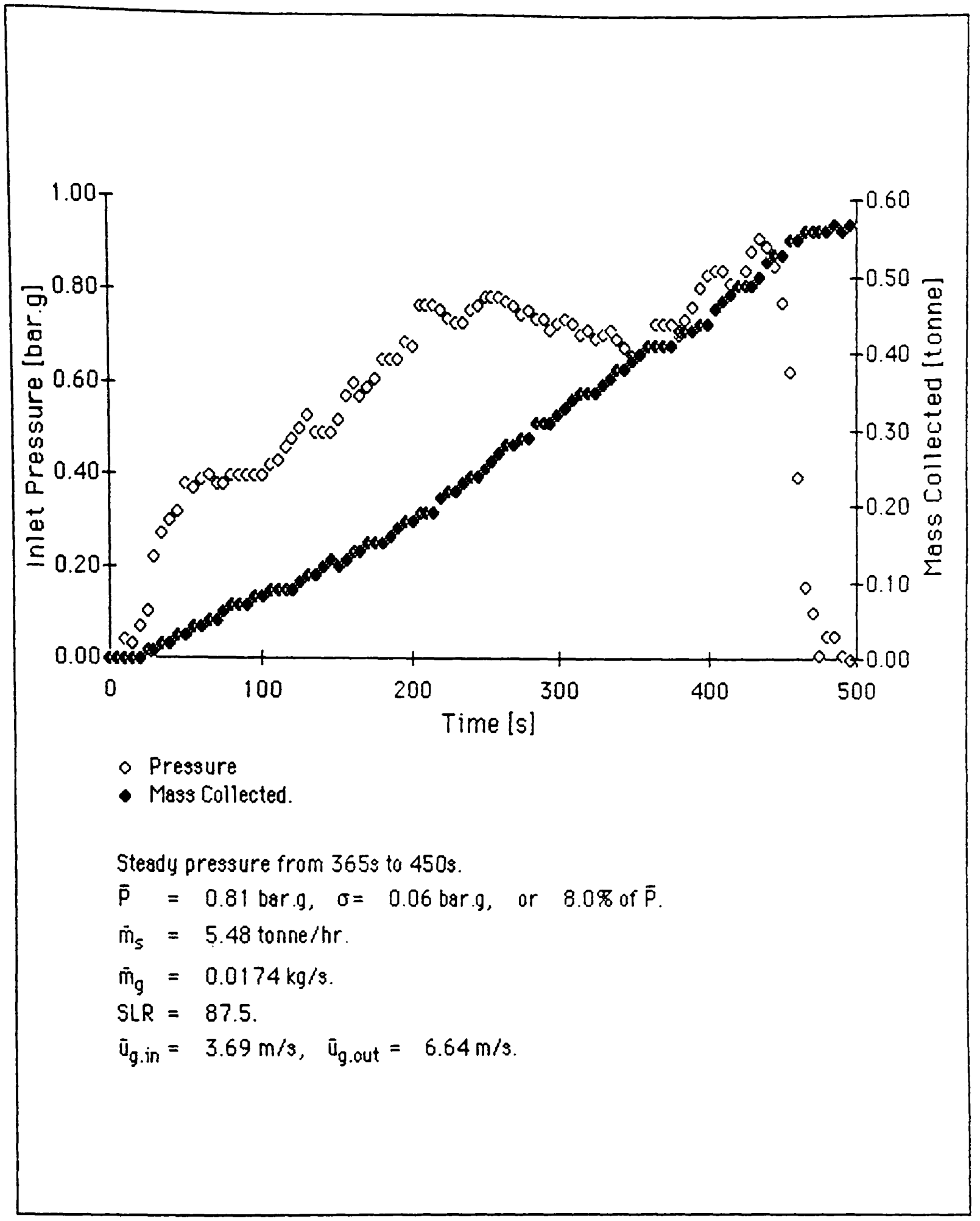

Figure 6.4.1.8 The variation of pipeline inlet pressure and mass collected in the receiving hopper during test 7.

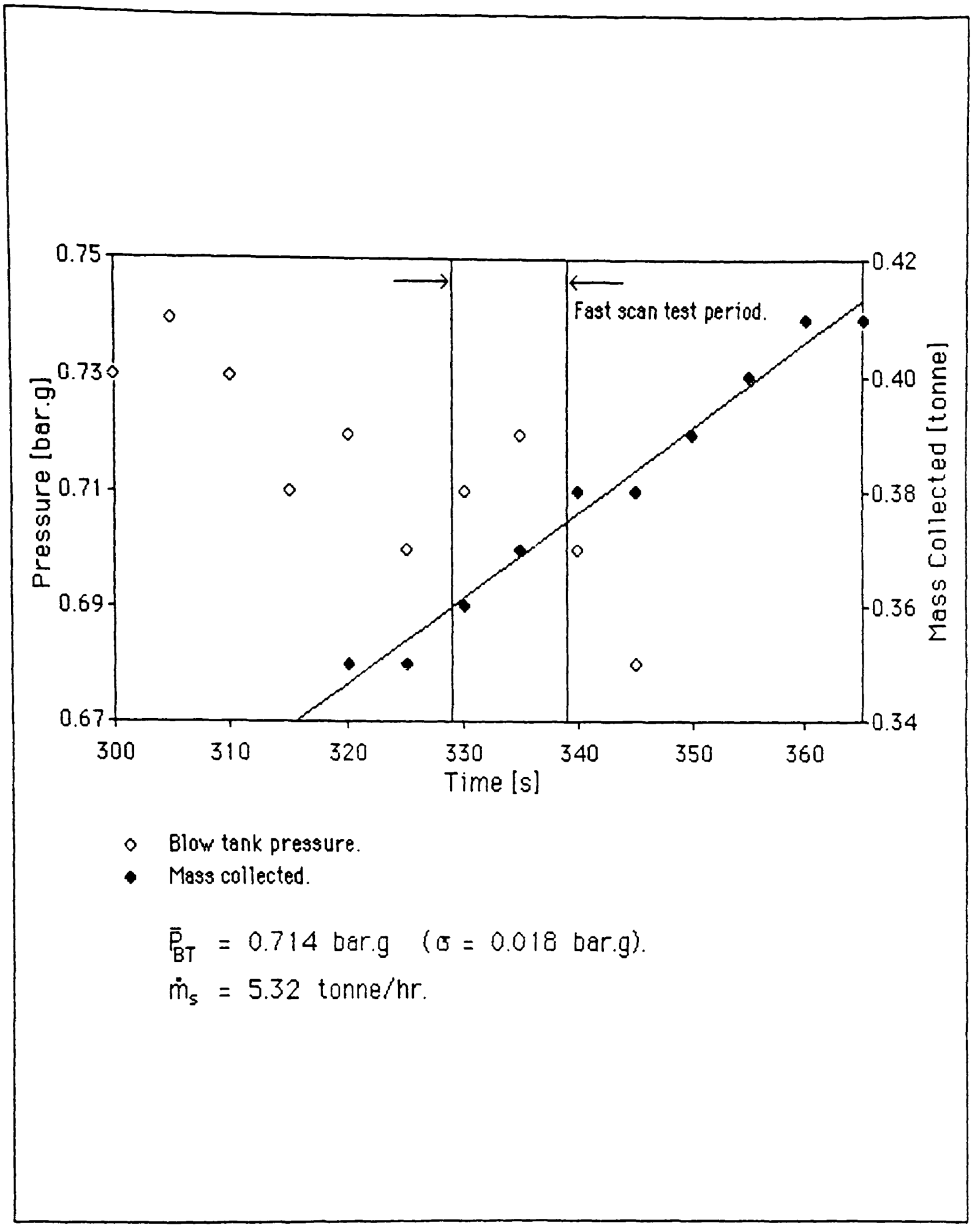

Figure 6.4.1.9 Flow conditions during the fast scan of test 7.

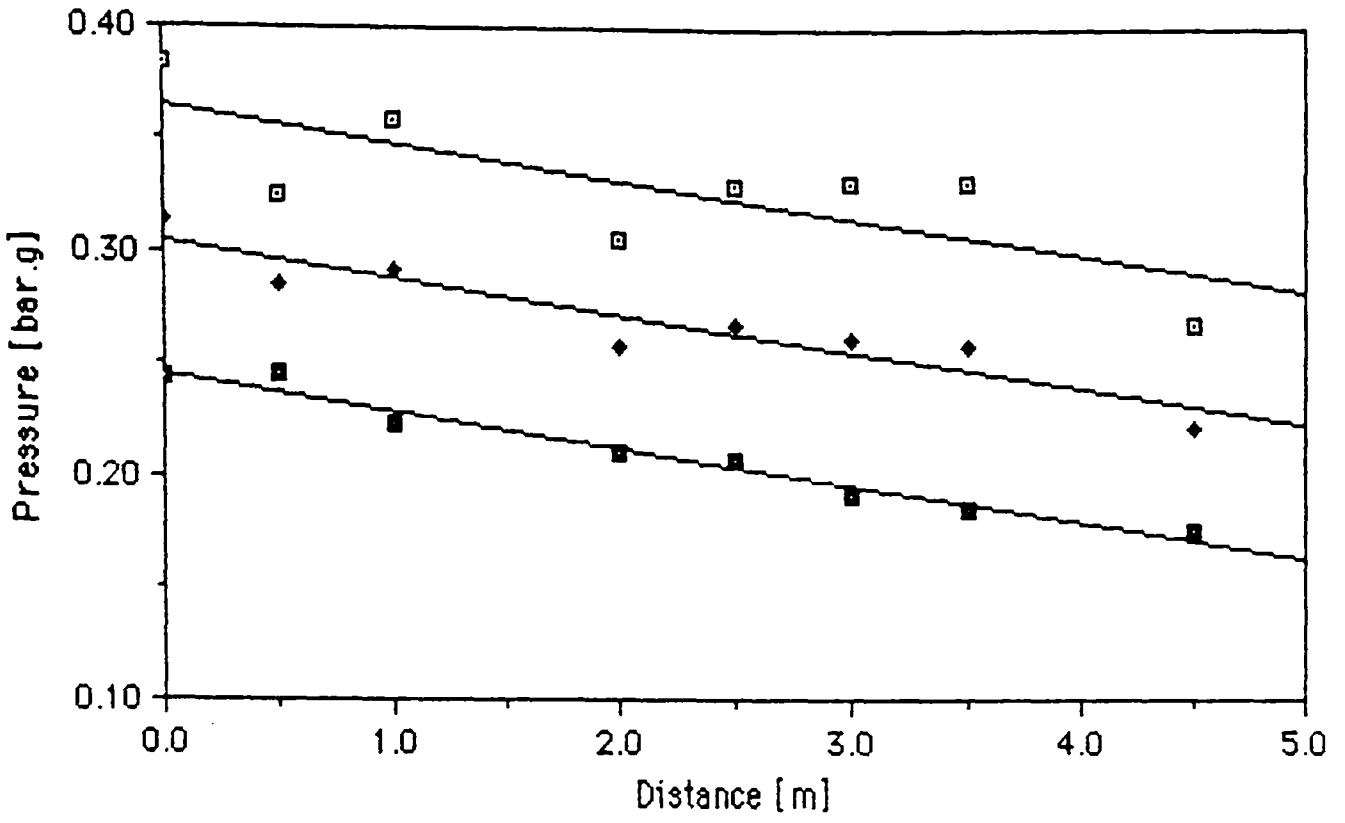

- ▫ $\bar{P} + \sigma$ = 0.36463 - 1.6595E-2.x, ρ^2 = 0.572.
- ◆ $\bar{P}$ = 0.30532 - 1.6559E-2.x, ρ^2 = 0.876.
- ■ $\bar{P} - \sigma$ = 0.24602 - 1.6523E-2.x, ρ^2 = 0.965.

At each transducer location, $\bar{P}$ represents the mean of 500 readings sampled every 0.02s for 10s.

The mean pressure gradient = 0.0166 bar/m = 1656 Pa/m.

The mean standard deviation = 0.0592 bar = 5922 Pa.

Figure 6.4.10 The time averaged mean pressure gradient during the fast scan of test 7.

6.4.2 REFINEMENT OF THE MODEL

Figure 6.4.2.1 shows the variation of predicted solids volume fraction at two instances in time. The effect of the inlet boundary condition is clearly illustrated. The uniform mass flux of both phases across the inlet results in an unrealistic distribution of solids in the first 2 m of the pipeline (the first four control volumes in the axial direction). After this point the influence of the gravitational source has established a more reasonable distribution of the solids. The solids volume fraction is not the only variable that is affected. The pressure gradient in this region is also higher.

An alternative to a uniform inlet is to specify a profile with the majority of the solids entering the pipeline in the bottom control volume. After a series of trials the following profile was found to reduce the scale of the inlet boundary condition effects:

CONTROL VOLUME	HEIGHT [mm]	PROPORTION OF THE TOTAL SOLIDS FLOW RATE
4	46.375	1%
3	33.125	5%
2	19.875	39%
1	6.625	55%

It can be seen from figure 6.4.2.2 that the pressure gradient in the first metre is similar to that for the remainder of the pipeline. Comparison of the predicted profile of the solids volume fraction at a number of cross-sections through the pipe are shown in figure 6.4.2.3. The variation in the profile is now much less than that with the uniform inlet condition. The increase in the solids volume fraction in control volume 2 indicates an increase in the depth of the moving-bed of solids.

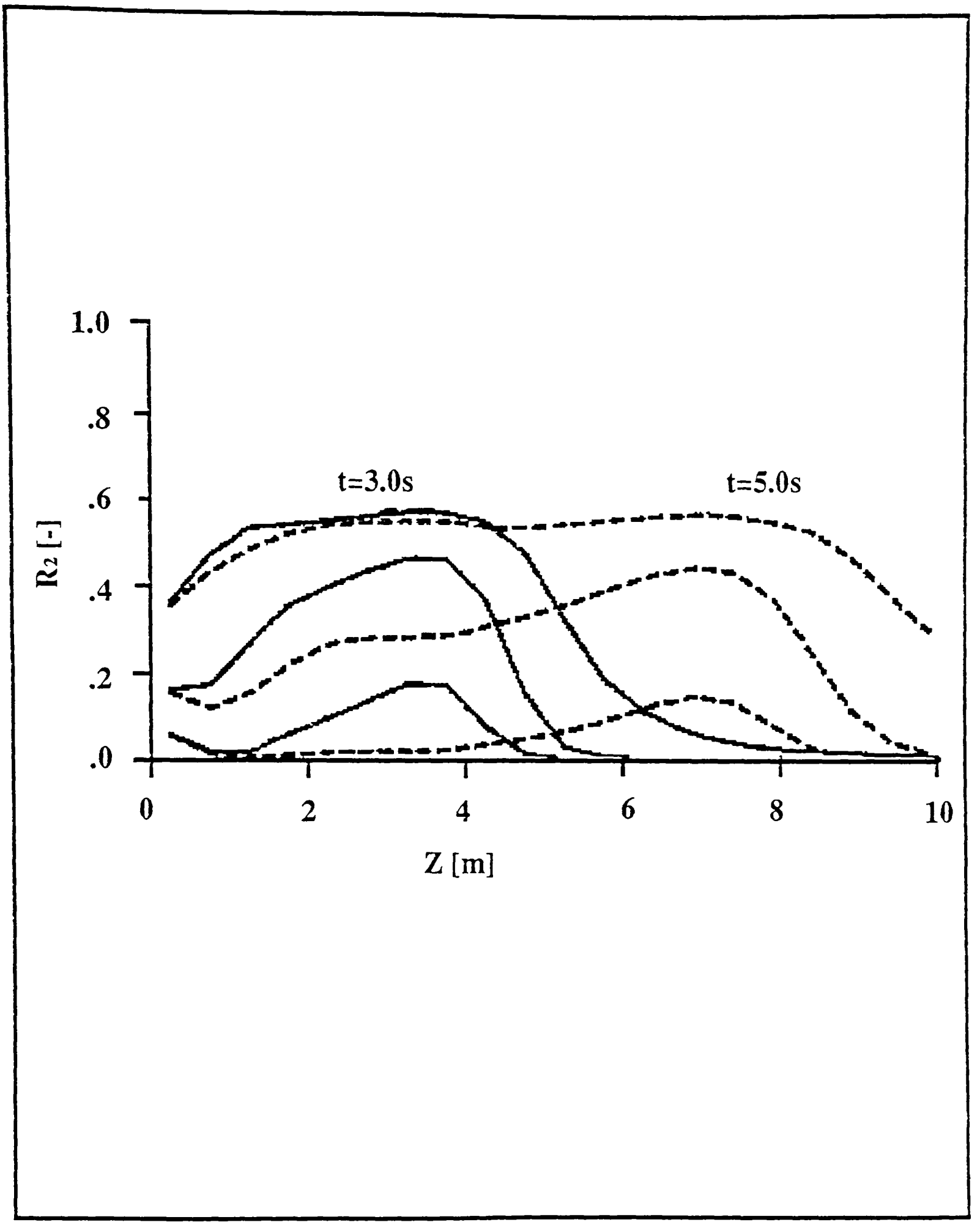

Figure 6.4.2.1 The variation of predicted solids volume fraction with time.

The influence of the outlet boundary condition can also be seen in figure 6.4.2.1. The outlet boundary condition is a fixed pressure condition where:

$$S_{outlet} = R_i C (V - P) \qquad 6.4.2.1$$

where
- R_i is the volume fraction of the phase
- C is the coefficient of the source term set to a large value, $C < 10^{10}$
- V is the value of the external pressure 0 barg
- P is the pressure in the last axial control volume

The size of the coefficient ensures that the mass flow out of the control volume is proportional to the pressure gradient between the cell and the external value. The volume fraction weights the source term so that the outflow from the control volume is proportional to the respective volumetric concentration of the gas and solids in the control volume. This was modified by multiplying the coefficient by the density of the phase. This change results in the outflow being proportional to the mass concentration in the control volume. Figure 6.4.2.4 shows the benefit of this adjustment.

The simulation results shown in figure 6.4.2.2 are for a higher solids mass flow rates than the previous case. The conveying trial operating point was:

i. gas mass flow rate, $\dot{m}_g$ = 0.05 kg/s;

ii. solids mass flow rate, $\dot{m}_s$ = 13.76 tonne/hr;

iii. inlet pressure, P = 1.85 bar_g.

During the fast scan test:

i. mean solids mass flow rate, $\dot{m}_s$ = 12.86 tonne/hr;

ii. mean inlet pressure, P = 1.73 bar_g

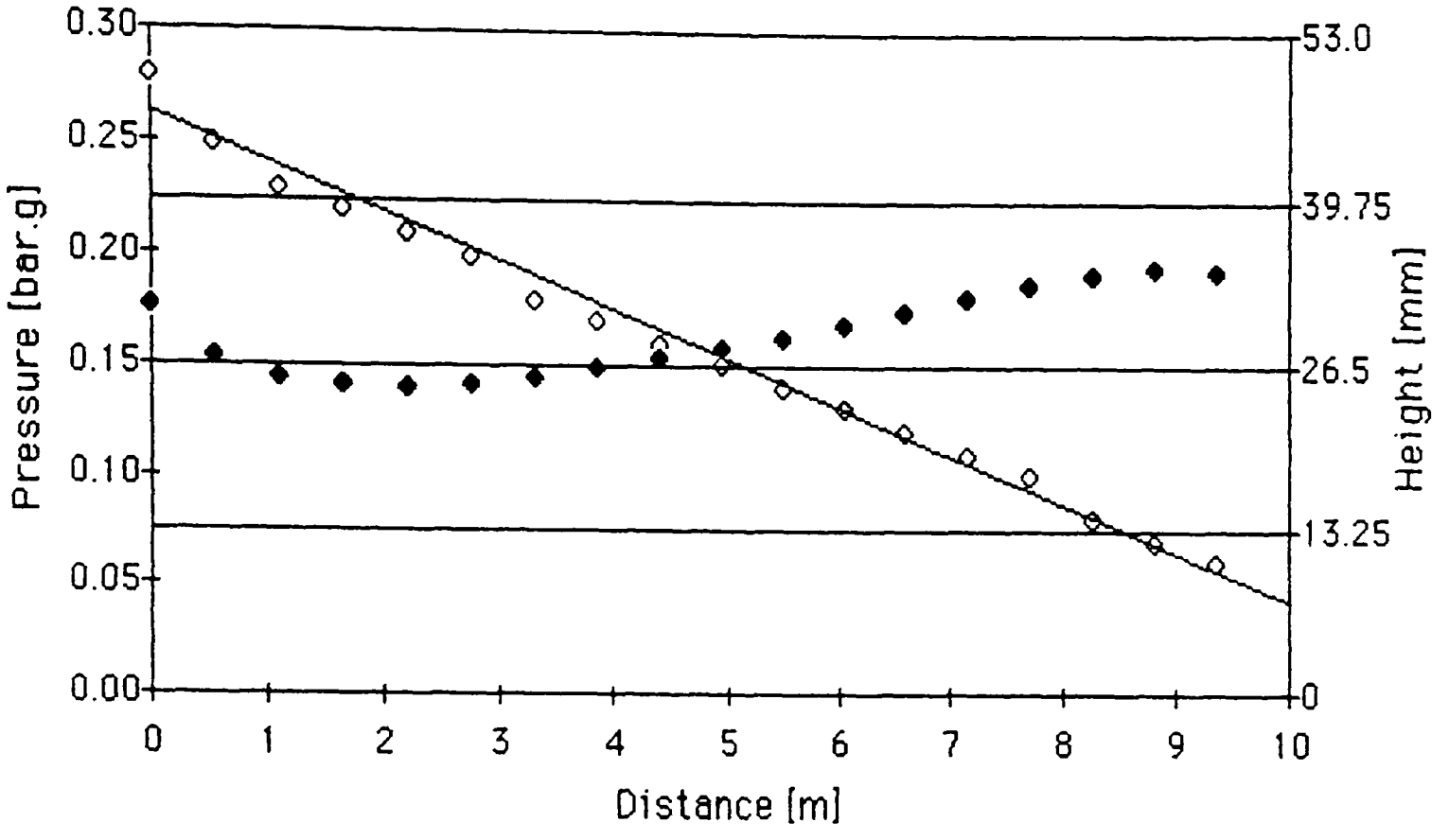

$\bar{m}_g$ = 0.05 kg/s
$\bar{m}_s$ = 12.86 tonne/hr
$\frac{\Delta P}{L}$ = 2178.6 Pa/m

Height estimated by assuming the bed is at the bulk density of the cement
ie R_{sbed} = 0.35

$$(R_{s.av})ix = \frac{1}{4} \left(\sum_{iy=1}^{4} R_{s.iy}\right)ix$$

Height found by using figure 6.3.4.9

Figure 6.4.2.2 The predicted pressure drop and bed height variation after the pipe had been filled.

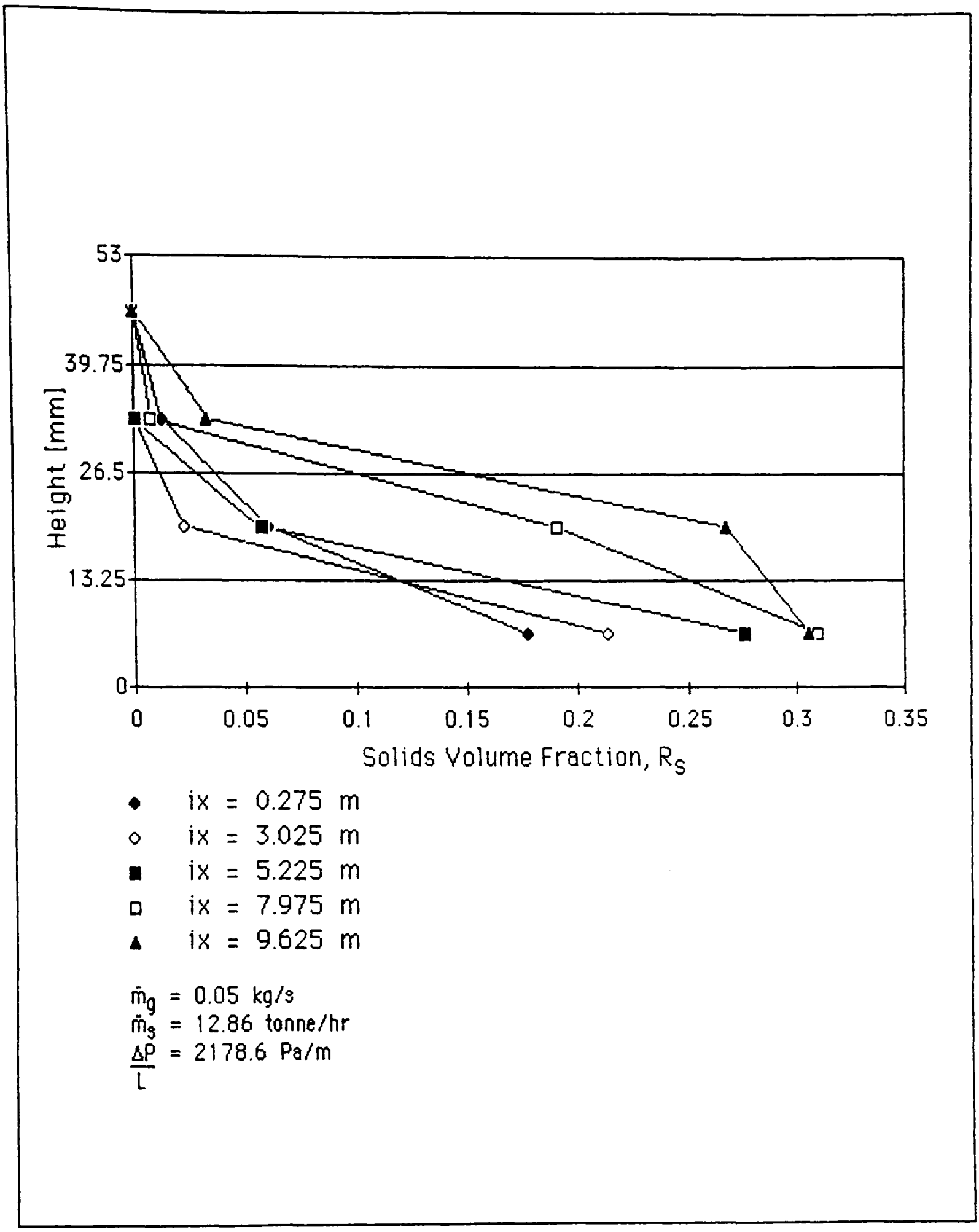

Figure 6.4.2.3 The predicted profile of the solids volume fraction at several cross-sections along the pipeline.

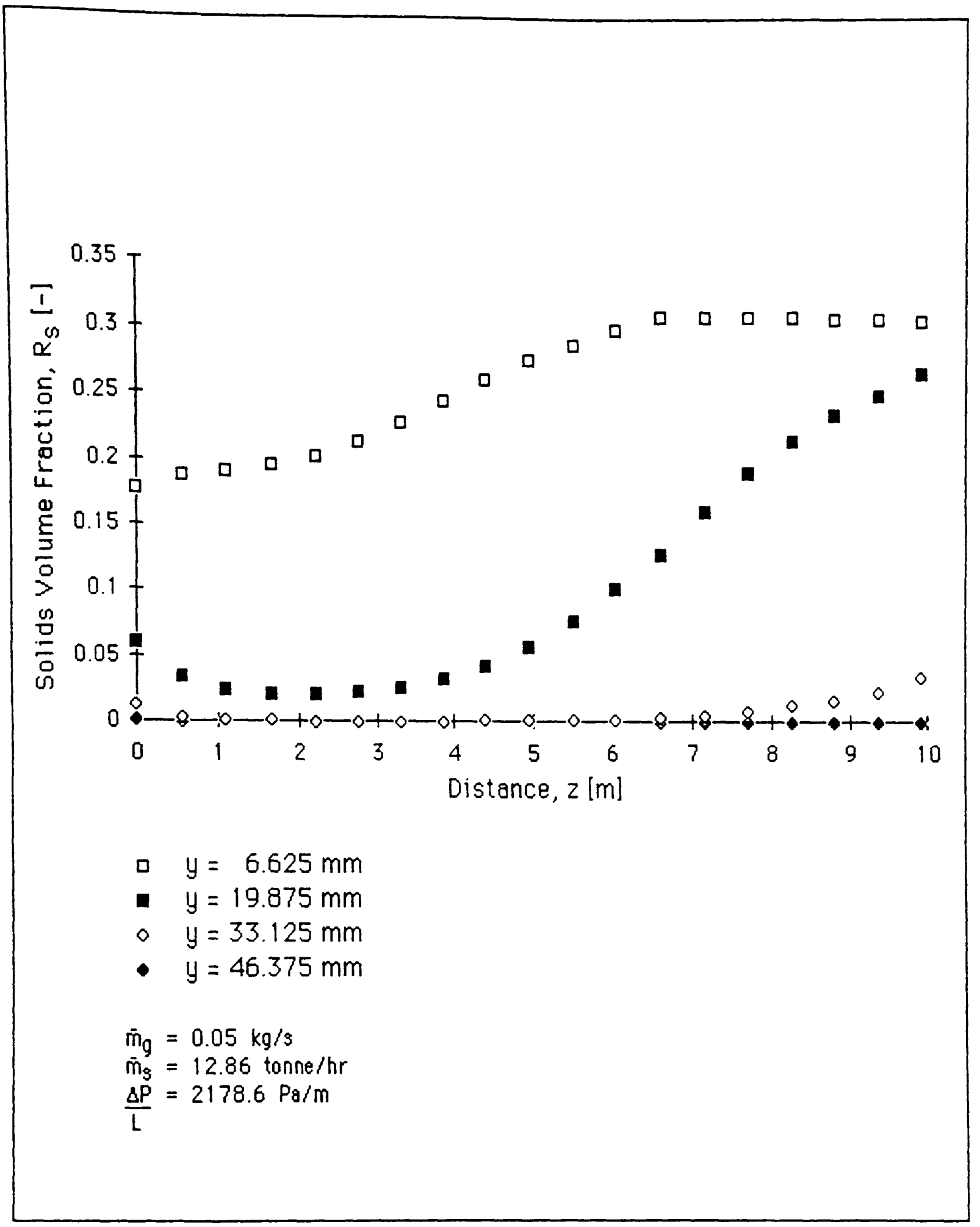

Figure 6.4.2.4 The variation of solids volume fraction with axial distance and height.

The time averaged values for the pressure at each location in the measuring section are shown in figure 6.4.2.5:

i. mean pressure gradient, $\frac{\Delta P}{L}$ = 3061 Pa/m

ii. standard deviation of the pressure = 1308 Pa

The predicted value of the pressure gradient is only 71% of the measured value. This difference points to a deficiency in one of the mathematical models.

The wall friction model for the solids makes a number of assumptions. The first problem is that the calculation was for a two dimensional channel rather than a cylindrical pipe. The comparison of the relative effects of these two geometries is not straightforward. Depending upon the depth of the moving-bed of solids:

i. the ratio of the surface areas of the walls in contact with the solids;
ii. the ratio of the cross-sectional areas occupied by the solids;

will have effects that tend to balance each other, as shown in figure 6.4.2.6. In addition to the geometric considerations the wall shear stress will vary for the pipe, unlike the channel where the height of solids above the wall is constant. The wall friction model assumes that the shear force at the wall is proportional to the normal force at the wall. The constant of proportionality was taken as the wall friction coefficient from a shear cell test. In this test the bulk material is compacted by an applied load. The physical situation in the pipeline is quite different, since the bulk material is aerated (a dynamic situation rather than the static one in the test). A number of conflicting factors have been noted relating to the geometry and the material property data used in the wall friction model. None of these factors would be expected to significantly increase the wall friction and hence the pressure gradient.

If the sole aim was to increase the pressure gradient until it matched the experimental value then the constants associated with the interphase friction and the diffusion coefficient could be altered to achieve the desired result. This exercise would not solve the problem since the constants would be different for each combination of flow rates.

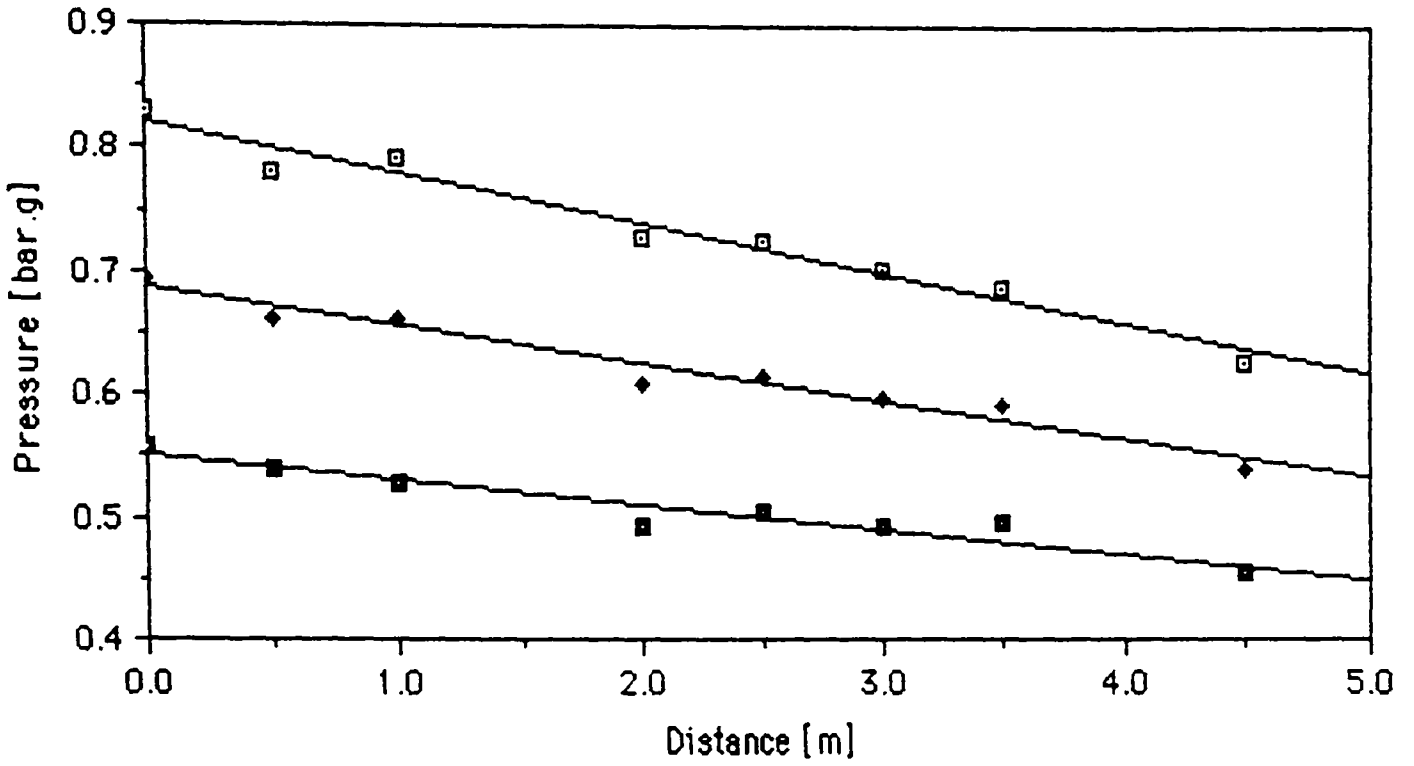

□ $\bar{P} + \sigma$ = 0.82209 - 4.1145E-2.x, ρ^2 = 0.967.

◆ $\bar{P}$ = 0.68640 - 3.0612E-2.x, ρ^2 = 0.961.

■ $\bar{P} - \sigma$ = 0.55071 - 2.0079E-2.x, ρ^2 = 0.914.

At each transducer location, $\bar{P}$ represents the mean of 200 readings sampled every 0.02s for 4s.

The mean pressure gradient = 0.0306 bar/m = 3061 Pa/m.

The mean standard deviation = 0.0131 bar = 1308 Pa.

Figure 6.4.2.5 The time averaged mean pressures in the measuring section during the fast scan in conveying trial 5.

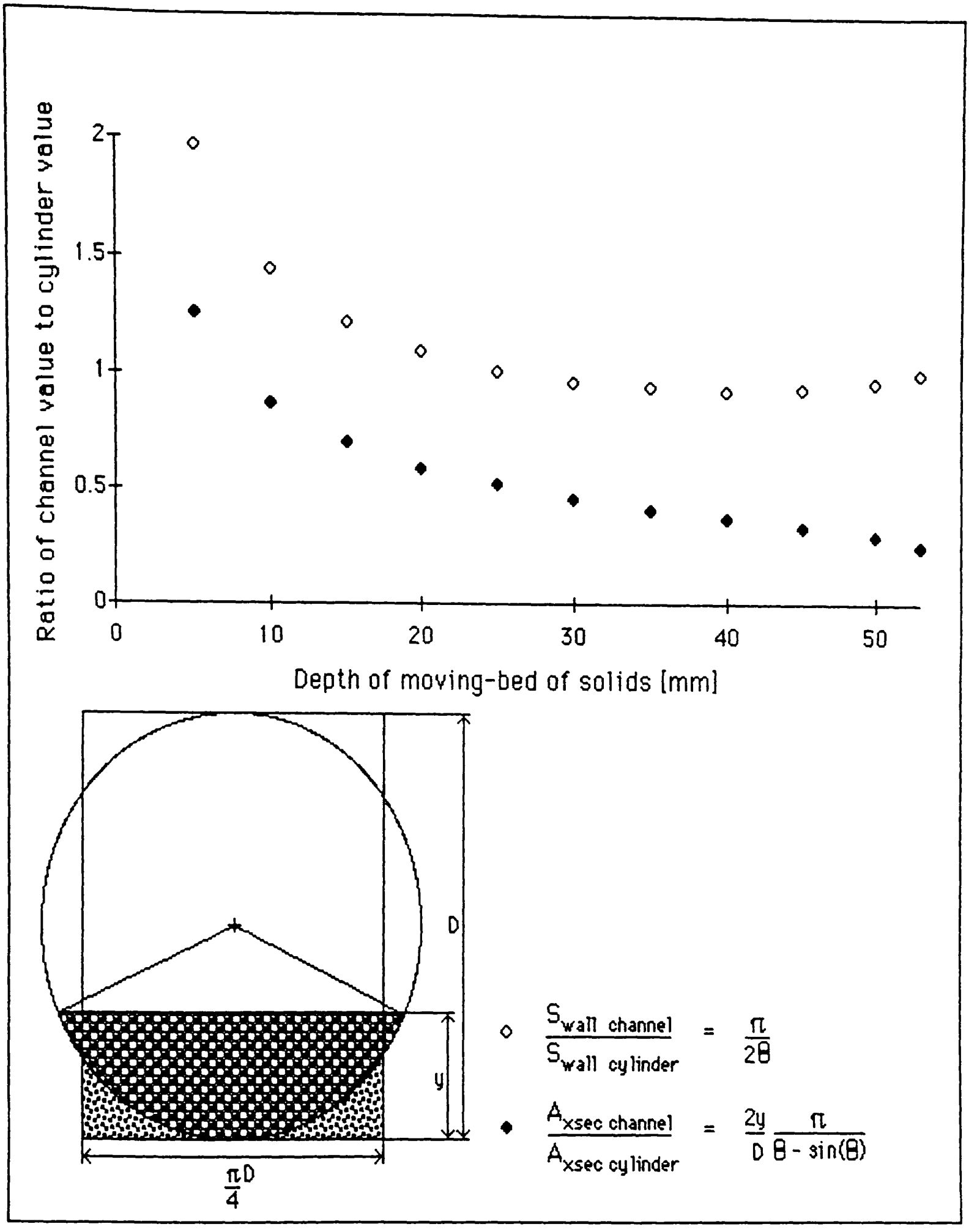

Figure 6.4.2.6 A geometric comparison of the assumption of a 2D channel against a 3D cylinder for the calculation of the solids wall friction.

A major contribution to the source term in the momentum equations is made by the interphase friction force. This term is calculated by taking the force on a single particle and modifying it according to the volume fraction of the solids phase. This practice has been used to correlate the behaviour of fluidised beds with single particle equations, for example Richardson and Zaki (1954). Figure 6.4.2.7 shows the variation of the function used with solids volume fraction. Also shown is a modified function that would increase the interphase force by the margin necessary to minimise the difference between the experimental and predicted values for the pressure gradient. Foscolo and Gibilaro (1984) reviewed a number of works and concluded that $(1-R_s)^{-3.8}$ is well supported by the experimental evidence as the modifying function. Care must be taken when reviewing these works since most correlate with the superficial gas velocity, thus:

$$\overline{U}_g = \frac{\dot{m}_g}{A\rho_g} = R_g u_g \qquad 6.4.2.2$$

$$\overline{U}_g . R_g^{-4.8} = u_g . R_g^{-3.8} \qquad 6.4.2.3$$

Two possibilities exist:

i. the conditions in the fluidised bed and the moving-bed type flow in the pipeline are sufficiently different to justify an increase in the exponent of the modifying function;
ii. the mathematical model used does not account for all of the physical phenomena that occur in the flow.

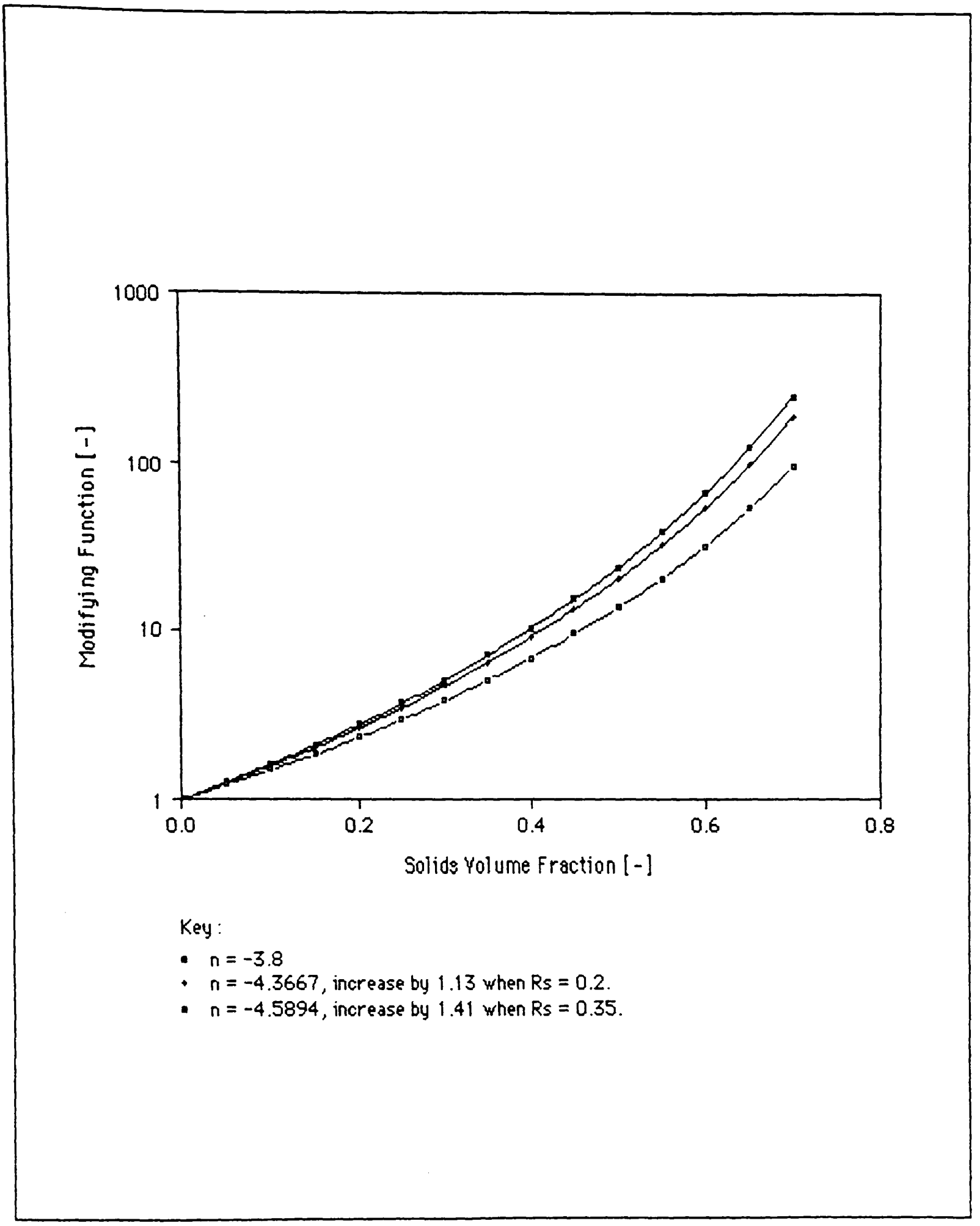

Figure 6.4.2.7 The function to modify single particle phenomena to account for multi-particle effects.

6.5 SUMMARY

A mathematical model for the non-suspension moving-bed mode of gas-solids pipeline flow has been developed. Experimental work was undertaken to validate this model. The results showed a reasonable agreement for lower flow rates of gas and solids. The deviation increased with higher flow rates of gas and solids.

The experimental investigation showed that the pressure in the pipeline can vary significantly with time at one location. Analysis indicates that this effect is due to the pulsatile nature of the flow. Thus the velocity of the fluctuations of the depth of the moving-bed could be estimated. These velocities were of the same order as the superficial gas velocity. This provides a useful basis for a non-intrusive flow rate measuring device for this particular mode of flow.

The development of the mathematical model showed that empirical results used to correlate single particle phenomena with multi-particle phenomena are extremely complex and need to be treated with care. These factors nearly always incorporate a number of physical phenomena so that the danger of accounting for an individual effect more than once exists.

7 NON-SUSPENSION PLUG TYPE FLOW

7.1 INTRODUCTION

7.1.1 PLUG FLOW MATERIALS

Bulk materials that can flow in a plug mode of flow exhibit high values of permeability and de-aeration rate, Jones and Mills (1989). These materials have a narrow particle size range and can be classified as Geldart group B, or D materials. Examples of such bulk materials are: mustard seeds; coarse grades of silica sand; and polyethylene pellets. This last material is widely used at trade exhibitions worldwide to demonstrate *dense phase* pneumatic conveying systems.

Early investigators of plug flow include: Lippert (1966); Muschelknautz and Krambrock (1969); and Flatt and Allenspach (1969). A number of pneumatic conveying systems were produced to promote plug flow with a variety of devices for controlling the formation and period of the plugs. The work of Konrad (1980), Hitt (1985), and Mainwaring and Reed (1986) indicate that it is the material properties and not the type of system that govern the potential of a bulk material to flow in a plug flow mode. These modified systems offer the greatest potential when considering borderline materials whose bulk properties are not sufficient in themselves to allow plug flow.

7.1.2 A DEFINITION OF PLUG FLOW

If the conveying gas velocity is maintained at a sufficiently high value a bulk material can be conveyed successfully in a pneumatic conveying system. Reducing the flow rate of the gas will result in particles falling out of suspension and either a pipeline blockage will occur, or flow in a non-suspension mode. Experimental investigations using this approach have often failed to identify bulk materials, with the potential to flow in a plug flow mode, as being capable of non-suspension flow.

The key to identifying such bulk materials is to start from zero gas velocity rather than reducing the gas velocity from that necessary to achieve suspension flow. Ramachandran et al (1970) and Hitt (1982) both describe the development of plug flow from very low conveying gas velocities. Figure 7.1.2.1 illustrates the development of the flow as the gas velocity is increased.

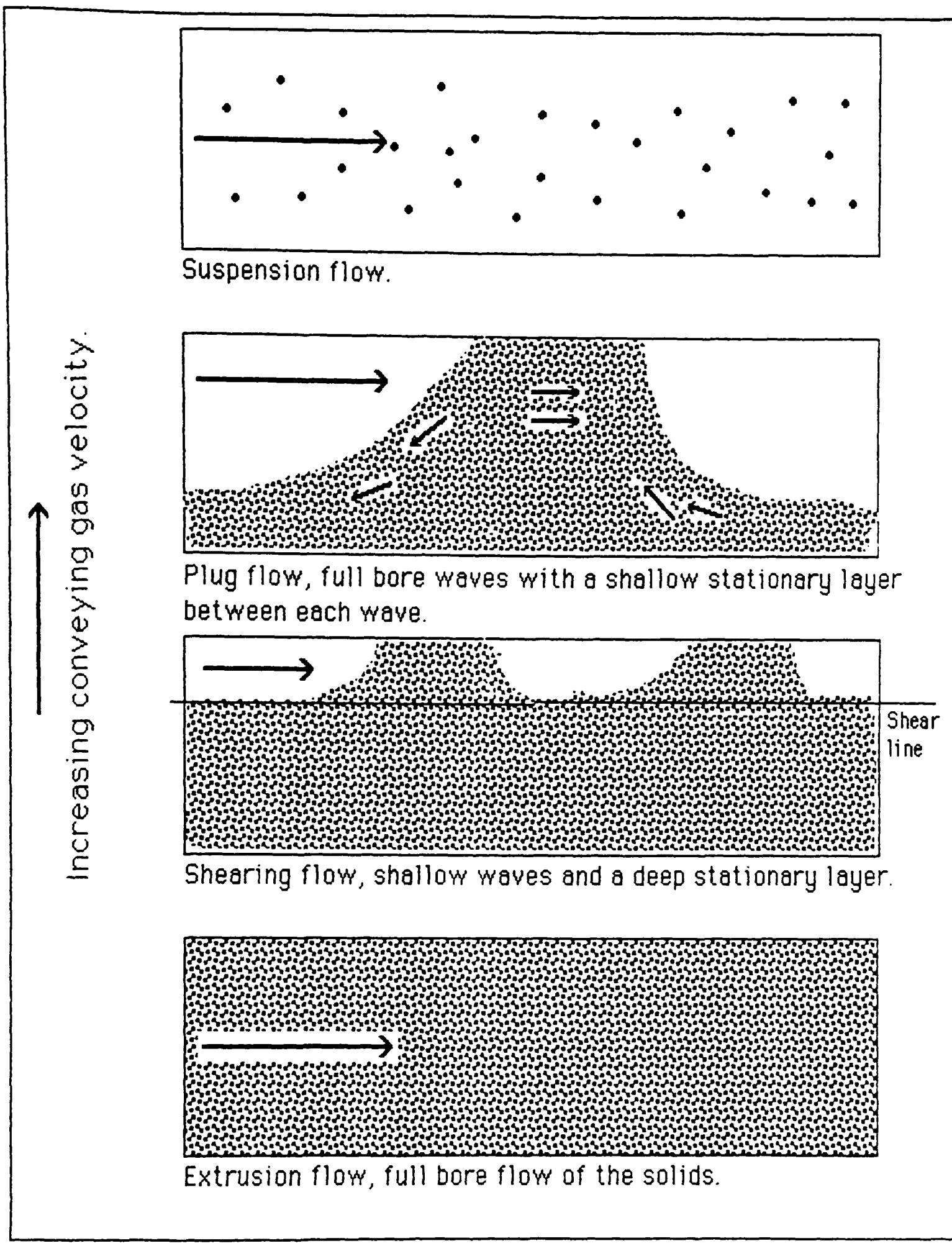

Figure 7.1.2.1 Flow patterns in the development of non-suspension plug type flow.

In this work the extrusion type of flow, at the lowest gas velocities, was only evident in the first glass section (5 m from the solids feed point). The shearing mode was only noticed with certain materials. In particular, it was possible to achieve this flow with silica sand (mean particle size 1 mm), but not with polyethylene pellets (mean particle size 4 mm). This was also reported by Hitt (1985). As the gas flow rate is increased the flow regime commonly described as plug flow is achieved. This type of flow is a series of waves. The name plug flow has often caused confusion, since the plug is often assumed to be comprised of the same particles throughout its journey along the pipeline. This is not the case in reality, but the terminology is consistent with that used to describe stratified gas-liquid flows. Baker (1954) and Wallis and Dobson (1973) define plug flow in horizontal channels as the case where gas bubbles are formed by the crest of the liquid wave being permanently in contact with the upper channel wall.

As the gas flow rate is increased further there is an uncontrolled acceleration of the flow. Visual observation of the flow in the glass sections is difficult though the flow is still pulsatile. During this mode of flow considerable vibration was induced in the pipeline by the impact of clumps of particles on bends in the pipeline. Figure 7.1.2.2 shows the conveying characteristic for polyethylene pellets. The locus of the maxima of the pressure contours marks the boundary between non-suspension plug type flow on the left and suspension flow on the right. The region close to this boundary is where this pulsatile flow occurs. In practice it is difficult to obtain reliable system operating points in this region.

Pulsatile flow can be observed at the end of the discharge cycle of pneumatic conveying systems fed by blow tanks. With an empty pressure vessel (but with material still in the pipeline) the pipeline pressure gradient falls rapidly as the pipeline is cleared. Since the gas is supplied at a constant mass flow rate the velocity of the conveying gas increases and the pulsatile mode of flow is achieved during line clearance. In order to minimise degradation of the bulk material the conveying gas can be shut off as the pressure begins to decay. This results in a layer of material being left in the pipeline. For plug flow materials this does not present a problem, since after refilling the pressure vessel conveying can be recommenced. This is in marked contrast to bulk materials that flow in a moving-bed mode of non-suspension flow were it is critical to keep the material *live* (fluidised and moving) in order to maintain non-suspension flow.

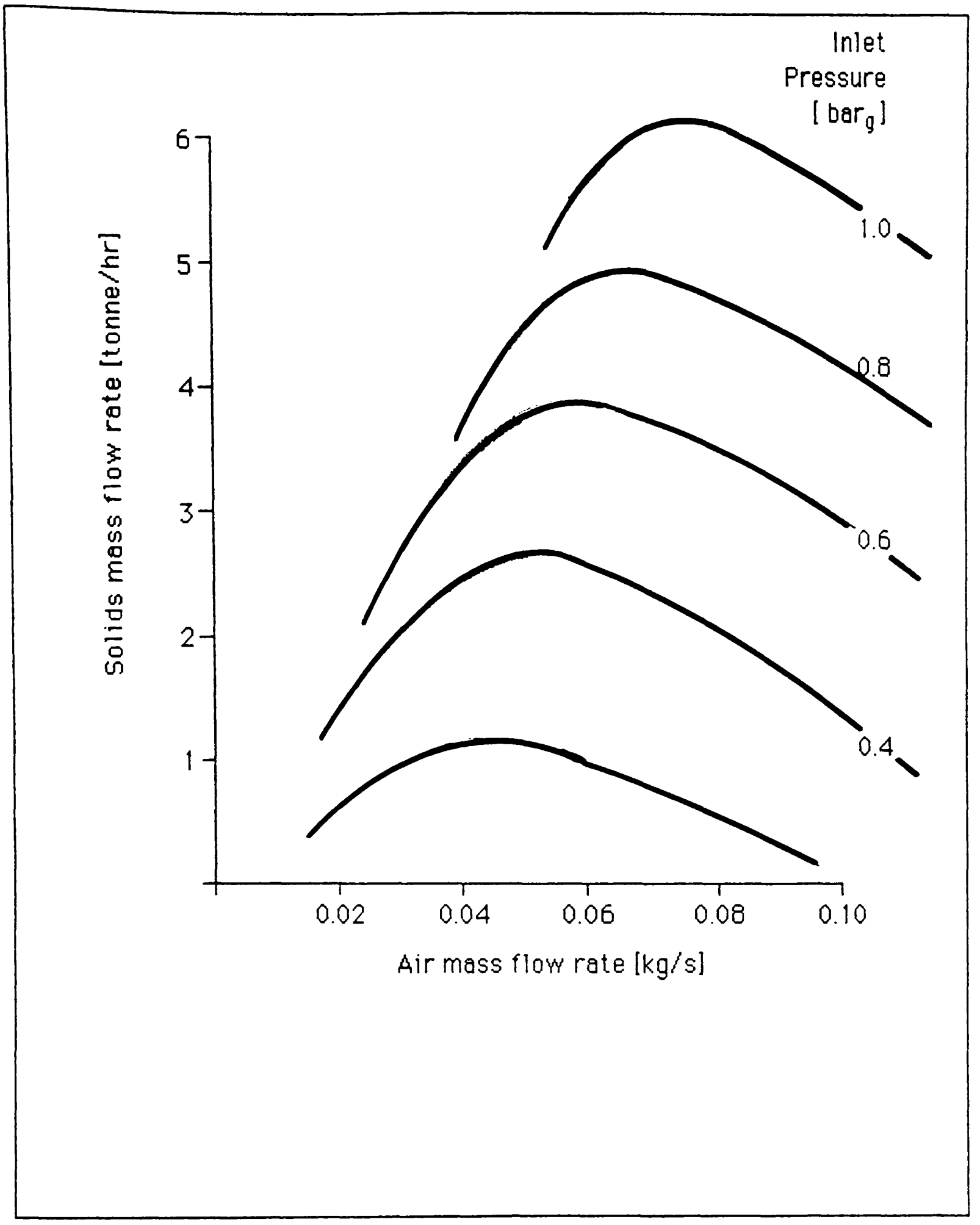

Figure 7.1.2.2 Conveying characteristics for polyethylene pellets.

7.2 MODELS FOR PLUG FLOW

7.2.1 ANALYSIS OF A SINGLE PLUG

Konrad (1980) and Legel (1980 and 1984) based their analyses of plug flow on a balance of forces on a single plug. Figure 7.2.1.1 illustrates the difference between the models of the plug used by each author. Legel used an extra force to model the momentum transfer between the plug and the stationary layer, whereas Konrad assumed a transition portion of the plug where the velocity was half of that in the main portion of the plug.

In both these studies the scale of the experimental rig was small:

i. a straight horizontal pipe D = 100 mm and L = 6.0 m was employed by Konrad;
ii. a straight horizontal pipe D = 40 mm and 65 mm and L = 22 m was used by Legel.

This limits the analysis since tests with longer pipelines in this work have shown that plugs of material will combine and then decompose. In addition Legel used a pulsed feed (the air supply was alternated between the blow tank and the supplementary line) though the measuring section was sufficiently far downstream for this to have a negligible effect.

The equations for pressure gradient across a moving plug have been converted to a common set of symbols, with the equations presented in the form:

$$\frac{\Delta P}{L_P} = \rho_B g \tan(\phi_w)\left(\beta_1 + \beta_2 . \frac{u_s^2}{Dg}\right) \qquad 7.2.1.1$$

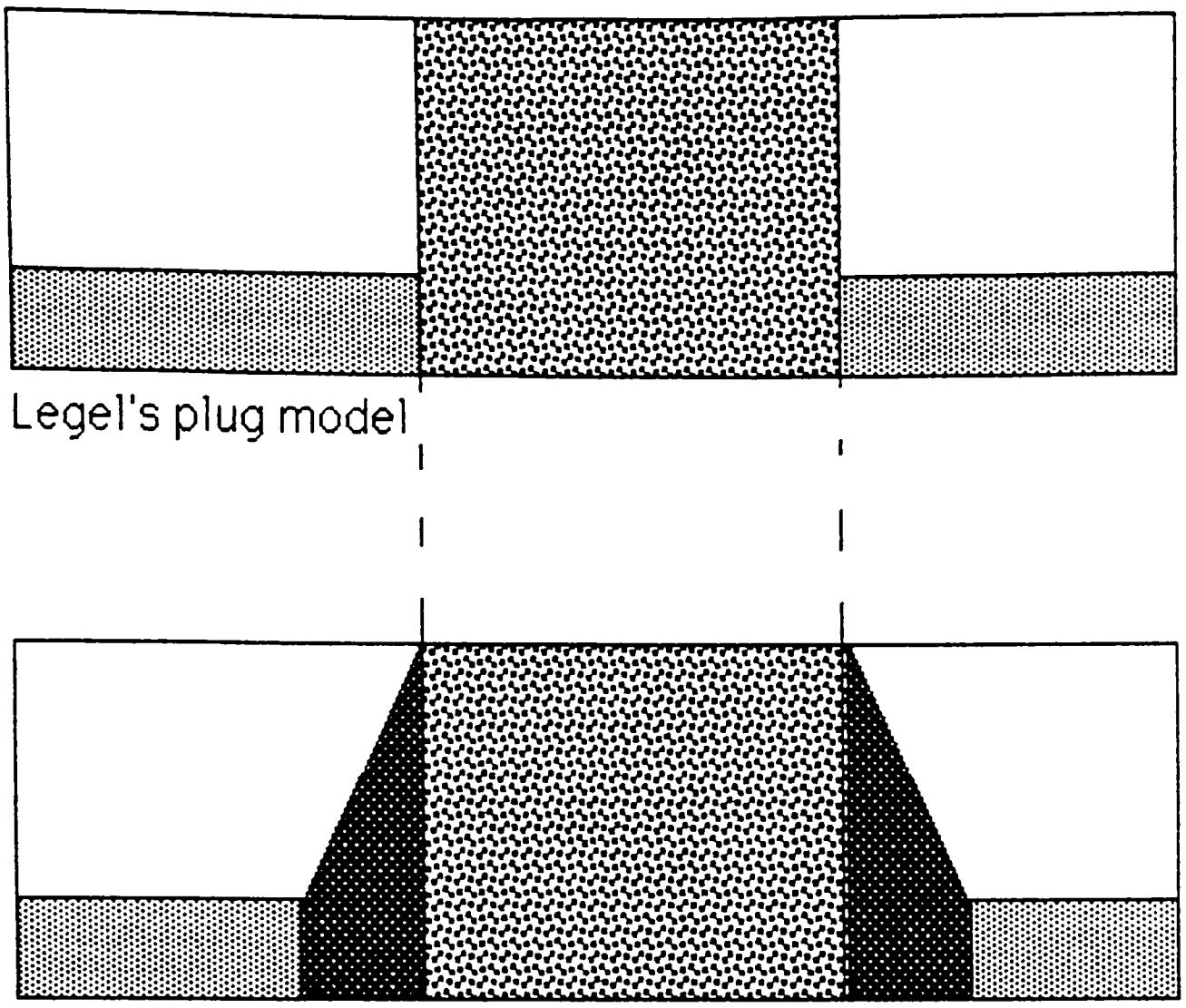

Figure 7.2.1.1 The plug models of Legel and Konrad.

Legel's analysis produced:

$$\frac{\Delta P}{L_P} = \rho_B g \tan(\phi_w)\left(1 + \frac{\rho_{B,st}}{\rho_B}.\frac{A_{st}}{A}.4\lambda B_c.\frac{u_s^2}{Dg}\right) \qquad 7.2.1.2$$

and from Konrad's analysis:

$$\frac{\Delta P}{L_P} = \rho_B g \tan(\phi_w)\left(2 + \frac{A_{st}}{A-A_{st}}.4K_w.\frac{u_s^2}{Dg}\right) \qquad 7.2.1.3$$

Comparing the equations 7.2.1.2 and 7.2.1.3.

	Legel	Konrad
β_1	The force on the pipe wall due to the weight of material in a plug.	The hydrostatic pressure in the plug along the pipe axis.
β_2	The bulk density of the material in the plug and in the stationary layer are assumed to be different. λ is the ratio of radial to axial stress in the plug. B_c is the ratio of compressive stresses in the plug, equal to 1 for ideal plugs. A_{st}/A is the ratio of the cross-sectional area of the stationary layer to that of the pipe cross.	For polyethylene pellets as tested by Konrad the bulk density will vary by less than 5%. K_w is the ratio of radial to axial stresses in the plug at the pipe wall. $A_{st}/(A-A_{st})$ is the ratio of the cross-sectional area of the stationary layer to that of the gas bubble.

The two approaches diverge in the method used to evaluate the plug velocity. Legel uses an experimental approach and by correlating pressure gradient and Froude number, u_s^2/Dg, determines β_2. Konrad makes an analogy between this type of flow and gas-liquid flow and *borrows* an expression for the bubble velocity in an inviscid liquid. Konrad's final equation is then in terms of material properties and this is compared with experimental data.

7.2.2 ANALYSIS OF SHEARING TYPE FLOW

As previously mentioned shearing type flow occurs at velocities below that for plug flow. Hitt (1982) compared the shear strength of the bulk materials with the shear stress due to the axial pressure gradient, for a pipeline completely filled with material. From this analysis the depth of the stationary layer during shearing type flow could be predicted. Figure 7.2.2.1 shows an idealised conveying characteristic for a bulk material capable of plug flow. The transition from shearing to plug flow is modelled by:

$$\frac{\Delta P}{L} = 2.\mu_w.\rho_B.g \qquad 7.2.2.1$$

Using this expression for silica sand with a mean particle size of 215 μm:

$$\frac{\Delta P}{L} = 2 * 0.306 * 1350\,kg/m3 * 9.81\,N/kg = 8105\,Pa/m$$

The experimentally measured transition occurred when the pressure gradient was 7500 Pa/m. For polyethylene pellets with a mean diameter of 3.83 mm:

$$\frac{\Delta P}{L} = 2 * 0.266 * 558\,kg/m3 * 9.81\,N/kg = 2912\,Pa/m$$

No transition point was measured by Hitt. This experience was confirmed in this work, with shearing flow achieved with sand, but not polyethylene pellets. Both Hitt's investigation and this work employed 2 inch nominal bore pipelines. This results in a ratio of pipe diameter to particle diameter of 250 for the sand, but only 14 for the polyethylene pellets. There was obviously an insufficient depth of material to produce shearing flow with polyethylene pellets. This would be expected to change with larger bore pipelines.

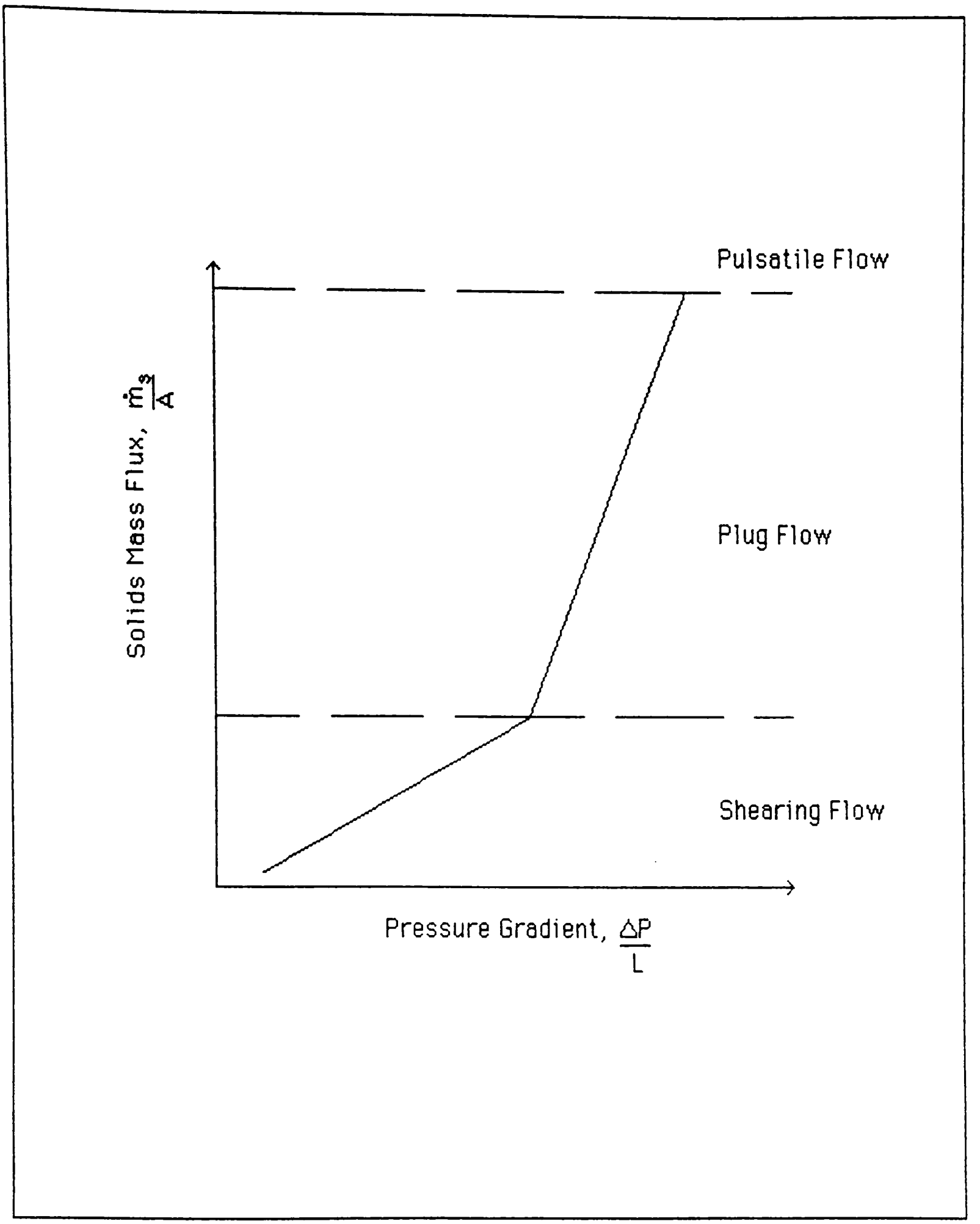

Figure 7.2.2.1 An idealised conveying characteristic for a bulk material capable of plug type non-suspension flow.

7.2.3 DISCRETE VERSUS CONTINUUM MODELS

Previous mathematical models presented in this work for suspension flow and non-suspension moving bed type flow, described the particles as a continuum. Extending this model to non-suspension plug type flow proved difficult. The main problem are the moving *free surfaces* such as the plug front. The control volume formulation of the conservation equations relies upon averaging between the centres and faces of control volumes. With a *free surface* this averaging procedure requires some modification.

The Donor-Acceptor method was employed by Ramshaw and Trapp (1976) to address this problem. Considering two neighbouring control volumes, the one with mass outflow is the donor and the other the acceptor. The principle of the Donor-Acceptor method may be stated as follows: when computing the transport of a mixture from a donor control volume to an acceptor control volume, the single component or phase values are determined by the donor, whereas the composition or proportions are determined by the acceptor. For example, consider a gas-liquid system. A control volume can be either:

i. a pure gas control volume;
ii. a two-phase control volume;
iii. a pure liquid control volume.

If the donor control volume is two-phase and the acceptor control volume is pure gas then only gas will be transported from the donor control volume until all the gas in the two-phase control volume is exhausted. A test is required to determine whether a control volume is a donor, or acceptor of a phase. This is of the form of a lower and an upper limit for the volume fraction of the phase. When the volume fraction exceeds the upper limit for a particular phase in a control volume, the control volume will be considered as full of that phase, and thus only donate or accept that phase.

A number of additional points need to be considered to prevent unreal physical situations occurring. One of the most important is to compare the volume fraction of the phase in both control volumes. If the difference is small then all phases can flow into the acceptor control volume. This prevents the Donor-Acceptor method operating in two-phase regions where the phases are well mixed and would be expected to stay mixed. This method has been successfully used in the modelling of gas-liquid

systems. Koh et al (1987) used this method to describe the flow of gas bubbles injected into a vertical column of liquid.

Unfortunately, this method cannot be applied to the plug type mode of non-suspension gas-solids flow. When a bulk material flows in the plug type mode the percolation of gas through the plug of material is critical to maintain the flow. Indeed without sufficient permeability to allow this process a blockage, and hence no flow, would occur! This was demonstrated by the author during conveying trials with silica sand. The sand would flow in the plug flow mode, but after a number of trials some particle degradation had occurred. This increased the amount of fines and reduced the permeability of the material resulting in the pipeline eventually becoming blocked.

Using the Donor-Acceptor method to prevent the diffusion of the plug boundaries in the flow model would preclude the percolation of gas through the plug, since control volumes in the plug would only be able to donate or accept solids. So, although the flow may appear to be visually similar to gas-liquid flows (indeed Konrad (1980) employed this analogy in his analysis of plug flow) this approach cannot be used without discounting important physical phenomena.

The alternative to modelling the solids phase as a continuum is to describe each particle individually. Tsuji et al (1990) used this approach to model plug flow. With this approach the interaction between particles is modelled as a spring, damper and slider system. Ergun's equation was used to evaluate the fluid force on each particle. Tsuji found that the value of the *spring stiffness* was a key factor in achieving realistic results. The *coefficient of friction* (for the slider) was determined by assuming Coulomb type friction and the *damping coefficient* was derived from the *spring stiffness*.

In his work the flow in a horizontal pipe with L = 1.0 m and D = 50 mm was modelled. The particles had a diameter of 10 mm and a density of 1000 kg/m^3. From discussions with Professor Tsuji, to achieve realistic results the value of the *spring stiffness* needed to be of the order of 4000 N/m. This required a time step of 2×10^{-5} s and resulted in a computation time of 150 minutes (using an NEC ACOS 2000) for a simulation of 1.2 s of flow. Initially 1000 particles were stacked at one end of the pipe. After being released they flowed to the outlet, and were recirculated to the inlet plane at the same height above the bottom of the

pipe as they had been at the outlet plane.

Some problems exist with this approach:

i. with fewer particles the flow degenerated to a stationary layer along the bottom of the pipe;
ii. with a uniform inflow of particles across the whole cross-section the predicted flow patterns are not realistic, hence the use of a cyclic boundary condition for the outlet.

The use of a discrete model avoids the problems of describing the solids phase as a continuum, but creates other difficulties especially in terms of the computer power required to solve problems of a realistic scale.

7.3 EXPERIMENTAL OBSERVATIONS

7.3.1 FLOW VISUALISATION AND TRIALS WITH DIFFERENT FEEDERS

The experimental test rig used in this work could be fed using either:

i. a pressure vessel;
ii. a high pressure rotary valve.

Both of these arrangements are discussed in chapter 4. The arrangement used to alter the feed arrangement to the rotary valve resulted in the first section of the pipeline running along the floor. This meant that the first glass section could not be fitted. Figure 7.3.1.1 illustrates the difference between these feed arrangements. Apart from these changes the pipeline geometry was not altered.

While using the pressure vessel as a feeder, the flow in both glass sections was observed. This allowed a comparison between the flow near the feed point and that near the end of the pipeline to be observed.

The modifications to facilitate the use of the rotary valve feeder were part of a separate project. Part of this project was to measure the air leakage through the valve. This was reported by Reed et al (1988). With the availability of this alternative feeding device a number of comparative tests were conducted.

Firstly it was found that provided the pressure and flow rate conditions in the pipeline just after the feed point were the same, then the flow patterns observed were the same. Though this seems a very straightforward statement a number of manufacturers sell special feeding devices to promote plug flow. A number of examples are based upon the use of an *air-knife* as developed by the Warren Spring Laboratory in the late 1960's. Examples of the application of an *air-knife* are shown in Figure 7.3.1.2. Observation of plug flow in this work has confirmed the author's opinion that special feeding devices are not required for materials that are capable of the plug type mode of non-suspension flow.

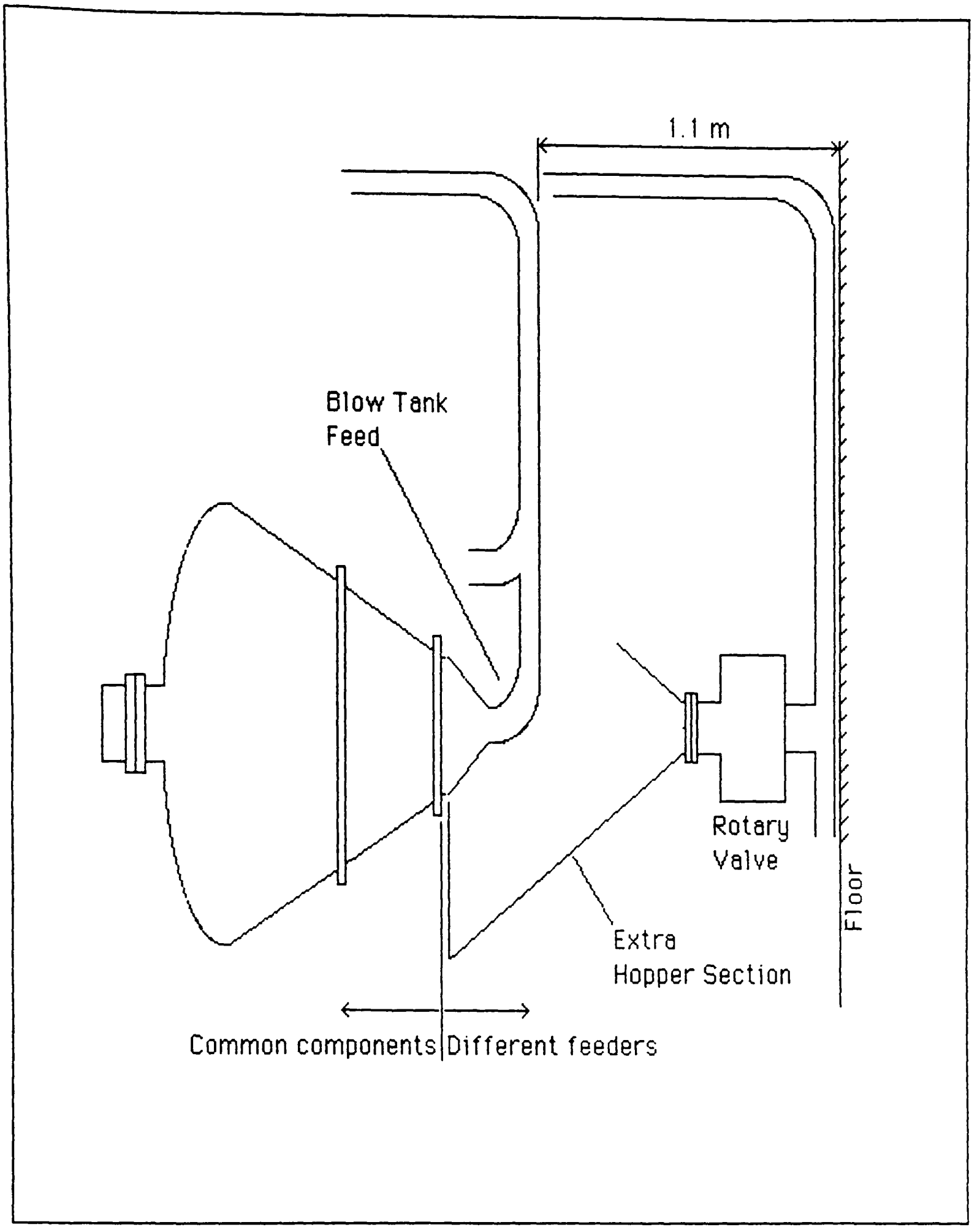

Figure 7.3.1.1 Alternative solids feed arrangements for conveying trials.

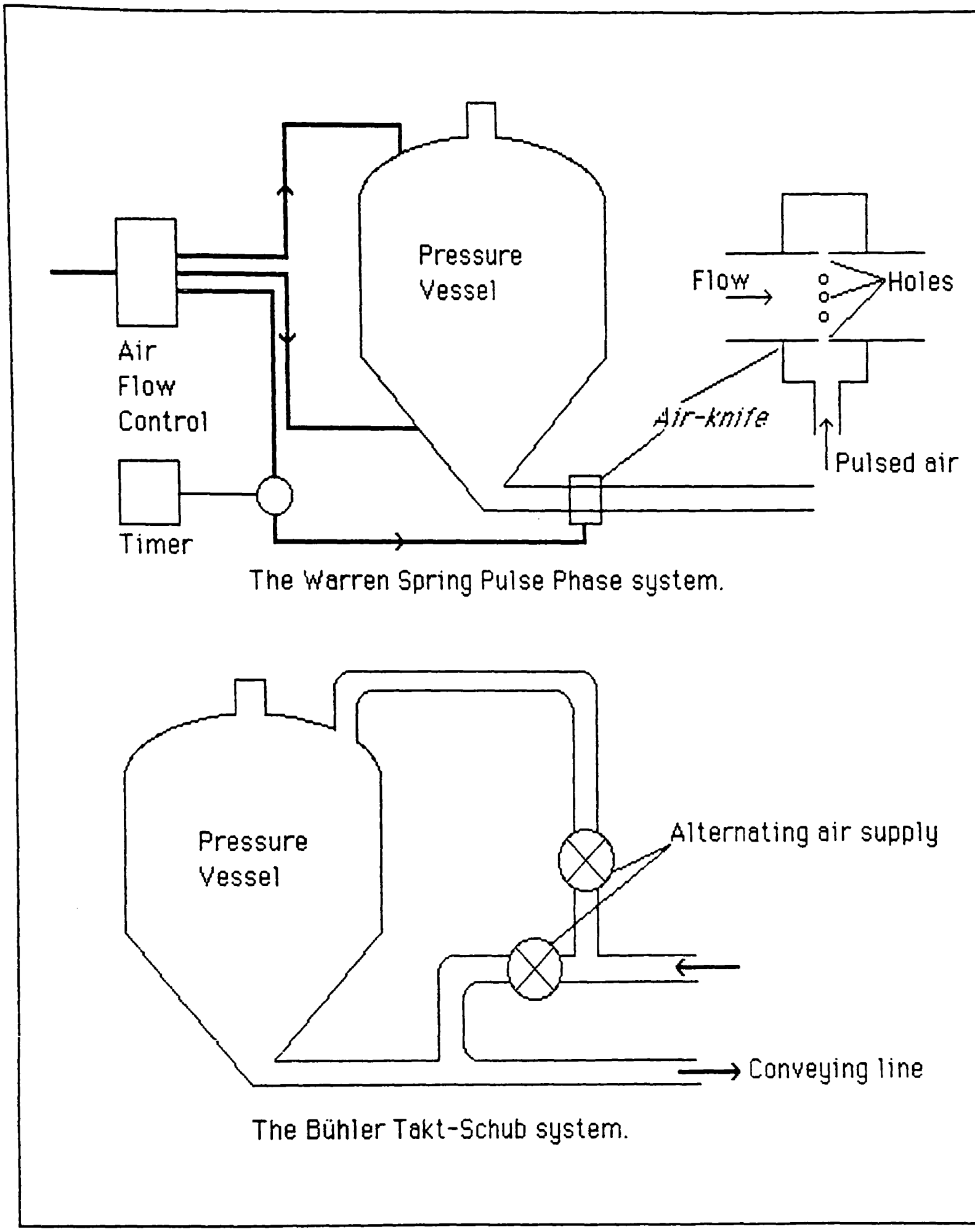

Figure 7.3.1.2 Various *air-knife* type feeding devices.

Legel and Schwedes (1984) employed a feeding device that alternated the air supply between the pressure vessel and an *air-knife*. The time ratio for the air supply (total time to time air was supplied to the *air-knife*) was 2. In the pipeline the ratio of the time for a plug plus air bubble to pass to that for a plug to pass was measured and found to be in the range 3 to 9. This is explained in terms of increasing plug velocity implying that the plug length does not alter. From the results of Hitt (1985) and this work the plug length would be expected to increase over the initial portion of the pipeline (up to about 20 m from the inlet in a pipeline with D = 53 mm when conveying polyethylene pellets).

Conveying trials using the rotary valve as a feeder showed that the air leakage during conveying was the same as that for the *air only* tests conducted by Reed et al (1988), within the limits of experimental error. This was as expected, since a reduction of a few percent in the leakage is normally quoted when a rotary valve is feeding a granular material into a pressurised line.

7.3.2 ANALYSIS OF EXPERIMENTAL DATA

Experimental measurements of the flow by Hitt (1985) observed that:

i. the pressure gradient varied linearly with solids mass flow rate when conveying in the plug flow mode of non-suspension flow, see figure 7.3.2.1;
ii. the length of plugs was proportional to the axial distance from the solids feed point, as shown in figures 7.3.2.2 and 7.3.2.3;
iii. the ratio of plug to gap duration was assumed to be constant due to the scatter in the experimental data.

Using a plug model similar to that of Legel, shown in figure 7.3.2.4, this data can be analysed further. The frequency of the plugs can be related to the average solids mass flow rate by:

$$\dot{m}_{solids} = \frac{t_{plug}}{t_{total}} \dot{m}_{plug}$$

$$= f_{plug} t_{plug} A R_{plug} \rho_{solids} u_{plug} \qquad 7.3.2.1$$

$$= f_{plug} A \rho_{bulk} (1-\alpha) L_{plug}$$

$$f_{plug} = \frac{\dot{m}_{solids}}{(1-\alpha) A \rho_{bulk} L_{plug}}$$

α is the ratio of the area occupied by the stationary layer to the pipeline cross-sectional area.

ρ_{bulk} is the bulk density, which can be used in this case since the materials which flow in the plug flow mode (such as polyethylene pellets) exhibit only a small change in bulk density from the poured to the tapped states.

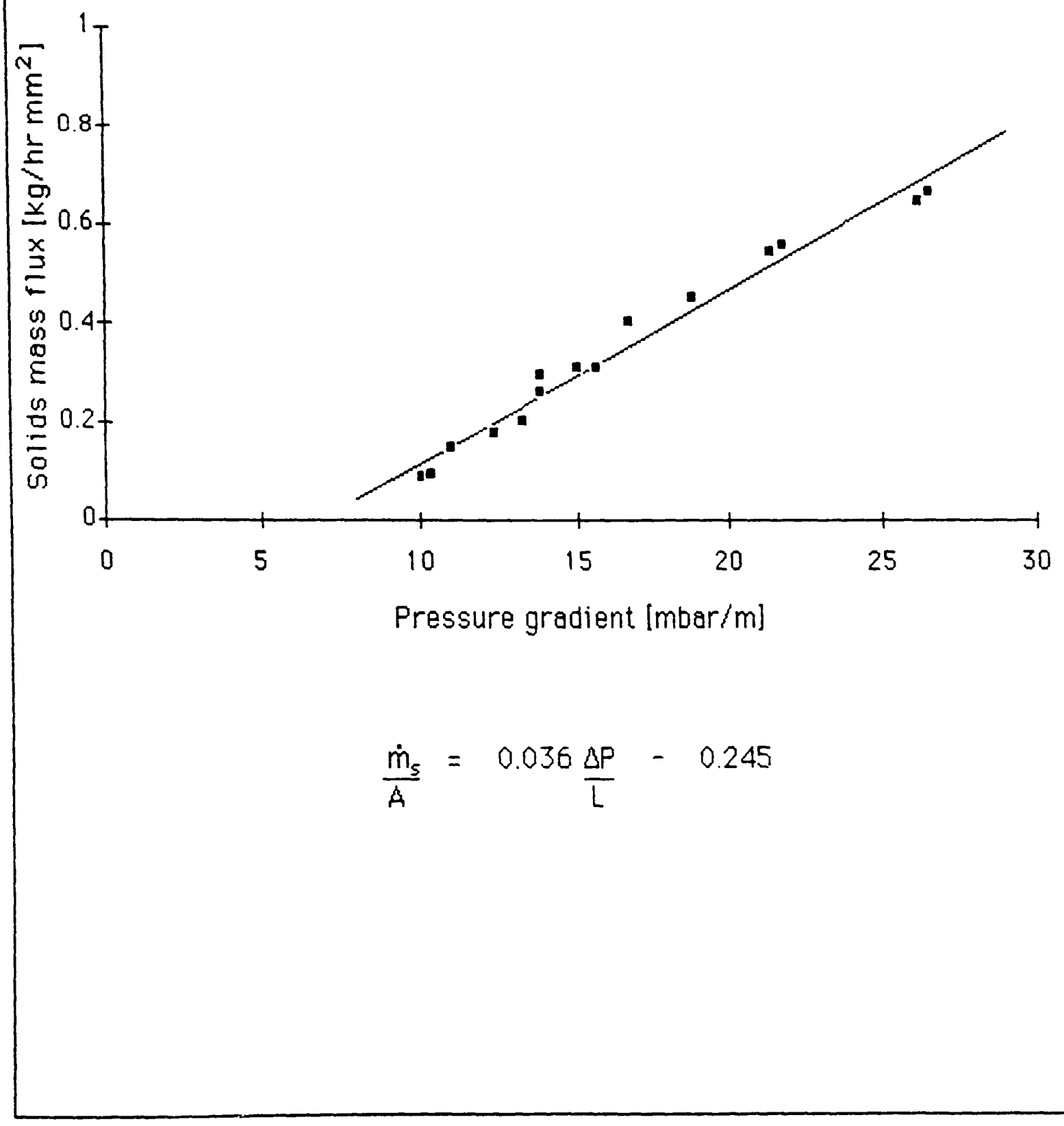

Figure 7.3.2.1 The variation of solids mass flux with pipeline pressure gradient for polyethylene pellets.

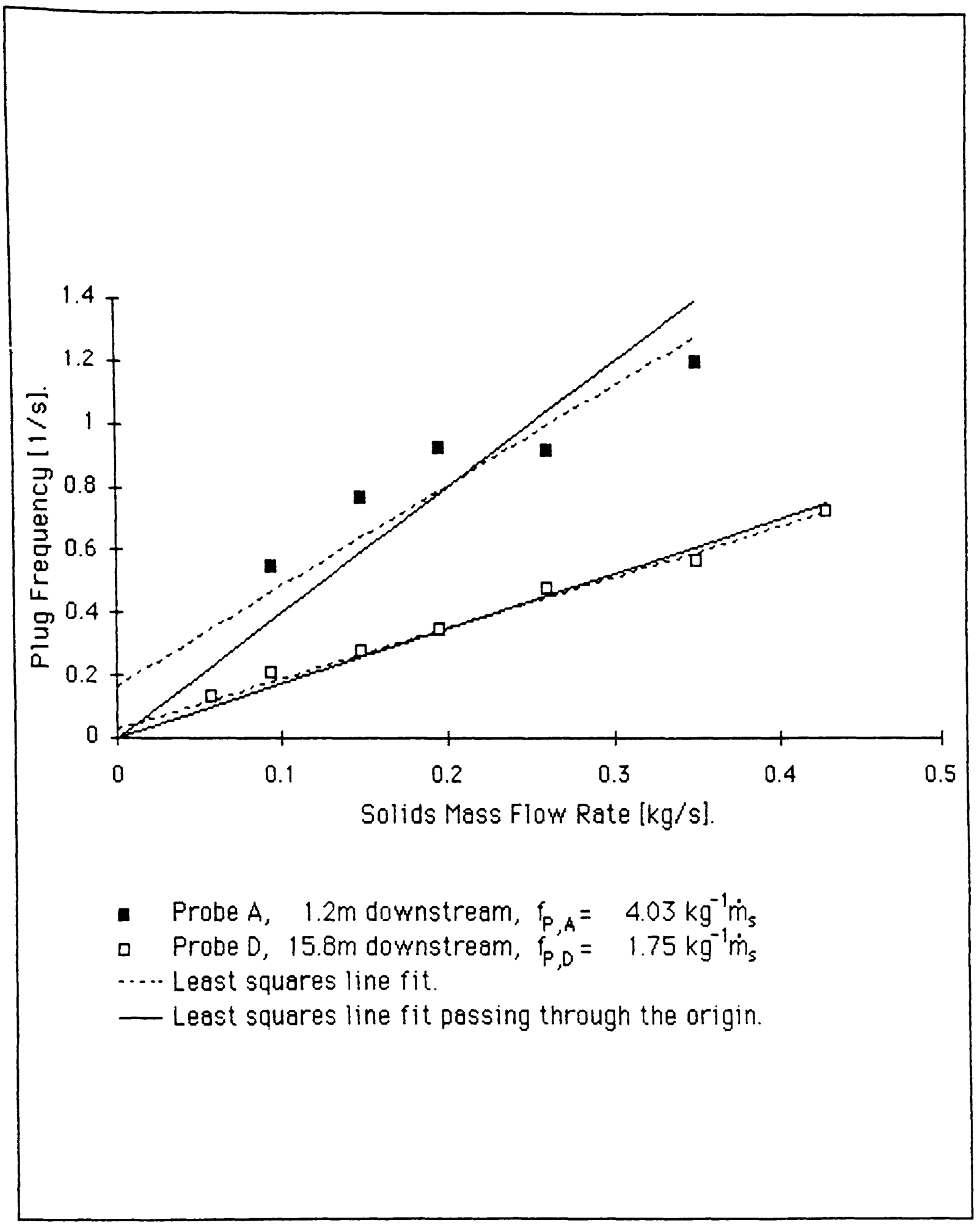

Figure 7.3.2.2 The variation of plug frequency with solids mass flow rate for polyethylene pellets.

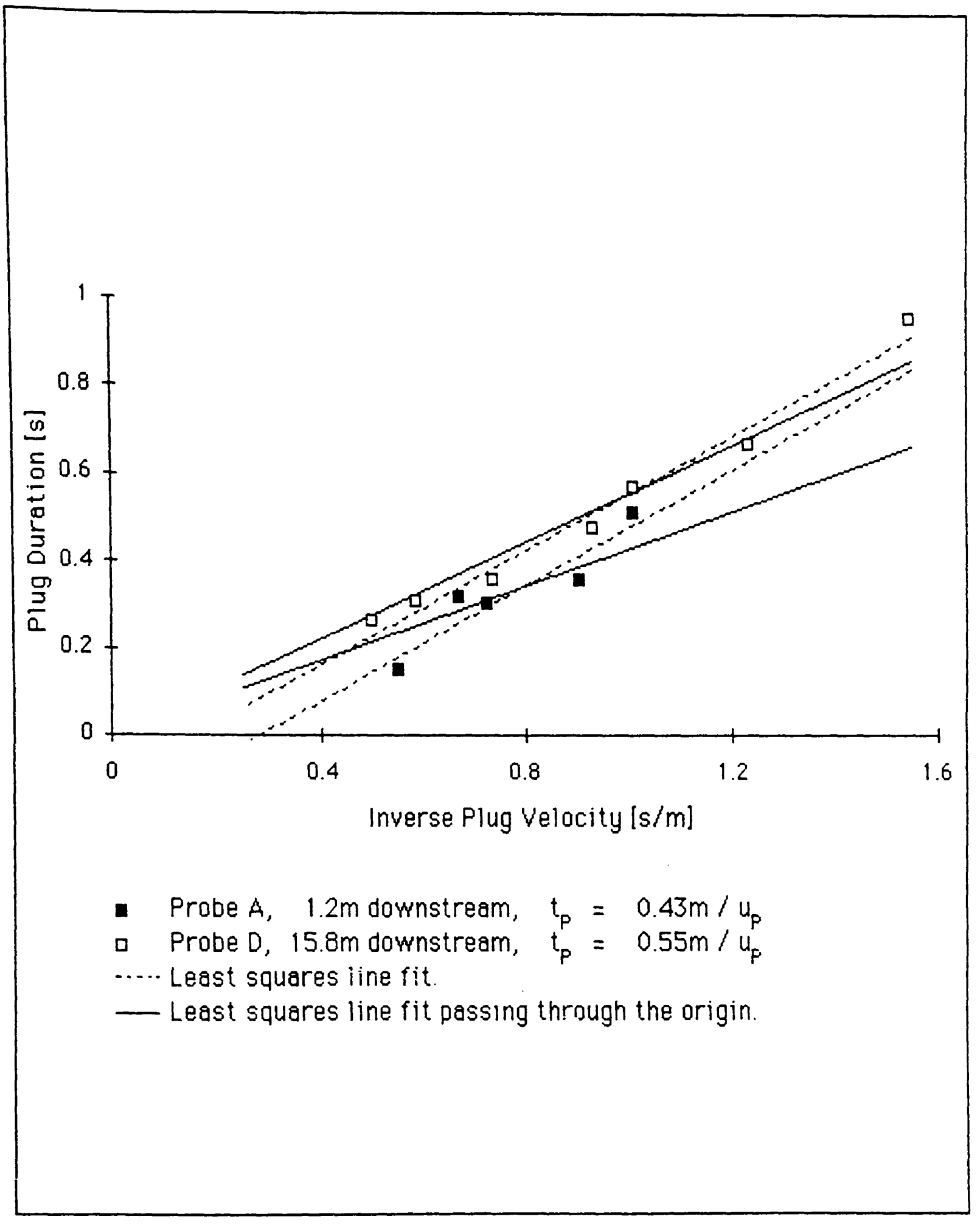

Figure 7.3.2.3 The variation of plug duration with inverse plug velocity for polyethylene pellets.

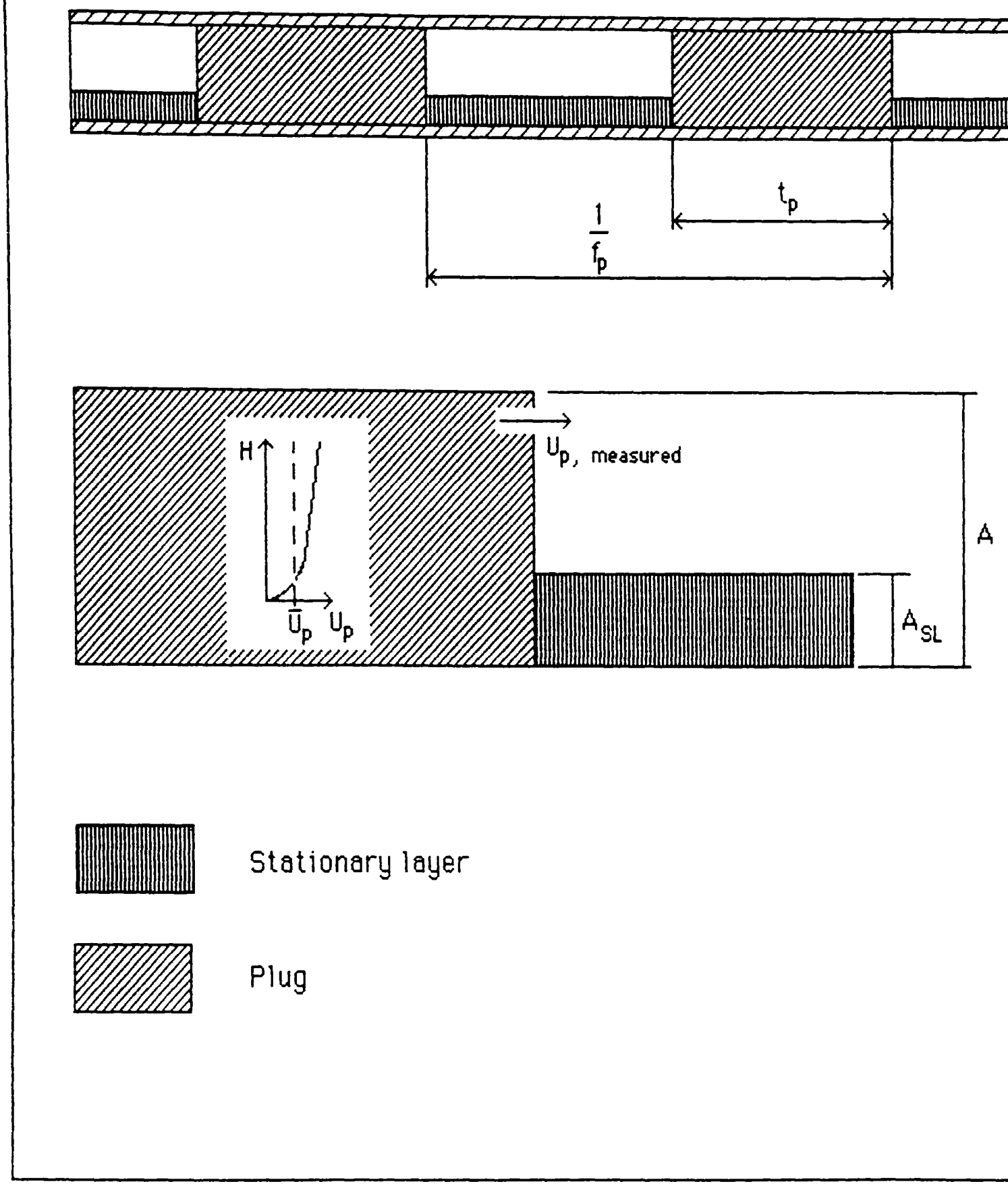

Figure 7.3.2.4 The plug model used to analyse Hitt's data.

Noting that the plug frequency must be zero when the solids mass flow rate is zero, then the data in figure 7.3.2.2 indicates that $(1-\alpha)A\rho_{bulk}L_{plug}$ is constant and changes with axial distance travelled. The duration of the plugs is related to the velocity by:

$$t_{plug} = \frac{L_{plug}}{u_{plug}} \qquad 7.3.2.2$$

$$\bar{u}_{plug} = (1-\alpha)\, u_{plug}$$

Figure 7.3.2.2 allows the length of the plug to be calculated. From this and the previous result α can be determined and the depth of the stationary layer calculated. The depth of the stationary layer decreases with distance. Figure 7.3.2.3 shows the variation of plug to gap ratio with values calculated from:

$$\frac{t_{plug}}{t_{gap}} = \frac{t_{plug}}{\frac{1}{f_{plug}} - t_{plug}} \qquad 7.3.2.3$$

This shows that the gap between plugs decreases. Thus material has been taken from the stationary layer to increase the length of the plug. Differences between the change in volume of the stationary layer and the plug are due to neglecting the transition area where material is swept up into the plug and where it slides off the back of the plug. Eventually the plug would be expected to join up. This is not observed in practice. After achieving a certain length the plugs are broken up by the process of bubble formation analogous to the phenomena that occurs in fluidised beds with Geldart group B and D materials. As the plug becomes longer the pressure drop along it becomes larger and the bubbling point is reached. This has been observed at the start of the pipeline during the initial pressure transient of the blow tank conveying cycle.

The result of this is that further down the pipeline shorter plugs with small gaps between them followed by a long gap are observed ie a consequence of each long plug being broken up. The implication of this

analysis for methods such as Legel's and Konrad's is that the plug length must be treated as a variable and not a constant.

7.4 SUMMARY

The plug flow mode of non-suspension gas-solids flow has been examined. Three distinct flow patterns have been identified:

i. full bore flow which occurs at the lowest gas mass flow rates;
ii. shearing flow which consists of small waves and a deep stationary layer;
iii. plug flow which consists of full bore waves and a shallow stationary layer of material between the waves.

Shearing flow could only be achieved with certain bulk materials that achieved the other modes of flow. This was probably because the pipe diameter was insufficient to achieve a deep enough stationary layer with the materials that did not exhibit this mode of flow.

The mathematical models that were successfully applied to suspension flow and to non-suspension moving-bed type flows failed when applied to plug flow. This was due to the diffusion of the wave boundaries by the numerical averaging procedures employed by the model. Procedures such as the Donor-Acceptor method for averaging, which have been successfully applied to solve this problem in gas-liquid systems, could not be applied without excluding important physical phenomena. Models describing discrete particles do not exhibit this problem, but require large computational power.

A mechanism for the development of plug flow along a pipeline has been proposed. Initially plugs increase in length until the pressure gradient across them is sufficient to cause gas bubbles in the plug. These bubbles break up the plug and result in several plugs travelling in close proximity. This mechanism explains the measurement of increasing plug length up to 16 m from the inlet and the observation of shorter plugs travelling in *convoy* 45 m from the inlet.

8 CONCLUSION

8.1 SUMMARY OF ACHIEVEMENTS

8.1.1 GENERAL SUMMARY

Three possible modes of gas-solids flow in pipelines have been identified:

i. suspension flow;
ii. non-suspension moving-bed type flow;
iii. non-suspension plug type flow.

Within each mode there are several possible flow patterns which, in general, vary with conveying gas velocity. Mathematical models for each of these modes of flow have been developed. Experimental work to validate these models has been undertaken. In addition to providing data to validate the predictions of the mathematical models, the experimental works has provided some new insight into the flow of gas-solids mixtures in pipelines.

8.1.2 SUSPENSION FLOW

The mathematical model for suspension flow predicted the developing flow region well. When the flow had become established the prediction was less good. This demonstrates the weakness of the model's description of particle-wall effects. This may not be a serious drawback, since the pressure drop in the developing flow region is often the major contribution to the overall pressure drop for the pipeline. The exception would be for pipelines with very long straight sections.

8.1.3 NON-SUSPENSION MOVING-BED FLOW

The mathematical model for non-suspension moving-bed type flow showed reasonable agreement with experimental data. The major weakness of this model was the prescription of the frictional force between the moving-bed and the pipe wall. The experimental investigation showed good agreement with other workers in terms of the system operating points (pressure drop, gas mass flow rate and solids mass flow rate) though a lower minimum conveying gas velocity was achieved. The data collected on the flow was in terms of observation of flow patterns and measurement of pressure fluctuations along the pipeline. These

pressure fluctuations were shown to be a function of the varying depth of the moving-bed. The velocity of the moving-bed calculated from the speed of these fluctuations showed good agreement with calculations based upon the solids mass flow rate and an assumed bed depth.

8.1.4 NON-SUSPENSION PLUG FLOW

In the mathematical models developed for suspension flow and non-suspension moving-bed flow the solids were modelled as a continuum. This approach was not successful when applied to non-suspension plug type flow. The main reason for this was the inability to maintain well defined boundaries between the waves of material (plugs) and the gas pockets between the waves. This is a result of the averaging techniques used in the general mathematical model. This problem has been overcome for gas-liquid boundaries, but applying this to a gas-solids flow would exclude physical phenomena that have a significant effect on the flow. The experimental investigation showed that the characteristics of this mode of flow is related to the properties of the bulk material and not to the mechanism of introducing the gas and solids into the pipeline. From experimental observations and analysis a mechanism for the development of the flow along the pipeline has been proposed.

8.2 AREAS FOR FURTHER INVESTIGATION

The potential of the mathematical modelling techniques used in this work to describe gas-solids flows in pipelines has been demonstrated. There are two possible avenues for further investigation:

i. extension of the models to describe the whole pipeline of a pneumatic conveying system;
ii. investigations to clarify the nature of certain physical phenomena in the flow and refinement of the mathematical models.

The first avenue will require models to describe the effect of the pipeline components that link the straight lengths of pipe. The operation of the system could then be simulated. For non-suspension flow, the simulation would predict the variation of system performance with time. In practice the system operating point may become steady even though the flow is not steady. This suggests a trade-off between:

i. predicting the flow in the pipeline, with a transient analysis;
ii. establishing the system operating point by time averaging certain effects and using a steady analysis.

The second approach would provide a convenient design tool without the requirement for huge computer power and the production of large amounts of unused data. The first approach would allow a more detailed investigation into phenomena such as particle degradation and pipeline blockages.

The mathematical models developed in this work have shown some weaknesses. These are a result of insufficient information about certain physical phenomena. One area of particular interest is the effect of particles on turbulence. With small particles ($d_s < 100\ \mu m$), an effect on the scale of turbulence has been noted by several workers, especially at low solids concentrations. The effect of larger particles and high solids concentration would be of particular interest. This would be especially useful for the model of suspension flow, but also for the model of non-suspension moving-bed flow where particles are carried in suspension above the moving-bed.

One point not addressed by this work is flow up vertical pipes. For non-suspension flows co-current and counter-current flow of particles have been reported. With the present model, as the solids are described by only one phase, simulation of vertical non-suspension flow is not possible.

REFERENCES

ADAM, O (1957).
Chemie Ing Techn, Vol 29, p 151.

ALBRIGHT, C W, HOLDEN, J H, SIMONS, H P, and SCHMIDT, L D (1949).
Pneumatic Feeder For Finely Divided Solids.
Chem Eng, pp 108-111.

ANON 0 (1887).
Duckham Pneumatic Grain Elevator
Engineering 29th January, p 151 and 2 ill.

ANON 1.
Deliquescent Compressed Air Dryers VAN AIR Systems Inc, British Agents, Awcitrol, Thomas House, 65-67 Kingston Road, New Molden, Surrey.

ANON 2.
Bühler-Miag Literature on High Pressure Rotary Valves, Buhler Brothers Ltd, CH-9240, Uzwil, Switzerland.

ANON 3 (1989).
Chemical Engineers handbook.

BAKER, O (1954).
Simultaneous Flow of Oil and Gas.
Oil and Gas J, V 53, pp 185-195.

BIRCHENOUGH, A and MASON, J S (1976).
Particle velocity and axial turbulence intensity measurements in a dilute gas-solid suspension flowing vertically upwards.
J Powder and Bulk Solids Technol, pp 6-12.

BIRCHENOUGH, A and MASON, J S (1980).
An Industrial Application of the Laser Velocimeter in Gas-Solid Flows.
Proc Pneumotransport 5 conf.

BIRKHOFF, G (1964).
Averaged Conservation Laws in a Pipe.
J Math Analysis and Apps Vol 1 pp66 - 77.

BOOTHROYD, R G (1966).
Pressure drop in duct flow of gaseous suspensions of fine particles.
Trans Inst Chem Engnrs, Vol 44, p 306.

BRADLEY, M S A (1989).
Pressure Losses Caused by Bands in Pneumatic Conveying Pipelines: Effects of Bend Geometry and Fittings.
Proc Powder and Bulk Solids conf.

BRAUER, H (1980).
Powder and Bulk Solids Technol, Vol 4.

BRAIN, T J S and REID, J (1974).
Performance of Small Diameter Cylindrical Critical Flow Nozzles.
NEL Report N 546 National Engineering Laboratory, East Kilbride, Glasgow.

BS1042.
British Standards institution, (1964), British Standards House, 2 Park Street, London, W1, UK.

CRAMP, W and PRIESTLY, A (1925).
Pneumatic Grain Conveyors,
Engineer.

CROWE, C T (1982).
Review - Numerical Models for Dilute Gas-Particle Flows.
Trans ASME J Fluids Eng V 104 pp297 - 303.

CROWE, C T, SHARMA, M P and STOCK, D E (1977).
The Particle-source-in Cell (PSI - Cell) Model for Gas-droplet Flows.
Trans ASME J Fluids Eng Vol 99 No 2 pp325 - 332.

DI GIACINTO, M, SOBETTA, F and PIVA, R (1982).
Two-way Coupling Effects in Dilute Gas-particle Flows.
Trans ASME J Fluids Eng Vol 104 pp304 - 312.

DIXON, G (1979).
The Impact of Powder Properties on Dense Phase Flow.
Proc Int Conf on Pneumatic Conveying Powder Advisory Centre, UK.

DONGARRA, J J (1985).
Performance of various computers using standard linear equations software in a FORTRAN environment.
Technical memo 23, Argonne National Lab, USA.

ERGUN, S (1952).
Fluid flow through packed colums.
Chem Eng Progress, Vol48 No2, pp89-94.

FLATT, W and ALLENSPACH, W (1969).
Increasing the Feed Performance and Improving the Efficiency of Pneumatic Feed Systems. (In German)
Chemie Ing Techn, V 41, N 21, pp 1173-1176.

FOSCOLO, P U and GIBILARO, L G (1984).
A Fully Predictive Criterion for the Transition Between Particulate and Aggregate Fluidisation.
Chem Eng Sci Vol 39 No 12 pp1667 - 1675.

FOSCOLO, P U and GIBILARO, L G (1987).
Fluid Dynamic Stability of Fluidised Suspensions : The Particulate Bed Model.
Chem Eng Sci Vol 42 No 6 pp1489 - 1500.

GELDART, D (1973).
Types of Gas Fluidisation.
Powder Tech, Vol 7, pp 285 - 292.

GIDASPOW, D (1986).
Hydrodynamics of Fluidisation and Heat Transfer : Supercomputer Modelling.
Appl Mech Rev Vol 39 No 1.

HARLOW, F H and WELCH, J E (1965).
Numerical cacluation of time-dependent vicous incompressible flow of fluid with a free surface.
Phys Fluids Vol 8 pp2182.

HISHIDA, K, TAKEROTO, K and MAEDA, M (1987).
Turbulence Characteristics of Gas-solids Two-phase Confined Jet (effect of particle density).
Jap J Multiphase Flow Vol 1, No 1 pp56 - 69.

HITT, R J, REED A R and MASON, J S (1982).
An Investigation into Two Modes of Slugging in Horizontal Dense Phase Pneumatic Conveying.
Proc PNEUMATECH 1 conf.

HITT, R J (1985).
An Investigation Into the Low Velocity Pneumatic Conveying of Bulk Solids.
PhD Thesis Thames Polytechnic London, UK.

JONES, M G (1983).
An investigation of the acceleration pressure drop and particle acceleration length in horizontal dilute-phase pneumatic conveying,
Tech Report, Dept Mech Eng, Thames Polytechnic, UK.

JONES, M G (1988).
The influence of bulk particulate properties on pneumatic conveying performance.
PhD Thesis Thames Polytechnic London, UK.

JONES, M G and MILLS, D (1989).
A Product Classification for the Design of Pneumatic Conveying Systems.
Proc 14th Powder and Bulk Solids conf.

KLINZING, G E and MATHUR, M P (1981).
The Dense And Extrusion Flow Regime In Gas Solid Transport.
Can J Chem Eng, Vol.59, part 5, pp596-594.

KOH, P T L, MARKATOS, N C and CROSS M (1987).
Numerical Simulation of Gas-Stirred Liquid Baths with a Free Surface.
Physico Chemical Hydrodynamics, V 9, N 1/2, pp 197-207.

KONRAD, K, HARRISON, D, NEDDERMAN, R M and DAVIDSON J F (1980).
Prediction of the Pressure Drop for Horizontal Dense Phase Pneumatic Conveying of Particles.
Proc Pneumotransport 5 conf.

KONRAD K (1980).
Dense Phase Pneumatic Conveying of Particles.
PhD Thesis University of Cambridge.

LAUNDER, B E and SPALDING, D B (1972).
Lectures In Mathematical Models Of Turbulence.
Academic Press, London, UK.

LEGEL D (1980).
Untersuchungen zur pneumatischen Föderung van Schüttgutpfropfen aus kohäsionslosem Material in horizontalen Rohren.
Dissertation TU Braunschweig.

LEGEL D and SCHWEDES J (1984).
Investigation of Pneumatic Conveying of Plugs of Cohesionless Bulk Solids in Horizontal Pipes.
Bulk Solids Handling, V 4, N 2, pp 399-405

LIPPERT A (1966).
Pneumatic Conveyance of Large Concentrations of Solids.
Chemie Ing Tech, V 38, N 3, pp350-355.

LOHRMANN, P C and MARCUS, R D (1982).
The Influence of Velocity, Pressure and Line Length on the Performance of A Blow Vessel.
Proc Pneumatech 1 conf.

McVEIGH, J C and CRAIG, R W (1972).
Metering of Solid Gas Mixtures Using An Annular Venturi Meter.
Proc Pneumotransport 1 conf.

MAINWARING, N J and REED, A R (1986).
Mechanisms for Gas-Solids Flows at Low Velocity in Pneumatic Conveying Pipelines.
Proc 11th Powder and Bulk Solids conf.

MAINWARING, N J and REED, A R (1987).
Permeability and Air Retention Characteristics of Bulk Solid Materials in Relation to Modes of Dense Phase Pneumatic Conveying.
Bulk Solids Handling Vol 7 No 3 pp415 - 425.

MAINWARING, N J (1988).
The Effect of the Physical Properties of Bulk Solid Materials on Modes of Dense Phase Pneumatic Conveying.
PhD Thesis Thames Polytechnic London, UK.

MARKATOS, N C (1986).
Modelling of Two-phase Transient Flow and Combustion of Granular Propellants.
Int J Multiphase Flow Vol 12 No 6, pp913-933.

MASON, D J MARKATOS, N C and REED, A R (1987).
Numerical Simulation of the Flow of Gas-Solids Suspensions in *Acceleration* Regions of Pipelines.
Proc. 2nd PHOENICS User conf.

MASON, D J, CROSS, M, PATEL, M K, and REED, A R (1989).
Numerical Modelling of *Dense-Phase* Pneumatic Conveying of Bulk Particulate Materials.
Proc 14th Powder and Bulk Solids conf.

MASON, D J, YENETCHI, G V and WOODCOCK, C R (1990).
A Computational Procedure for the Design of *Dilute-Phase* Pneumatic Transport Systems.
Proc 15th Powder and Bulk Solids conf.

MICHAELIDES, E E (1984).
A Model for the Flow of Solid Particles in Gases.
Int J Multiphase Flow, Vol 10 No 1, pp61 - 77.

MICHAELIDES, E E (1987).
Motion of Particles in Gases : Average Velocity and Pressure Loss.
Trans ASME J Fluids Eng, V 109, pp172 - 178.

MICHAELIDES, E E and Roy I (1987).
An Evaluation of Several Correlations Used for the Prediction of Pressure Drop in Particulate Flows.
Proc Pneumatech 3 conf.

MIGDAL, D and AGOSTA, V D (1967).
A Source Flow Model for Continuum Gas-particle Flow.
Trans ASME J Fluids Eng, Vol 35, No 4 pp860 - 865.

MILLS, D (1979).
The Determination of Product Conveying Characteristics For Pneumatic Conveying Systems.
Proc Int Conf PAC Conf London, January.

MILLS, D and MASON, J S (1985).
The influence of bend geometry on pressure drop in pneumatic conveying system pipelines.
Proc 10th Powder and Bulk Solids conf.

MORIKAWA, Y, TSUJI Y and TANAKA, T (1986).
Measurements of horizontal air-solid two-phase flow using an optical fibre probe (particle velocity and concentration).
Bulletin of JSME, Vol 29, No 249, pp802-809

MUSCHELKNAUTZ, E and KRAMBROCK W (1969).
Vereinfachte Berechnung horizontal er pneumatischer Föderleitungen bei hoher Gutbeladungen mit feinkörnigen Produkten.
Chemie Ing Techn, V 41, N 21, pp 1164-1172.

OWEN, P R (1969).
Pneumatic transport.
ASME J Fluid Mech, Vol 39, No2, pp407-432

PATANKAR, S V (1980).
Numerical Heat Transfer and Fluid Flow.
Pub Hemisphere

PATANKAR, S V and SPALDING, D B (1972).
A Calculation Procedure For Heat, Mass And Momentum Transfer In Three-Dimensional Parabolic Flows.
Int J Heat and Transfer, Vol.15, pp1797-1806.

PATEL, M K, CROSS, M, MARKATOS, N C and MACE, A C H (1987).
An evaluation of eleven discretization schemes for predicting elliptic flow and heat transfer in supersonic jets.
Int J Heat and Mass Transfer, Vol 30, No 9, pp1907 - 1925

RAMACHANDRAN, P S, BURKHARD, D G and LAUER, B E (1970).
Studies of Dense Phase Horizontal Flow of Gas Solids Mixtures.
Indian J Techn, Vol8, pp199 - 204

RAMSHAW, J D and TRAPP, J A (1976).
A Numerical Technique of Low-Speed Homogeneous Two-Phase Flow with Sharp Interfaces.
Journal of Computational Physics, V 21, pp 438-453.

REED, A R, KESSEL, S R, and PITTMAN, A N (1988).
Examination of The Air Leakage Characteristics of a High Pressure Rotary Valve.
Bulk Solids Handling V8 N6 pp725-730

REIF, F (1965).
Fundamentals Of Statistics And Thermal Physics.
Pub. McGraw-Hill.

RICHARDSON, J F and McLEMAN M (1960).
Pneumatic Conveying: Part II, Solids Velocities and Pressure Gradients in a One Inch Horizontal Pipe.
Trans Instn Chem Eng, Vol 38, pp 257 - 266.

RICHARDSON, J F and ZAKI, W N (1954).
Sedimentation and Fluidisation : Part I.
Trans Instn Chem Engrs, Vol 32, pp35-53

ROSE, H E and BARNACLE, H E (1959).
Flow of Suspensions of Non-cohesive Spherical Particles in Pipes.
The Engineer, V 203 N 5290, pp 898-901 and pp 939-941

ROSE, H E and DUCKWORTH, R A (1969).
Transport of Solid Particles in Liquids and Gases.
The Engineer, 14 March pp392 - 396, 21 March pp430 - 433, and 28 March pp478-483

ROSTEN, H I and SPALDING, D B (1986).
PHOENICS - Beginners guide and user manual.
CHAM TR/100

ROWE, P N (1961).
Drag Forces in a Hydraulic Model of a Fluidised Bed Part II.
Trans Instn Chem Engrs, Vol 39, pp175-180

SCHILLER, L and NAUMANN, A (1933).
Uber die grundlegender berechnungen beider schwerkraftanfbereitung.
VDI Zeits, Vol 77, No 12, pp318-320

SCHUCHART, P (1970).
Pneumatic Conveying.
Chem and Process Eng. May, pp76-80.

SHARMA, M P and CROWE, C T (1978).
A Novel Physico Computational Model for Quasi One Dimensional Gas Particle Flows.
Trans ASME J Fluids Eng, Vol 100, No 3, pp343-349

SOO, S L (1965).
Dynamics of Multiphase Flow Systems.
Ind Eng Chem Fund, Vol 4, pp426-433

SPALDING, D B (1980).
Numerical Computation of Multi-phase Fluid Flow and Heat Transfer.
Recent Advances in Numerical Methods, Vol 1, Ch 5, pp139 - 167
Ed. Taylor and Morgan, Pineridge Press Ltd Swansea, UK

SUTTON, H M, and RICHMOND, R A (1973).
How To Improve Powder Storage And Discharge In Hoppers By Aeration.
Process Engineering, September.

TSUJI, Y, OSHIMA, T and MORIKAWA, Y (1985).
Numerical Simulation of Pneumatic Conveying in a Horizontal Pipe.
Kona Power Sci and Tech in Japan, No 3, pp38-51

TSUJI, Y, MORIKAWA, Y, TANAKA, T, NAKATSUKASA, N and NAKATANI, M (1987).
Numerical Simulation of Gas-solid Two-phase Flow in a Two-dimensional Horizontal Channel.
Int J Multiphase Flow, Vol13, No 5, pp671-684

TSUJI, Y, SHEN, N Y and MORIKAWA, Y (1989a).
Numerical Simulation of Gas-solid Flows I (particle to wall collision).
Tech Report Osaka University, Vol 39, No 1975, pp233-241

TSUJI, Y, SHEN, N Y and MORIKAWA, Y (1989b).
Numerical Simulation of Gas-solid Flow II (calculation of a two-dimensional horizontal channel flow).
Tech Report Osaka Univerity, Vol 39, No 1976, pp243-254

TSUJI, Y, TANAKA, T and ISHIDA, T (1990).
Graphic Simulation of Plug Conveying.
Proc Pneumatech 4 conf.

WALLIS, G B and DOBSON J E (1973).
The Onset of Slugging in Horizontal Stratified Air-Water Flow.
Int J Multi-Phase Flow, V 1, N 1, pp 173-193.

WAGHORN, D (1977).
The Performance Characteristics of A Blow Tank for Feeding A Pneumatic Conveying System.
PhD Thesis Thames Polytechnic, London, UK

WELSCHOF, G (1962).
Pneumatische Forderung bei grossen Fordergutkonzentrationen (Pneumatic Conveying At High Particle Concentrations).
VDI-Forschungsheft 492.

WEN, C Y and SIMONS, H P (1959).
Flow Characteristics In Horizontal Fluidised Solids Transport.
AIChE J, Vol 5, No 2, pp263-267.

WEN, C Y and YU, Y H (1966).
Mechanics Of Fluidisation.
Chem Eng Progress Symposium Series, Vol.62, No.62, pp100-111.

WIRTH, K E and MOLERUS, O (1982).
Prediction Of Pressure Drop With Pneumatic Conveying Of Solids In Horizontal Pipes.
Proc Pneumatech 1 conf.

WOODCOCK, C R and MWABE, P O (1984).
An Approach to the Computed-aided Design of Dilute Phase Pneumatic Conveying Systems.
Proc Pneumatech 2 conf.

WOODHEAD, S R, BARNES, R N and REED, A R (1989).
A Review of Techniques For Measuring The Mass Flow Rate of Bulk Solid Materials in Pneumatic Conveying Pipelines.
Proc 14th Powder and Bulk Solids conf.

ZENZ, F A and OTHMER, D F (1960).
Fluidisation and Fluid-Particle Systems.
Pub Reinhold, Chem Eng Series.

ZENZ, F A and ROWE, P N (1976).
Particle Conveying In Extrusion Flow.
Fluidisation Technology Vol 2.
Ed. Keairns D L, Hemisphere Pub Co, Washington, USA

ZUBER, N (1963).
On the Dispersed Two-phase Flow in the Laminar Flow Regime.
Chem Eng Sci Vol 19, pp897-917

ZUKOSKI, E E (1966).
J Fluid Mech, Vol 25, Part 4, pp 821 - 837.

KEY TO CONFERENCES

Pneumotransport series organised by
BHRA Fluid Engineering, Cranfield, Bedford, MK43 OAJ, UK.

Pneumatech series organised by
Powder Advisory Centre, PO Box 78, London, NW11 OPG, UK.

Power and Bulk Solids series organised by
Cahners Exposition Group, Cahners Plaza, PO Box 5060, 1350 E. Touhy Avenue, Des Plaines, IL 60017-5060, USA.

PHOENICS User Conference organised by
CHAM Ltd, London, UK.